ISBN 978-82-326-3350-0 (printed version)
ISBN 978-82-326-3351-7 (electronic version)
ISSN 1503-8181

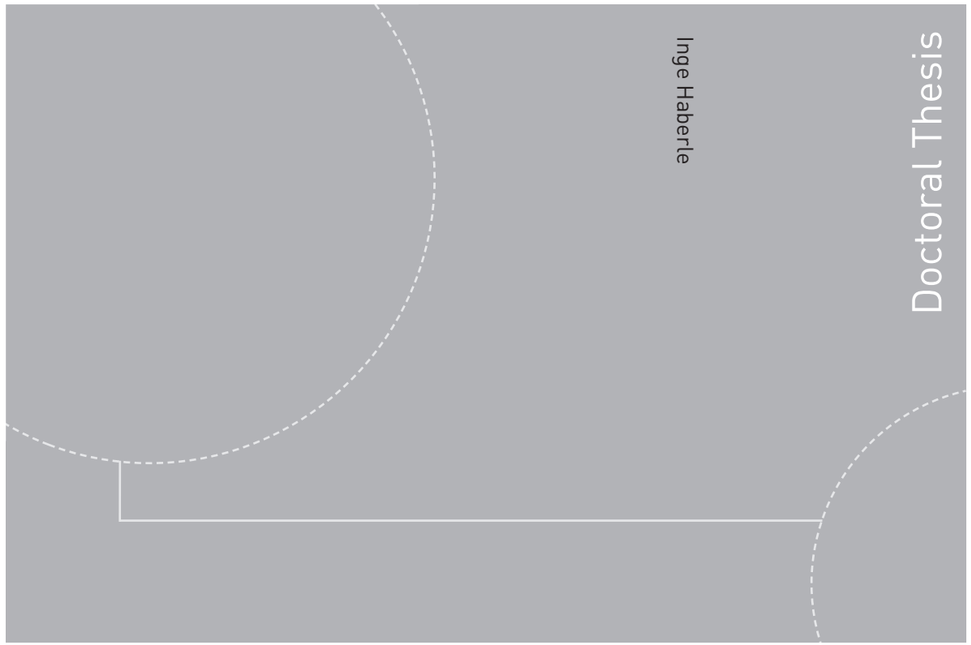

Doctoral theses at NTNU, 2018:280

Inge Haberle

Numerical simulation of transient behavior of wood log decomposition and combustion

NTNU
Norwegian University of
Science and Technology

NTNU
Norwegian University of
Science and Technology

NTNU
Norwegian University of
Science and Technology
Faculty of Engineering
Department of Energy and Process Engineering

Doctoral theses at NTNU, 2018:280

NTNU
Norwegian University of
Science and Technology

Inge Haberle

Numerical simulation of transient behavior of wood log decomposition and combustion

Thesis for the degree of Philosophiae Doctor

Trondheim, September 2018

Norwegian University of Science and Technology
Faculty of Engineering
Department of Energy and Process Engineering

NTNU
Norwegian University of
Science and Technology

NTNU
Norwegian University of Science and Technology

Thesis for the degree of Philosophiae Doctor

Faculty of Engineering
Department of Energy and Process Engineering

ISBN 978-82-326-3350-0 (printed version)
ISBN 978-82-326-3351-7 (electronic version)
ISSN 1503-8181

Doctoral theses at NTNU, 2018:280

Printed by Skipnes Kommunikasjon as

Preface

The doctoral work presented here was carried out at the Norwegian University of Science and Technology (NTNU) under the supervision of Associate Professor Nils Erland L. Haugen and Dr. Ing. Øyvind Skreiberg for partial fulfillment of the requirements for the degree of philosophiae doctor.

This work was performed within the WoodCFD project (243752/E20) led by SINTEF Energy Research. The project was funded by the Research Council of Norway as well as four industry partners, namely Norsk Kleber AS, Jøtulgruppen, Morsø AS and Dovre AS through the ENERGIX program.

Abstract

Heat from wood combustion in domestic wood stoves is a main contributor to the bioenergy in Norway. However, wood combustion in such small-scale combustion appliances can cause significant emissions, e.g. fine particulate matter. Therefore, optimization of old technologies and the development of new designs are required in order to manufacture wood stoves with reduced emission levels, higher efficiency and greater ease of use. To perform the required improvements, the combustion process inside the wood stove must be well understood. In the present thesis, thermochemical degradation of wood and successive char conversion were studied numerically by means of one-dimensional (1D) and two-dimensional (2D) models.

Common CFD platforms, e.g. Ansys Fluent, have well-established models for the gas phase, but lack detailed solid phase models. The solid phase model, developed as a standalone code as part of this Ph.D. work, has the potential to be coupled to the gas phase model via user-defined functions in the future. Since processes in the gas and solid phase influence each another, a dynamic coupling of the two models is required to obtain an accurate simulation tool. Fundamental studies on wood combustion can still be done by means of the standalone code. The wood combustion process, implemented in the 1D and the 2D model, included drying, devolatilization and char conversion of the solid fuel. Since all three stages are interrelated, the detailed modeling of all conversion stages with respect to a distinct location inside the wood log had to be done to derive an accurate solid phase combustion model.

The solid conversion model was developed for thermally thick particles, such that wood logs used in fired stoves or boilers could be modeled. Fundamental studies could be performed with the developed one-dimensional (1D) model, while detailed studies on the anisotropy of wood must use the extended two-dimensional (2D) model. Model validation was completed against experimental data, available for thermally thick particles' drying and devolatilization, as well as the combustion of a thermally thick near-spherical particle. The 2D model was validated against experimental data for a large, dry, hanging wood log, due to limited experimental data available on thermochemical degradation and combustion of wood logs, as used in domestic wood stoves.

Presented results include the studies on numerical efficiency of different models, as well as qualitative and quantitative results showing how wood logs degrade under combustion conditions. Furthermore, grid-independence studies were performed as part of the model development in this Ph.D. project.

Acknowledgements

First, I would like to express my sincere gratitude to my supervisors Nils Erland L. Haugen and Øyvind Skreiberg for all their support, valuable feedback and motivating encouragement. By sharing their knowledge within the field of numerical modeling, wood combustion and wood stove applications, they have helped me to increase my knowledge within those fields.

I would also like to thank the four industry partners Jøtulgruppen, Morsø AS, Dovre AS and Norsk Kleber for all their valuable input during our seminars.

My sincere gratitude goes to my wonderful family. The most valuable thing you have taught me is that even if I fail there is always a place I can come home to. Thank you Wolfgang, Ursula and Ralf!

I would also like to thank Betti, the most wonderful friend one could possibly have. Thank you for always motivating me during the last three years and thank you so much for being the amazing person that always makes me laugh, even when I was going through a rather frustrating period during my Ph.D.

I would also like to thank Anne, who has not only been there for me during the last three years, but actually most of the time over the last 25. Your honest opinion is something I can always count on.

Above all I would like to thank the person, that has helped me most through the ups and downs of my Ph.D. Christian thank you so much for understanding, helping, motivating me if necessary and ignoring me if appropriate. Thank you so much for giving me a home, no matter where we are in this world.

Last but not least, I would like to thank one of the most wonderful women I have had the honor to meet: my wonderful grandmother, who saw me start my Ph.D. but unfortunately not finish it. Oma, thank you so much for always having seen more in me than I did myself.

List of publications

The thesis is based on work presented in the following papers, referred to in the text by Roman numerals:

I. **Inge Haberle**, Øyvind Skreiberg, Joanna Łazar, Nils Erland L. Haugen. *Numerical models for thermochemical degradation of thermally thick woody biomass, and their application in domestic wood heating appliances and grate furnaces.* Progress in Energy and Combustion Science, **63**, 204-252, (**2017**).

II. **Inge Haberle**, Nils Erland L. Haugen, Øyvind Skreiberg. *Drying of thermally thick wood particles: A study of the numerical efficiency, accuracy and stability of common drying models.* Energy & Fuels, **31**, 13743-13760, (**2017**).

III. **Inge Haberle**, Nils Erland L. Haugen, Øyvind Skreiberg. *Combustion of thermally thick wood particles: A study on the influence of wood particle size on the combustion behavior.* Energy & Fuels, **32**, 6847 - 6862, (**2018**).

IV. **Inge Haberle**, Nils Erland L. Haugen, Øyvind Skreiberg. *Simulating thermal wood particle conversion: Ash-layer modeling and parametric studies.* (**accepted for publication in Energy & Fuels** in **2018**).

V. **Inge Haberle**, Nils Erland L. Haugen, Øyvind Skreiberg. *A two-dimensional study on the effect of anisotropy on the devolatilization of a large wood log.* (**submitted to Energy & Fuels** in **2018**).

Author's contribution

The papers are co-authored. The author of the thesis has performed the following work for the presented papers:

Paper I. The author reviewed the literature presented in the paper, processed the collected data and studied the effect of the data on the modeling results. A vast range of model input data for different wood species were presented in the paper. A critical analysis of current single particle models, as well as solid phase (= solid bed) models in domestic combustion units and large-scale grate furnaces was presented. The author wrote the paper in its current version. The author's main focus was the single particle modeling, as this review can be directly linked to the author's Ph.D. thesis. Literature was reviewed in collaboration with Joanna Łazar. Øyvind Skreiberg contributed to the section on wood chemistry and theoretical aspects of thermochemical degradation, as well as combustion. Nils Erland L. Haugen provided valuable support to the section on soot, as well as gas-phase related modeling aspects. Øyvind Skreiberg and Nils Erland L. Haugen both intensively contributed to the final version of the review paper.

Paper II. The author developed the drying and devolatilization model for a wet cylindrical thermally thick wood particle. Different drying models and the associated numerical efficiency, accuracy and stability were studied. Validation of the model was done by the author. The author was responsible for writing and interpreting the results. Nils Erland L. Haugen was involved in the model development and gave valuable support in the numerical aspects related to this paper. Øyvind Skreiberg and Nils Erland L. Haugen were both involved in the interpretation of the modeling results and provided valuable contributions to the final version of the paper.

Paper III. The author extended the existing drying and devolatilization model by adding char conversion reactions to cover the whole combustion process of a thermally thick wet wood particle. Validation of the model was conducted against experimental work as well as other modeling works. A grid-independence study was added, since this aspect of model development is not frequently discussed in the literature. Additionally the paper included a chapter that discussed how particle size (different radii) affected the particle combustion behavior. The author was responsible for the model development and validation, as well as the particle size study. The author was also responsible for writing the paper and interpreting the results. Nils Erland L. Haugen was involved in the model development and gave valuable support on the numerical aspects related to this paper. Øyvind Skreiberg and Nils Erland L. Haugen were both involved in the interpretation of the modeling results and provided valuable contributions to the final version of the paper.

Paper IV. The author used the thermochemical degradation and combustion model to compare the results of two different char conversion modeling concepts. One was based on fixed boundary conditions (consideration of ash) and the other was based on the concept of inward moving boundary conditions (absence of ash). The author also studied the sensitivity of the model to the thermal conductivities of char and wood, as well as to assigned specific surface areas and gas permeabilities. The author was responsible for the model development, the comparison between the two concepts and the parametric study. The author was responsible for writing the paper and interpreting the

results. Nils Erland L. Haugen was involved in the model development and gave valuable support to the numerical aspects related to this paper. Øyvind Skreiberg and Nils Erland L. Haugen were both involved in the interpretation of the modeling results and provided valuable contributions to the final version of the paper.

Paper V. The author extended the existing 1D model to 2D. Devolatilization of a large hanging, cylindrical wood log was modeled. The effect of anisotropy was studied by changing radial and longitudinal char permeabilities. Based on the predicted flow of gases, the volatile release rate at the bottom and top of the wood log was expected to differ from the release rate via the lateral surface. Nils Erland L. Haugen was involved in the model development and gave valuable support to the numerical aspects related to this paper. Øyvind Skreiberg and Nils Erland L. Haugen were both involved in the interpretation of the modeling results and provided valuable contributions to the final version of the paper.

Additional publications and presentations

Conference publications and presentation

I. **Inge Haberle**, Øyvind Skreiberg, Nils Erland L. Haugen. *Numerical simulation of devolatilization of wood logs and pressure generation in the wood log center.* Proceedings of 25th European Biomass Conference & Exhibition (EUBCE), 12 - 15 June 2017, Stockholm, Sweden, 561 - 565.

II. **Inge Haberle**, Nils Erland L. Haugen, Øyvind Skreiberg. *Comparison of numerical efficiency of the thermal and the kinetic rate drying model applied to a thermally thick wood particle.* Energy Procedia, **142**, 37 - 42, (**2017**). (Presented at the 9th International Conference on Applied Energy, 21 - 25 August 2017, Cardiff, UK).

Contents

Organization of the thesis

Chapter 1 outlines the role of wood as a renewable energy source. Wood combustion which in this thesis was used for heat generation on a domestic-scale is discussed and the constraints to related technologies are shortly outlined. The concept of numerical modeling is subsequently discussed in Chapter 2, as the working tool used in this Ph.D. work. In combination with experimental research it is a very promising research and development route toward new and optimized combustion technologies.

The results of the Ph.D. are presented in the attached papers, which can be found in **Selected papers**. Initially, a 1D model for wood combustion was developed. In fact, the main focus of **Paper II** was the development and validation of the drying and devolatilization model. **Paper III** focused on the extension of the existing drying and devolatilization model by including the char conversion stage. Char consumption was modeled as char oxidation and gasification. Both papers discussed thermally thick wood particles. Validation of the entire wood combustion model was conducted. The effect of particle size on combustion behavior was also investigated. This began to build a bridge from the validation case, which was conducted on a comparatively small near-spherical particle with a diameter of 9.5mm. In contrast to the validation test case, however, domestic stoves use very large cylindrical wood logs. In **Paper IV** the author confronted whether or not an up-building ash-layer must be considered in a wood combustion model. This question is relevant since wood contains very little ash with ash chemistry that yields a rather porous ash. It was thus a valuable approach to simplify the model, by assuming that the ash layer had a negligible influence on heat and mass transfer.

In a later stage of the Ph.D. project, the 1D model was extended to a 2D model. This extension was described in **Paper V**. By means of the 2D model, the anisotropy of wood was studied in detail. It was expected that the anisotropic nature of wood affected the internal distributions of temperature, mass fractions of gaseous species, gas density and consequently also internal pressure. Since the wood internal temperature field was expected to depend on heat transfer properties, the wood and char densities also varied in radial and axial direction, since the degree of devolatilization, which depends on temperature, also differed. **Paper V** also determined if fundamental studies on wood degradation dynamics require multi-dimensional models or if 1D models were sufficient.

In addition to the papers discussing model development, **Paper I** presented an extensive literature review on current single particle models. Modeling works regarding domestic wood-combustion units as well as large-scale grate furnaces were beyond the scope of this thesis but were still reviewed. However, the section in the review paper discussing numerical models for single particles was directly linked to this Ph.D. work.

Results obtained throughout the duration of this Ph.D. work are presented in Chapter 3. The complete papers that this thesis was based on are also attached. The thesis closes with conclusions and recommendations for future work (Chapter 4).

Abbreviations

BDF	Backward Differentiation Formula
Bi-CGStab	Bi-Conjugated Gradient Stabilized method
CFD	Computational Fluid Dynamics
DAE	Differential-Algebraic system of Equations
d.b.	dry basis
FDE	Finite Difference Equation
GMRES	Generalized Minimal RESidual
HACA	Hydrogen-Abstraction-Carbon-Addition
IDA - solver	Implicit Differential Algebraic equations system solver
PAH	Polycyclic Aromatic Hydrocarbons
PDE	Partial Differential Equation
SUNDIALS	SUite of Nonlinear and DIfferential/ ALgebraic equation Solvers
T.E.	Truncation Error
TFQMR	Transpose-Tree Quasi Minimal Residual method
w.b.	wet basis

Symbols

General symboles

a_n	coefficient (of time integrator)	[-]
h_{conv}	convective heat transfer coefficient	[W/(m^2 K)]
h_{eff}	effective heat transfer coefficient	[W/(m^2 K)]
h	time step size (of time integrator)	[s]
T	temperature	[K]
V	volume	[m^3]
A	surface	[m^2]
l	length	[m]
k	reaction rate constant	[1/s]

Greek letters

ω	emissivity	[-]
λ	thermal conductivity	[W/(mK)]
σ	Stefan Boltzmann constant	[W/m^{2}K^4]

Subscripts

c	characteristic
$conv$	convective
eff	effective
n	number of applied time steps
$particle$	particle
$surface$	wood particle/ log surface
1	reaction path 1: wood $\rightarrow$ non-condensable gases
2	reaction path 2: wood $\rightarrow$ tar
3	reaction path 3: wood $\rightarrow$ char

List of Figures

Chapter 1

Introduction

1.1 The role of wood in today's energy mix

Since wood is a renewable energy source, it is preferred over fossil fuels [1]. Continuous extensive use of fossil fuels causes rising carbon dioxide concentrations, with the undesirable consequences of global climate change [2]. Stricter demands for energy sustainability and intensified interest in renewable energy sources have arisen, due to the growing awarenesss and concern regarding global warming [3]. In fact, enhanced use of biomass, which includes wood, can reduce CO_2 emissions as well as yield an increased independence of society from fossil fuels [4]. Enhanced usage of biomass can antagonize rising carbon dioxide concentrations in the atmosphere, because it balances production and consumption of carbon dioxide.

The use of wood as fuel is unevenly distributed across the world. In 2005, 49% of roundwood usage was for fuel purposes in developing countries, while it was only 5% in developed countries [2]. Even though the contribution of wood for fuel purposes in developed countries seems more limited, current trends show that the use of bioenergy is still increasing. *Bioenergy* is defined as energy from biomass, and the carrier of this energy if often referred to as *biofuel*, within which solar energy is stored as chemical energy [5]. Besides its renewable character, the enhanced used of bioenergy can not only lead to a renewable energy system but can also result in the compensation of other fluctuant renewable energy sources [6].

In fact, it is estimated that there are about 65 million domestic wood burning installations within Europe, with the most common domestic technology being wood log combustion technologies [7]. However, it needs to be mentioned that the wood log combustion technologies implemented on a domestic scale are commonly used as a heat source in addition to oil and gas heating [7]. Users install such additional heating sources mainly due to the aesthetic combustion process (i.e. visible bright yellow flame).

Figure 1.1: Jøtul F 520, as depicted by Jøtul AS [8]. The aesthetic side effect of a wood stove is clearly shown by the intense yellow flame. The nominal output of this stove is 7 kW.

In 2013, about 1.2 million tons of wood logs were burned in Norway, with 1 million being burned in small-scale combustion units that were used for household heating [9]. In 2008, small-scale combustion technologies accounted for 50% of total Norwegian bioenergy use [10]. This proves that wood combustion is an important heat source even in developed countries. This already large use was expected to further increase by 8 TWh until 2020 [10].

This use of wood combustion units on a small-scale suggests that enhanced research within this field is required, since these units must also operate with low emissions, high efficiency and should remain user-friendly [11].

1.2 Fuel properties of wood

There are many different compositions for biomass fuels. Common biomass fuels are categorized as starch-containing, protein-containing, sugar-containing, oil containing and lignocellulosic [12].

Wood, as a lignocellulosic biomass, is mainly composed of cellulose, hemicellulose and lignin. In addition, there are also minor amounts of lipids, fats, proteins and inorganics. With respect to the three main constituents, some small variations can be observed when comparing different wood species, e.g. hard- and softwoods, but cellulose is typically the main compound with 40wt.% (dry basis) [13]. Hemicellulose accounts for 25 - 35wt. % (dry basis) [14], such that the total carbohydrate fraction varies from 65 - 75wt.% (dry basis). This combined fraction is also referred to as holocellulose. The residual mass fraction is mainly lignin, with small amounts of ash and extractives.

Cellulose is the main substance forming the cell wall. It is composed of D-glucose-molecules that are linked together via β-(1,4)-bondings (see Figure 1.2). The degree of polymerization of cellulose, which is defined by the number of sugar units within one molecule, ranges from 9 000 to 10 000 [14].

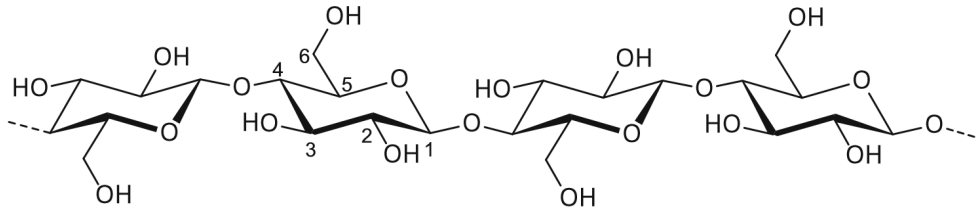

Figure 1.2: Chemical structure of cellulose, as depicted in Heinze [15].

In contrast to hemicellulose, cellulose is linear, while hemicellulose has a more branch-like structure [13]. Furthermore, hemicellulose has a lower molecular weight than cellulose and while cellulose is formed of glucose-molecules, hemicellulose is a mixture of different polysaccharides, e.g. glucose, xylose and arabinose. The two carbohydrates, cellulose and hemicellulose, are typically found in the secondary cell wall [14].

Lignin is the third main constituent of lignocellulosic biomass, and acts as a filler. It only occurs in combination with cellulose. Lignin is the generic term for a range of different aromatic polymers. Its structure is significantly more complex than the structure of cellulose, since it has a three-dimensional structure composed of phenylpropane-units with different numbers of hydroxyl- and methoxyl-groups. Lignification of a plant is responsible for its structural strength, even though the capillary pressure is low [13]. Basic information of wood chemistry can also be found in **Paper I**.

With respect to the elemental composition, wood is 47 to 50wt.% (dry basis) of carbon (C), 40 to 45wt.% (dry basis) of oxygen (O) and 5 to 7wt.% (dry basis) of hydrogen (H). In comparison to coal, wood contains a significant amount of oxygen and the difference in this elemental composition is due to the formation of wood and coal [13]. The heating value of the wood is influenced by its elemental composition. The amounts of C and H lead to an increase in the heating value, since these two compounds are the two main oxidable elements of wood. In contrast, increased amounts of oxygen in the fuel's elemental composition lead to a reduction of its heating value. The heating value for wood is commonly between 17.5 to 19 MJ/kg (dry and ashfree basis). Softwood has a slightly higher heating value than hardwood, since it has a higher lignin and extractives content. Both lignin and extractives having a higher C content than cellulose, also have higher heating values [13].

Further elements that can be found in wood, are nitrogen (N), potassium (K), phosphor (P), calcium (Ca), magnesium (Mg), chlorine (Cl) and sulfur (S). There are further elements with even lower contributions. Nitrogen, chlorine and sulfur are critically relevant when discussing emissions. However, in comparison to other biomass types, wood contains limited amounts of N, which is mostly due to a limited protein content. The nitrogen content is also low since wood is not subject to fertilization. Therefore, the fuel-bond NO_x in wood is low compared to other biomass sources [13]. Sulfur can

also be critical since it defines the SO_2-emissions. Chlorine, even though relevant for general emission studies, is less relevant for wood thermochemical conversion. Cl in wood is even lower than Cl in other biomass types that have been in contact with fertilizers. Cl only contributes to 0.005 to 0.02wt.% of wood (dry basis). Nonetheless, emissions from chlorine contained in wood still need to be studied, since chlorine is responsible for corrosion, which can significantly affect the conversion unit [13].

The ash content of wood is commonly very low, e.g. <1wt.% (dry basis). Knowledge of the ash content of a fuel is relevant, because it affects the operation and therefore the entire design of the combustion technology. For domestic wood stoves, ash deposition-related studies are not a main concern, since a low ash-content fuel is converted. The maximum ash fraction used in this Ph.D. was 1wt.% dry basis (see **Paper III** to **Paper V**).

A main fuel property of wood that defines its combustion behavior is its high volatile content (74 to 83 wt.% (dry basis)) [13]. The high volatile content can be directly linked to the main motivation for installing a domestic wood stove; i.e. the visible flame. As soon as the volatiles are released from the solid during devolatilization, and are mixed sufficiently well with oxygen at a high enough temperature in the combustion chamber, the combustible gases are oxidized and the flame is established.

Fuel properties are, however, not purely defined by the fuel's chemistry. A fuel's physical appearance can also affect its combustion behavior. [13]. It is obvious that particle size has an influence on the combustion behavior, e.g. see **Paper III**. On domestic scales, wood pellets, wood chips and wood logs are commonly fired, which are all considered thermally thick particles, but the dimensions and shapes differ significantly.

For a *thermally thick* particle, the internal heat transfer is slower (higher heat transfer resistance) than the external heat transfer, and therefore a temperature gradient can be observed within the particle, which is in contrast to *thermally thin* particles where the internal heat transfer is fast compared to the external heat transfer. For thermally thin particles, the particle can be modeled as isothermal. However, if this *isothermal modeling approach* is used also for large particles, significant errors are introduced.

The thermal thickness of a particle is defined by the Biot number (Bi), where external and internal heat transfer resistances are related to each other by [16]

$$Bi = \frac{h_{\text{eff}} l_{\text{c,particle}}}{\lambda_{\text{particle}}} \tag{1.1}$$

with $l_{\text{c,particle}} = \frac{V_{\text{particle}}}{A_{\text{particle,surface}}}$ being the characteristic length [m], $\lambda_{\text{particle}}$ being the particle's thermal conductivity [W/(mK)], V_{particle} being its volume [m^3] and $A_{\text{particle,surface}}$ being its external particle surface [m^2]. The effective heat transfer coefficient for heat transfer from the surroundings of the particle to the particle, h_{eff}, takes into account both convection and radiation, being defined as [1]

$$h_{\text{eff}} = h_{\text{conv}} + \sigma \omega_{\text{particle}} (T_\infty + T_{\text{surface}})(T_\infty^2 + T_{\text{surface}}^2) \tag{1.2}$$

with ω_{particle} being the particle emissivity [-], and σ being the Stefan-Boltzmann-constant [W/(m^2K^4)].

The separation between *thermally thick* and *thermally thin* is at a Biot number of 0.1 [16, 17] (see Figure 1.3). If Bi $<$ 0.1, the assumption of an isothermal particle is valid, without introducing significant errors to the model. For such a case, intra-particle temperature gradients are negligible. If isothermal particles are to be modeled, drying, devolatilization and char conversion occur in series. The larger the particle (Bi>0.1), the more likely the conversion stages will overlap in time on the particle-scale. This implies that drying, devolatilization and char conversion are occurring simultaneously within the particle, but at different locations [16].

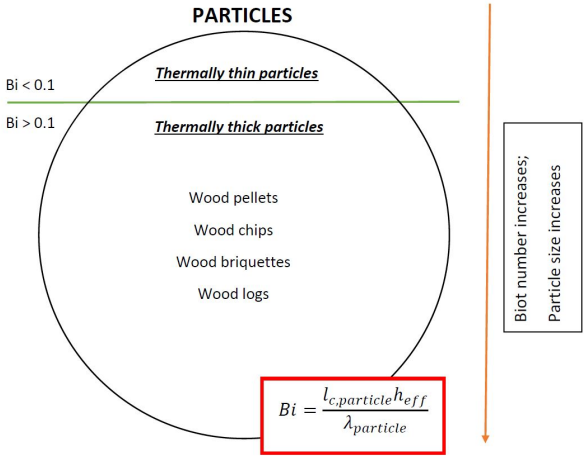

Figure 1.3: Thermal thickness of particles.

However, it needs to be added that the critical Biot number of 0.1 is not commonly accepted and that different researchers have used different limits for the split between thermally thin and thermally thick regimes [16, 18, 19]. Bryden et al. [18] even split the categorization according to relative heat transfer contributions into three different regimes; namely the thermally thin regime, the thermally thick regime and the thermal wave regime. They define the thermally thick regime as the regime where internal and external heat transfer are comparable and the thermal wave regime is given when internal heat transfer is significantly slower than external heat transfer. Thermally thin, according to the classification by Bryden et al. [18] only refers to Biot numbers smaller than 0.2. One can, however, expect that for both, the thermally thick and the thermal wave regime, intraparticle gradients, are expected to be modeled. In other works, however, a significantly higher Biot number of unity is used to serve as threshold value between thermally thin and thermally thick [19]. Compared to the other two suggested threshold values, we considered this value to be rather high and assume that at such high Biot numbers, intraparticle gradients cannot be neglected anymore without causing notable errors in modeling results.

Wood chips are commonly between 5 to 100 mm [20]. Wood chips are obtained by simply chipping the untreated wood, and therefore these wood particles must be modeled as anisotropic, since the original wood fiber structure is well maintained. Wood pellets, in contrast to wood chips, are formed by a densification step from finely ground wood powder. Wood pellets are of cylindrical shape and

are well-manageable, i.e. by a feeding system due to homogeneity [21]. In contrast to wood chips, wood pellets are also smaller, with a diameter less than 25 mm [20]. Another main difference between wood chips and wood pellets is that wood pellets, due to the precendent densification process can be considered as isotropic. The natural fiber orientation, which is well-maintained in wood chips, is also well-maintained in wood logs. Even though wood pellets are rather well-regulated, the definition of a wood log is not yet standardized. A common wood log is a large piece of wood, typically cylindrical or brick-shaped, that has a diameter within the cm-range and aspect ratios significantly larger than unity. The devolatilization of such a wood log was discussed in **Paper V**. Wood logs, when fired in wood stoves, commonly have moisture contents up to 16-20wt.% wet basis [22]. Wood logs are not homogeneous while pellets have a more homogenized character. Logs can still contain a bark layer. Therefore the composition, porosity etc. can vary depending on the location in the wood log.

This difference between wood logs and wood pellets requires models to be based on different simplifying assumptions. While isotropy can be assumed for densified-wood, eliminating the need for multi-dimensional models, a wood log is anisotropic and requires multi-dimensional models. Wood log modeling by 1D models can be considered very much simplified, since direction-depent properties enter the model as averaged values or by simply using one single value, e.g. only radial thermal conductivities. Consequently, it is more accurate for native wood to be described by multi-dimensional models, where anisotropy can be accounted for in detail.

The previous discussion with respect to fuel properties already outlined the significant number of model input parameters required. Of course this increases the complexity of the model, and as a consequence the model can become numerically inefficient or less user-friendly. Both aspects reduce its applicability as a tool for wood stove design and optimization. Simplifications are needed and simplifying assumptions are a key element of modern model development. Common simplifying assumptions are also discussed in the papers (see Chapter 3 and **Paper IV**).

1.3 Thermochemical conversion routes for wood

Thermochemical conversion technologies are commonly used to obtain heat or energy carriers, such as charcoal, a liquid or a gaseous product. Conversion routes include pyrolysis, gasification, liquefaction and combustion [12, 23]. A list of possible thermochemical conversion routes is shown in Figure 1.4.

Pyrolysis is a term describing thermochemical degradation in the absence of oxygen. This lack of oxygen refers to oxygen supplied from the exterior, and does not include oxygen contained in the biomass structure, which can theoretically contribute to the degradation reactions [12].

Normal temperature ranges of pyrolysis are 200 to 500°C, and the products are always a mixture of tar, non-condensable gases and a solid, i.e. biochar. The relative contribution of the different products to the product mixture is a function of residence time, heating rate, pressure as well as temperature. The products can be used in different ways. While the carbon containing solid, i.e. biochar, can be upgraded to activated carbon, finding its application in metallurgical processes, the produced non-condensable gas can be used to generate heat or power. It can also be further processed by synthesising it into methanol or ammonia. The tar fraction, which condenses to a crude oil when

cooled to room temperature, can be used as a precursor for high grade hydrocarbon liquid fuels used in the transportation sector or for heat and power generation [23]. The temperature range for pyrolysis of wood is large, since all three wood components; cellulose, hemicellulose and lignin, have different thermal stabilities. While hemicellulose is the least stable compound in wood, lignin starts to degrade at slightly higher temperatures and cellulose starts to decompose at the highest temperatures [24]. Lignin decomposition covers a broader temperature range than the other two wood compounds [25]. Lignin has the highest charring tendency of all compounds, while cellulose and hemicellulose contribute more to the tar fraction [24].

Gasification is a thermochemical conversion route used to obtain a product gas with a desirable heating value. Gasifying agents are most commonly H_2O, air or oxygen, though CO_2 could also be used. Partial oxidation ensures that the required energy for gasification reactions is supplied [12]. The gasifying agent influences the heating value of the product gas. While air gasification yields a gas with a heating value of 4 - 7 MJ/Nm^3, oxygen gasification produces a gas with a heating value of 10 - 18 MJ/Nm^3 [23]. Gasification normally occurs at temperatures between 800 to 1000°C, which is significantly higher than the peak temperature for pyrolysis. The main aim of gasification is the formation of significant amounts of non-condensable gas; a fuel gas. As the main product is aimed to be a gas, the solid remnants contain significant amounts of ash and some residual carbon [25]. The gaseous product does not contain only combustible gas species, but also contaminations by ash, tar or small char particles. The fuel gas can be used in different ways, e.g. upgrading to methanol, or burned in a boiler for hot water or steam production. In addition, it can be burned in a gas turbine for electricity production, where it becomes very crucial that contaminations have been removed [23].

Liquefaction is a thermochemical conversion route that describes the degradation of biomass in a liquid phase, occurring at high pressure and comparably low temperatures. Catalysts can be applied to enhance the degradation. The main product is a crude bio-oil [12]. The advantage of liquefaction is that since liquefaction can be performed with liquid water (hydrothermal liquefaction), wet biomass can be efficienctly converted, without requiring an energy-intensive pre-drying step [25].

Finally, there is combustion, which is a thermochemical conversion route applied to generate heat and electricity [12]. In combustion, the full oxidation of biomass is the objective. Therefore, combustion is the only thermochemical conversion route mentioned where the entire energy content stored in the biomass is directly released, which of course can only be reached if enough oxygen is available to fully oxidize all combustible components of the fuel [25]. Further details on combustion are found in Chapter 1.3.1. In contrast to this, pyrolysis, gasification and liquefaction yield secondary energy carriers, with different properties than the original wood log, e.g. gaseous or liquid [25].

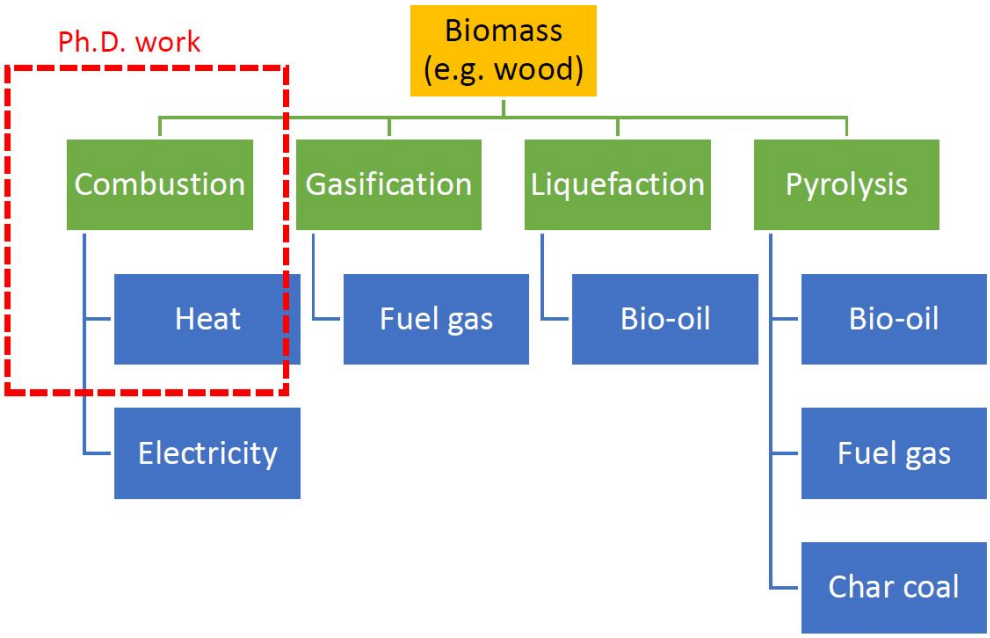

Figure 1.4: Thermochemical conversion routes.

The modeling of wood combustion was intensively studied in this work. A wood combustion model was developed, where drying, devolatilization and char conversion were considered.

1.3.1 Wood combustion

Combustion has been the main method of heating and food preparation for tens of thousand of years. Throughout history, wood, charcoal and other biofuels were used as a primary energy source that could be transformed. Only after large amounts of the forests in Europe were stripped due to the then upcoming technology of the steam engine, an additional source of primary energy had to be found in the industrialized world. Coal became the main source for primary energy; oil and gas followed suit. However, the interest in biomass as a primary energy source was always there, but it was only in the 1970s, as a consequence of the energy crisis at the time, that the focus was shifted again in the direction of biomass. The movement toward renewable sources started as society was then afraid of running out of oil, due to the more limited predicted reserves at that time [26].

Combustion refers to the complete oxidation of biomass after the stages of drying and devolatilization [23]. The combustion process of wood is the result of a strong coupling between heat and mass transfer phenomena as well as chemical reactions [3]. Details on the related phenomena can be found in **Paper I** to **V**.

The wood log initially fed to the wood stove is wet, since wood is naturally hydrophilic. During evaporation the liquid water, present as bound water or liquid free water [23], is reduced and water vapor fills the pores. Vaporization is an endothermic process, using energy released from the char

oxidation, and as a consequence potentially lowering the temperature in the combustion chamber. The drying stage can be crucial, since burning of a very wet wood log can result in a termination of the combustion process [5]. Drying in this study was modeled by the "kinetic rate" or the "thermal drying" model, and more details on the theory of these drying models can be found in **Paper II**. Once a part of the wood log has been dried and temperatures higher than 200°C are reached, devolatilization becomes very much enhanced [3]. The products of the organic mass loss due to devolatilization are lumped together into tar, char and non-condensable gases in models [3]. Such a combining procedure is required to allow for a reasonable computational cost. This is because the two gaseous product categories (non-condesable gases and tar (at temperatures higher than room temperature)) contain hundreds of different chemical species, which would imply the need for a signifcant number of species equations to be implemented in the model. Details on the devolatilization scheme can be found in **Paper I**, where different schemes are compared. Applied kinetics can be found in **Paper II** to **V**, where the "three competitive reaction scheme" was included in the thermochemical degradation model.

Secondary tar reactions occur, because the produced tar from the devolatilizing wood log has to pass through the hot char layer, where it can further react, either forming secondary char or non-condensable gases [17]. Reactions occur if the tar has a large enough residence time in hot particle areas, and therefore sufficient time to either further crack or re-polymerize. Therefore, the extent of secondary tar reactions depends on operational conditions as well as the fuel particle size.

The volatiles released during devolatilization may ignite in the vicinity of the wood log, such that a diffusion flame surrounds the wood log. Depending on the operation conditions, the volatiles can leave the vicinity of the wood log and burn further away from it in a partially premixed mode [12].

As a result of devolatilization, a char layer forms around the unreacted wood core [3]. The char layer starts to react, mostly with O_2 but also with CO_2 and H_2O, depending on the operational conditions, and as a consequence the char layer is consumed [3]. Ideally, only ash is left after the burnout has been accomplished. Depending on the quality of the combustion process, the residual carbon content in the ash is close to zero, but practically never exactly zero as assumed in models. During char conversion in wood stoves, mass transfer is the key mechanism because it defines the oxygen transfer to the active sites and therefore the char conversion rate and the total burnout time [3].

In addition to drying, devolatilization and char conversion reactions, as well as gas phase transportation through the porous system, a model is theoretically also required to consider structural changes, such as surface regression, crack formation, shrinkage and swelling [24]. Shrinkage is less important during drying, but becomes significant during devolatilization [27] due to the large organic mass loss occurring during this conversion stage. The wood log also decreases in size due to heterogeneous char reactions [3]. There are different approaches to model shrinkage, as outlined in **Paper I**. The implementation of a shrinkage model in the general thermochemical degradation and combustion model has been discussed in **Paper II**, **Paper III**, **Paper IV** and **Paper V**. It is now obvious that during wood log combustion, physical and chemical processes are strongly coupled. The complexity of all the processes related to combustion that must be considered outlines the challenges for model development.

1.4 Biomass combustion technologies

Common wood combustion technologies can be categorized into large-scale and small-scale. Large-scale technologies include fluidized-bed furnaces and grate-fired furnaces [12]. Grate-fired furnaces use large fuel particles that are transported through the combustion chamber on a grate. At the beginning of the grate the fuel bed dries, and close to the end of the grate the residual char is converted. This is a rather simple technology, still in use for biomass and waste combustion [28]. Current modeling works of solid bed conversion on such grates have been reviewed in **Paper I**, though this does surpass the scope of this Ph.D.

With respect to fluidized-bed combustion, the applied particle size is smaller than for grate-firing. The fuel is packed in the furnace together with an inert material; e.g. sand. The fuel and the inert bed material are kept in a fluidized state, while the fuel is converted [29].

Large-scale applications, however, are not the main concern of this thesis. This Ph.D. work focuses on a solid phase model applicable for small-scale combustion applications, specifically wood log fired stoves. Therefore, those combustion units were briefly reviewed in **Paper I**. In addition to wood stoves, other small-scale wood combustion applications include fireplaces and wood log or wood pellet boilers [12]. Fireplaces are the most simplistic wood combustion units, but cause significant emission levels due to incomplete combustion caused by low combustion temperatures. Small-scale wood log boilers can operate up to 20kW, and water is used as an energy carrier. In contrast to wood stoves, these boiler units are commonly used for central heating in detached houses and not for single-room heating, where wood stoves are used. Wood stoves, as already mentioned earlier, normally operate at lower heat output; i.e. up to 10 kW. The low heat output compared to other small-scale technologies led to the designation as micro-scale applications within this study. The main disadvantages of wood log stoves are the high emission rates, due to the batch-wise operation of those units, which does not allow stable combustion conditions [12].

In a wood stove, the combustion process is commonly split into three stages based on experimental observations. First, the stove and the initial biomass batch must be heated. This stage includes drying and is related to high CO and total volatile hydrocarbon (THC) emissions. The high emissions are due to the initialization of the devolatilization stage, where volatiles start to be released, but are not yet fully oxidized in the combustion chamber [30]. This lack of oxidation is due to low temperatures in the combustion chamber at the beginning of the combustion-cycle. Temperature, residence time, turbulence and availability of oxidant affect the combustion of gases. This initial stage is followed by a sudden drop in O_2 in the exhaust gas, occurring when the combustible volatiles start reacting with the available oxygen. In return, the temperature increases due to exothermic oxidation reactions. An increasing temperature in the combustion unit leads to an enhanced solid fuel conversion rate, because devolatilization is heat-transfer controlled. Experimentally, an intense yellow flame can be observed above the solid fuel during this stage. Significant organic mass loss occurs, due to the enhanced devolatilitzation reactions, and only charcoal remains. The conversion of charcoal occurs in the third stage of the combustion-cycle, and is linked to a rather slow mass loss [30]. During this stage more CO is emitted, which is due to the dropping temperature [12]. Shortly before the char conversion has been fully accomplished, the wood stove user commonly inserts a new and wet wood

log into the combustion chamber.

Significant amounts of products from incomplete combustion are emitted from wood log stoves due to the batch-wise combustion. This batch-wise firing causes continuously changing conditions in the interior of the combustion chamber; e.g. excess air ratio, combustion temperature and fuel composition, which affects the emission levels [12].

Even though combustion has been around for thousands of years, and humans are already quite acquainted with it, it is still not as developed as other technologies. The maturity of a technology can be measured by whether or not the development of new designs can be based on computational models. This partly implies that the underlying physics is well understood and can be efficiently implemented and used in those simulation tools. For wood log combustion technologies, however, computer models are still in a fledging state and it is more common to develop new designs based on experiments and experience. This deficiency does not arise from a lack of research activities with respect to modeling development, but rather from the fact that combustion (gas and solid phase) is a multi-scale and multi-dimensional problem, including highly non-linear processes that are strongly coupled [26]. It is not yet possible to fully and numerically efficiently reproduce the related real-world physics of combustion in a computer model.

Even though there are still restrictions, computational fluid dynamics (CFD) has become more and more important with respect to combustion modeling in particular for gas phase combustion. Due to improved computational capabilities, the role of computer simulations in the design and optimization of combustion is quite prominent already [31]. It has been used to study phenomena occurring in the furnace or the boiler and has already been used to analyze the flow of gaseous products from the combustion process through the post-combustion systems. Modeling has already allowed for a greater understanding of the combustion process [32]. Currently, the focus of research is also on studying the influence of different chemistry, turbulence and combustion sub-models on the modeling results and finding the most suitable choices for different biomass combustion technologies [33]. Even though CFD has become a common simulation tool for modeling gas phase combustion, CFD software does not contain solid phase combustion models for wood logs, which instead have to be implemented by the user.

1.5 Emissions from domestic wood stove applications

One main problem with wood stoves is that older and poorly operating technologies are still used, which are responsible for significant amount of emissions. Of the 1 million tons of burned wood logs in Norwegian households in 2013, 54% were burned in new technologies, and 46% were thermally converted in old wood stove technologies [9]. Those units are responsible for significant emissions, suggesting that optimization is required.

Not only are particulate emissions influenced by the batch-wise operation of wood stoves, but also gaseous emissions depend on the wood stove's operation mode. High emissions are observed in the beginning of the combustion cycle and in the final burnout phase [34]. The increased emissions imply that incomplete combustion is one of the main problems associated with domestic systems [30, 35].

If the use of wood combustion increases, as predicted, these technologies would become a dominant source of fine primary particle air pollution in Europe from 2020 onward [7]. Automation could be a solution, but most of the current technologies on the market are not automated [34], even though some manufacturers offer fully automated wood log combustion units [36].

However, emissions cannot be purely controlled by advanced technologies since user-behavior and fuel quality also play a role [7]. Emission levels are influenced by the type of fuel, the amount of fuel load as well as fuel quality; i.e. moisture content, size of the wood particle burning and contamination of the fuel. All these parameters affect burning conditions [37, 38, 39, 40, 41]. An example of the influence of user-behavior on emission levels is the manually operated regulation of combustion air, which affects oxygen availability in the reaction zones. If too little oxygen is available, combustible gases cannot be fully converted to water vapor and carbon dioxide, and if too much air is available, the temperature in the combustion chamber becomes too low, also leading to incomplete combustion. In general, incomplete combustion can be linked to inadequate mixing of combustion air and fuel, the overall lack of available oxygen, low combustion temperatures, residence times that are too short and low radical concentrations [5].

Particle matter emissions from wood stoves are within the sub-micrometer range (smaller than 1 μm) [40, 42]. The particle size is crucial when defining related health issues, as particle size decides where and if deposition in the respiratory system during inhalation occurs. In addition to particle size, the chemical composition of particle matter is important when defining health issues. Mainly polycyclic aromatic hydrocarbons (PAH) have been studied, which are toxic, mutagenic and carcinogenic [43, 44], but the oxygenated PAHs can be even more toxic [7]. The operational mode of the wood stove influences the emissions of PAHs more than the fuel species. The available oxygen in the combustion chamber as well as the combustion temperatures also influenced the formation of PAHs.

Soot emission is an additional problem related to wood combustion technologies. Soot is formed over a set of steps, including inception, surface growth, coagulation and oxidation. The coagulated particles can further increase in size, by forming clusters via agglomeration, up to 1μm [45]. With respect to soot formation from biomass combustion, the inception stage is still not very well understood, which makes it difficult to model. The limitation is that the traditional hydrogen-abstraction-carbon-addition (HACA) route does not account for oxygenated PAHs, which can contribute to to soot formation during wood combustion as has been found for e.g. pine [46]. A short discussion on soot modeling is presented in **Paper I**.

With respect to biomass combustion, NO_x emissions are also important. NO_x can be formed through three different paths; thermal, prompt and fuel-bond NO_x. Thermal NO_x, which is formed from nitrogen and oxygen in the combustion air at high temperatures (higher than 1400°C) is less relevant for wood stove applications, since the required temperatures are not commonly reached in wood stoves. Prompt NO_x is also formed from nitrogen and oxygen supplied by the combustion air, but requires the presence of hydrocarbon radicals together with temperatures that are not possible in a wood stove combustion [13]. Therefore, it can be concluded that most of the NO_x measured in small wood combustion appliances comes from fuel-bond nitrogen. Aspects of NO_x modeling have also

been discussed in **Paper I**.

Emission requirements are becoming stricter [47], demanding more advanced and optimized wood combustion technologies. Optimization is possible, because efficiency and emission performance of older technologies have been found to vary greatly from new technologies [48, 49].

Optimization can only occur after understanding thoroughly the combustion-related chemical and physical processes. In micro-scale domestic wood combustion technologies, secondary flue gas cleaning technologies, which could reduce high emission rates, are not commonly used due to too high cost. Emission levels therefore have to be reduced by cost-efficient primary reduction methods [34].

Wood stove designs are not only studied with respect to optimization required for reduced emission levels. Thermal comfort also has to be considered when designing new and optimizing old wood stove technologies. The current research with respect to thermal comfort when using wood stoves is focused on a reduction of the peak heat release commonly observed in old wood stove technologies. Other research focuses on stable heat release during the entire combustion process. The research focus is thus on the combustion process and the materials used for wood stoves.

1.6 Thesis objective

Wood is a very important renewable energy source, with a wide range of applications and wood combustion will play an important role in current and future energy mixes. Combustion units, such as wood stoves, have been developed primarily based on experiments and experience. However, modeling is a faster and less expensive tool for wood stove manufacturers to derive optimized designs. The need for simulation tools was the main motivation for this Ph.D. project. Computational fluid dynamics (CFD) softwares, such as ANSYS Fluent can be used for wood stove design and optimization, but are primarily only well-established for gas phase modeling. Detailed solid-phase models are not included. Therefore, the development of such solid phase models is required. A suitable model for wood log conversion can then be dynamically coupled to the gas phase model, leading to the development of more accurate simulation tools.

The objectives of this Ph.D. thesis are therefore as follows:

1. Obtain fundamental understanding of wood combustion related processes, both chemical and physical.
2. Develop a numerical simulation tool that describes wood combustion. The starting point is a 1D model that can be used to obtain a fundamental understanding of drying, devolatilization as well as char conversion of a thermally thick wood particle.
3. Develop a 2D model, where the anisotropy of wood can be studied in detail and where the standalone code can then be coupled to an existing gas phase model.

Chapter 2

Modeling approach

Even though thermochemical biomass conversion has been a field of intensive research already for decades, much of it remains unknown. In order to gain deeper understanding of the chemical and physical processes occurring during thermochemical degradation and combustion of wood particles and logs, modeling is a useful tool. By describing the conversion process by mathematical equations, computing the conversion and comparing the modeling results to experimental observations, much can be studied with respect to physical and chemical phenomena occurring during conversion. Furthermore, input data to the model can be quickly changed, such that a range of different operating conditions can be easily studied [25]. A vast range of different modeling approaches and degrees of simplification of the thermochemical conversion are available [50]. How well a specific model perfoms is defined by the fuel as well as the reactor conditions to be tested [51].

In this Ph.D. work a comprehensive model for thermochemical degradation and combustion was developed. A comprehensive thermochemical degradation model is defined as a model that considers chemical kinetic schemes describing the degradation as well as conservation principles for heat and mass transfer. However, not all comprehensive models contain the same degree of detail. The applied kinetic schemes can be subject to varying degrees of simplification and heat and mass transfer phenomena can equally be simplified to various degrees in different comprehensive models [50].

The transient thermochemical degradation of the solid fuels interrelates different phenomena; for example heat transfer (convection as well as conduction), heat sink and sources due to chemical reactions, phase changes such as moisture drying, outwardly convective transport of gas products, diffusion of gases inward, as well as wood internal pressure up-build and resulting structural changes such as cracking. Many of the involved processes are not yet well understood, such that all currently available comprehensive thermochemical wood conversion models are subject to simplification.

The development of such a numerical model requires a set of governing equations describing

- continuity in the gas phase
- mass of wood
- mass of char

- mass of ash
- mass fractions of gas species, e.g.tar, O_2, CO, CO_2, H_2O (g)
- temperature
- liquid phase mass (bound and liquid free water)

during the thermochemical degradation and char conversion of a particle. The set of required governing equations is repeatedly listed in different papers that were written as part of this Ph.D. work, **Paper I** to **V**. In addition to the governing equations, wood properties need to be described. As a consequence, a combination of partial differential equations and algebraic equations must be solved for, which can only be done by means of a numerical solution procedure [23].

As already mentioned earlier those governing equations, when implemented in a thermochemical wood conversion and combustion model, are subject to simplifications. The most common simplifications are [50]

- The wood is assumed to have a homogeneous porous structure.
- Structural changes are simplified, e.g. negligence of cracking, swelling and shrinkage or shrinkage is considered uniform.
- The complex chemistry of wood is simplified by either only considering a mixture of its different species (only wood is considered in the degradation kinetics) or by tracking the evolution only of the main consitutents.
- It is assumed that local thermal equilibrium exists between all phases.
- Darcy's law is used to describe the movement of gas phase in the pores.
- Gases are assumed to be ideal.
- Thermochemical degradation products are simplified and lumped together.
- The number of reactions involved in thermochemical degradation are significantly simplified and reduced.

In order to find the values of temperature, wood density, char density, mass fractions of gas species, gas and liquid phase density at distinct locations within the wood log at different times, the continuous information contained in the differential equations must be transformed into discrete positions. Various discretization methods can be employed, and because the discretized equations are generally derived from the integral or differential form of the governing equations, they express the same physical information [52]. The most common discretization methods applied for wood conversion modeling are the finite difference method, e.g. in [53] and the finite volume method, e.g. in [1].

The finite-difference method is based on the Taylor expansion series, where the derivatives are approximated by truncated Taylor series [52]. The finite-difference method is applicable for very simple

geometries and structured grids [54]. Typically wood logs are simplified and described by idealized shapes such as bricks or cylinders and the wood log surface is smoothened out and simplified. These simplifications make the finite-difference method a valid approach. Finite differencing was used in this work.

The order of the discretization depends on the discretization method. In this work, as mentioned in **Paper III**, the convective term was discretized by first order upwinding, while the diffusive term was discretized by a second order difference scheme. The spatial discretization was therefore of first order accuracy, (i.e. $O(\triangle r)$). As mentioned in **Paper III** as well as in **Paper V** such a degree of accuracy was considered sufficient, primarily due to a smooth gas flow without discontinuities within the wood log pores.

The IDA solver included in the SUNDIALS software package [55] was used as a time integrator. It implicitely solved the set of equations by a backward differentiation formula, with an order of 1 to 5. The order was chosen by the solver depending on the local error. The IDA solver followed the same concept as the DASSL solver written in Fortran, which was used for thermochemical degradation modeling of wood by Grønli [23]. More details on the IDA solver can be found in Chapter 2.1.

Besides the discretization method, an accurate and reliable numerical model requires suitable boundary conditions. This was especially critical for the thermochemical degradation and combustion of wood logs. The heat and mass transfer from the surroundings of the particle to its external surface was affected by the gases leaving the particle during conversion. Such an interaction had to be considered in the model. Symmetry conditions could be applied to the center lines of the wood log in order to save computational time, as discussed in **Paper V**. When large wood logs were considered, modeling only e.g. one fourth of the solid instead of the entire wood log, yielded a significant reduction of grid points. This resulted in reduced computational cost. However, if boundary conditions are not homogeneous, as for example when logs are stacked, the boundary conditions of each wood log will change, such that symmetry conditions are not an appropriate choice. If heat and mass transfer vary greatly over the external surface, then the entire wood log must be modeled.

The numerical model developed as part of this Ph.D. work was written in C. In its current form it operates as a standalone code. Drying, devolatilization and char conversion of the solid wood particle can be studied, as presented by **Paper II** to **V**. The current model was first developed for a simple one-dimensional (1D) case. The model development with respect to the 1D set-up was discussed in detail in **Paper II**, **Paper III** and **Paper IV**. The numerical set-up of the 1D case was then extended to a 2D model, where the anisotropic nature of wood could be studied. Details on this extension can be found in **Paper V**.

In the future, the model will be coupled to Ansys Fluent via user-defined-functions. Only after such a coupling can the dynamic interaction between solid and gas phases be realistically accounted for. The consideration of the dynamic interaction between solid and gas phases refers to the fluctuating radiative feedback of the flame to the solid. The wood log is then a solid fuel with a temperature boundary affected by a dynamically changing heat flux. As a consequence, volatile release rates will change, which affects the input data to the gas phase model.

In its current form the model can be used to fundamentally study chemical and physical processes that occur within the solid as it thermochemically degrades. 1D models were sufficient, as was shown by the validation against experiments presented in **Paper II** to **IV**, for fundamental conversion studies. To study the internal distributions in wood, the anisotropic nature of wood has to be captured by the model. Details on the 2D model can be found **Paper V**. Large wood logs, as used in wood stoves, are not an intensive subfield of research within the general biomass thermochemical degradation and combustion research. This lack of experimental data resulted in using a large hanging wood log experiment for the validation of the 2D model.

The number of required grid points depend on the size of the wood log as well as operating conditions affecting the temperature and oxygen mass fraction gradients within the wood particle. A grid-indendependence study was performed, as mentioned in **Paper III** and **V**. For the 1D model, a rather dense mesh was found to be required, due to the steepness of temperature and oxygen mass fraction gradients during the char conversion stage (see **Paper III** for details). The required number of grid points for the 2D model was expected to have a significant effect on the computational time. In order to save time, symmetry boundary conditions were applied (see **Paper V**). For both the 1D and the 2D model, structured grids were applied to the wood log, and the grid spacing was not reduced towards the wood log boundaries, where higher gradients can be expected. The number of grid points was strictly coupled to the particle size and the operational conditions.

For the 1D case, where only drying and devolatilization were studied, cylindrical particles with an aspect ratio of four were modeled (see **Paper II**). However, due to limited experimental data describing thermochemical degradation as well as char conversion of a wood particle, the entire conversion, including drying, devolatilization and char conversion, was modeled for a near-spherical particle; i.e. a cylinder with an aspect ratio of one, (see **Paper III** and **Paper IV**).

The 2D model was then applied to a significantly larger wood log, comparable to those used in wood stoves. The diameter for this case was in the cm-range and the aspect ratio was six. Details on the modeled wood log can be found in **Paper V**.

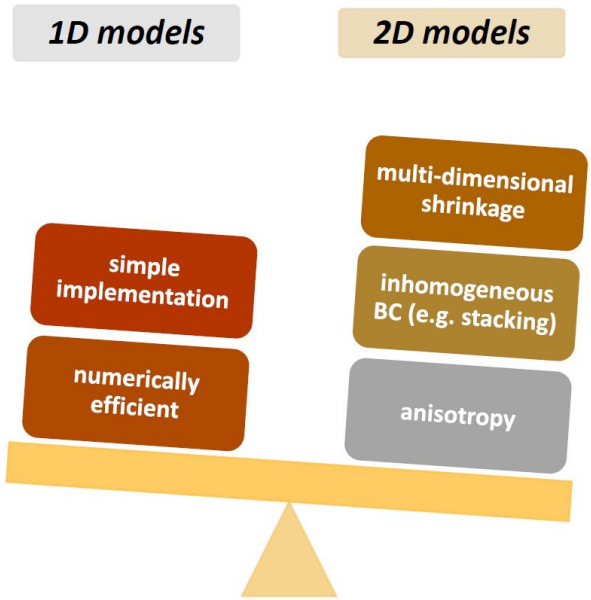

Figure 2.1: Comparison of 1D and 2D model advantages.

In Figure 2.1 the advantages of 1D and 2D models are presented. The main advantages of 1D models are simple implementation and numerical efficiency. 1D models can be effectively used to perform fundamental studies on thermochemical degradation and combustion within a comparably short time frame. Conversion times can be rather well predicted even with simplified 1D models. However, with 2D models a significantly larger amount of detail can be simulated. For example, wood anisotropy, which alters heat and mass transfer, can be accounted for. As a result, the distribution of temperature, mass fractions of different gasoues species and the position of the conversion zones can be well predicted. Also, the wood internal pressure peak can be well predicted. This information cannot be accurately obtained from 1D models. Since flow conditions within the anisotropic wood log are better mimicked by higher dimensional models, volatile release rates at different positions in the wood log, e.g. top and bottom in contrast to lateral shell, are expected to be predicted more realistically by multi-dimensional models. This provides a more accurate input to the gas phase model, which would as a consequence increase the accuracy of the wood stove simulation tool.

In contrast to 1D models, multi-dimensional models can account for inhomogeneous boundary conditions. If wood logs are stacked, a single wood log may be in contact with another log on one side, blocking volatile release and altering radiative heat transfer to this wood log side, while other sides are still well exposed to the furnace wall. Such conditions can only be implemented in mutli-dimensional models. Shrinkage can also only be considered within a multi-dimensional model. However, as mentioned in **Paper V**, even though 2D models are closer to the real combustion process in a stove, suitability cannot be generically assumed to be higher than the 1D models since the purpose of a model defines its required dimensionality.

Wood was considered as a mixture of its constituents in all of the papers presented in this thesis. Bark was not considered. The complexity of the wood chemistry was simplified by modeling the degradation of wood, instead of describing the degradation of hemicellulose, cellulose and lignin in detail. This means that only one governing equation had to be solved for wood, which saved computational time. Based on the assumption that wood reacted as a mixture of its components, the "three independent competitive reactions scheme" was applied to model devolatilization. Applied kinetics for this scheme are listed in **Paper II** through **V**. It is beyond any doubt that this reaction scheme is very much simplified, since it is known that wood conversion involves a significant number of reactions, forming a compelling number of intermediates as well as products. Finding an exact reaction mechanism and implementing such a detailed mechanism is therefore not the common modus operandi in single wood particle conversion modeling where also computational time is a main concern. There are more advanced models available (e.g. the detailed multi-step kinetics in [56]), but for this study, the increased computation cost was not justified. The model developed in this Ph.D. thesis also lumps together the devolatilization products. This is again mainly done to save computational time, since only a reduced number of gas species has to be tracked. For details on the considered gas species see e.g. **Paper III** and **Paper IV**.

One additional aspect of devolatilization that was considered was that the produced gaseous species have a longer residence time in the inner pore structure and must cross the hot char layer as they are leaving the particle, such that secondary tar reactions occur. The applied secondary tar kinetics are surely a simplification, especially the description of heterogeneous secondary char formation from tar, expressed as a homogeneous reaction (e.g. **Paper V**), but are chosen due to limited knowledge with respect to this conversion stage. Because the aim was to model very large wood logs, it was crucial to consider secondary tar reactions, due to the expected long residence time of tar in the wood pores and its passing through the hot char layer.

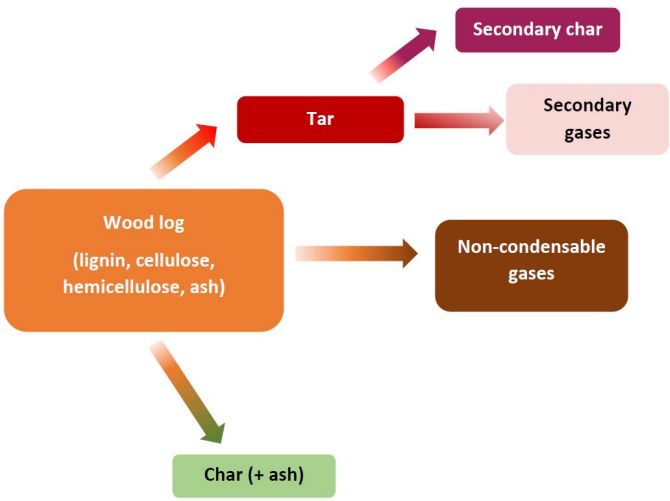

Figure 2.2: Three independent competitive reactions scheme describing the thermochemical degradation of wood to tar, non-condensable gases and char via three independent competing reactions.

However, even though wood is not described in detail, the model can describe how different wood species react, since heat and mass transfer, which are controlling the particle conversion, are linked to certain wood properties that are all entering the model as input data. The model can therefore describe different combustion behavior of different wood species even though it is not explicitely considering evolution of cellulose, hemicellulose and lignin. The difference between hardwoods and softwoods can be considered by altering properties accordingly.

2.1 IDA solver

The IDA solver (Implicit Differential Algebraic equations system solver) was used in this Ph.D. work. The IDA solver is part of the SUNDIALS [55] software package. The time integrator was chosen such that it could handle a system of differential and algebraic equations, even though equations may be stiff. The IDA solver uses the backward differentiation formula (BDF) [57]

$$\sum_{i=0}^{q} a_{n,i} y_{n,i} = h_n \dot{y}_n, \tag{2.1}$$

with h_n being the time step size, y_n being the computed approximate for $y(t_n)$, $\dot{y}_n$ being the computed approximate for $\dot{y}(t_n)$and $a_{n,i}$ being a coefficient. The coefficient depends on the order of the BDF as well as the step size history, with both being adapted based on the local error [57]. The time integrator implicitely solves the equations. The BDF order is limited from 1 to 5 [57]. The same time integrator was succcessfully used by Grønli [23] in a previous study on wood drying and devolatilization. Since no numerical instabilities were reported by Grønli [23] it was assumed the the time integrator can also be used to describe the drying, devolatilization and char conversion model developed as part of this Ph.D. work.

The solution of the linear system of equations was found by a Krylov-subspace-method. Since the wood log model results in a large DAE-system, it was expected that only iterative solvers were a feasible choice, and therefore, direct methods were not considered. In the IDA solver GMRES (generalized minimal residual method), Bi-CGStab (Bi-Conjugated Gradient stabilized method) or TFQMR (transpose-free quasi minimal residual method) can be chosen, though GMRES is generally recommended by the IDA-guide [57]. From the testing, it was found that GMRES was most robust and promising [57].

The GMRES method is a Krylov-subspace method that can be used to iteratively solve a system of equations. Krylov-subspace methods solve a system of the form [58]

$$[A]\mathbf{x} = \mathbf{b} \tag{2.2}$$

by repeatedly performing matrix-vector mutliplications involving [A]. GMRES is a modified form of the conjugated gradient method, with the latter requiring that the coefficient matrix is symmetric and positive definite. Thus, the conjugated gradient method is somewhat limited when it comes to the many equations that are relevant in CFD. GMRES was therefore a suitable choice, as it can be used for a more general system of equations and it does not have the same restrictions with respect

to the coefficient matrix [58].

The main concept of GMRES is that at every iteration, a vector is searched for that minimizes the residual, $\mathbf{r}$, [58]

$$\mathbf{b} - [A]\mathbf{x} = \mathbf{r}. \tag{2.3}$$

As it is the case for all iterative methods, convergence can be improved by preconditioning both sides of the equation using a preconditioning matrix. However, since suitable preconditioning must be tested, which in itself is a complex research field, it was beyond the scope of this thesis.

With respect to the current model development based on finite differencing, a series of errors can affect the quality of the modeling results [54]. The *truncation error (T.E.)* arises from the truncated representation of the exact partial differential equation (PDE) by the finite difference equation (FDE), such that [58]

$$T.E. = PDE - FDE. \tag{2.4}$$

The order of the *T.E.* is defined by the order of accuracy of the discretization scheme. Secondly, *round-off errors* need to be considered, because calculated data is only represented by a finite number of digits in the arithmetic operations. Most importantly though are the *discretization error* and the *iteration error*, since both can be easily avoided by simple adjustments to the IDA solver. The *discretization error* occurs when a continuous problem is replaced by a discrete representation. It can be reduced by refining the grid, i.e. by choosing small $\triangle r$, $\triangle z$ etc. [58], which highlights the important role of grid-independence studies when using the finite differencing. The *iteration error* can be easily reduced by lowering the tolerance of the IDA solver, which of course increases the number of required iterations and to some extent also the computational time.

Chapter 3

Summary of papers

3.1 Paper I: Numerical models for thermochemical degradation of thermally thick woody biomass, and their application in domestic wood heating appliances and grate furnaces.

In this paper a literature review on single particle modeling, as well as solid phase modeling in small-scale domestic wood heating appliances and large-scale grate furnaces was conducted. The state-of-the-art of numerical models used for thermochemical degradation and combustion of thermally thick woody biomass particles was discussed in detail. The theory of drying, devolatilization and char conversion with respect to the implementation of conversion stages in the numerical simulation tools was discussed. Common drying models and devolatilization reaction schemes were discussed in detail. Wood chemistry was also shortly described, in order to highlight the challenges for wood conversion modeling that arose from the complex composition of wood.

Furthermore, it was mentioned that there were physical differences between wood logs or wood chips, both being naturally anisotropic wood supplies, and wood pellets or briquettes, where both were obtained after densification, which altered their physical characteristica. Based on the related properties, which were altered by densification, the modeling input data and assumptions were said to vary significantly. The validity of the assumptions therefore was found to depend significantly on the input fuel. The different modeling approaches were categorized by the dimensionality of the model (1D, 2D or 3D), and the 1D models were separated into mesh-based and interface-based models. Additionally, the applicability of solid phase models for wood stoves was discussed, and an overview of the existing literature on numerical simulations of small-scale wood stoves and domestic boilers was given. The available literature for wood stove applications was very limited. Current bed modeling approaches in large-scale grate furnaces were presented and compared against single particle models.

Bed models in large-scale grate furnace modeling were found to be subject to significant simplifications compared to single particle models, since computational cost was a main concern of those simulation tools. Large-scale grate furnace modeling was not the main focus of the review paper, as it was also not related to the Ph.D. work, but this section in the review paper can still serve as an extended reading.

3.2 Paper II: Drying of thermally thick wood particles: A study of the numerical efficiency, accuracy and stability of common drying models.

The primary focus of this paper was on studying different numerical models for the drying of wet cylindrical wood particles. The advantages and disadvantages of the models, with respect to numerical efficiency, stability, and accuracy were investigated. The thermal drying model and the kinetic rate drying model were discussed in this paper as the most common drying models for combustion applications. The drying models were tested using a 1D cylindrical wood particle. The choice of drying model was found to have an influence on the computational time associated with the thermal conversion. The occurrence of numerical pressure oscillations in the thermal drying model was found and investigated. The numerical oscillations were reduced by introducing an evaporation fraction, which smeared out the very steep drying front, which was found to cause numerical instabilities, such as the observed oscillations. When the thermal drying model was applied, the drying zone was very thin, only including one grid point, which could result in numerical instabilities. The evaporation fraction allowed the smearing of the drying zone by reducing the heat flux used for evaporation and using the residual heat flux for heating the grid points. Reducing the evaporation fraction also resulted in reduced CPU times. It was found that model accuracy was not significantly influenced by the choice of drying model.

3.3 Paper III: Combustion of thermally thick wood particle: A study on the influence of wood particle size on the combustion behavior.

A 1D comprehensive combustion model for thermally thick wet wood particles was developed. Since the model was developed for thermally thick particles, where the intraparticle temperature gradient was considered in detail, this model was also applicable for large wood logs, e.g. those used in wood stoves. The model included drying, devolatilization, and char conversion, which was modeled by gasification and oxidation.

CO oxidation was modeled, since part of the combustible gases that were formed by devolatilization as well as char consumption, could consume oxygen via oxidation on the way out. Oxygen transfer through the ash layer and to the active sites was therefore even further restricted.

Model validation was completed against experimental data for the combustion of near-spherical wood particles, due to a lack of experimental data for thermochemical degradation and combustion of larger wood logs and particles. Measured and modeled mass loss trends were in good agreement, allowing for the conclusion that the model yielded acceptable accuracy. Model accuracy could still be improved, especially with respect to temperature predictions, if the solid phase model was coupled to a gas phase model, which allowed for the accurate prediction of the additional radiative heating of the solid by the flame.

The validated model was up-scaled and the effect of wood log diameter on the thermal conversion time, as well as the position of drying, devolatilization, and char conversion zones were studied. The up-scaling was done for cylindrical wood logs with an aspect ratio of four. The thermal conversion

time significantly increased with the size. It was also found that the relative extent of the drying, devolatilization, and char conversion zones decreased as wood log size increased. The paper concluded with recommendations for future work.

3.4 Paper IV: Simulating thermal wood particle conversion: Ash-layer modeling and parametric studies.

In this paper, the thermochemical degradation and combustion of wet wood particles were studied. The work was split in two main parts: 1) the effect of the ash layer handling approach and 2) a parametric study.

In the study of the ash layer handling, the effect of allowing the ash to remain on the surface of the particle when the char was converted (*Model A*) was contrasted with removing the ash such that the reacting char layer was always exposed (*Model B*). It was found that the two modeling concepts yielded significantly different mass losses as well as surface and center temperature predictions. *Model B* presented a faster thermal conversion while the results predicted by *Model A* were in better agreement with experimental results.

A parametric study was completed, where the sensitivity to variations in thermal conductivity, specific surface area and gas permeability were studied. Thermal conductivity influenced the time when drying and devolatilization were accomplished. This was because these conversion stages were heat-transfer controlled. Char conversion was only affected by a shift to earlier times for the initialization of the char conversion when higher thermal conductivities were used.

The specific surface area can significantly affect the final char conversion time. Since char conversion is a key stage of wood combustion, the full conversion time was also affected.

The gas permeability affected oxygen diffusion into the particle. It was found that up until a critical effective gas permeability, the modeling results were sensitive to assigned permeabilities.

3.5 Paper V: A two-dimensional study on the effect of anisotropy on the devolatilization of a large wood log.

In this work an existing 1D model for wood particle drying, devolatilization and char conversion was extended to a 2D model, applicable to a large cylindrical wood log. The tested wood log was a dry, birch wood cylinder. A grid-independence study was performed, in order to see how fine the 2D-mesh had to be to guarantee grid-independent solutions. It was found that under the given external heating conditions, the devolatilizing wood log with a radius of 25 mm and an aspect ratio of six required a mesh of 37×61 grid points. Furthermore, the wood log internal distributions of temperature, solid species densities, gas density and gas species mass fractions were studied. In addition, the wood internal 2D pressure field was analyzed and in combination with this study on the wood log internal pressure peak, the gas flow velocities in radial and longitudinal directions were studied. It was found that the internal pressure peak significantly depended on the permeabilities of char, even though devolatilization dynamics were hardly affected by the choice of permeabilities. Furthermore,

the relative contributions of radial and longitudinal gas flow to the total gas flow outward depended significantly on the permeabilities, which highlighted the importance of modeling anisotropy in detail.

In addition to this study on wood anisotropy, the authors compared the detailed anisotropy study results to 1D modeling results, where only radial properties were considered.

Chapter 4

Conclusions and recommendations for future work

This Ph.D. thesis discusses the development of a 1D (**Paper II**, **Paper III** and **Paper IV**) as well as a 2D model (**Paper V**) describing thermochemical wood degradation and char conversion either of a thermally thick wood particle or a large wood log. Char conversion is described by steam and CO_2 gasification reactions as well as char oxidation (as discussed in **Paper III**).

In the first development stage of the model, the modeling of drying and devolatilization was studied in detail. With respect to the drying stage it was found that re-condensation of water vapor does not have to be modeled, since it does not have a significant influence on the prediction of the overall degradation dynamics. When studying the thermal drying model in more detail it was found that the thermal drying model resulted in oscillatory numerical solutions. Those oscillations do not contain any physical information and need correction. In order to correct the oscillations an evaporation fraction was introduced, which caused smearing of the drying-front. As a result, the oscillations were reduced. Furthermore, it was found that combining the thermal drying model with the kinetic rate drying model, and using the drying model dependent on whether liquid free water or bound water evaporate, did not increase the accuracy of the modeling results. Numerical efficiency tests showed that a corrected thermal drying model with an evaporation fraction of 0.85 operated at lower computational cost than the uncorrected thermal drying model.

The 1D model has proven to be a good approach to fundamentally study the combustion behavior of wood particles. Nonetheless, obtained temperature data requires further validation, despite accurate mass loss prediction. Accurate surface temperature prediction, is not possible with a standalone solid phase combustion model, since dynamic coupling between gas phase and solid phase is required to accurately predict wood particle surface temperatures. The current solid phase model seems to capture the relevant chemical and physical phenomena very well, though suggesting that coupling it to a gas phase model is a promising advancement for future research.

As part of the study on wood particle combustion by means of the 1D model, it was found that with respect to model input data, such as wood properties, or even reaction kinetics, as well as

char reactivity, noteable uncertainties exist. Despite these potential sources of error, for the case studied here, the presented model has proven to capture physical and chemical phenomena related to combustion well enough.

During the study of wood particle combustion it was furthermore found that the consideration of an up-building ash layer or its negligence can significantly affect modeling results. However, it was concluded that no generic conclusion can be drawn on whether the consideration or negligence of the ash-layer yields better results. It was found that also idealized conditions, such as commonly found in lab-scale single particle reactors, allow the unhindered up-building of an ash-layer even though for real wood stoves the external physical phenomena might antagonize the up-build of an ash layer. It was therefore concluded that not only the fuel defines on whether or not ash needs to be conidered, but it is also the testing enviroment of the experiments that need to be replicated by the model.

Performing a parametric study by means of the wood combustion model led to the conclusions that the modeling results are sensitive to the thermal conductivity of wood and char. The reason is that drying and devolatilization are both heat-transfer controlled phenomena. In addition, the model is sensitive to the specific surface area if it is lower than a critical value. If the char surface area is large, such that diffusion controls char conversion, the assumed specific surface area is a less critical input data. A parametric study of the gas permeability led to the conclusion that total wood combustion depended significantly on permeabilities up until a critical value was reached.

Summing up, it was found that fundamental studies, performed by means of the 1D model, showed that drying and devolatilization are heat-transfer controlled phenomena, while char consumption is limited by oxygen diffusion into the particle, see **Paper III** and **Paper IV**.

The 2D model outlined the importance of a proper consideration of anisotropy, since the modeling results change depending on how direction-dependent wood properties are modeled, see **Paper V**. As a general rule, we found that higher dimensional simulations (>1) are required when

- the wood logs have non-uniform boundary conditions (like in e.g. wood stoves),
- the detailed distribution of any variable within the log is studied,
- the ratio between the longitudinal and the radial extent of the log is low,
- the log cannot be approximated as neither cylindrical nor spherical.

In fact it was concluded, that only a multi-dimensional solid phase model (i.e. wood log model) is suitable for a coupled solid- and gas-phase-model because only then realistic physics are mimicked and also with sufficient detail in order to guarantee that the profiles entering the gas phase model are accurate enough to allow accurate modeling of the gas phase combustion in the freeboard. A high accuracy with respect to gas phase modeling is required since it defines the predicted emissions as well as heat release rates, and therefore the heat release rate to the surrounding room. Knowledge of those aspects is a key element in wood stove design and optimization.

Furthermore, it is recommended, that even though shrinkage is already included in the current model, its consideration should be improved. The reason herefore arises mainly from the planned application

of the model, which is for large wood logs combusting in wood stoves. It has been found that degradation dynamics and product yield predictions are strongly controlled by structural changes, such as shrinkage, especially for lagre wood logs [50].

Furthermore, it is emphasized that a detailed consideration of cracking can improve the model accuracy. Since the model developed in this thesis predicted comparably high wood internal pressures, it may be a promising improvement of the model to account for pressure drop when cracking occurred. Hereby, it can be avoided that the model predicts unphysically high wood internal pressures. In its current version, the model does not control the physicality of the predicted pressure, since its prediction is purely controlled by the permeability. Especially during the ongoing conversion of wood to char and the decreasing structural integrity of the solid fuel, the consideration of cracking might become very important. Capturing such a sudden structural failure of a wood log does not only improve the validity of predicted wood internal pressures. It can as well predict how volatile release rates are altered by such a structural change, since cracks facilitate the volatiles to leave the wood particle or log.

Based on the literature review, (**Paper I**), it can be concluded that current wood log combustion models, used for wood stove modeling, are very much simplified, i.e. by developing empirical models instead of developing a multi-dimensional model based on conservation principles. The mutlidimensional model developed as part of this Ph.D. work (see **Paper V**) can be applied more flexibly for wood stove design and optimization purposes by wood stove manufacturers compared to empirical models. This is primarily due to the fact that empirical models require empirical data obtained under very specific operation conditions. Therefore, the input data is then restricted to exactly the same or at least very similar operation conditions and stove set-ups, while at the same time it can predict very wrong combustion trends for deviating conditions. This drawback is not present for mathematical models purely based on conversion principles catching physics well enough.

Future research is recommended to couple the current standalone 2D wood combustion model to the gas phase models of existing CFD softwares, e.g. ANSYS Fluent. At the same time the 1D model, developed as part of this thesis, can still be used for fundamental studies on degradation dynamics. Therefore, it is concluded that both 1D and 2D models can play a fundamental role in wood conversion modeling, since both numerical set-ups can be used to gain differently detailed information at different computational cost. The user though, has to know the degree of detail he expects from the model and also balance it against the required computational cost.

It is also recommended that future research intensifies the experimental focus on large wood log combustion, since experimental data is scarce. As a consequence, validation of large wood log combustion modeling can only be done very limitedly. In order to assure a well-working simulation tool, validation is a key stage of model development. It is beyond any doubt that the combined modeling and experimental validation route is a very promising route toward the develoment of more efficient and emission-reduced domestic wood-stove combustion technologies.

Bibliography

[1] A. K. Biswas and K. Umeki, "Simplification of devolatilization models for thermally-thick particles: Differences between wood logs and pellets," *Chemical Engineering Journal*, vol. 274, pp. 181 – 191, 2015.

[2] M. Ek, G. Gellerstedt, and G. Henriksson, *Pulp and paper chemistry and technology: Volume 1: Wood chemistry and wood biotechnology*, M. Ek, G. Gellerstedt, and G. Henriksson, Eds. Berlin: De Gruyter, 2009.

[3] H. Fatehi, "Numerical simulation of combustion and gasification of biomass particles," Ph.D. thesis, Lund University, Lund, Sweden, 2014.

[4] T. Li, "Gasification of biomass for second generation biofuel production," PhD thesis, Norwegian University of Science and Technology, Trondheim, Norway, 2015.

[5] S. Van Loo and J. Koppejan, *The handbook of biomass combustion and Co-firing*, 1st ed. London: Earthscan, 2008.

[6] V. Burg, G. Bowman, M. Erni, R. Lemm, and O. Thees, "Analyzing the potential of domestic biomass resources for the energy transition in Switzerland," *Biomass and Bioenergy*, vol. 111, pp. 60 – 69, 2018.

[7] R. Nyström, R. Lindgren, R. Avagyan, R. Westerholm, S. Lundstedt, and C. Boman, "Influence of wood species and burning conditions on particle emission characteristics in a residential wood stove," *Energy & Fuels*, vol. 31, no. 5, pp. 5514–5524, 2017.

[8] Jøtul AS, "Jøtul F 520," 2016, [Online]. Available: https://jotul.com/uk/products/wood-stoves/jotul-f-520. [Accessed: 2018 - April].

[9] M. Seljeskog, A. Sevault, A. Østnor, and Ø. Skreiberg, "Variables affecting emission measurements from domestic wood combustion," *Energy Procedia*, vol. 105, pp. 596 – 603, 2017.

[10] M. Bugge, Ø. Skreiberg, N. E. L. Haugen, P. Carlsson, and M. Seljeskog, "Predicting NOx emissions from wood stoves using detailed chemistry and computational fluid dynamics," *Energy Procedia*, vol. 75, pp. 1740 – 1745, 2015.

[11] Ø. Skreiberg, M. Seljeskog, and L. Georges, "The process of batch combustion of logs in wood stoves - transient modelling for generation of input to CFD modelling of stoves and thermal comfort simulations," *Chemical Engineering Transactions*, vol. 43, pp. 433– 438, 2015.

[12] Ø. Skreiberg, "Theoretical and experimental studies on emissions from wood combustion," Ph.D. thesis, Norwegian University of Science and Technology, Trondheim, Norway, 1997.

[13] M. Kaltschmitt, H. Hartmann, and H. Hofbauer, *Energie aus Biomasse - Grundlagen, Techniken und Verfahren*. Berlin Heidelberg: Springer Science & Business Media, 2009.

[14] R. C. Pettersen, "The chemical composition of wood," in *The Chemistry of Solid Wood*, R. M. Rowell, Ed. Washington, DC: American Chemical Society, 1984, pp. 57–126.

[15] T. Heinze, "Cellulose: Structure and properties," in *Cellulose Chemistry and Properties: Fibers, Nanocelluloses and Advanced Materials*, O. J. Rojas, Ed. Cham: Springer International Publishing, 2016, pp. 1–52.

[16] H. Ström and H. Thunman, "CFD simulations of biofuel bed conversion: A submodel for the drying and devolatilization of thermally thick wood particles," *Combustion and Flame*, vol. 160, no. 2, pp. 417 – 431, 2013.

[17] I. Haberle, Ø. Skreiberg, J. Łazar, and N. E. L. Haugen, "Numerical models for thermochemical degradation of thermally thick woody biomass, and their application in domestic wood heating appliances and grate furnaces," *Progress in Energy and Combustion Science*, vol. 63, pp. 204 – 252, 2017.

[18] K. M. Bryden and M. J. Hagge, "Modeling the combined impact of moisture and char shrinkage on the pyrolysis of a biomass particle," *Fuel*, vol. 82, no. 13, pp. 1633 – 1644, 2003.

[19] Y. B. Yang, V. N. Sharifi, J. Swithenbank, L. Ma, L. I. Darvell, J. M. Jones, M. Pourkashanian, and A. Williams, "Combustion of a single particle of biomass," *Energy & Fuels*, vol. 22, no. 1, pp. 306–316, 2008.

[20] L. Nikolaisen and P. Jensen, "Biomass feedstocks: categorisation and preparation for combustion and gasification," in *Biomass Combustion Science, Technology and Engineering*, 1st ed., L. Rosendahl, Ed. Cambridge, United Kingdom: Woodhead Publishing, 2013, pp. 36 – 57.

[21] S. Caillat and E. Vakkilainen, "Large-scale biomass combustion plants: an overview," in *Biomass Combustion Science, Technology and Engineering*, 1st ed., L. Rosendahl, Ed. Cambridge, United Kingdom: Woodhead Publishing, 2013, pp. 189 – 224.

[22] Ø. Skreiberg, "Performance history and further improvement potential for wood stoves," *Chemical Engineering Transactions*, vol. 65, pp. 199–204, 2018.

[23] M. G. Grønli, "A theoretical and experimental study of the thermal degradation of biomass," PhD thesis, Norwegian University of Science and Technology, Trondheim, Norway, 1996.

[24] C. Di Blasi, "Modeling and simulation of combustion processes of charring and non-charring solid fuels," *Progress in Energy and Combustion Science*, vol. 19, no. 1, pp. 71 – 104, 1993.

[25] K. Weber, "Production and properties of biochar," PhD thesis, Norwegian University of Science and Technology, Trondheim, Norway, 2018.

[26] R. W. Bilger, "The role of combustion technology in the 21st century," in *Turbulent Combustion Modeling*, ser. Fluid Mechanics and Its Applications, vol. 95, T. Echekki and E. Mastorakos, Eds. Dordrecht, Netherlands: Springer, 2011, pp. 3 – 18.

[27] R. Mehrabian, S. Zahirovic, R. Scharler, I. Obernberger, S. Kleditzsch, S. Wirtz, V. Scherer, H. Lu, and L. L. Baxter, "A CFD model for thermal conversion of thermally thick biomass particles," *Fuel Processing Technology*, vol. 95, pp. 96 – 108, 2012.

[28] C. Yin, L. A. Rosendahl, and S. K. Kær, "Grate-firing of biomass for heat and power production," *Progress in Energy and Combustion Science*, vol. 34, no. 6, pp. 725 – 754, 2008.

[29] B. G. Miller and S. F. Miller, "Fluidized-Bed firing systems," in *Combustion Engineering Issues for Solid Fuel Systems*, 1st ed., B. G. Miller and D. A. Tillman, Eds. Burlington: Academic Press, 2008, pp. 275 – 340.

[30] A. Calvo, L. Tarelho, C. Alves, M. Duarte, and T. Nunes, "Characterization of operating conditions of two residential wood combustion appliances," *Fuel Processing Technology*, vol. 126, pp. 222 – 232, 2014.

[31] J. Krüger, "Numerical investigation of the effect of flow turbulence on heterogeneous reaction rates," Ph.D. thesis, Norwegian University of Science and Technology, Trondheim, 2017.

[32] M. Santucci, J. Scavuzzo, and J. Hoffman, "Some computer applications for combustion engineering with solid fuels," in *Combustion Engineering Issues for Solid Fuel Systems*, 1st ed., B. G. Miller and D. A. Tillman, Eds. Burlington: Academic Press, 2008, pp. 393 – 421.

[33] M. Farokhi, M. Birouk, and F. Tabet, "A computational study of a small-scale biomass burner: The influence of chemistry, turbulence and combustion sub-models," *Energy Conversion and Management*, vol. 143, pp. 203 – 217, 2017.

[34] H. Lamberg, O. Sippula, J. Tissari, A. Virén, T. Kaivosoja, A. Aarinen, V. Salminen, and J. Jokiniemi, "Operation and emissions of a hybrid stove fueled by pellets and log wood," *Energy & Fuels*, vol. 31, no. 2, pp. 1961–1968, 2017.

[35] J. Zhang, K. Smith, Y. Ma, S. Ye, F. Jiang, W. Qi, P. Liu, M. Khalil, R. Rasmussen, and S. Thorneloe, "Greenhouse gases and other airborne pollutants from household stoves in China: a database for emission factors," *Atmospheric Environment*, vol. 34, no. 26, pp. 4537 – 4549, 2000.

[36] RIKA Innovative Ofentechnik GmbH, "Ricatronic3 - Öfen mit eingebauter Intelligenz," 2015, [Online]. Available: http://www.rika.at/de/rikatronic/. [Accessed: 2018-07-24].

[37] L. S. Johansson, B. Leckner, L. Gustavsson, D. Cooper, C. Tullin, and A. Potter, "Emission characteristics of modern and old-type residential boilers fired with wood logs and wood pellets," *Atmospheric Environment*, vol. 38, no. 25, pp. 4183 – 4195, 2004.

[38] J. Tissari, K. Hytönen, J. Lyyränen, and J. Jokiniemi, "A novel field measurement method for determining fine particle and gas emissions from residential wood combustion," *Atmospheric Environment*, vol. 41, no. 37, pp. 8330 – 8344, 2007.

[39] J. Muhlbaier Dasch , "Particulate and gaseous emissions from wood-burning fireplaces," *Environmental Science & Technology*, vol. 16, no. 10, pp. 639–645, 1982.

[40] A. Kocbach Bølling, J. Pagels, K. E. Yttri, L. Barregard, G. Sallsten, P. E. Schwarze, and C. Boman, "Health effects of residential wood smoke particles: the importance of combustion conditions and physicochemical particle properties," *Particle and Fibre Toxicology*, vol. 6, no. 1, p. 29, 2009.

[41] E. Vicente, M. Duarte, A. Calvo, T. Nunes, L. Tarelho, D. Custódio, C. Colombi, V. Gianelle, A. Sanchez de la Campa, and C. Alves, "Influence of operating conditions on chemical composition of particulate matter emissions from residential combustion," *Atmospheric Research*, vol. 166, pp. 92 – 100, 2015.

[42] J. Slama Lighty , J. M. Veranth, and A. F. Sarofim, "Combustion aerosols: Factors governing their size and composition and implications to human health," *Journal of the Air & Waste Management Association*, vol. 50, no. 9, pp. 1565–1618, 2000.

[43] U. Pöschl, "Atmospheric aerosols: Composition, transformation, climate and health effects," *Angewandte Chemie International Edition*, vol. 44, no. 46, pp. 7520–7540, 2005.

[44] M. Kampa and E. Castanas, "Human health effects of air pollution," *Environmental Pollution*, vol. 151, no. 2, pp. 362 – 367.

[45] G. L. Borman and K. W. Ragland, *Combustion Engineering*, 1st ed. Boston, USA: WCB McGraw-Hill, 1998.

[46] E. M. Fitzpatrick, J. M. Jones, M. Pourkashanian, A. B. Ross, A. Williams, and K. D. Bartle, "Mechanistic aspects of soot formation from the combustion of pine wood," *Energy & Fuels*, vol. 22, no. 6, pp. 3771–3778, 2008.

[47] R. Scharler, C. Benesch, A. Neubeck, and I. Obernberger, "CFD based design and optimisation of wood log fired stoves," in *Proceedings of 17th European Biomass Conference and Exhibition*, Hamburg, Germany, 2009, pp. 1361–1367.

[48] L. S. Bäfver, B. Leckner, C. Tullin, and M. Berntsen, "Particle emissions from pellets stoves and modern and old-type wood stoves," *Biomass and Bioenergy*, vol. 35, no. 8, pp. 3648 – 3655, 2011.

[49] H. Lamberg, K. Nuutinen, J. Tissari, J. Ruusunen, P. Yli-Pirilä, O. Sippula, M. Tapanainen, P. Jalava, U. Makkonen, K. Teinilä, K. Saarnio, R. Hillamo, M.-R. Hirvonen, and J. Jokiniemi, "Physicochemical characterization of fine particles from small-scale wood combustion," *Atmospheric Environment*, vol. 45, no. 40, pp. 7635 – 7643, 2011.

[50] B. Moghtaderi, "The state-of-the-art in pyrolysis modelling of lignocellulosic solid fuels," *Fire and Materials*, vol. 30, no. 1, pp. 1–34, 2006.

[51] C. Di Blasi, "Kinetic and heat transfer control in the slow and flash pyrolysis of solids," *Industrial & Engineering Chemistry Research*, vol. 35, no. 1, pp. 37–46, 1996.

[52] S. V. Patankar, *Numerical heat transfer and fluid flow*, 1st ed. Washington: Hemisphere Publ., 1980.

[53] K. M. Bryden, "Computational modeling of wood combustion," PhD thesis, University of Wisconsin - Madison, Madison, WI, 1998.

[54] R. Scharler, "Entwicklung und Optimierung von Biomasse-Rostfeuerungen durch CFD-Analyse," Ph.D. thesis, Graz Univeristy of Technology, Graz, Austria, 2001.

[55] National Laboratory Lawrence Livermore, "SUNDIALS: SUite of Nonlinear and DIfferential/ALgebraic Equation Solvers - IDA," 2016, [Online]. Available: http://computation.llnl.gov/projects/sundials/ida. [Accessed: 2017-04-07].

[56] E. Ranzi, A. Cuoci, T. Faravelli, A. Frassoldati, G. Migliavacca, S. Pierucci, and S. Sommariva, "Chemical kinetics of biomass pyrolysis," *Energy & Fuels*, vol. 22, no. 6, pp. 4292–4300, 2008.

[57] A. Hindmarsh, R. Serban, and A. Collier, "User documentation for IDA v2.9.0 (SUNDIALS v2.7.0)," September 26, 2016.

[58] D. Anderson, J. Tannehill, and R. Pletcher, *Computational Fluid Mechanics and Heat Transfer*, 3rd ed., ser. in Computational and Physical Processes in Mechanics and Thermal Sciences. Boca Raton, FL: CRC Press, Taylor & Francis Group, 2016.

Selected papers

Paper I

Inge Haberle, Øyvind Skreiberg, Joanna Łazar, Nils Erland L. Haugen, Numerical models for thermochemical degradation of thermally thick woody biomass, and their application in domestic wood heating appliances and grate furnaces, Progress in Energy and Combustion Science, 63,2017,204-252.

Progress in Energy and Combustion Science 63 (2017) 204–252

Contents lists available at ScienceDirect

Progress in Energy and Combustion Science

journal homepage: www.elsevier.com/locate/pecs

Numerical models for thermochemical degradation of thermally thick woody biomass, and their application in domestic wood heating appliances and grate furnaces

Inge Haberle[a,*], Øyvind Skreiberg[b], Joanna Łazar[a,b], Nils Erland L. Haugen[a,b]

[a] Department of Energy and Process Engineering, Norwegian University of Science and Technology, NTNU, Kolbjørn Hejes vei 1 B, 7491 Trondheim, Norway
[b] Department of Thermal Energy, SINTEF Energy Research, Postboks 4761 Torgard, 7465 Trondheim, Norway

ARTICLE INFO

Article History:
Received 10 November 2016
Accepted 19 July 2017
Available online 12 September 2017

Keywords:
Thermochemical conversion
Wood
Numerical modeling
Single particle
Stove
Boiler
Grate furnace

ABSTRACT

This paper reviews the current state-of-the-art of numerical models used for thermochemical degradation and combustion of thermally thick woody biomass particles. The focus is on the theory of drying, devolatilization and char conversion with respect to their implementation in numerical simulation tools. An introduction to wood chemistry, as well as the physical characteristics of wood, is also given in order to facilitate the discussion of simplifying assumptions in current models. Current research on single, densified or non-compressed, wood particle modeling is presented, and modeling approaches are compared. The different modeling approaches are categorized by the dimensionality of the model (1D, 2D or 3D), and the one-dimensional models are separated into mesh-based and interface-based models. Additionally, the applicability of the models for wood stoves is discussed, and an overview of the existing literature on numerical simulations of small-scale wood stoves and domestic boilers is given. Furthermore, current bed modeling approaches in large-scale grate furnaces are presented and compared against single particle models.

Contents

* Corresponding author.
E-mail address: inge.haberle@ntnu.no (I. Haberle), oyvind.skreiberg@sintef.no (Ø. Skreiberg), nils.e.haugen@sintef.no (N.E.L. Haugen).

http://dx.doi.org/10.1016/j.pecs.2017.07.004
0360-1285/

1. Introduction

Currently, intense research is concentrated on the thermal conversion of biomass, which is due to the more attractive character of biomass compared to traditional fossil fuels for technologies based on thermal conversion, such as combustion [1]. The superiority of biomass-based technologies compared to fossil fuel technologies is related to the environmentally friendly character of botanic biomass, also including lignocellulosic biomass. A plant can only release the carbon dioxide (while burning) that it has stored during growth. The net CO_2 emission is therefore zero, making biomass carbon-neutral [2]. Hence, more research within the field of thermal conversion of biomass can contribute significantly to a sustainable energy mix.

Biomass combustion is one of the main routes of biomass conversion [3]. Different combustion technologies require differently sized lignocellulosic biomass particles [4]. Wood pellets, logs and chips are usually used, and are considered to be thermally thick particles [5]. When modeling thermally thick wood particles, heat and mass transport have to be considered. Overall, there is a large difference between thermally thin and thermally thick particles, which is classified by the Biot (Bi) number. The Biot number is defined as [6]

$$\mathrm{Bi} = \frac{h_{\mathrm{eff}} d}{\lambda}, \quad (1)$$

where the thermal conductivity (λ), characteristic length (d) and effective heat transfer coefficient (h_{eff}) are used. The Biot number defines the ratio between heat transfer resistance in the interior of the particle and at the surface of the particle [7]. For low Biot numbers (< 0.1), a thermally thin regime is present, whereas large Biot numbers (> 0.1) indicate the presence of a thermally thick regime [8]. In thermally thick particles, intra-particle gradients of temperature are important [9]. Due to varying temperatures, different conversion stages occur simultaneously within the wood log or particle, and intra-particle transport phenomena also have to be considered. In contrast, thermally thin particles have a uniform temperature distribution. This results in sequential conversion stages [10]. Independent of the applied combustion technology, the conversion steps that occur during combustion are drying, devolatilization and char burnout.

In addition to the fundamental research on thermal conversion of biomass particles, the application of the corresponding models to wood-fired boilers and stoves has recently been intensively studied. The main aim of current research is to improve the combustion process with the aid of modeling tools to help yield an improved design and operation of boilers or stoves. Improvement is required since emissions of carbon monoxide, particulates, organic pollutants such as polycyclic aromatic hydrocarbons (PAH), soot and nitrogen oxides of current small-scale units may be very high [11]. Furthermore, the use of bioenergy will increase in the future, thereby highlighting the importance of optimized stove and boiler designs [12]. In Norway today, domestic heating applications such as wood stoves account for almost 50% of bioenergy use, and the use of wood logs in small-scale units, as well as the utilization of pellets in pellet stoves and boilers, is predicted to increase even further. The Norwegian objective is to increase the rate of energy conversion in wood and pellet stoves by a factor of 2 from 2008 until 2020 [13]. The need for optimization of wood log fired stoves is due to decreasing emission limits and changing market demands [14]. Modern simulation techniques, such as computational fluid dynamics (CFD), are an efficient way to reach these objectives [14]. CFD for the optimization of combustion systems is considered an alternative way of improvement (compared to experiments) that is usually less expensive [15]. Even though numerical simulations are a more time-saving and less expensive optimization route, experiments are needed for the validation of models applied [12].

In order to apply commercial CFD tools, numerical sub-models have to be developed [15]. The sub-models aim to fully describe the thermal conversion of the solid fuel, and eventually link these results

to gas phase modeling, which is commonly performed with commercial CFD tools. It is of importance to develop numerical models for drying, devolatilization and char burnout of wood particles that optimize the balance between the degree of accuracy and the required computational time [10]. Both aspects need to be considered when the purpose is to apply the model as an engineering tool for the optimization of wood heating appliances.

Currently, most of the research within the field of CFD-aided design and optimization of biomass combustion units is restricted to large-scale biomass fixed bed and grate furnace applications. Only a few works have been done on CFD models for wood log combustion in domestic heating appliances [14]. In this work, the domestic scale is limited to 30 kW, which is more accurately rather micro-scale than small-scale, but is referred to as small-scale in this review. This review focuses in part on such domestic applications, but further also discusses current single particle models. The third part of the paper focuses on large-scale grate furnaces and the corresponding bed models. With respect to large-scale grate furnaces, it is outlined how currently applied bed models are simplified when compared to detailed single-particle models. While large-scale grate furnaces have a moving bed and the fuel is transported through the furnace while undergoing different stages of conversion, the previously discussed domestic heating applications have a fixed bed, e.g. wood stoves.

The current state-of-the-art for large-scale grate furnace design and optimization is that also within this field furnace design is primarily based on experience or empirical data. However, experiments are difficult and expensive, which highlights the necessity for a CFD analysis [16]. CFD also gains increasing importance within this field, due to the constant improvement of computer performance [17]. Despite this increasing importance, simplifications are still needed in order to make large-scale grate furnace modeling affordable [16].

The purpose of this review is to convey theoretical knowledge of physical and chemical phenomena related to the thermal conversion of woody biomass. The focus is on drying, devolatilization and char conversion of thermally thick wood particles (incl. logs). The aim is to discuss current modeling approaches for single particles in detail, and to identify their strengths and weaknesses.

A number of reviews on thermochemical degradation of wood and related physical processes is already available. The current review does not only cover chemical and physical processes modeling for single particle applications but also discusses models for the solid phase that can be applied in small-scale heating appliances as well as large-scale furnaces. Anca-Couce [18] presented an extensive review on pyrolysis of wood and related chemical and also partly physical processes. The full thermal conversion of particles though has not been reviewed. Furthermore, no direct linkage between the single particle models and how solid phase is modeled in small-scale heating appliances has been discussed. A detailed review on pyrolysis of biomass was also presented by Neves et al. [19]. The focus was on factors influencing secondary pyrolysis of gases and the product distribution and composition. Furthermore an empirical model for the volatile composition was presented. Di Blasi [20] reviewed literature on modeling of chemical and physical processes of wood during pyrolysis. Primary devolatilization kinetics were discussed in detail, as well as secondary reaction modeling approaches. They also reviewed pyrolysis reactor models, even though they found that only very limited work had been done in that field. Fixed-bed reactors and fast-pyrolysis reactors were included in their review. However, no review on stove models was performed and we also found that a significant amount of work has been done since Di Blasi's review [20] in 2008.

The purpose of the small-scale furnace modeling section is to review the current state-of-the-art, and to identify which modeling aspects need more attention. The purpose of the large-scale grate furnace section is to outline how current bed models for grate furnaces deviate from single particle models. Such deviation is due to the complexity of large-scale grate furnaces, which requires simplifying assumptions in order to operate at a reasonable computational cost.

2. Chemistry of woody biomass

Wood is classified as lignocellulosic biomass, and can be split into hardwood and softwood [21]. Table 1 outlines the composition of typical Scandinavian wood species.

In Table 1, fractions of lignin, cellulose and hemicellulose are presented for some woody biomasses. Lignocellulose describes three-dimensional composites of polymeric substructures, and is primarily composed of lignin, a phenolic polymer, as well as carbohydrate macromolecules, namely cellulose and hemicellulose. Besides these main compounds, small percentages of proteins, acids, salts and minerals are also identified in lignocellulosic feedstock [24].

Lignin is the natural binding material in the cell walls of lignocellulosic plants [22]. It is amorphous, and its units are randomly linked [18]. Lignin is a co-polymer, including three types of phenylpropane monomeric units, which are p-coumaryl, coniferyl and sinapyl alcohols [25]. Lignin varies with respect to its O, C and H composition, and can therefore be either hydrogen-rich, carbon-rich or oxygen-rich [26]. As it is later outlined, such a detailed classification of lignin is only used by Ranzi et al. [27] for developing a detailed devolatilization reaction model. However, a detailed description of the reacting fuel is required if the purpose of the model is to accurately predict volatile species and their release rates.

Cell walls mainly contain cellulose [22]. The cellulose content in wood can vary depending on the age of the plant, as well as the plant type. Cellulose is built up by linear chains of 1,4-β-bonded anhydroglucose units. These units contain OH-groups, which form hydrogen bonds inside the macromolecule. Not only do these bonds connect within one macromolecule, but they also link different macromolecules [28]. Cellulose molecules are characterized by their linearity, which is one of the primary differences compared to hemicellulose and lignin. The degree of polymerization, describing the number of sub-units forming the entire polymer of cellulose (>10000), is much higher than for hemicellulose (20–500) [22].

Hemicellulose is the third main component forming cell walls. It is less linear than cellulose, and has a more branch-like character [22]. In hardwoods, the main hemicellulose macromolecule is methylglucuronxylan [29]. This differs from hemicellulose macromolecules found in softwood, which are mainly built up by galactoglucomannan and arabinomethylglucuronoxylan [29]. Therefore, reaction schemes in case of thermal degradation for

Table 1
Chemical composition of typical Scandinavian hardwoods and softwoods.

Wood type	Lignin	Cellulose	Hemicellulose	Extractives	Ref.
Hardwoods:					
Silver birch	22%	41%	30%	3.2%	[22]
American beech	22%	48%	28%	2%	[22]
Softwoods:					
Scandinavian spruce	29%	43%	27%	1.8%	[22]
Scandinavian pine	29%	44%	26%	5.3%	[22]
Douglas fir	29%	39%	23%	5.3%	[22]
Scots pine	28%	40%	25%	3.5%	[22]
Hardwood	20–22%	40–42%	30–35%	2–3%	[23]
Softwood	27–28%	40–43%	21–23%	3–5%	[23]

these two types of hemicellulose also differ. Modeling hemicellulose in hardwood is often done by modeling the chemical characteristics of xylan [26].

One can clearly see that wood is a mixture of many components, and an accurate description of its devolatilization accordingly includes numerous reactions. Such a broad range of reactions increases both the complexity of the model and the computational cost, since reactions will be of different stiffnesses, which require finer temporal resolution. Simplifying assumptions are therefore needed, which can be either modeling wood as a mixture of all components, or modeling cellulose, hemicellulose and lignin separately. Both modeling approaches have their strengths and weaknesses, which are discussed in a later chapter.

3. Physical characteristics of woody biomass

Woody biomass particles vary significantly in their physical characteristics. Table 2 illustrates the major differences between wood logs and densified wood particles, which can both be categorized as thermally thick woody particles.

Pellets are compressed biomass particles made from pulverized biomass, either with or without additives (binder). The shape is most commonly cylindrical and the particles have a length of 5–40 mm [31].

The allowed diameter for wood logs is rather narrow for birch wood with a nice appearance (8–15 cm), as suggested by the Norwegian quality standard for firewood [32]. For other wood species, including birch, oak, ash and maple (hardwoods), the minimum diameter is 4 cm, while the maximum diameter is 18 cm. This diameter range is applicable to almost all wood species, whereas the corresponding standard lengths of the wood logs vary between 20, 30 and 60 cm.

Pellets and briquettes have a lower water content than wood logs. More specifically, both wood pellets and briquettes typically have an average water content of approximately 8wt% on wet basis, even though bark briquettes can also have a higher water content (18wt% on wet basis). This variation in water content has an effect on net calorific value, combustion efficiency and temperature of combustion [30]. In contrast to densified wood, freshly harvested wood has a higher water content. However, small-scale units can only operate sufficiently well if the moisture content does not exceed a critical value, and wood logs should be used with a water content that is not higher than 12–20wt% wet basis [23].

A primary difference between wood pellets and wood logs is the density, which for wood pellets is commonly assumed to be about twice as high (1100 kg/m^3) as the density of wood logs (500 kg/m^3) [1]. It has to be added though that especially the wood species significantly affects the density of undensified wood. In addition to the variation in densities, wood pellets are also often considered isotropic, while wood logs are considered anisotropic [1]. Wood is formed by elongated cells, whose walls are formed by micro-fibrils aligned along the longitudinal axis of the cell [22]. These fundamentals of the wood structure explain the naturally anisotropic properties of wood. Therefore, e.g. the thermal conductivity of wood is smaller in the radial and the tangential direction to the grains compared to the longitudinal direction [33]. Due to the analogies between heat and mass transfer, similar behavior is expected for permeabilities. The anisotropy of wood also affects shrinkage during drying and devolatilization. The highest degree of shrinkage occurs tangentially to the grains, which means in the direction of annual growth rings. Radial shrinkage is only half of tangential shrinkage but is still more significant than longitudinal shrinkage [33].

These physical differences between undensified and densified wood particles highlights that simplifying assumptions, required for modeling, have to be applied with caution as they might be suitable for describing pellets and briquettes, e.g. isotropy, but can lead to false predictions, when applied to undensified particles.

4. Particle degradation modeling

New modeling approaches for drying, devolatilization and char conversion of single wood particles and logs are continuously being developed. There is a vast variety of such models, and there may be large differences between them. The differences are primarily due to the simplifying assumptions that have been made. The purpose of the subsequent comparison is to outline the differences between current models, and to identify their strengths and weaknesses. The comparison of models in Table 3 is for thermally thick particles only.

Table 3 shows that a number of models only include certain stages of thermal conversion (e.g. only drying and devolatilization, while neglecting char conversion), instead of modeling the entire thermal conversion process. This can lead to inaccuracies if the purpose of the model is to predict overall conversion times and product yields, rather than only developing a model for the fundamental research on a certain conversion stage, since the conversion stages have an influence on each another.

The heating rate affecting the wood particle during thermal conversion has a signficant influence on the devolatilization product yields. At lower heating rates, more char is produced, while at higher heating rates depolymerization of the wood compounds to permanent gases and tar is enhanced [65]. This fundamental understanding of product yields was used by Pozzobon et al. [62] to outline how evaporation can influence char conversion. Pozzobon et al. [62] found that the char yield is largest at intermediate moisture contents. This is related to the fact that at very low moisture contents (about 1wt%), drying does not slow down the overall heating up significantly, such that char formation is not significantly enhanced, while it is enhanced at an intermediate moisture content (9wt%). At a moisture content of 50wt%, it was found that char yield decreases again. This is because water vapor is formed, which leaves via the porous structure of wood and char, and hereby heterogeneously reacts with char, such that the char yield decreases [62]. Nothing comparable has been found in earlier works, which again highlights that an accurate thermal conversion model of a thermally thick particle has to account for all three main conversion stages simultaneously, as they significantly influence one another.

With respect to Table 3, it has to be mentioned that some of the models have been applied to packed-bed modeling. However, they were added to the table if their single particle models were separately validated. It is therefore assumed that these single particle

Table 2
Different physical properties of commercially available woody biomass.

Wood	Diameter [cm]	Length [cm]	Anisotropy/Isotropy	Density [kg/m^3]	Ref.
Densified wood:					
Wood pellets:	0.59–1.02	0.5–4.0	Isotropic	1180	[1,30,31]
Wood briquettes:	5.2–9.3	7.4–31.3	Isotropic	1060	[30]
Wood log	8–15	20–60	Anisotropic	430–650 [a]	[22,32]

[a] Density given on oven-dry basis.

Table 3
Comparison of current single particle models. [a] refers to the one-step global mechanism, [b] refers to the three independent parallel reactions, [c] refers to the three independent competitive reactions and [d] refers to the every other devolatilization model. If a column in the table is marked with "–" this indicates that it was explicitly mentioned in the paper that this aspect was not considered. In case of column "Log/Particle" , "–" indicates that neither of them is modeled, but instead only densified particles are modeled. If a field is marked with ✓ it means that it has been considered. "K" in the drying column refers to kinetic rate model, "T" refers to thermal drying model and "E" refers to equilibrium model. "NA" stands for "not announced".

Author (year)	Dimension	Wood species/ type	Log (=1) / Particle (=2)	Densified wood	Isotropic (=1) \Anisotropic (=2)	Volumetric shrinkage	Drying	Devolatilization: one[a]	Devolatilization: 3 i.p.[b]	Devolatilization: 3 i.c.[c]	Devolatilization: others[d]	Secondary reactions	Char oxidation	Char gasification	Interface (=I) / Mesh based (=M)
Alves and Figueiredo (1989) [34]	1D	Pine	2	–	1	–	K/E	–	–	–	✓	–	–	–	M
Koufopanos et al. (1991) [35]	1D	NA	2	–	1	–	–	–	–	–	✓	–	–	–	M
Di Blasi (1994) [36]	2D	Cellulose	2	–	2	–	–	–	–	–	✓	–	–	–	M
Di Blasi (1996) [37]	1D	Maple	2	–	1	✓	–	–	–	✓	–	✓	–	–	M
Melaaen (1996) [38]	1D	NA	2	–	1	–	E	–	–	–	✓	✓	–	–	M
Di Blasi (1998) [39]	2D	Cellulose	2	–	2	–	–	–	–	–	✓	–	–	–	M
Grønli and Melaaen (2000) [40]	1D	Spruce	2	–	1	–	–	–	–	✓	–	✓	–	–	M
Larfeldt et al. (2000) [41]	1D	Birch	1	–	1	✓	–	✓	–	✓	✓	–	–	–	M
Bryden et al. (2002) [42]	1D	Basswood/ Poplar/ Red oak/ Southern Pine	2	–	1	✓	K	–	–	✓	–	✓	–	–	M
Hagge and Bryden (2002) [43]	1D	Poplar	2	–	1	✓	–	–	–	✓	–	✓	–	–	M
Thunman et al. (2002) [44]	1D	Birch/ Spruce	2	–	1	✓	K	–	–	✓	–	–	✓	✓	I
Wurzenberger et al. (2002) [45]	1D	Beech	2	–	1	–	E	–	–	–	✓	✓	✓	✓	M
Bruch et al. (2003) [46]	1D	Beech	2	–	1	–	T	✓	–	–	–	–	✓	–	M
Bryden and Hagge (2003) [47]	1D	Poplar	2	–	1	✓	K	–	–	✓	–	✓	–	–	M
Babu and Chaurasia (2004) [48]	1D	NA	2	–	1	✓	–	–	–	–	✓	✓	–	–	M
de Souza Costa and Sandberg (2004) [49]	1D	NA	1	–	1	–	T	–	–	–	✓	–	✓	–	I
Galgano and Di Blasi (2006) [50]	1D	Poplar	1	–	1	–	T	✓	–	–	–	–	✓	✓	I
Galgano et al. (2006) [51]	1D	Poplar	1	–	1	–	T	✓	–	–	–	–	✓	✓	I
Porteiro et al. (2006) [52]	1D	Densified wood	–	✓	1	✓	T	–	–	✓	–	–	✓	–	I

(*continued on next page*)

Porteiro et al. (2007) [53]	1D	Densified wood	–	✓	1	✓	T	–	–	✓	–	–	✓	–	I
Shen et al. (2007) [54]	1D	Birch	2	–	1	–	K	–	–	–	✓	–	–	–	M
Yuen et al. (2007) [55]	3D	Beech	2	–	2	–	E	✓	–	–	–	–	–	–	M
Sand et al. (2008) [56]	2D	Birch	1	–	2	✓	T	–	–	✓	–	✓	–	–	M
Yang et al. (2008) [57]	2D	Willow	2	–	1	✓	T	✓	–	–	–	–	✓	–	M
Sadhukhan et al. (2009) [58]	1D	Casuarina wood	2	–	1	✓	–	–	–	–	✓	✓	–	–	I
Haseli et al. (2012) [59]	1D	Pine/ Red Oak/ Spruce/ Douglas Fir/ Redwood/ Plywood	2	–	1	–	–	–	–	–	✓	–	–	–	I
Mehrabian et al. (2012a) [7]	1D	Poplar/ Beech/ Spruce/ Spruce pellet	2	✓	1	✓	T	–	✓	–	–	–	✓	✓	I
Mehrabian et al. (2012b) [10]	1D	Poplar	2	–	1	✓	T	–	✓	–	–	–	✓	✓	I
Ström and Thunman (2013a) [8]	1D	Beech / Poplar	2	–	1	✓	T	–	–	✓	–	–	–	–	I
Ström and Thunman (2013b) [5]	1D	Beech	2	–	1	✓	T	–	–	✓	–	–	–	–	I
Galgano et al. (2014) [60]	1D	Oak	2	–	1	–	T	✓	–	–	–	–	✓	–	I
Kwiatkowski et al. (2014) [61]	3D	Pressed wood shavings	2	–	1	✓	E	–	–	–	✓	✓	–	✓	M
Pozzobon et al. (2014) [62]	2D	Beech	2	–	2	–	K	–	–	–	✓	✓	–	–	M
Seljeskog and Skreiberg (2014) [63]	1D	NA	1	–	1	–	T	–	✓	–	–	–	–	–	I
Biswas and Umeki (2015) [1]	1D	Katsura	1	–	1	✓	–	–	–	✓	–	✓	–	–	M
Biswas and Umeki (2015) [1]	1D	Pine and Spruce	–	✓	2	✓	–	–	–	✓	–	✓	–	–	M
Ding et al. (2015) [64]	1D	Birch	2	–	1	–	K	✓	–	–	–	–	✓	–	M

models can also be used to model single particles alone, as only boundary conditions have to be adjusted accordingly.

Moreover, it has to be added that independent of the choice of single particle model, the validation of models against experiments is very challenging due to various reasons [40]. The first problem is that chosen properties can vary a lot, and also show a significant dependency on wood species. Furthermore, the values for the properties of charred and partially charred solids are related to a significant uncertainty. The values of properties of the solid then also have to take into consideration the structural changes (e.g. cracking, fragmentation) and shrinkage that can occur during the entire thermal conversion process. It is also not possible to know the detailed chemical composition of each wood particle modeled. This is because the same sample cannot be produced twice, since it is expected that there always is a small variation in the percentage of contributing cellulose, hemicellulose and lignin fractions. Inorganic matter that is contained in the experimental wood sample, and which catalyzes primary devolatilization, is often not taken into consideration in modeling applications. Finally, the influence of chosen kinetic data is related to uncertainty, since the kinetic models themselves are also a gross simplification. In addition, the obtained kinetics are restricted to the operational conditions for which they were derived [40].

The models listed in Table 3 are of different complexity. The two most simplified models [49,59] in Table 3, were primarily based on pre-defined temperatures and geometrical relations. To a certain extent, they were based on interfaces moving through the wood particle, even though they included a higher number of simplifying assumptions compared to the rest of the listed interface-based models. Models of medium complexity listed in Table 3 are the interface-based models, where conversion fronts move through the particle from the surface to the center, and the highest complexity is related to the very detailed mesh-based models, where the full single particle is discretized. Nonetheless, more details on mesh-based and interface-based models are mentioned in the following sections. With respect to Table 3, however, it must be pointed out that, depending on the purpose of a model, simplistic models can be more suitable than very comprehensive mesh-based models. Even though mesh-based models result in higher accuracy, they might not be suitable for certain purposes (e.g. as a fast and simple engineering tool) due to increased computational cost.

4.1. Evolution equations

A model's accuracy and complexity increase with increasing detail in the mathematical description of physical and chemical processes. Therefore, the relevant evolution equations for thermochemical wood degradation and combustion modeling need to be discussed.

As shown in Fig. 1, the wood volume is formed by a solid matrix, and embedded in this solid matrix there are openings (pores) that contain gas and liquid phase. The dimensions of these pores can vary quite a bit. Pore size distribution, and consequently the overall porosity of wood, influence mass and heat transfer, which consequently affects thermal degradation [66]. This combined structure of solid matrix and gas- or liquid-filled pores leads to the assumption that wood can be described as a porous medium.

Based on the structure of wood, the describing equations need to include the influence of all current phases. Given the porous multiphase structure of wood, the evolution equation for temperature is given by

$$\begin{aligned}&\left(c_{\mathrm{P},s}\rho_s + c_{\mathrm{P,l}}\rho_\mathrm{l} + c_{\mathrm{P,b}}\rho_\mathrm{b} + \epsilon_\mathrm{g}(c_{\mathrm{P,g}}\rho_\mathrm{g}^\mathrm{g})\right)\frac{\partial T}{\partial t}\\ &+(\rho_\mathrm{l}\mathbf{v}_\mathrm{l}c_{\mathrm{P,l}} + \rho_\mathrm{b}\mathbf{v}_\mathrm{b}c_{\mathrm{P,b}} + \rho_\mathrm{g}\mathbf{v}_\mathrm{g}c_{\mathrm{P,g}})\nabla T\\ &= \nabla\cdot(k_\mathrm{eff}\nabla T) + \Phi_\mathrm{evap} + \Phi_\mathrm{dev} + \Phi_\mathrm{char}\end{aligned} \tag{2}$$

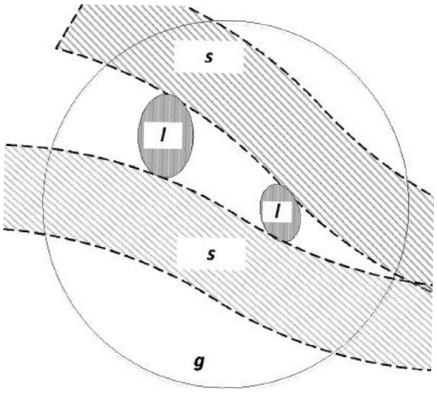

Fig. 1. Wood as a porous medium. The lined areas illustrate the solid phase (marked with s), the crossed areas are occupied by the liquid phase (marked with l) and the plain white areas illustrate areas where the gas phase (marked with g) is present. The pores themselves can contain both liquid and gas phase. The circle illustrates a certain representative sub-volume of the entire wood log.

where the subscripts s, l and g refer to the solid, the liquid and the gas phase, respectively. In the case of ongoing devolatilization reactions in a thermally thick particle, the solid phase includes the virgin wood as well as the produced char. During the stage of char conversion, char and ash form the solid phase. The effective thermal conductivity, k_eff, includes the influence of virgin wood, char, free liquid and bound water, in addition to gases. A linear variation of thermal conductivity from virgin wood to char, based on the degree of conversion, is commonly assumed [22,34,36–40,42,43,54,55,58,61]. A general assumption is that material properties vary linearly from virgin wood to char, and this does not solely apply to thermal conductivity, but also to specific heat capacity and permeability. The last three terms on the right-hand-side of the equation are source and sink terms due to the heat of reactions of drying, devolatilization and char conversion. The specific heat capacities are given by $c_{\mathrm{P,\,i}}$, where subscript i represents the phase, which can be either for solid (s), liquid (l), bound (b) or gas phase (g), respectively. One of the major simplifying assumptions that has been used in obtaining Eq. (2), and which is also applied by many researchers [1,7,10,22,34–43,45–55,57–62,64], is the assumption of thermal equilibrium between all the phases (solid, liquid and gas).

Large Peclet numbers, defined as

$$Pe = \frac{du\rho c_\mathrm{p}}{\lambda} \tag{3}$$

for heat transfer [67] justify the simplifying assumption of a local thermal equilibrium. Here, d is the characteristic length, u is the velocity, ρ is the density, λ is the thermal conductivity and c_P is the specific heat capacity. The Peclet number is the ratio of convective and diffusive transport. The assumption of thermal equilibrium reduces the number of required temperature equations to one, and consequently reduces the computational cost. Some deviation between modeling results and experimental results can be due to this assumption [68,69], as it results in longer conversion times, which increase by approximately 20%, compared to the case where separate temperature equations are solved for each phase.

Some authors neglect convection in the porous structure [48,64]. It has to be mentioned, however, that the gas phase that is flowing through the pores will result in a cooling of the solid particle, and that this effect cannot be modeled accurately if convection is neglected. Neglecting the convection should actually be considered

as a gross over-simplification because it is known that a high gas flow along the grain direction can limit the heating rate, and accordingly the entire temperature evolution is closely coupled to the gas flow within the pores. Another consequence is that a slower heating of the wood log, due to high gas flows out of the wood log center, yields different product yields and also gives a different conversion time comparable to what is obtained when neglecting convection. Di Blasi [39] identified an interesting dependency of particle size in relation to the influence of the convective term. With increasing particle size, the influence of the convective term decreases, as the maximum velocity is also reduced. This finding can therefore justify why the convective term in the temperature equation can by neglected in the case of very large wood particles.

Another common simplification is to neglect the influence of the heat capacity of the gas phase [34,42,43,47,50,51,60]. This is a fair assumption, since the thermal mass (defined as $m_i c_{P,\,i}$, with m being the mass of a species) of wood char is 650 times larger than the thermal mass of gases [47]. In Eq. (2), two different phase averages, the intrinsic average and the phase average, are used, which are explained hereafter.

The intrinsic phase average is the averaged value within a single phase. This means that the intrinsic average of the variable φ within the phase i, is defined as [22]

$$\phi_i^i = \frac{1}{V_i}\int_{V_i} \phi dV \tag{4}$$

where i can be l, g or s and V is the volume over which the average is performed, while V_i is the sub-volume of V occupied by phase i. In contrast to this, the phase average is defined as [22]

$$\phi_i = \frac{1}{V}\int_{V_i} \phi dV. \tag{5}$$

The relation between phase averaging and the intrinsic phase average is given as [22]

$$\epsilon_i \phi_i^i = \phi_i \tag{6}$$

where $\epsilon_i = V_i/V$ is the volume fraction of phase i. This relation is valid for all three phases present in wood. The continuity equation for the liquid free water is given as [38]

$$\frac{\partial \rho_l}{\partial t} + \nabla\cdot(\rho_l \mathbf{V}_l) = \dot{\omega}_{evap,l} \tag{7}$$

where ρ_l is the liquid free water density, $\dot{\omega}_{evap,l}$ is the rate of evaporation of the liquid-free water, and $\mathbf{V}_l$ is the velocity of the liquid free water.

The evolution equation of bound water is similarly constructed [22,38] as

$$\frac{\partial \rho_b}{\partial t} + \nabla\cdot(\rho_b \mathbf{V}_b) = \dot{\omega}_{evap,b} \tag{8}$$

where ρ_b is the bound water density, $\dot{\omega}_{evap,b}$ is the rate of evaporation of the bound water, and $\mathbf{V}_b$ is the velocity of the bound water. The velocities for liquid free water and bound water transportation are calculated differently, based on whether convective or diffusive transport is dominant.

The bound water movement is modeled as [22]

$$\rho_b v_{bx} = -\rho_{wood,dry} D_b \left(\frac{\partial\left(\frac{\rho_b}{\rho_{wood,dry}}\right)}{\partial x} \right) \tag{9}$$

where D_b is the bound water diffusivity, which depends on temperature and the bound water content itself. Commonly, one can assume $\rho_{wood,\,dry}$ to be constant during drying, which therefore cancels out and the equation is further simplified.

In contrast, the liquid free water transport is dominated by advection, which is commonly modeled by Darcy's law, such that [22]

$$\mathbf{V}_l = -\frac{K_l K_{rl}}{\mu_l}\nabla P_l. \tag{10}$$

As can be seen from the equation, the permeability contains the influence of a relative permeability, K_{rl}, and the intrinsic (absolute) permeability, K_l. The liquid phase pressure is based on a correlation between the gas phase pressure, P_g, and capillary pressure, P_c, such that [22]

$$P_l = P_g - P_c. \tag{11}$$

A common approach for modeling the capillary pressure is based on experimental work by Spolek and Plumb [70]. The mathematical expression for capillary pressure as a function of temperature, T, and liquid free water content (M_l) was derived by Perre and Degiovanni [71] as

$$P_c = 1.364\times 10^{-5}\sigma(M_l - 1.2\times 10^{-4})^{-0.63}, \tag{12}$$

where σ is the surface tension between the gas phase and the liquid phase, which is defined as

$$\sigma = \frac{128 + 0.185T}{1000}. \tag{13}$$

The above expressions are, however, based on experiments, which reduces the validity of the mathematical expression not only to softwood species, but also to certain operational conditions that the experiments were performed with.

The gas phase continuity equation is given by [22]

$$\frac{\partial(\epsilon_g \rho_g^g)}{\partial t} + \nabla.(\rho_g \mathbf{V}_g) = \dot{\omega}_{evap} + \dot{\omega}_{dev} + \dot{\omega}_{char} \tag{14}$$

where ϵ_g, ρ_g^g, $\mathbf{V}_g$ are the volume fraction of the gas phase, the intrinsic phase average density of the gas phase and the velocity of the gas phase, respectively. On the right-hand side in the above equations are the source terms due to water evaporation $\dot{\omega}_{evap}$, wood devolatilization $\dot{\omega}_{dev}$ and char conversion $\dot{\omega}_{char}$. The gas phase species continuity equation reads [38]

$$\frac{\partial(\epsilon_g \rho_i^g)}{\partial t} + \nabla\cdot(\rho_i \mathbf{V}_g) = \nabla\cdot\left[\rho_g^g D_{eff}^i \nabla\left(\frac{\rho_i^g}{\rho_g^g}\right)\right] + \dot{\omega}_i \tag{15}$$

where ρ_i^g is the intrinsic phase average density of a species i in the gas phase, and $\dot{\omega}_i$ is the source term of species i. The effective diffusion coefficient, D_{eff}, has to be used in the gas phase species continuity equation because it accounts for the constrictions due to diffusion in a porous medium, such as wood. It is suggested by Fogler [72] that it can be related to the binary diffusion coefficient, D, such that

$$D_{eff} = \frac{\epsilon_g \sigma_c D}{\tau}, \tag{16}$$

where τ is tortuosity, σ_c is a constriction factor and ϵ_g is the volume fraction occupied by the gas phase, which is equal to the porosity in the case of dry wood. In some works, diffusion of the gas species is neglected, since it is assumed that it is much smaller compared to convection [50,51,60]. The convective term of the volatile species equation was adjusted by Galgano et al. [60], such that the influence of the formation of cracks was partly considered in their work. They assumed that only a fraction of the entire gas phase is actually transported out by convection, and therefore has to pass the entire thickness of the hot char layer [60]. This means that a fraction of gases is modeled to leave the wood particle immediately along cracks and fissures.

The velocity of the gas phase is calculated such that [38]

$$\mathbf{V}_g = -\frac{K_g K_{rg}}{\mu_g}\nabla P_g, \tag{17}$$

where the effective permeability again is a combination of intrinsic, K_g and relative permeability, K_{rg}. Generally speaking, the intrinsic permeability is higher for softwoods than for hardwoods, and higher for sapwood than for heartwood [22]. Eq. (17) is also known as Darcy's law. Using Darcy's law to model gas phase advection is a common approach [1,22,36–43,45,55,61,62]. Since one expects a laminar flow in the pores, and since the viscous forces dominate over the inertial forces in the woody biomass structure, the computation of liquid and gas phase advection inside the wood with Darcy's law is reasonable [73].

It has been experimentally shown that significant pressure peaks can form inside a wood log [74]. It was also found that the pressure has an influence on the distribution of the devolatilization products within the solid, since the mass transfer is linked to the effect of pressure gradients on mass transfer velocity and thus also on residence times of products in the interior of the particle [75].

There are works in which the gas flow was not based on Darcy's law. Sand et al. [56] modeled gas phase behavior inside and outside of the wood log by fully solving the momentum equation, and were thereby able to identify a gas plume leaving the wood log. The influence of such a plume on the entire wood log degradation processes has not been investigated intensively so far, and accordingly, the importance of such a detailed description of the gas flow inside and outside the wood log needs to be investigated in more detail in the future.

The direction of the gas flow is often restricted, as it is common to assume that gases can only move away from the wet core [34,46,49,52,60]. Such a simplifying assumption neglects entirely the fact that gaseous products of thermal conversion can also move inwards, towards cooler regions and condense there. This would then require the modeling of tar and water vapor recondensation, which is not commonly done. Only a few works model the inwards and outwards movement of produced gases [36,39,45,54], even though in those works, condensation reactions are still neglected. Wurzenberger et al. [45] experimentally found condensation reactions of gases moving inwards. It is therefore suggested that condensation reactions are relevant. It would also be interesting to see how an asymmetric flow field, due to the anisotropy of wood, affects the importance of tar condensation reactions during thermal conversion modeling. Additionally, it is not yet known how anisotropic heating affects the importance of tar re-condensation modeling.

In order to solve the previously discussed governing equations, suitable boundary conditions have to be chosen and the most common ones are discussed hereafter.

4.1.1. Boundary conditions

For temperature evolution in a wood particle, it is most common to consider the influence of radiation and convection at the boundaries [5,8,10,22,34,35,38,40,42,49,52–54]. Some works set a fixed uniform radiant heat flux to heat up the wood log, and assigned losses to the boundaries, which result from convection and re-radiation [22,37,50,54,60,62]. It is also a common approach to assign fixed background temperatures, either one single temperature [36,39,42,43,47,52,53] or a combination of radiation temperature (commonly furnace temperature), T_{rad}, and convective temperature (from the surrounding gas phase), T_{conv}, [7,10], which results in heating of the wood particle.

The value of the applied heat flux has a significant effect on the produced char, since at higher heat fluxes the char density will decrease at the boundaries, while it will be higher in the interior of the wood log, due to slower heating inside. Faster heating at the boundaries, as a result of applying high heat fluxes, yields enhanced tar production and reduced char production [40]. Seljeskog and Skreiberg [63] set their boundary conditions such that two different heat fluxes could be applied at the bottom and top surface of the wood log. Accordingly, this model grants the flexibility to its user to also model asymmetric heating conditions that are more realistic in stoves.

None of the works has considered that the steam, exiting from the interior of the particle primarily during drying, can build a layer around the particles outer surface and absorb some of the radiation that heats up the particle [52]. Consequently, it is of interest for future work to identify how large the influence of such a layer on the temperature history of the particle really is.

The radiative heat flux from the flame was only mentioned in a limited number of works [64]. Even though this was a first step towards considering the back-radiation of the flame to the wood particle surface, it has to be pointed out that the validity is restricted, as a constant uniform heat flux was applied [64]. However, in the case of a real flame, the radiant heat flux will fluctuate significantly, mainly due to the highly transient thermal conversion process.

The particle emissivity is an important parameter that couples the exterior conditions of the solid with the drying, devolatilization and char burnout processes occurring inside the particle. Particle emissivity has been assigned a value of 0.85 [7,10,40,52,53,55] but also higher values of 0.9 [1,38,42,43] and 0.95 [48] and 1 [37,39] have been applied. A comparably low particle emissivity of 0.78 [54] has rarely been used. Surprisingly, some works even assume the emissivity of wood to exceed the emissivity of char [56]. In addition, some works did not account for significant changes of emissivity as wood converted to char [62,64] which is considered a weakness of a model, as one expects the emissivities to vary, because there is a significant change in elemental composition as wood degrades to char.

The applied emissivities do not follow a certain trend (a dependency on the composition of the initial wood species) or a dependency on the degree of conversion. It seems that the value of the emissivity is fitted in order to obtain better agreement between numerical and experimental results. It is also assumed that the ambiguous choice of emissivity values is due to the overall limited range of values for different wood species available in literature.

For external heat and mass transfer, heat and mass transfer coefficients have to be defined. Some authors therefore assume constant values [34,37,40,54,59], while others have started to work on a more detailed description of heat and mass transfer to the particle surface. A primary influence on these two coefficients is due to outflowing gases, which will reduce the transfer coefficients. This indicates that the gases leaving the particle act as a convective barrier [52,53]. One of the effects of the outflowing gases is also that they tend to react with oxygen before it can reach the active char sites. Porteiro et al. [52,53] considered such a reaction only for the exiting hydrogen. They corrected heat and mass transfer coefficients due to the blowing by the model suggested by Moffat and Kays [76]. In this correlation, a geometrical parameter and a blowing factor are related to the Stanton number with blowing, and a Stanton number without blowing. From the adjusted Stanton number the heat transfer coefficient can be calculated. De Souza Costa and Sandberg [49] also considered the blowing effect of exiting gases by the following expression of the heat transfer coefficient

$$h_s = h_0 \frac{ln(1 + B_s)}{B_s} \tag{18}$$

where B_s is the smoldering transfer number, which is a function of mass fractions of oxygen [49]. Transpiration effects influencing heat and mass transfer coefficients are accounted for in some works [50,51].

Bruch et al. [46] took this outflow of gases into consideration by using the Stefan correlation. The Stefan correlation corrects the transfer coefficients for mass and heat, which are not influenced by blowing of gases, by the influence of the mass flow of gases exiting

the particle such that [77]

$$h_c = \frac{\dot{m}_g c_{P,g}}{\exp\left(\frac{\dot{m}_g c_{P,g}}{h_{c0}}\right)-1} \quad (19)$$

and

$$h_m = \frac{\dot{m}_g/\rho_g}{\exp\left(\frac{\dot{m}_g}{\rho_g h_{m0}}\right)-1} \quad (20)$$

where $\dot{m}_g$ is the mass flux of gases, h_{c0} is the not-influenced heat transfer coefficient and h_{m0} is the not-influenced mass transfer coefficient. The corrected mass and heat transfer coefficients are h_c and h_m, respectively [77].

The influence of blowing factors on the temperature profile of a particle significantly depends on whether radiation or convection dominate the heat transfer to the particle. It is acceptable to neglect the influence of the blowing factor with respect to heat transfer phenomena if radiation dominates the heat transfer to the particle [78]. However, if convection dominates, the blowing factor has to be considered, as it can slow down the particle devolatilization process by about 20% [78]. The conclusion is that depending on the choice of boundary conditions, the blowing effect on heat and mass transfer has to be considered (convection dominates) or can be neglected (radiation dominates).

The pressure at the boundary is handled in such a manner, that it is commonly set equal to the atmospheric pressure, e.g. [37,40,43].

The layer model, applied by a number of researchers [7,10,44,52,53], used homogeneous boundary conditions for its implementation. The original work by Thunman et al. [44] was based on an Eulerian discretization, which does not require homogeneous boundary conditions as such. In fact, the boundary conditions can vary and instead of relating conversion to the external surface of the particle it was related to the surface area per unit volume. A significant spatial variation in boundary conditions can only be accurately modeled if the discretization is finer than the size of the particle.

However, in order to include highly diverse boundary conditions, it is recommended to develop a multi-dimensional mesh-based model in order to yield sufficient accuracy.

After having discussed how the particle is linked to its exterior, it is now of further interest to discuss how the thermal conversion processes in the interior of the particle are modeled.

4.2. Drying

This section describes the theory of drying of thermally thick woody biomass. Water is present as bound water, liquid free water and water vapor in the porous structure of wood. Bound water is attached to cell walls as OH-groups bound to structures of cellulose and hemicellulose (and not that many attachments to lignin). The presence of bound water is considered to be significant due to the hygroscopic nature of wood materials. Free water is liquid water in voids in the biomass, which is held in place due to capillary forces. Water vapor is considered as a species in the gas phase resulting from evaporation [18].

Drying is an endothermic process [23] that is prolonging the heat-up time [5]. There will not be any mass loss of the organic solid fuel until devolatilization starts. Water evaporates and leaves the wood as vapor, and if the heating rates are sufficiently high, the cell walls might be affected by higher pressures due to vapor formation in the pores. In special cases, extractives, such as resins, can melt and block the pores. The result is that the convective transport of the gas phase through the pores is slowed down or entirely hindered, which explains such a pressure increase in the porous body as previously mentioned. Physical changes in the wood related to drying can also be explained with respect to different dilatation rates along and across the wood fibers. Due to this variation of dilatation in different spatial directions, the resulting tension increase can lead to cracking of wood structures. These cracks can eventually help to accelerate the drying process, since the surface of the wood log exposed to the heat source is increased [23] and also permeability increases.

During evaporation, water vapor can move towards higher temperature regions, but it can also move towards cooler regions and condense there [79]. The simplifying assumption of negligible re-condensation of water vapor is a common approach when drying is modeled. Only a very limited number of works considered re-condensation of water vapor [42,47,78]. It is said that the effect of re-condensation on the overall modeling results of thermal conversion is negligible. However, since hardly any works include re-condensation, it is not fully known how such a re-condensation of water vapor affects the overall heating-up of the wood log and the conversion time, in comparison to the modeling of an ideal irreversible evaporation of water vapor. This should be studied for anisotropic heating of large wood particles.

One highly interesting aspect has been discussed by Lu et al. [78], who split water into bound water and liquid free water when modeling the drying of a poplar wood particle. Lu et al. [78] found that bound water and liquid free water do not vaporize in the same manner, which outlines that the present liquid water has to be split accordingly. They assumed that bound water can only be irreversibly reduced in heterogeneous Arrhenius expressions reflecting the evaporation of water, while liquid free water evaporation can be reversible and re-condensation reactions can also increase the amount of present liquid free water.

One expects the pressure distribution within the wood log to vary if water vapor re-condenses, so it therefore seems reasonable to assume that the convective transport of gaseous species out of the porous medium, and accordingly the entire heat and mass transfer within a wood log, are likewise affected. However, the identification of the degree of this influence is recommended to be an objective of future work. In the case of biomass with a lower moisture content, the influence of re-condensation reactions is also less compared to woody particles with a significantly higher moisture content.

Shrinkage is also occurring during drying, though in modeling it is mostly neglected [10] since it occurs to a significantly smaller extent compared to the volumetric shrinkage occurring during devolatilization, or even the particle size reduction due to heterogeneous reactions taking place during char conversion.

The reason for shrinkage during drying is that the cell walls lose the bound water that has been attached to hydroxyl-groups of cellulose and hemicellulose via hydrogen bonds. In comparison, the free water does not have any influence on shrinkage, as it only affects the density of the wood particle [10]. This relation indicates that wood does not show any change in size if moisture above the fiber saturation point is evaporated, while it is affected by shrinkage if moisture is lost below the fiber saturation point [33]. Shrinkage during drying accounts for 5–10% of size reduction of the entire particle [43]. Shrinkage related to the stage of drying is reversible, since the particle can swell again if exposed to humidity [10].

What is most interesting is that due to various shrinkage rates in longitudinal, radial and tangential direction, the wood particle can be distorted. This is also valid for shrinkage during devolatilization, and any comparable physical change of the wood particle results in an influence on heat and mass transfer, and accordingly the overall thermal conversion. It is a natural consequence that such a diversity of shrinkage, which varies significantly with direction, can only be accurately replicated in a multi-dimensional model, while 1D models focus on shrinkage in only one preferential direction.

Shrinkage during drying, often defined as the percentage of the green dimension, depends on the wood species [33]. The green

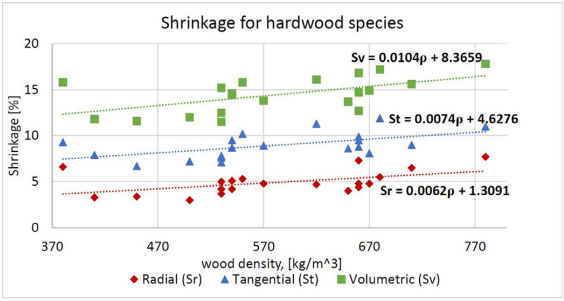

(a) Shrinkage, radial, tangential and volumetric, dependency on hardwood species.

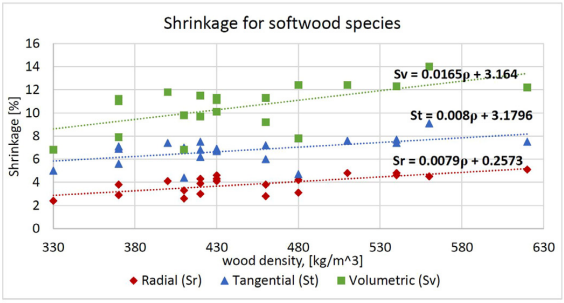

(b) Shrinkage, radial, tangential and volumetric, dependency on softwood species.

Fig. 2. Shrinkage dependency on wood species. The figure illustrates the shrinkage for a range of different hardwood and softwood species. Shrinkage occurs when green wood is dried to an oven-dry basis. Trend lines have been added to indicate that the shrinkage values increase as the density of certain wood species increases (= higher shrinkage for wood species of a higher density). More detailed information on shrinkage for different hardwood and softwood species can be found elsewhere [33]. The figure was based on data provided in a reference work for the various properties of wood [33]. (For interpretation of the references to color in this figure legend, the reader is referred to the web version of this article.)

dimension relates to the dimension of the green wood particle. Moreover, the shrinkage is also affected by the moisture content [33] such that

$$S = S_0 \frac{M_{fsp} - M}{M_{fsp}} \tag{21}$$

where S is shrinkage, %, from green wood to wood of a certain residual moisture content (M), S_0 is the total shrinkage, and M_{fsp} is the moisture content at the fiber saturation point is fulfilled. The fiber saturation point, M_{fsp}, is defined as the critical point where the cell walls of the wood contain the maximum quantity of bound water but no liquid free water is yet present. This relation is only valid if $M < M_{fsp}$.

When comparing shrinkage for different hardwood species and softwood species, it was found that the shrinkage also depends on the wood species. It appears to be the case that radial, tangential and volumetric shrinkage tend to increase for wood species of higher densities, even though it has to be pointed out as well that the dependency is modest. Fig. 2 shows the dependency of shrinkage, %, on different hardwood and softwood species.

In current models, shrinkage during drying is usually neglected. One can therefore conclude that an enhanced modeling focus on physical changes during drying can be a field of interest in future research.

4.2.1. Mathematical modeling of drying

Due to evaporation, the source term in the energy equation Eq. (2) is given by

$$\phi_{evap} = -\Delta h_{vap} \dot{\omega}_{evap} \tag{22}$$

where h_{vap} represents the vaporization enthalpy of water. The rate of evaporation, $\dot{\omega}_{evap}$, is determined based either on a thermal, kinetic rate or an equilibrium drying model [10]. Attention has to be paid when modeling the heat of evaporation. Only in a limited number of works [22,38,40] have the influences of bound water and liquid free water been explicitly modeled. Depending on whether the available moisture content exceeds the fiber saturation point or not, the heat of evaporation has to be calculated differently. If the moisture content exceeds the fiber saturation point, the heat of vaporization Δh_{evap} is calculated such that [22]

$$\Delta h_{evap} = \Delta h_l \tag{23}$$

where Δh_l is the latent heat of vaporization of water, which is independent of the porous material. If the moisture content drops below the fiber saturation point, the heat of vaporization is calculated as a combination of the latent heat of vaporization of water and the differential heat of sorption, Δh_{sorp}, such that [22]

$$\Delta h_{evap} = \Delta h_l + \Delta h_{sorp}. \tag{24}$$

The differential heat of sorption mainly depends on the structure of the wood, and is hence important in a regime lacking liquid free water but with bound water present [38].

Also, only limited works [22,38,40] have introduced an additional source term in the temperature equation

$$\Phi_{sorp} = \rho_b \mathbf{v}_b \Delta h_{sorp}, \tag{25}$$

which highlights that the level of enthalpy of the bound water depends on the bound water itself [22]. The consideration of bound water in current models is very limited, and the water is not commonly split into liquid free water and bound water. This is considered a weakness since the transport of bound water and liquid free water have to be modeled differently. It is also not uncommon to neglect both the diffusion and convective transport of water all together [5,7,8,10,52,53].

Based on the available literature, it seems that the scientific world is in favor of the thermal drying model [5,7,8,10,46,50–53, 56,60,63]. This method is based on the assumption that drying occurs at a fixed boiling temperature at atmospheric pressure, 373.15 K, and that any amount of heat above this temperature will be consumed by the drying process in order to vaporize the moisture [10]. The advantage of thermal drying models is that they are easy to implement in numerical codes. However, the robustness of the thermal model is limited because it results in a step-function, which can result in numerical instabilities. The operational conditions, under which the thermal model can be applied, require that a high-temperature environment is given, and also that the size of the drying front is comparably small in contrast to the entire particle dimension [10]. Furthermore, it was found that the assumption of evaporation at exactly 373 K is wrong, since due to significant water vapor formation the pressure in the wood log interior increases, such that the actual pressure significantly differs from atmospheric pressure [77]. This suggests that higher boiling point temperatures are given and it is recommended to model the actual evaporation temperature as a function of wood internal pressure.

The equilibrium model employs the assumption of a thermodynamic equilibrium between the liquid water and the water vapor in the gas phase. The difference between the equilibrium concentration and the current vapor concentration in the gas phase is the driving force for the drying process. The equilibrium method is usually considered in low-temperature drying models [10]. This approach has been employed by several researchers [22,55,61]. Alves and

Figueiredo [34] assumed that drying based on the equilibrium model is only valid for a moisture content below 14.4%, while above this value, the thermal model is applied.

Even though it has been stated that the equilibrium model is generally applicable in low-temperature processes, it has also been applied in these works in a high-temperature environment, such as in combustion and gasification processes. It is considered that especially at lower heating rates, where the time to reach the boiling point temperature is significantly long, the influence of an accurate modeling of drying below the boiling point temperature is significant; even so, it is presumed that for most combustion processes, a high-temperature environment can be assumed, which justifies the neglecting of drying below 100 °C.

Based on these strengths and weaknesses of the present drying models, it can be concluded that a combination of equilibrium and a thermal model can result in a good prediction of drying over a broad temperature range, because the implementation of such a combined model results in a good description of both low-temperature and high-temperature drying.

An alternative to the thermal drying model is the kinetic rate model, which has the primary advantage that it is more numerically stable, since it lacks the discontinuity. Furthermore, one can model drying to occur over a broader temperature range (depends on how kinetic data is adjusted), and therefore also consider drying below the boiling point temperature to some extent by fitting the kinetic data. In addition one can account for bound water, which evaporates at higher temperatures than 373 K. In the kinetic rate models, the drying is considered a heterogeneous reaction, and an Arrhenius equation is used to calculate its rate [44]. The pre-exponential factor and activation energy are set such that the evaporation mainly occurs around the water boiling temperature [10]. In contrast to the common application of thermal models, there is a smaller number of papers that apply the kinetic rate model [42,44,47,54,62,64]. Three different combinations of activation energy and pre-exponential factor were found. Bryden et al. [42,47], Shen et al. [54] as well as Ding et al. [64] used 5.13×10^{10} s^{-1} as a pre-exponential factor and an activation energy of 88 kJ/mol. Pozzobon et al. [62] used the same activation energy but applied a lower pre-exponential factor of 5.13×10^{6} s^{-1}. Thunman et al. [44] used an activation energy of approximately 207 kJ/mol, while the pre-exponential factor was set to $10^{27} s^{-1}$ by Thunman et al. [44]. With respect to the pre-exponential factors applied in these works, one can identify a clear discrepancy between the chosen values, since Thunman et al. [44] modeled a layer model, in which infinitely fast reactions, in this case phase change, are expected, such that the zone where reactions occur is very narrow (= infinitely thin) and high pre-exponential factors are required. This model is based to a certain degree on assuming very fast conversion stages, while Bryden et al. [42,47] developed a mesh-based model, where reaction zones can also be thicker and accordingly phase change due to drying does not have to be infinitely fast.

Finally we will now discuss the numerical efficiency of the thermal drying model and the kinetic rate model. The equilibrium model is not included in the discussion, since it is only relevant for low-temperature drying conditions, while the combustion environment in wood stoves requires models that are suitable for high-temperature conditions. Due to the fact that it has frequently been pointed out that the thermal drying model is lacking numerical robustness, the authors aimed to investigate this drawback of the drying model by comparing it to the more stable kinetic rate model.

For this comparison, a model, based on the one developed by Di Blasi [37] is used. Kinetic data was taken from Font et al. [80] (K3 in Di Blasi's work [37]). Because Di Blasi only discussed a dry particle, we just added the two drying models, after having successfully validated the dry particle modeling against Di Blasi [37]. The transport equations for drying were taken from Melaaen [38]. The moisture content was 5 wt%, wet basis. For both the thermal drying and kinetic rate model, the tolerance of the iterative solver defining the convergence criteria of the model was set to 10^{-4}. Time discretization was done with a backward differentiation formula (BDF). It was found that using the kinetic rate model with kinetic data by Chan et al. [81] (pre-exponential factor being 5.13×10^{6} s^{-1} and the activation energy being 88 kJ/mol), resulted in the applicability of a significantly larger temporal resolution compared to the thermal drying model. The chosen time step using the kinetic rate model was as large as 2.5×10^{-4} s, whereas the thermal drying model required time steps as small as 1×10^{-6} s. Most interesting was also that by increasing the external heat flux, the numerical stability of the thermal drying model was significantly affected. The temporal resolution had to be refined from 1×10^{-6} s to 5×10^{-7} s when increasing the external heat flux from 70 kW/m^2 to 100 kW/m^2.

When increasing the stiffness of the kinetic drying model, by using a higher pre-exponential factor ($5.13 \times 10^{10} s^{-1}$) as suggested by Bryden et al. [42], the temporal resolution had to be refined. In this case, the time step size had to be reduced to 7.5×10^{-6} s. Such an increase in stiffness mimics the reduction of the size of the drying zone, because it concentrates evaporation reactions in a more narrow temperature region. Accordingly, by increasing the pre-exponential factor, the kinetic rate model approaches the principle of very thin drying zones, as commonly implemented in layer models.

It was found that the choice of drying model has a significant influence on the numerical efficiency of the overall thermal conversion model of a thermally thick wood particle. This is the case, since the time step size is determined by drying and not by devolatiliztion reactions. It was also found that the low robustness of the thermal drying model is a key weakness of this model, and that the kinetic rate model is less complex to implement in a code.

Besides these numerical aspects all three models are capable of demonstrating that the overall heating time of wet wood is greatly affected by the amount of moisture in the wood log.

4.3. Devolatilization

Devolatilization is a thermochemical degradation process that occurs by definition in the absence of oxygen. While tar and permanent gases are formed and leave the wood log via the pores, oxygen can only enter the wood log via diffusion, since these gas compounds build up a convective barrier to inflow.

In some works, there is a clear differentiation between pyrolysis and devolatilization, as pyrolysis is assumed to occur in a reducing environment, while devolatilization is related to thermochemical degradation in oxidizing environment. However, most particles that are thermochemically degrading are within a volatile cloud that to some extent mimics a reducing atmosphere, so these two expressions can be used interchangeably [78].

Chemical reactions, as well as physical processes that occur during thermal conversion, have to be modeled simultaneously since they influence one another [82]. The fresh green wood (=moist wood) is primarily heated by conduction. After drying, the heated part subsequently undergoes thermochemical degradation and the release of volatiles starts. In thermally thick particles, drying and devolatilization can overlap, even though they never overlap in space. The permanent gases that are formed during devolatilization include a vast variety of chemical species, with the main compounds being CO, CO_2, CH_4 and H_2. Produced in lower quantities are also light hydrocarbons such as ethene, propene and nitrogenous compounds [18]. In addition tar is formed, which is organic compounds that are liquid at ambient temperature [18]. This broad range of different gas phase compounds makes it clear that modeling all the species related to devolatilization reactions is a challenge, and the so-called lumping procedure has therefore been introduced. As part of this method, various products of thermochemical biomass

degradation are collected in different product categories, namely char, tar and permanent gases [83].

After all the gases have been removed, only a char layer remains [82]. Mostly due to higher pressure inside the particle (and due to a higher char permeability), the flow of the gases is directed towards the heated surface. In the high-temperature region, which the gases have to pass, secondary tar reactions, cracking or re-polymerization, occur. These reactions may occur homogeneously in the gas phase, or might also be heterogeneous and occur on the char surface. The gases can also be directed towards the virgin wood, which has a lower temperatures, leading to condensation. However, only a small fraction of the entire gases will be directed towards the colder wood region. As a result, the convective inward transport of heat and mass is often neglected in models. The condensed gas phase compounds can evaporate again if the temperature at the spatial location in the wood log increases over a critical value due to ongoing heat transfer phenomena [82].

The char layer forming on the biomass tends to build up on the non-devolatilized wood as devolatilization continues. This leads to an increased residence time of tar, thereby enhancing cracking or re-polymerization. As thermal degradation continues, the physical parameters of wood logs change due to shrinkage and cracking of the solid fuel, which again have to be considered in cases of heat, mass and momentum transfer [82]. During devolatilization, mass loss of wood will be around 80% due to the formation of gaseous products [23].

Furthermore, shrinkage becomes more important during devolatilization compared to its relevance during drying. This process is not reversible, and its degree depends on wood species, peak temperature and temperature history. It is also interesting that lignin can swell during devolatilization, which adds even more complexity to numerical modeling [43]. Shrinkage is influenced by the anisotropic properties of wood. The theoretical discussion of devolatilization underscores that considering detailed chemistry and detailed changes in wood structure yields a high-complexity model. Consequently, it is of interest to review all the chemical and physical aspects of devolatilization and identify the most relevant ones and some additional simplifications, such that future models can easily find the balance between accuracy and complexity, and therefore save computational time.

4.3.1. Mathematical modeling of wood devolatilization

The modeling of devolatilization of wood requires the description of chemical and physical phenomena in a mathematical form. Therefore, the most relevant governing equations for devolatilization modeling are discussed in this chapter. When modeling gas phase continuity Eq. (14) the devolatilization source term $\dot{\omega}_{\mathrm{dev}}$ occurs, which is defined as [37]

$$\dot{\omega}_{\mathrm{dev}} = (k_1 + k_2)\rho_{\mathrm{wood}} - \epsilon_g k_5 \rho_{\mathrm{tar}} \tag{26}$$

where k_i with i = 1,2,5 are reaction rate constants modeled with Arrhenius expressions. This is only an exemplary reaction pathway where three independent competitive reactions describe wood degradation. However, in a more generic way one can state that the first term in Eq. (26) represents primary devolatilization reactions and the second term describes secondary devolatilization reactions. Reaction rate constants k_1 and k_2 are due to permanent gases and tar formed from wood, respectively, whereas k_5 refers to the reaction where tar is converted to char again. The mass change of solid wood is defined as [1]

$$\frac{\partial M_{\mathrm{wood}}}{\partial t} = R_{\mathrm{wood}} = -(k_1 + k_2 + k_3)M_{\mathrm{wood}}, \tag{27}$$

where k_3 is due to the formation of char from wood. The species mass fractions are calculated from Eq. (15) and the corresponding source terms are given as [37]

$$\dot{\omega}_{\mathrm{tar}} = k_2 \rho_{\mathrm{wood}} - \epsilon_g (k_4 + k_5)\rho_{\mathrm{tar}} \tag{28}$$

for tar, where k_4 is the reaction rate constant for the cracking of tar to permanent gas. The source term of permanent gas is modeled similarly as

$$\dot{\omega}_{\mathrm{vol}} = k_1 \rho_{\mathrm{wood}} + \epsilon_g k_4 \rho_{\mathrm{tar}}. \tag{29}$$

The permanent gas phase includes a broad range of different species and the range of compounds that form this product group [19] is discussed hereafter. A detailed discussion on gas phase products from devolatilization is found in Neves et al. [19].

Commonly, one lumps together CO, CO_2, H_2 and CH_4, as well as other light hydrocarbons, when modeling permanent gases. Additional light hydrocarbons are C_2 species, as well as C_3 species. It was found that the main compounds of the permanent gas phase species are CO and CO_2, and light hydrocarbons and H_2 are also commonly present in lower amounts. This composition is little influenced by heating rate. In fact, CO, CH_4 and H_2 show similar temperature dependencies as far as their formation trends are concerned. It is also found that the higher light hydrocarbons (mostly C_2 species) increases linearly with methane, thereby suggesting that they have similar reaction pathways. However, the formation of CO_2 with respect to temperature changes deviates from what is observed in the case of the other compounds [19]. If the temperature is approximately 500 °C, it is expected that the major contribution of volatile species is derived from primary devolatilization reactions. In such cases, CO and CO_2 are the main compounds while small amounts of CH_4 are also present. At approximately 450 °C, 2/3 of the entire mass of dry gas species are CO_2, while the residual fraction is primarily CO. It has also been found that at temperatures below 500 °C the composition of the volatile species does not show a strong temperature dependency. However, as temperatures increase and exceed 500 °C, the yields of combustible gases in the volatile species become strongly temperature-dependent. Such a change in composition above 500 °C is mainly related to secondary reactions. As the temperature increases from about 500 °C to 850 °C, the mass fraction of CO increases from 2 to 15% to 30–55% (based on dry and ash-free fuel) [19]. Accordingly, the tar yield decreases. Some tars are also converted to light hydrocarbons (including CH_4), which thereby increases from 1% at around 500 °C to 10% at temperatures higher than 850 °C. Hydrogen shows a similar temperature dependency, and increases from $<0.2\%$ at around 500 °C to $>1\%$ at above 850 °C. It is therefore suggested that if a significant increase in CO and H_2 can be found in experiments, the presence of secondary tar reactions is highly relevant for an accurate prediction of permanent gas phase species product distribution. As mentioned earlier, the temperature dependency of CO_2 deviates from the temperature dependency of the residual species forming the volatile fraction. In the case of CO_2, no significant change with respect to an increasing temperature is found. This highlights that CO_2 is a main product of primary reactions [19].

The change of char mass due to devolatilization reactions is modeled as being influenced by primary and secondary devolatilization reactions, but also gasification reactions $\dot{\omega}_{\mathrm{gasif}}$ and oxidation reactions $\dot{\omega}_{\mathrm{oxid}}$ influence the char yield

$$\frac{\partial M_{\mathrm{char}}}{\partial t} = R_{\mathrm{char}} = k_3 M_{\mathrm{wood}} + k_5 V_{\mathrm{gas}} \rho_{\mathrm{tar}} - \dot{\omega}_{\mathrm{gasif}} - \dot{\omega}_{\mathrm{oxid}}. \tag{30}$$

The overall mass change of char, Eq. (30), is modeled similarly to wood degradation in Eq. (27). Here, V_{gas} is the volume occupied by pores, which equals the volume occupied by the gas phase, since liquid water has entirely been evaporated as char conversion initiates [37]. The porosity of the dry wood can be expressed as the

ratio between the volume occupied by the gas phase and the total volume, as shown in Eq. (31)

$$\epsilon_g = \frac{V_{gas}}{V}. \tag{31}$$

Modeling the degradation of wood occurring during devolatilization is a vast field of research. Di Blasi [84] stated in her work that the field of chemical kinetics of biomass is highly debated. The complexity is that wood is a mixture of many different compounds that degrade differently. Not only does the raw material differ, but also a high number of different products needs to be modeled, which even further challenges researchers. Mathematically, this indicates a high number of required equations. The kinetics of these models can vary a lot in their stiffness, so the computational efficiency is also affected [85]. However, the computational cost and accuracy need to be balanced, and researchers inevitably have to apply simplified models to overcome this challenge [86]. The most common models are discussed in the following sections.

Finally the influence of devolatilization reactions on the temperature of the wood log has to be modeled. Due to devolatilization, the source term in the energy equation Eq. (2) is given by

$$\Phi_{dev.} = \sum_{k=1,2,3} r_k \Delta h_k + \sum_{k=4,5} \epsilon_g r_k \Delta h_k \tag{32}$$

where Δh_k is the heat of reaction, due to devolatilization reactions, with the first term representing primary devolatilization and the second term secondary reactions. As will be outlined later, it is a challenge to define accurate values for the heat of reaction for devolatilization, since it tends to vary from endothermic to exothermic reactions as conversion proceeds. We will go more into detail on how heat and mass source terms related to devolatilization reactions are modeled in those governing equations, and which challenges arise with certain model approaches.

4.3.2. One-step global mechanism model

The reaction mechanism of a one-step global mechanism can be illustrated as [20]

$$\text{dry woody biomass} \rightarrow \text{gases} + \text{char}. \tag{33}$$

This is the most simplified reaction scheme applied in a number of works as shown by the number of different kinetic data used in the models (see Fig. 3). The temperature dependency of the Arrhenius expression defining kinetic rate constants is plotted in Fig. 3.

The kinetic rate constant by Ding et al. [64] seems to be inconsistent with the rest of the data used to model the one-step global reaction mechanism. It shows a steep increase of the reaction rate with respect to temperature increase, and eventually highly exceeds all the other values for reaction rate constants already at 500 K. It is therefore suggested that this set of data predicts too fast devolatilization. The inconsistency of kinetic data in the case of Ding et al. [64] is also highlighted by the fact that for the devolatilization modeling of birch wood, Larfeldt et al. [41] used a much lower kinetic rate constant, which agrees with what has been used for other hardwoods [46,55,57]. There is also a slight discrepancy in kinetic data used for beech devolatilization modeling by Yuen et al. [55] and Bruch et al. [46]. However, none of those two reaction rates increase unreasonably fast, and therefore both models are assumed to yield reasonable conversion rates.

The primary disadvantage of the one-step global model is that the produced gas phase is not automatically split into tar and permanent gases [22]. In order to clearly split the gaseous fraction, a stoichiometric coefficient for tar has to be known prior to modeling [22]. It is expected that the mass fractions of these two products are inversely linked, and that the ratio between the two products depends on operational conditions. In this approach, the reactant (wood) is considered to be homogeneous [37]. Considering only one

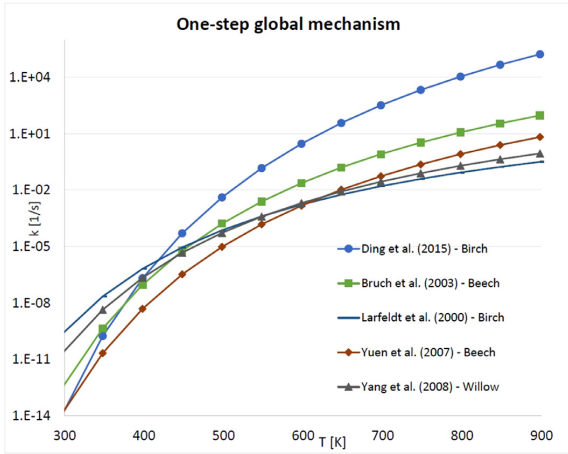

Fig. 3. Reaction rate constants of one-step global reaction mechanisms. In this plot the reaction rate constant, k [1/s] is plotted against the temperature, [K]. Kinetic data, used in a number of independent models in which different wood species were modeled, are plotted.

reactant, and consequently only defining kinetics with respect to a single reaction rate constant is often considered to be a rather crude approximation, even though the justification of this model is that the thermal behavior of biomass reflects the behavior of the sum of its compounds and tt is not the response of every single compound [37].

Many researchers work with single first-order reactions (one-component mechanism) when modeling devolatilization [41,50,51, 55,57,60,64]. Some works [50,51] fitted the modeled mass losses and therefore the kinetics to experiments, such that surface reactions could be used to model devolatilization. This was done, since the model was based on an interface-based approach, and it was assumed that devolatilization only occurs at the surface of the dry wood layer. Such a fitting can be considered a weakness.

Even so, the primary advantage of the one-step global mechanism is that product yields, as well as overall decomposition rates, can be predicted accurately enough at a reasonable computational cost [10]. It is suggested that this is acceptable for most engineering applications. However, one might think that for larger particles this does not apply, since there is a large temperature difference in the particle and in one-step global reaction mechanisms, such a temperature influence on the char yield cannot be modeled precisely [20,87]. Furthermore, it is concluded that for the purpose of fundamental research on devolatilization, a more detailed devolatilization reaction model is recommended.

4.3.3. Independent competitive reactions model

In the three independent competitive reactions model, the solid input material degrades competitively to char, tar and permanent gases. The principle scheme of the independent competitive reaction model is presented in Fig. 4. The only linkage between the product

$$\text{Dry wood} \begin{cases} \xrightarrow{k1} \text{Permanent gases} \\ \xrightarrow{k2} \text{Tar} \\ \xrightarrow{k3} \text{Char} \end{cases}$$

Fig. 4. Independent competitive reactions scheme. This reaction model describes the thermochemical degradation of wood to tar, permanent gases and char via three independent competing reactions.

yields is through the mass fraction (the sum of all mass fractions at a certain time equal unity) [88].

A broad range of kinetic data for the three independent competitive reactions model is currently available and used in wood particle degradation modeling. Some of the most commonly applied kinetic data is discussed hereafter.

Thurner and Mann [89] present kinetics that are commonly used and that are derived from experiments with oak. The main disadvantage of this set of kinetic data is that the experiments were only conducted in a temperature range from 300–400 °C, which is very narrow and low. It is known that e.g. devolatilization reactions for cellulose can start below 300 °C, and overall devolatilization is expected to be finished at approximately 500 °C. The experiments were conducted with oak sawdust, which suggests that the kinetic data is mainly applicable to hardwood species. The influence of secondary reactions was aimed to be avoided during these experiments by keeping the temperature low. This suggests that if the kinetic data by Thurner and Mann [89] is to be used for modeling thermally thick particles, the modeling approach always has to be coupled with secondary reactions in order to predict the thermal conversion of a thermally thick particle with an acceptable accuracy. In general, it is more accurate to include secondary reactions as particle size increases.

A second set of commonly applied kinetic data was presented by Font et al. [80], who conducted experiments in a temperature range from 400 to 605 °C. This therefore leads to the conclusion that the kinetic data may not be valid in the temperature range from 200 to 400 °C, in which the degradation of holocellulose (combined cellulose and hemicellulose) in particular will occur. Furthermore, almond shells were tested, and no specific wood species can thus be directly related to this set of kinetic data.

The third very common set of kinetics was presented by Chan et al. [81], who based their kinetic model on two references. The kinetics for char formation were estimated from a previous work by Shafizadeh (obtained via personal communication, see [81]). The modeling results are highly sensitive to the kinetic data of char formation. Permanent gas and tar formation reactions and corresponding kinetic data were taken from Hajaligol et al. [90]. In this work, the rapid pyrolysis of cellulose was tested (1000 °C/s), and the temperature range of the experiments was between 300 and 1100 °C.

These three sets of kinetics are very often used when modeling thermochemical degradation of a single particle with the three independent competitive reactions scheme. The three independent competitive reactions model is commonly coupled to secondary tar reactions. If secondary tar reactions are neglected, this is linked to the simplifying assumption of produced gases exiting the wood particle or log immediately as they are formed. Such a simplifying assumption has been the basis for a number of works [44,52,53,59]. Bruch et al. [46] claimed that in the particle size range they were modeling (5 to 25 mm), only less than 10 % of the primary tars are cracked or re-polymerized, and accordingly, secondary reactions can be neglected.

One can also assume that without a correct inclusion of secondary charring or tar cracking reactions, the pressure field in the interior of the wood log is not predicted accurately, hence influencing the calculation of the gas phase velocity. However, this influence on the pressure prediction is assumed to be less important, since the overall prediction of the pressure is related to a number of uncertainties. These uncertainties include the common neglect of the formation of cracks in the char, in addition to a high uncertainty concerning commonly used permeability values.

Tar condensation reactions can also occur in a second stage after primary devolatilization, but such condensation reactions are commonly neglected (all works listed in Table 3 have neglected tar condensation). It is said that their influence on the thermal conversion process is somewhat limited, and in 1D simulations, where this was investigated in detail, it was found that the influence of tar condensation on overall conversion is negligible [91]. However, it is assumed that if asymmetric heating at the boundary of the wood log is given, the gaseous tar can flow to cooler regions and condense there. One can then expect that this will lead to a blocking of the pores, and a subsequent hindering of the convective transport of gaseous species, which can affect the pressure field in the wood interior. However, since the majority of the gases is transported outwards, this tar condensations can be neglected without significantly affecting modeling accuracy. The dependencies of devolatilization models on the temperature are shown in Fig. 5 a–c.

The mass loss rate of the center cell volume of the wood log versus the temperature in the center cell volume for different sets of kinetic data is shown in Fig. 6.

Fig. 6 shows that wood mass starts degrading fastest with the kinetic data suggested by Biswas and Umeki [1], while the kinetic data of Chan et al. [81], Thurner and Mann [89] and Font et al. [80] follow, respectively exhibiting lower mass loss rates. The modeled wood mass loss rate by Biswas and Umeki [1] increases steeply until it reaches a certain peak (a peak much higher compared to the other models). The mass loss behavior is comparable to what has been found for the other three sets of kinetic data, but occurs at a lower temperature range. The conversion is over at about 580 °C, when applying kinetic data by Biswas and Umeki [1]. This is a fast devolatilization compared to the other kinetic models resulting in devolatilization being finished at approximately 600 to 620 °C. It is also interesting that the models by Chan et al. [81], Thurner and Mann [89] and Font et al. [80] show a maximum mass loss rate at approximately 480 °C, which is close to what is commonly assumed to be the temperature where most of the devolatilization reactions should be finished (500 °C). With the kinetic data used by Biswas and Umeki, the peak in the mass loss rate occurred at slightly lower temperatures, around 460–470 °C. With respect to the data used by Biswas and Umeki, it has to be added that they used data originally derived by Di Blasi and Branca [92], who tested thermally thin particles and comparably high heating rates. It can also be seen from Fig. 7 that Biswas and Umeki predicted the lowest residual solid mass, which is consistent with the test conditions for the originally derived data. With respect to the kinetics found by Font et al. [80], where almond shells were tested, it has to be added that this data is assumed relevant for wood degradation modeling, since it is similar to the kinetic data obtained by Nunn et al. [93] for hardwood.

Fig. 7 shows that the kinetic data suggested by Font et al. [80] yields the highest residual solid. It is interesting to see that the amount of residual solid decreases as mass loss rates shown in Fig. 6 speed up, and also have their peak at lower temperatures. Thus, one explanation is that the mass loss rates with a peak at a lower temperature suggest that most of the mass losses are related to the degradation of cellulose and hemicellulose. In the case of Font et al. [80], the mass loss peaks at a slightly higher temperature, which agrees more with the devolatilization temperature of lignin.

A disadvantage of the three independent competitive reactions model is that wood as a reactant is not described in detail. Therefore, the validity of this reaction model is limited, since only wood species similar to the experimentally tested wood species for obtaining the kinetic data can be used. The main advantage of the this reaction scheme is, that one can predict char, tar and permanent gas yields, without pre-defining a stoichiometric coefficient that is required to split the product yields.

Overall, it can be concluded that the three independent competitive reaction scheme is a well-established concept that yields good results compared to experimental work, even though it misses a very detailed prediction of the product species.

Commonly, the secondary tar cracking reactions, which are often coupled with the three independent competitive reaction model, are of first order [94]. There are also models where the primary tar does

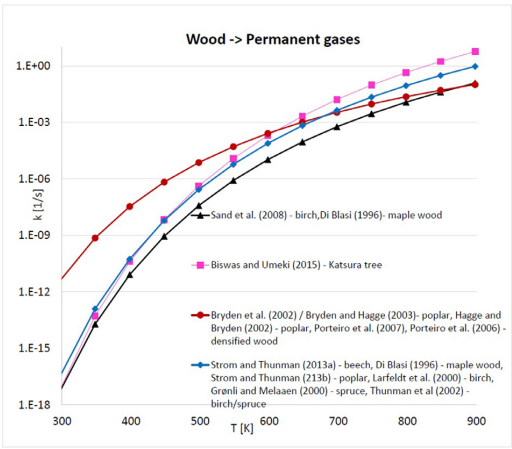

(a) Reaction rate constants of applied three independent competitive reaction schemes for the reaction of wood degrading to permanent gases.

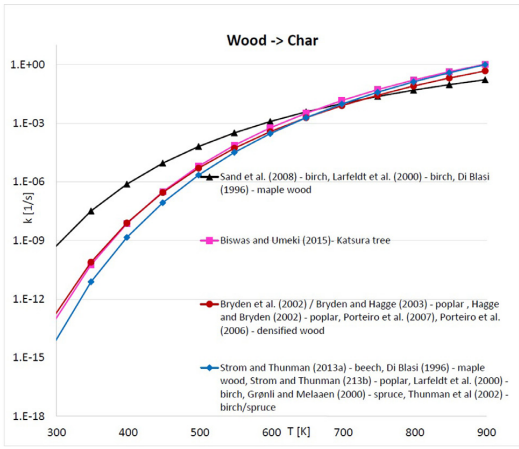

(b) Reaction rate constants of applied three independent competitive reaction schemes for the reaction of wood degrading to char.

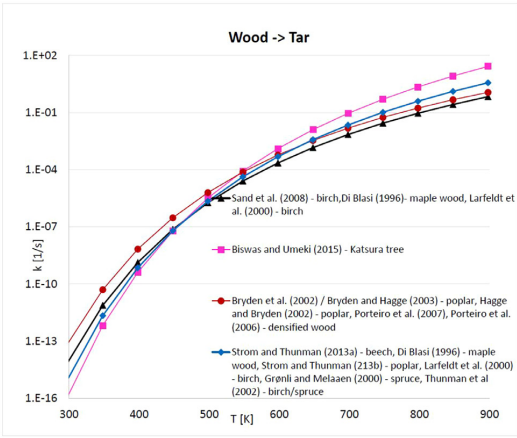

(c) Reaction rate constants of applied three independent competitive reaction schemes for the reaction of wood degrading to tar.

Fig. 5. Reaction rate constants of three independent competitive reaction schemes. The applied kinetic data was plotted also considering which wood species was modeled. The red lines having circles as markers refer to kinetic data originally derived by Thurner and Mann [89], the black lines having triangles as markers refer to kinetic data originally derived by Font et al. [80], the magenta colored lines having rectangles as markers refer to kinetic data used by Biswas and Umeki [1] and the blue colored lines having diamonds as markers refer to kinetic data originally derived by Chan et al. [81]. In the figures the lines are then related to the models that used these sets of kinetic data. (For interpretation of the references to color in this figure legend, the reader is referred to the web version of this article.)

not directly form char due to re-polymerization reactions and permanent gas phase compounds due to cracking, but instead yields secondary tar and permanent gases [22]. Various researchers have recently extended their kinetic models of thermal wood degradation to include secondary tar cracking [1,5,22,37,40,42,43,56,58,61].

The kinetic data used in their work is plotted against the temperature in Fig. 8a and b.

Fig. 8a shows the range of variation between the maximum reaction rate constant applied by Di Blasi [37] are the minimum reaction rate constant used by Kwiatkowski [61].

Fig. 8b shows that the reaction rate constant used by Kwiatkowski [61] is much slower than the reaction rate constant applied by other researchers [1,37,42,43,47,56,57,62]. Comparing Fig. 8a and b shows that heterogeneous reactions of tar to char are slower compared to homogeneous gas phase reactions of tar to permanent gas phase compounds.

Furthermore, different values for the heat of reaction of pyrolysis were used. A common value for all primary reactions is -418 kJ/kg, and the heat of pyrolysis of the two competing secondary reactions is commonly set to 42 kJ/kg, e.g. [37,56]. Slight deviation from these values is common [42,43,47]. Accordingly, it is a common assumption to define primary devolatilization as endothermic reaction and secondary devolatilization as exothermic reaction. Grønli and Melaaen [40] chose different values (primary reactions endothermic with –150 kJ/kg and secondary reactions exothermic with 50 kJ/kg). By comparing all these previously mentioned values, it is suggested that there is no common consensus on heat of reactions. This lack of common consensus can even be illustrated by the heat of pyrolysis

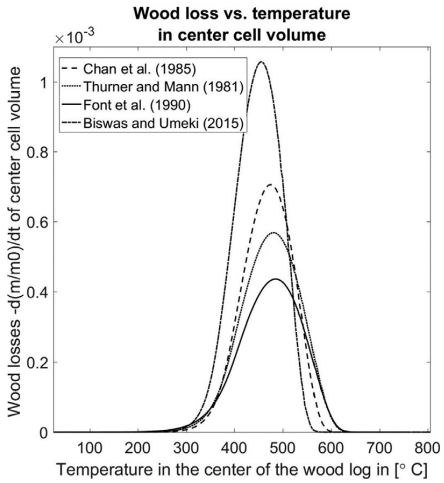

Fig. 6. Mass loss rate versus temperature of the center cell volume of a wood log. This is based on a mesh-based model, developed by the authors. The model is based on work by Di Blasi [37], and the same conditions and properties have been used; except a lower density of 410 kg/m^3, a smaller particle size ($1 \times 1 \times 3$ cm^3) and the varying set of kinetic data tested for three independent competitive reaction scheme models. The external heat flux heating up the wood log is 70 kW/m^2 (perpendicular to the grain). The heat flux to the boundary of the wood log was constant. The permeability was set to 1×10^{-15} m^2, and was therefore lower compared to Di Blasi, although it was found here that the influence of the convective term on the presented results was negligible.

of the primary devolatilization reaction of beech wood, which was found to vary between –156.1 and 145.3 kJ/kg [95]. The range of variation for the secondary pyrolysis reaction for beech wood is more narrow, only ranging from –65.7 to 17.3 kJ/kg [95]. Since beech wood can be assumed to represent hardwoods, one can also discuss the variation in the heat of pyrolysis for the degradation of spruce as a softwood species. In this case, the heat of pyrolysis of the primary degradation reactions ranges from 41.9 to 387.3 kJ/kg, while the secondary reactions range from –60.8 to –23.8 kJ/kg [95]. One of the reasons for these significant spans of values is that the experimental determination of heat of reaction of devolatilization reactions is very

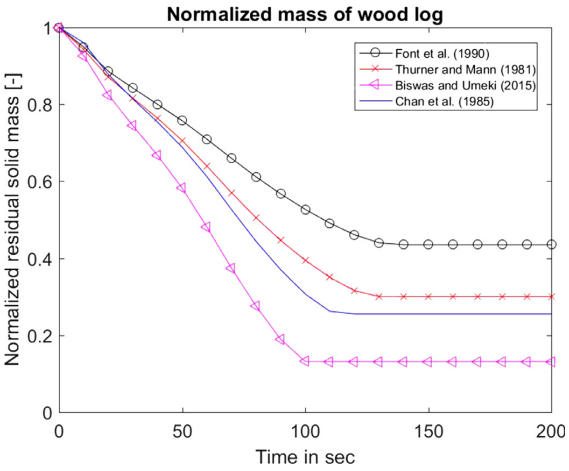

Fig. 7. Normalized residual mass of a wood particle based on most common kinetic data used in current three independent competitive reactions models. This is based on a mesh-based model, developed by the authors (description was provided earlier).

sensitive to the conditions under which the experiments are performed [19,95,96]. Moreover, it is also the case that many values for the heat of reaction for primary and secondary devolatilization reactions have been obtained by fitting the heat of pyrolysis to the measurements [8]. This instead suggests that the applied values are again based on a series of modeling assumptions, rather than being taken from realistic experiments.

4.3.4. Independent parallel reactions model

According to Papari and Hawboldt [94], many researchers prefer to predict the products of pyrolysis by modeling three independent parallel reactions. This means that they independently model the degradation of lignin, cellulose and hemicellulose [94]. The reaction scheme is illustrated in Fig. 9.

Mehrabian et al. [7,10] have implemented the three independent parallel reactions model, using pre-exponential factors of 2.202×10^{12}; 1.379×10^{14} and 2.527×10^{11} s^{-1} for lignin, cellulose and hemicellulose degradation, respectively [97]. The corresponding activation energies for lignin, cellulose and hemicellulose decomposition were 181; 193 and 147 kJ/mol, respectively, experimentally obtained by Branca et al. [97].

The basic assumption for the three independent parallel reactions mechanism is that components in the mixture degrade the same way they would if they were decomposing separately [98]. Many authors have claimed that the degradation processes for hemicellulose and cellulose should be modeled as first-order reactions, whereas lignin degradation is modeled as a higher order reaction [99]. However, this is not a common consensus, since it is more commonly assumed that the degradation reactions of all pseudo-components are first-order reactions [98].

Furthermore, there are only a few studies that also include extractives in the independent parallel reaction model [20]. One advantage of such a split into three independent parallel reactions is that such a model can be applied to a variety of biomass types, since they differ by mass fractions of lignin, cellulose and hemicellulose. Because these compounds are all handled individually, it is relatively easy to adjust their fractions and take into account their influence in the model [100]. However, a more practical point of view causes the criticism that the modeling of three independent parallel reactions needs more input parameters (e.g. activation energy, pre-exponential factors, etc.) than the one-step global mechanism, which are primarily obtained by experiments or previous assumptions [22].

A main disadvantage of this model is that the interaction between cellulose and lignin, as well as hemicellulose and cellulose, is entirely neglected, even though such interactions have been found within certain temperature ranges [101]. Before being able to state whether ongoing cross-reactions limit the applicability of the three independent parallel reactions model with respect to the thermal degradation modeling of thermally thick wood particles in combustion environments, it is recommended to experimentally test the relevance of potential cross-linking reactions.

4.3.5. Broido–Shafizadeh scheme

In the Broido–Shafizadeh scheme, an activated intermediate is formed, which continues to degrade into tar, char and permanent gases [102]. The Broido–Shafizadeh scheme was originally developed for cellulose only, thereby suggesting that the initiation reaction leads to the generation of activated cellulose from cellulose. The activated cellulose will then competitively react to permanent gas, tar and char in first-order reactions [102]. It is very important to realize that the formation of the activated intermediate from the reactant (such as cellulose) is not related to any mass loss [103]. The principle of the reaction is shown in Fig. 10.

The Broido–Shafizadeh scheme, which was originally established for cellulose, has been used for modeling thermochemical wood degradation, even though in some works pure cellulose was

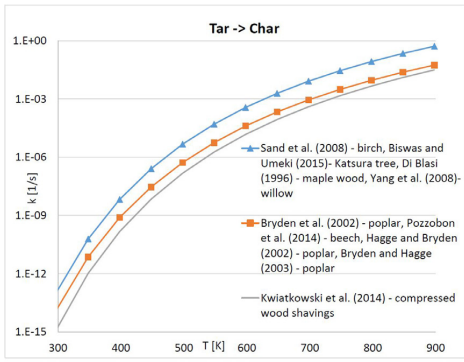

(a) Reaction rate constants of applied secondary reactions of tar reacting to char.

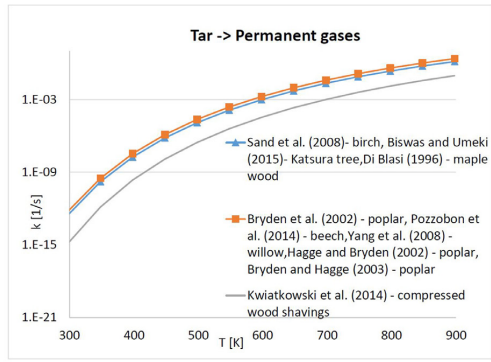

(b) Reaction rate constants of applied secondary reactions of tar reacting to permanent gases.

Fig. 8. Common kinetic data used for modeling secondary tar reactions. The kinetic rate constants applied in certain models are illustrated, and it is shown how the reaction rate constant increases as the temperature increases. The kinetic data discussed was applied for modeling different wood species. Even though there will most commonly not be a differentiation between tars derived from certain parent biomass fuels, the relation is still mentioned in the legend.

modeled [36,39]. This model is typically applied based on the assumption that wood can be modeled as pure cellulose, since holocellulose accounts for 75% of the wood [39], and it has already been applied for modeling thermochemical degradation of birch [41]. The typical reaction products resulting from lignin decomposition, which are mostly phenolic compounds, cannot be predicted with this model. One instead expects that even a more simplified scheme, based on the actual degradation of wood as a mixture of cellulose, hemicellulose, lignin and extractives results in a more accurate model of thermal conversion than the Broido–Shafizadeh scheme.

Furthermore, it is considered a main disadvantage that the reaction forming the activated intermediate, is considered less important at low temperatures, since based on new kinetic measurements, it has been found that such reactions are superfluous at 250 to 370 °C [37].

Furthermore, the kinetic parameters required for deriving the chemical reaction rate constant for the conversion stage of wood to the activated intermediate can hardly be derived experimentally. This conclusion agrees with what has been stated by Mamleev et al. [103], who claimed that the reactions related to the Broido–Shafizadeh scheme cannot be easily found experimentally, and interpretations of experimental results are difficult, since there is no mass loss related to the conversion to activated intermediate and it seems arbitrary to define when the activated intermediate has been created. From a more practical point of view, the Broido–Shafizadeh scheme also does not provide advantages compared to the more suitable three independent parallel reactions scheme or the three independent competitive reactions scheme, since in all cases three kinetic rate constants have to be determined. Due to these facts, one cannot identify any major advantages or strengths of the Broido–Shafizadeh scheme.

$$\text{Dry wood} \begin{cases} \rightarrow \text{Lignin} \xrightarrow{k1} \text{Gases} + \text{Char} \\ \rightarrow \text{Cellulose} \xrightarrow{k2} \text{Gases} + \text{Char} \\ \rightarrow \text{Hemicellulose} \xrightarrow{k3} \text{Gases} + \text{Char} \end{cases}$$

Fig. 9. Independent parallel reactions model. This reaction model describes the thermochemical degradation of wood as three independent parallel reactions of its main components.

$$\text{Reactant} \xrightarrow{k1} \text{activated intermediate} \begin{cases} \xrightarrow{k2} \text{Char} + \text{permanent gas} \\ \xrightarrow{k3} \text{Tar} \end{cases}$$

Fig. 10. Broido–Shafizadeh scheme. This reaction model assumes the formation of an intermediate that eventually forms the final products char, permanent gas and tar.

4.3.6. Ranzi scheme

A multi-step lumped mechanism for the pyrolysis of woody biomass has also been developed by Ranzi et al. [27]. The most important aspects of this model are a detailed description of the parent biomass fuel, the devolatilization of it and its products. A simplifying assumption of the model is that similar components are grouped together, and related reactions are lumped together but in more detailed sub-groups of educts, products and reactions than the previously discussed models. This aims to sufficiently well balance the computational cost of modeling devolatilization and the accuracy of the predictions [27].

Cellulose reacts to activated cellulose, levoglucosan, hydroxyacethaldeyde (HAA, $C_2H_4O_2$), glyoxal ($C_2H_2O_2$), CO, CH_2O, CO_2 and char, as well as H_2O in a number of reactions [27]. Levoglucosan is the main product at lower temperatures. At higher temperatures, the formation of other products such as HAA is dominant. Hemicellulose reacts to intermediates that subsequently decompose with different activation energies and charring propensities. One of the intermediates can form xylose, which is one of the primary components of the tar fraction. In addition, a number of species contributing to the permanent gas fraction are also released from the intermediates. Lignin is described by three sub-categories, which are either rich in carbon, oxygen or hydrogen, while the main products from lignin degradation are phenol and phenoxy species [27].

Advantages of the Ranzi scheme are that a broad range of volatile species can be predicted, with levoglucosan being the main product, due to high percentages of cellulose in both hardwood and softwood. Additionally, permanent gases such as CO, CO_2, H_2, CH_4 and C_2H_4 can be predicted. Alcohols, carbonyls, phenolics and water vapor can also be predicted. Moreover, the model can be applied to describe hardwood or softwood devolatilization, since the parent fuel can also be described in detail based on defining the contributions by its three main pseudo-components. It is also claimed that the model is applicable for a broad range of operational conditions, which enhances is applicability. One disadvantage is that secondary gas-phase reactions forming char are not included in the model, since char is only derived either from lignin or cellulose in the chemical wood structure, or the activated intermediates of cellulose and hemicellulose. Another weakness of this model is that the presence of extractives or inorganics, and their catalytic effect, are neglected.

Nevertheless, it is known that minerals contained in the parent fuel have an effect on the char yield, and can even catalyze cellulose and hemicellulose fragmentation [18]. Moreover, no nitrogen-containing species are included in the list of predicted products, i.e. the presence of fuel-bound nitrogen is also entirely neglected. The interaction between cellulose and lignin, as well as hemicellulose and cellulose, is neglected, even though, as previously mentioned, at temperatures comparable to temperatures in wood stoves, cross-linked reactions cannot be fully excluded. With respect to numerical efficiency it is also assumed that this model has its drawbacks. It is concluded that due to the increased number of modeled equations (compared to e.g. three independent competitive reactions model or the three independent parallel reactions model), the CPU time per time step is larger.

4.3.7. Other schemes

In Table 3, there is an extra column for "other schemes" and in this category some less common reaction schemes are listed. Alves and Figueiredo [34] modeled six parallel reactions. They provided kinetic data for cellulose and hemicellulose degradation, and further provided kinetic data for four additional reactions describing degradation of parts of the phenolic lignin macromolecule. Their kinetic data was obtained from isothermal TGA experiments performed with pine wood sawdust, with a particle size range of 180–595 μm. The temperature range was very broad (265-650 °C), and accordingly the kinetic data obtained is less restricted in its validity. One has to consider though, when using this set of kinetic data for large wood log modeling, that this set of kinetic data has originally been derived for thermally thin particles, and that experimentally derived correlations are needed to validate this model for thermally thick particles. Because the kinetics were originally derived for pine sawdust, a correlation was implemented [34] that was aimed to convert the mass loss obtained with the kinetics for thermally thin particles to the mass loss of large particles. The experimentally determined final char yield of large particle conversion entered this correlation as an empirical factor.

Wurzenberger et al. [45] based their devolatilization model on work by Alves and Figueiredo [34], and therefore also split the solid into various species that react in parallel. However, the kinetics for those reactions were taken from a TGA test, with a heating rate of 5 K/min and a beech wood particle of 1 mm, where the peak temperature of the tests was 1173 K [104]. The heat of pyrolysis was chosen such that it was correlated with a final char yield, as it was said that the actual value of heat of pyrolysis depends on wood species, particle size and the final char yield [45]. This broad dependency emphasizes again that it is very challenging to apply suitable values for the heat of reaction, and that the model is rather sensitive to this input data.

Larfeldt et al. [41] also implemented a reaction scheme with four independent parallel reactions, but it is not clearly stated which wood compounds are described by this degradation mechanism. They showed that a scheme with four independent parallel reactions was able to predict the correct devolatilization temperature for their application, while other models (one-step global mechanism, Broido–Shafizadeh and three independent competitive reactions scheme) over-predicted the initiation temperature of the devolatilization process. Even though the three independent competitive reactions scheme can be considered as an advanced devolatilization model, it is less advanced than the four independent parallel reactions model.

Babu and Chaurasia [48], as well as Sadhukhan et al. [58], based their devolatilization model on two competing reactions. In case of Sadhukhan et al. [58] the frequency factors and activation energies for secondary tar reactions were obtained by fitting the measured mass loss data of the tested wood sphere. The definition of the heat of reaction for secondary tar reactions was done in the same manner. Therefore, doubt arises concerning the broad applicability of this model, as it appears to be significantly attached to the experiments it was validated against. Furthermore, this two-competitive reactions model only splits between gases and char, and even though changing operational conditions will affect the predicted yields of gases and char, such a variation in operational conditions cannot be linked to varying yields of tar and permanent gas. In order to know the yields of tar and permanent gases, one has to set a predefined ratio that does not vary with operational conditions.

Shen et al. [54] also modeled two independent competitive reactions yielding char and gases. It is not specified if this gas fraction included permanent gas and tar, but based on the applied kinetic data, one assumes that only permanent gas is modeled. Kinetic data by Thurner and Mann [89] was used, which was originally derived for the three independent competitive reactions scheme. In the work by Shen et al. [54], tar formation was therefore neglected. For this reason, it is concluded that both product yields and conversion times cannot be computed correctly. The same reaction principle was used by Koufopanos et al. [35], who added one consecutive secondary reaction, in which primary char and gases could react to secondary char and gases. For modeling secondary reactions they required a deposition coefficient that described the fraction of gas species deposited on char sites. This coefficient is a function of residence time inside the degrading particle, so it is also dependent on particle dimensions.

Melaaen [38] used a devolatilization model suggested by Glaister [105], which differs slightly from the common three independent competitive reactions scheme. In the model by Glaister, the solid parent fuel can also react to water vapor. In this model, the formed tar does not exit the particle immediately, since consecutive tar cracking reactions occur. However, the disadvantage of these secondary reactions is that one has to predefine a factor defining how much permanent gas, tar and water vapor are produced by such a consecutive cracking reaction. This again limits the applicability of the model, since such values do not consider changing operation conditions well enough. In addition to the predefined coefficient for splitting the products of the secondary tar cracking reactions, even more empirical values are required, since the other two reaction pathways forming permanent gas or char also produce water vapor simultaneously. Hence, one can conclude that this model, even though a broader range of products can be predicted, has to be applied with caution, since the application of such a predefined coefficient for conditions different from what they have been obtained in, can lead to false predictions.

Kwiatkowski et al. [61] assumed that wood does not react directly to char, but instead is converted to an intermediate solid, also referred to as temporary char, which then reacts to form the final char. However, since there is no clear definition of what is defined as char and how it differs from temporary char, such a classification seems ambiguous. One also cannot evaluate how the correlating kinetic data has been obtained if there was no clear differentiation between temporary char and char. A reaction model, following the same concept as suggested by Kwiatkowski et al. [61], has been introduced by Pozzobon et al. [62]. Kwiatkowski et al. [61] performed their own experiments on compressed wood shavings in order to obtain kinetic data. However, according to the given material properties, e.g. a density of 750 kg/m^3, it is found that the sample of compressed wood shavings behaves comparably to an undensified wood sample.

Very simplified devolatilization models of a dry wood particle, also available in the current literature [59], model the devolatilization based on the assumption of a constant devolatilization temperature. The rate of devolatilization was accordingly linked to a constant pre-defined temperature, which acted as a boundary value between virgin dry wood and char. The decomposition rate was linked to the initial biomass density and the time-dependent evolution of the

char layer thickness. The disadvantage of this model is that detailed knowledge about the devolatilization products cannot be obtained, since only the overall thermal conversion time and the final residue can be obtained as model results. Moreover, the choice of pyrolysis temperature is ambiguous as this value highly varies with wood species, as well as heat flux [59].

A large number of devolatilization models are available. All of them are related to simplifications, but the degree of simplification differ significantly. It is clear that an extensive research focus, both modeling and experimental, is on devolatilization. The research within the field of devolatilization is more intense than within the other thermal conversion stages; drying and char conversion.

4.4. Char conversion

The solid product of the devolatilization process is a mixture of ash and mainly carbon, which further reacts as combustion proceeds. Modeling char conversion is challenging since heterogeneous reactions, which are influenced by mass transfer and kinetics, have to be modeled. When a particle with a low ash content, such as wood, is reacting, it will also shrink in size as the reactions proceed [106]. The gaseous products of char conversion will exit the reaction surface, and are transported into the freeboard by convection and diffusion. The carbon will primarily react with oxygen and form CO_2 and CO. Depending on the temperature and pressure conditions and the gas composition, the following reactions can be related to gasification and char oxidation [23]

$$C + O_2 \rightarrow CO_2 \quad (R1)$$

$$C + 0.5\ O_2 \rightarrow CO \quad (R2)$$

$$C + H_2O \rightarrow CO + H_2 \quad (R3)$$

$$C + CO_2 \rightarrow 2\ CO \quad (R4)$$

$$C + 2\ H_2 \rightarrow CH_4 \quad (R5)$$

Commonly applied kinetic data for the previously discussed char oxidation and gasification reactions are mentioned in Table 4.

The stoichiometric ratio, Ω, in Table 4 relates the moles of carbon to the moles of oxygen. Oxidation reactions of various ratios can be generically described by the reaction in Table 4 (listed in the first and fifth column). As one can see from Table 4, the same kinetic data is commonly used for char conversion. However, this entirely neglects that char reactivity is affected by operational conditions of a thermal conversion process. A higher heating rate would result in a highly porous and reactive char, with an extremely damaged structure, which is due to a fast and sudden gas phase release [107] compared to slower heating rates, as in the case of large particle heating. Such a variation in reactivity cannot currently be reflected well enough, as in current models similar kinetic data is used for the most common oxidation and gasification reactions independent of the previous drying and devolatilization history of the particle. Yang et al. [57] stated that the kinetics will vary with the potassium content in the wood. It is also interesting to note, that in their approach the diffusion of oxygen is implicitely included in the kinetic expression.

The kinetics of char conversion are one of the most significant uncertainties in the current modeling of thermal conversion of thermally thick woody biomass particles. Using always the same kinetic data for char conversion does therefore not allow the consideration of the influence of varying operational conditions, e.g. pressure or residence time of char at certain temperatures, in a model. Furthermore, the influence of catalytic ash elements can hardly be correctly modeled. Because the diversity of available literature on single biomass particle combustion data is limited [78], this is recommended as a field of future research.

4.4.1. Mathematical modeling of char conversion

Char conversion is either kinetically or mass transfer controlled. The kinetically controlled regime is predominant at low temperatures, whereas the mass transfer controlled regime is dominant at higher temperatures. In addition to this, the mass transfer controlled regime is more important for larger particles, because intra-particle and external mass transfer are much slower than chemical reactions [52,53,61]. A limited mass transfer means that the gas reactant penetration into the particle is limited. Char conversion is heterogeneous and the rate at which conversion occurs is calculated based on intrinsic kinetics, the oxygen diffusion rate as well as the evolution of the specific surface area that is available for reactions [60]. The mass fraction of oxygen, Y_{O_2} is required to be determined if the rate of char conversion is aimed to be determined. Mathematically this can be expressed as [60]

$$k_m(\rho_{e,O_2} - \rho_{O_2}) = \dot{\omega}_C \frac{n_{O_2}}{n_C}\frac{M_{O_2}}{M_C} \quad (34)$$

with n_i being the moles of oxygen or char, M_i being the molecular masses of oxygen or char, k_m being the mass transfer coefficient, and $\dot{\omega}_C$ being the reaction rate of char oxidation. The oxygen densities are calculated as [60]

$$\rho_{O_2} = \frac{P\overline{M}}{RT_s} Y_{O_2} \quad (35)$$

if the oxygen density at the surface is calculated, since the temperature at the surface, T_s, is used to define the density. If the external oxygen density is calculated, it is defined as [60]

$$\rho_{e,O_2} = \frac{P\overline{M}}{RT_e} Y_{e,O_2} \quad (36)$$

Table 4
Comparison of kinetic parameters for char conversion. The most commonly applied kinetics for char conversion modeling (either gasification or oxidation reactions) are listed in this table. Models from Table 3 were only included here, if intrinsic kinetic data was given for char conversion modeling.

Ref.	$\Omega C + O_2 \rightarrow 2(\Omega-1)CO + (2-\Omega)CO_2$	$C + H_2O \rightarrow CO + H_2$	$C + CO_2 \rightarrow 2CO$	$C + 2H_2 \rightarrow CH_4$	$\Omega C + O_2 \rightarrow 2(\Omega-1)CO + (2-\Omega)CO_2$	$C + H_2O \rightarrow CO + H_2$	$C + CO_2 \rightarrow 2CO$	$C + 2H_2 \rightarrow CH_4$
	Pre-exponential factor				**Activation energy**			
[10]	1.715 [a]	3.42 [a]	3.42 [a]	3.42×10^{-3} [a]	74.8287	129.703	129.703	129.703
[53]	3.01×10^{2} [b]	–	–	–	149.38	–	–	–
[52]	3.01×10^{2} [b]	–	–	–	149.38	–	–	–
[51]	–	4.45×10^{4} [c]	6.51×10^{3} [c]	–	–	217	217	–
[60]	1.73×10^{8} [c]	–	–	–	160	–	–	–
[50]	–	4.45×10^{4} [c]	6.51×10^{3} [c]	–	–	217	217	–
[7]	1.715 [a]	3.42 [a]	3.42 [a]	3.42×10^{-3} [a]	74.8287	129.703	129.703	129.703
[44]	1.715 [a]	3.42 [a]	3.42 [a]	3.42×10^{-3} [a]	74.8287	129.703	129.703	129.703
[46]	2.71×10^{5} [d]	–	–	–	149.38	–	–	–
[57]	10.3 [c]	–	–	–	74.9	–	–	-

[a] indicates that values are given as m/sK.[b] marks the unit of 1/s. [c]indicates that the pre-exponential factor is given in m/s. [d] indicates that the pre-exponential factor has the unit m^2/kg. E_a is given in kJ/mol.

where temeprature, T_e, and mass fraction Y_{e,O_2}, are taken from the external surrounding gas phase. Gasification, e.g. (R4) and (R3) is often modeled as an Arrhenius expression [50]

$$\dot{\omega}_{\text{gasif},1} = S_{\text{char}} A_1 \exp\left(\frac{-E_{a,1}}{RT}\right) \rho_{\text{char}} y_{s,CO_2}^{n,1} \tag{37}$$

which describes reaction (R4), while reaction (R3) is described as

$$\dot{\omega}_{\text{gasif},2} = S_{\text{char}} A_2 \exp\left(\frac{-E_{a,2}}{RT}\right) \rho_{\text{char}} y_{s,H_2O}^{n,2}. \tag{38}$$

where y_{s,H_2O} and y_{s,CO_2} are the surface mole fractions of the corresponding gasifying agent and S_{char} is the char specific surface area. The superscripts "n,1" and "n,2" mark the reaction orders of the corresponding reactions. The expressions in Eqs. (37) and (38) enter the equation for char mass loss calculations Eq. (30) as source terms, $\dot{\omega}_{\text{gasif}}$ Eqs. (37) and (38) show one approach on how gasification modeling can be done. However, the authors agree more with the char gasification and oxidation source term definition that was used by Fatehi and Bai [77].

The reaction of char with oxygen is faster than the gasification reactions for most practical applications. Hence, a common modeling assumption is that as long as residual oxygen is in the gas phase, char gasification reactions can be neglected [5,52,53,60]. Low oxygen supply rates to the particle result in a complete consumption of oxygen by the char and the leaving gas phase. A higher oxygen supply rate means that the reactions are limiting [108]. Accordingly, a model has to be flexible, such that it is valid over a broad range of operational conditions, which indicates the importance of a simultaneous consideration of both mass transfer and kinetic limitations for char conversion.

Despite this significant influence of operational conditions on char conversion, several authors modeled the char oxidation reaction as only diffusion controlled [46,50–53]. More flexible works are available where char conversion is a function of both reaction rate and mass transfer rate [7,10,44,60], which suggests that these models are more flexible to varying operational conditions.

Even though it is theoretically true that char oxidation is always faster than gasification reactions, which could therefore be neglected, it is not possible to pre-define when the critical oxygen mass fraction in the gas phase will be reached in practical applications. As a consequence, it is concluded that in order to be able to model a broad range of operational conditions and possible combustion conditions in a combustion unit, the implementation of both gasification and oxidation reactions is required. The model is then recommended to be able to freely model the most dominant reaction pathway depending on operational conditions.

In models where only the reaction of carbon and oxygen with carbon dioxide as a product (R1) is assumed to describe the char burnout process; e.g. [5,50,51], the production of CO from char conversion is entirely neglected. This assumption restricts char conversion to a temperature where CO_2 formation is dominant. By far, the char combustion in the majority of models is based on the reaction of carbon and oxygen, with both carbon monoxide and carbon dioxide as products [7,10,44–46,52,53,60]. The ratio between CO and CO_2, η, is commonly modeled as a function of temperature [52,53]

$$\eta = \frac{2\left(1 + 4.3\exp\left(\frac{-3390}{T}\right)\right)}{2 + 4.3\exp\left(\frac{3390}{T}\right)}. \tag{39}$$

It is assumed that modeling such a temperature dependency of CO/CO_2 increases the model's accuracy, and also broadens its applicability to a vast range of operational conditions.

Especially for large wet particles, it is suggested that the importance of gasifying reactions with H_2O is significant. In a thermally thick particle, the char layer will build up in the outer zones of the particle, even though in the core of the wood particle, evaporation still occurs. The formed water vapor has to pass through the hotter char layers, so it is reasonable to assume that the water vapor will react with the char. This of course also applies to CO_2 and H_2, which are products of wood devolatilization. These permanent gas phase species are also formed in the interior of the wood particle, and accordingly have to pass the hot char layer. A detailed modeling of leaving water vapor and permanent gas phase reactions with char are therefore considered essential for accurate prediction of product yields, both solid and gaseous.

However, gasification reactions described by reactions (R3) and (R4) have only been taken into consideration in some of the papers [7,10,44,61]. The formation of methane due to reactions of char with hydrogen have been included by even fewer works [7,10,44].

A further assumption in several models is that char only contains pure carbon [45,46,49–53,57,60,61,64]. In reality, char will also include ash and some reduced mass fractions of H, N and O, which remain after all the carbon has been consumed. The ash can build up an additional layer surrounding the particle, which results in an increasing resistance to mass and heat transfer. When this is taken into account, additional computations for the ash layer must be performed [7,10,44].

Furthermore, besides the influence of ash on mass transfer modeling, the catalytic influence of impurities on char conversion has not been modeled in any of the reviewed works. A general conclusion on whether considering impurities in a model is hard to draw, since there will be significant variations between different biomass species and also the extent to which specific inorganics are present will vary. However, one can expect that neglecting impurities is acceptable in the case of large woody biomass particles, because in larger particles diffusion is primarily controlling char conversion.

It was further found that there is no common approach on how the specific surface area available for heterogeneous reactions is modeled. However, the prediction of char conversion is highly dependent on the specific surface area. Because the formation of cracks and fissures leads to changes in the surface area, this also significantly affects heterogeneous reactions. Galgano et al. [60] considered the influence of cracks and fissures by introducing an enhancement factor when describing heterogeneous char conversion reactions. This enhancement factor is rather ambiguous, since it is not related to any detailed information concerning external and internal structural changes of a wood particle. Furthermore, it does not account for the fact that not all gas species can penetrate into any size of a newly formed opening (less relevant for cracks but more relevant for pore size), even though an increase of surface area enhances heterogeneous reactions.

It is common in current models to neglect the change in physical structure of the wood log and therefore the change in specific surface area. Overall, the change of specific surface area during thermal conversion, especially during char conversion, is very complex.

In the case of biomass char, it is likely that the pore size increases monotonously [109]. This contradicts with what is expected from coal char pore size evolution, since in such a case it is more likely that pores grow and also suddenly merge, which again results in a reduction of the specific surface area. It is therefore suggested to model the specific surface area of the biomass char to continuously increase during thermal conversion [110]. This can be achieved by modeling the evolution of the specific surface area which is defined as [110]

$$S_{\text{char}} = S_{\text{char},0}\sqrt{1 - X\left(1 - \frac{1}{\epsilon_0}\right)} \tag{40}$$

where $S_{\text{char},0}$ is the initial specific surface area and ϵ_0 is the initial porosity. Furthermore, S_{char} is the actual specific surface area and X

is defined as [110]

$$X = \frac{\rho_{char}}{\rho_{char,0}}. \quad (41)$$

The specific surface area is closely linked to the char porosity and the pore size seems to be a crucial parameter. One can distinguish between three main pore size groups, which are macro-pores ($d_p >$ 50 nm), meso-pores ($d_p =$ 2–50 nm) and micro-pores ($d_p <$ 2 nm). However, even though the micro-pores contribute greatly to the specific surface area, they do not influence the overall conversion significantly, since reactants cannot enter these pores sufficiently well. The complexity in their case is that even though this pore size category is initially negligible, pore size will increase such that these pores will eventually become big enough to significantly contribute to conversion. It also has to be pointed out that for different reactions, different pore sizes are relevant [110]. Hurt et al. [111] also found that char and CO_2 mainly react outside of the micro-pores network. Furthermore, it was found that O_2 cannot enter micropores [112], while H_2O can penetrate into this pore size category [113]. It is therefore suggested that pore sizes also evolve differently and that an accurate description of heterogeneous reactions requires a good enough description of the available specific surface area.

A change of availability of reactive surface during reactions was considered by Wurzenberger et al. [45]. In their definition of reaction rates of char conversion, the amount of unreacted char was linked to an experimentally defined exponent, which expressed the change of reactive sites [114,115]. This experimentally defined exponent is highly dependent on operation conditions.

A detailed description of the evolution of the specific surface area evolution is lacking in current works. In order to reduce uncertainties related to char conversion modeling, a detailed knowledge of time dependent change of active sites and specific surface area is required.

After having focused on the main chemical processes of thermal conversion, the required data for physical characterization of woody particles are reviewed.

4.5. Dimensionality

Describing the thermal conversion of a single thermally thick biomass particle with a one-dimensional model is a very common simplification [1,5,7,8,10,34,35,37,38,40–54,58–60,63,64]. Utilizing a one-dimensional modeling approach effectively reduces both the complexity and required computation time of the model. On the other hand, the anisotropic structure of wood cannot be taken into account by 1D approximations, as this aspect has to be managed by multi-dimensional modeling approaches. Two-dimensional [36,39,56,57,62] and three-dimensional [55,61] single particle numerical models exist in the literature, but they are rare. A more detailed discussion on dimensionality of models follows hereafter.

4.5.1. One-dimensional interface-based models

In so-called interface-based models, the chemical reactions and phase changes take place at the boundaries between different layers in the particle. The layers are composed of either wet virgin wood, dry wood, char or ash, and the thickness of these layers is defined by the available mass of these solid compounds. A pre-requisite for the interface-based models is that chemical reactions, as well as phase changes, are much faster than the intraparticle diffusion of heat and mass. Only then can one assume very sharp fronts, thus indicating that the reactions are limited to very narrow regions only. These models can only be applied if the Biot number and thermal Thiele modulus describing the ratio between characteristic heat penetration time and devolatilization reaction time are large [8].

In the layer model, due to conversion of the fuel particle, solid matter leaves one layer to enter the layer assigned to the next conversion stage and the drying, devolatilization and char combustion fronts move from the surface to the center of the particle [44]. Thunman et al. [44] adapted the concept of infinitely thin reaction fronts from Saastamoinen et al. [79] (only done for drying in their work), and assumed that devolatilization (and char conversion) also occurs in such infinitely thin reaction zones. This modeling work [44] has been the basis for a number of following models [5,7,8,10,52,53]. Galgano et al. [60], called their approximation a “front-based model”, which still describes the same phenomena as all interface-based models.

The layer models are related to a high numerical efficiency and rather decreased computational cost, mainly due to the fact that only a somewhat limited number of governing equations is solved, and also partly due to a rather coarse spatial discretization in the interior of the wood particle. In fact, only equations for temperature and mass have to be solved in the layer model. Mehrabian et al. [10] found that the layer model resulted in the same accuracy as the much more extensive model by Lu et al. [78,116], who solved a set of 14 governing equations, whereas the layer model by Mehrabian et al. [10] only contains the energy and the mass equation. At the same time, their layer model was significantly faster.

A conclusion is that if the main purpose of the solid phase model is to be coupled with CFD simulations of large-scale furnaces, in which a bed has to be modeled, a reduced computational cost is the most relevant aspect and the layer model is considered a suitable choice. The solid phase models are also used to describe large wood log conversion in a heating unit. However, if the purpose of the wood degradation model is to predict crack formation and the transportation of species inside the pores, the interface-based models are not suitable. In such cases, mesh-based models are recommended.

However, the low robustness of the interface-based model can still be considered as a weakness of the model, independent of its application purpose. The sharp fronts where reactions occur result in mathematical discontinuities, which may cause numerical instabilities [8].

4.5.2. One-dimensional mesh-based models

In a mesh-based model, the equations for thermal conversion are related to grid points. The particle is therefore fully discretized. One-dimensional mesh-based models are applied by many authors [1,34,35,37,38,40–43,45–48,54,64] and solve a higher number of governing equations than the layer model, which inevitably leads to higher computational costs. Accordingly, these models need to be significantly simplified if coupled to CFD simulations, and if they are aimed to be able to compete with the numerical efficiency of layer models. Nevertheless, if reasonable simplifying assumptions can be found and computational costs are low, it is assumed that mesh-based models provide much more information than the layer model, e.g. since also liquid and gas phase can be modeled in detail.

4.5.3. Two-dimensional models

Sand et al. [56] as well as some other researchers [36,39,62] developed a higher dimensionality model, which is rarely done as the current focus is on 1D. They also considered anisotropy to some extent and modeled wood logs of very large sizes, which are comparable to what is used in wood stoves. Di Blasi [36,39] has also accomplished work within the field of 2D modeling of wood degradation. By considering anisotropy, one expects an asymmetric velocity field that affects heat and mass transfer. Di Blasi [39] found that heat conduction, both across and along grains, differs. It was found that the propagation of a devolatilization front inwards is first faster across the grain direction, because a larger surface heat flux occurs in that direction. However, the difference between across and along the grain continuously decreases with time, since for longer times the influence of convective transport values decreases (less cooling along the grains). Furthermore, the thermal conductivity across the grain directions is smaller than the thermal conductivity along the

grain direction. Di Blasi [39] found that 2D and 1D models yield results that are quantitatively relatively similar. 1D models showed slightly lower temperatures and velocities of gases in the pores of the wood particle in the cross-grain direction compared to 2D models. Consequently, the propagation of a conversion front was predicted to be slower, the final char density higher and the conversion times longer. Along the grain direction, 1D models over-predicted temperatures and velocities, which resulted in faster propagation speeds and reduced char densities [39].

Overall, it is important to consider that the discrepancy between 1D and 2D modeling results increased with an increasing particle size, so it is suggested that large wood log modeling requires 2D or even 3D models [39].

4.5.4. Three-dimensional models

The three-dimensional model of Kwiatkowski et al. [61] was based on the discretization of a wood cylinder in a mesh composed of hexahedral elements of 0.1 mm, which was found to be sufficient for solving the temperature gradient inside the particle. Yuen et al. [55] developed a three-dimensional model for the pyrolysis of wet wood with a detailed consideration of the drying process, anisotropy and pressure-driven internal convection of gases. The main disadvantage of 3D models is the higher computational cost, compared to 1D and 2D models. Higher dimensionality models are recommended if anisotropy is investigated or the influence of highly varying boundary conditions is considered. Furthermore, due to the fact that radial and tangential properties do not vary significantly, 3D models will not necessarily result in a significantly higher accuracy compared to 2D models. However, no comparison between 2D and 3D models has yet been made, and it is therefore recommended that future research investigates the difference between these two approaches.

4.6. Feedstock

Feedstock can vary in many aspects, such as particle size, shape, density, wood species and therefore also thermo-physical properties. Different values for certain properties of wood, relevant for thermal conversion, are used in current models. Some models are derived for the combustion of wood logs [1,41,49–51,56,63] or smaller wood particles [5,7,8,10,34–40,42–48,54,55,57–62,64] and others for densified wood [1,52,53]. Even though densified wood models are partially relevant, since intra-particle gradients are modeled, they are less relevant for wood log-fired heating applications. Most of the differences between densified and non-densified wood are due to different fuel properties, such as a higher density for compressed wood, as well as a lower porosity, lower water content and anisotropy. The thermochemical degradation process of densified wood will therefore be different from what is expected in wood log applications.

4.6.1. Isotropy

The assumption of isotropy is rather obvious when the conversion of densified wood is modeled. The densification process, including grinding of the wood to sawdust size particles, which is required for pellet formation, leads to homogeneity in the physical-mechanical characteristics of solid fuels [23]. Models for densified wood are commonly based on the assumption of isotropic conditions [1,7,10,52,53]. Raw wood should be considered an anisotropic material. For undensified wood particles and logs, the isotropic assumption is nevertheless applied in many models [5,7,8,10,34,35,37,38,40–51,54,57–64]. In other works, the anisotropy of wood is taken into consideration by using a bridge factor [1,56]. This simplified consideration of anisotropy of wood is based on averaging between parallel-to-the-grains- and perpendicular-to-the-grains-properties, and does not account for actual properties that depend on different directions. This consideration can be considered as an intermediate step between the fully isotropic and fully anisotropic modeling of a wood log. Only a very limited amount of work has been done by actually implementing anisotropy, and consequently developing a higher dimensionality model without the usage of the bridge factor [36,39,55]. E.g. Yuen et al. [55] developed a 3D model, while Di Blasi [36,39] as well as Pozzobon et al. [62] implemented a 2D model. Due to this, it is of interest to focus on the influence of anisotropy on modeling predictions in the future.

4.6.2. Particle shape

It has been found that the particle shape has a significant influence on thermal conversion and that spherical particles have a lower mass loss rate than non-spherical particles. This is related to the smaller surface to mass ratio of spherical particles, which results in lower heat and mass transfer [10]. In the case of the layer model, a geometrical shape factor is used to model different shapes of the particle, and it was found that the layer model can sufficiently well describe the thermal conversion of particles of various shapes [10].

However, there is no model currently available that works with an irregular shaped particle, and the influence of cracks on thermal conversion is hardly ever included in a model. The particle shape is commonly assumed to be well-defined, though this is not the case, since wood particles are very irregular in most combustion applications. Therefore, it is of interest to identify how a more realistic description of particle shape affects the accuracy of the model.

It is not only that the virgin wood particles do not have ideal spherical or cylindrical shapes; the shape of the biomass char particles can be even more irregular. They are highly affected by the influence of the lignin structure of parent wood species, and by the mechanical process applied to form the wood particle [57].

It is therefore suggested to include the irregular shape of a particle undergoing thermal conversion. However, a very detailed description of the irregular shape of a particle and its evolution over time is expected to result in high computational cost as this will also require multi-dimensional models. Consequently, future models are challenged to find a balanced approach, including the description of high irregularity of particles while being computational low-cost models.

4.6.3. Particle size

The size of the particles varies from application to application, however, all the modeling approaches presented here are derived for predicting the thermal conversion of thermally thick wood particles and logs. Sadhukhan et al. [58] investigated a range of different particle sizes (the maximum being 10 cm and the minimum 1 cm). Their purpose was to identify the influence of the particle size on the entire devolatilization process. They found that the particle size has a significant influence on the history of the residual solid mass fraction, and accordingly the devolatilization time. The particle size influences when certain conversion stages are reached, even though the final residue mass fraction does not vary significantly.

In a particle thickness range of 0.1 cm - 2.0 cm it was found that for smaller particles, a high enough heat flux can result in a fast production of tar and permanent gas, and the leaving gases leave immediately, resulting in a single peak of leaving mass flow [64]. For larger particles, two peaks were found for the mass flow leaving the particle, which is related to an increasing influence of the char layer, which prevents the pyrolysate from exiting immediately [64].

Very few numerical simulations [41,56] have been performed on the thermochemical degradation and combustion of wood logs with sizes of the order of what is used in domestic wood stoves. Future work is therefore also encouraged to enhance research within the field of large wood log modeling. It is of interest to investigate how such comparably large particles and their shrinkage affect thermal conversion times and above all product yields, as it is expected that in case of such large particles the impact of the

char layer building up around the unreacted wood particle center has a significant influence. It is also assumed that leaving tar has a much longer residence time within hot char layers, so it is of interest to investigate to what degree the tars are converted within the char layer.

4.6.4. Density

Various wood species, and therefore also varying densities, are found in the existing literature. This variation limits the potential comparison of the modeling results (Table 5).

Based on a reference literature [33], that provides detailed information about wood and its properties, including density, the authors now investigate if the applied densities, used in current models are consisted. By investigating if the density is suitable for modeling a certain wood species, the authors were able to present a database for different wood species, that can be used for future model development. Furthermore, inconsistent values can outline that the model was fitted to agree with experiments. Bryden et al. [42] modeled basswood with a density of 420 kg/m^3, which deviates slightly from the reference density of American basswood, which is defined to be 380 kg/m^3 [33]. However, it has been concluded that the chosen density is still suitable for modeling basswood, since it is assumed that the choice of other fuel properties, e.g. thermal conductivity, will have a more significant effect on thermal conversion times and product yield predictions.

For beech wood, the values for dry wood density ranged from 680 kg/m^3 [7] to 750 kg/m^3 [46]. Overall, this span is comparably narrow, with American beech, as a representative of beech wood, having a density of 680 kg/m^3 [33].

In the case of birch wood, it was found that a much broader range of densities was applied. The value span reached from 410 kg/m^3 [41,56] to a maximum of 740 kg/m^3 [54,64]. Based on reference values from the literature for sweet birch and yellow birch, having densities of 710 and 660 kg/m^3 [33], respectively, it is concluded that

Table 5
Comparison of wood densities.[a] states that this is the specific density (oven dry cell-wall substance); [b] aims to differ between the density for different charcoal samples with different diameters. If no superscript is given, the apparent density is given, which is the density of wood, if porosity is taken into consideration. If "–" is in one cell of the table, this highlights that the information was not mentioned in the paper. Structuring of the table was done by wood species.

Ref.	Name and year	Wood species and/or type	$\rho_{dry,\ wood}$[kg/m^3]	ρ_{char}[kg/m^3]
[42]	Bryden et al. (2002)	Basswood	420	–
[46]	Bruch et al. (2003)	Beech	750	200
[7]	Mehrabian et al. (2012a)	Beech	680	–
[62]	Pozzobon et al. (2014)	Beech	701	–
[8]	Ström and Thunman (2013)	Beech and poplar	–	–
[55]	Yuen et al. (2007)	Beech	700	91.56
[64]	Ding et al. (2015)	Birch	740	–
[41]	Larfeldt et al. (2000)	Birch	410	150/ 100[b]
[56]	Sand et al. (2008)	Birch	410	125
[54]	Shen et al. (2007)	Birch	740	–
[44]	Thunman et al. (2002)	Birch/ spruce	540 (± 40)/ 420 (± 40)	1950[a]
[58]	Sadhukhan et al. (2009)	Casuarina wood	682	–
[36]	Di Blasi (1994),			
[39]	Di Blasi (1998)	Cellulose	420	–
[61]	Kwiatkowski et al. (2014)	compressed wood shaving	750	170
[1]	Biswas and Umeki (2015)	Densified wood (Pine and Spruce)	1100	1950[a]
[10]	Mehrabian et al. (2012b)	Densified wood (spruce)	1200	–
[52]	Porteiro et al. (2006),			
[53]	Porteiro et al. (2007)	Densified Wood	1480[a]	1957[a]
[59]	Haseli et al. (2012)	Douglas fire	504	50
[1]	Biswas and Umeki (2015)	Katsura tree	500	1950[a]
[37]	Di Blasi (1996)	Maple wood	650	–
[42]	Bryden et al. (2002)	Red oak	660	–
[60]	Galgano et al. (2014)	Oak	670	–
[59]	Haseli et al. (2012)	Oak	753	75
[34]	Alves and Figueiredo (1989)	Pine	590–640	–
[42]	Bryden et al. (2002)	Southern Pine	508	–
[59]	Haseli et al. (2012)	Pine	380	60
[59]	Haseli et al. (2012)	Plywood	462	60
[42]	Bryden et al. (2002)	Poplar	504	–
[47]	Bryden and Hagge (2003)	Poplar	504	–
[50]	Galgano and Di Blasi (2006)	Poplar	460	–
[51]	Galgano et al. (2006)	Poplar	460	–
[43]	Hagge and Bryden (2002)	Poplar	504	–
[7]	Mehrabian et al. (2012a)	Poplar	545	200
[10]	Mehrabian et al. (2012b)	Poplar	545	200
[59]	Haseli et al. (2012)	Redwood	354	50
[40]	Grønli and Melaaen (2000)	Spruce	450	–
[59]	Haseli et al. (2012)	Spruce	450	60
[7]	Mehrabian et al. (2012b)	Spruce	420	–
[57]	Yang et al. (2008)	Willow	820	–
[48]	Babu and Chaurasia (2004)	–	650	–
[35]	Koufopanos et al. (1991)	–	650	–
[49]	de Souza Costa and Sandberg (2004)	–	360	–
[38]	Melaaen (1996)	–	550	–

the very low values of 410 kg/m^3 [41,56] are not consistent with what has been reported elsewhere.

The higher density of compressed wood compared to uncompressed wood is a good assumption, since a lower porosity is also expected in densified wood particles due to the densification process. The comparably low density found by Kwiatkowski et al. [61] makes it hard to identify a clear differentiation between uncompressed and compressed wood, as the density is rather typical for uncompressed wood, while still compressed wood shavings were tested.

Maple wood was modeled [37] with a density of 650 kg/m^3, which lies within the range of reasonable maple densities, whereby the maximum density is 660 kg/m^3 (maple, sugar) and the minimum value 500 kg/m^3 (maple, silver) [33]. The density for oak used in models [60] is also considered a suitable choice, since the overall values for oak densities found in the reference literature range from 660 to 720 kg/m^3 [33].

When comparing the pine density chosen for different models [34], it was found that the value agrees well with the reference pine densities [33]. Still, the overall range of potential pine densities is significant, with a minimum value of 370 kg/m^3 and a maximum value of 620 kg/m^3. In case of pine wood modeling, one must therefore specify the type of pine wood in more detail and choose the properties for modeling thermal conversion accordingly.

When modeling poplar, the applied densities range from 460 [50,51] to 545 kg/m^3 [7,10]. When compared to reference data [33], the lower density limit agrees with the density of yellow poplar.

Modeling spruce was done by assuming a density of 450 kg/m^3 [40], which exceeds the maximum reference value by 20 kg/m^3 [33]. However, it is assumed that this deviation is not very significant, since the density range of different spruce types ranges from 370 to 430 kg/m^3, such that the difference between chosen and maximum reference value is comparably small. The modeled Redwood densities [59] agree well, with the reference value for young growth Redwood being 370 kg/m^3 [33].

With respect to porosity, the documentation of applied values in the literature is scarce. Most commonly, only apparent densities of wood are given, and because there is no detailed information on either the porosity or true density of wood, no back-calculation or proper discussion can be performed. However, the conclusion is that if acceptable wood densities are used in the model, both for hardwood and softwood, a proper porosity has been chosen as well. Accordingly, one would expect that since the densities previously discussed agree well with literature data from the reference literature [33], the porosities applied in current models are within reasonable ranges. Fig. 11 shows what porosity is expected when assuming a true density of 1500 kg/m^3 [117] and relating it to the previously listed apparent densities, such that

$$\epsilon = 1 - \frac{\rho_{\text{wood apparent}}}{\rho_{\text{wood true}}} \tag{42}$$

is fulfilled and the corresponding porosity, ϵ, can be calculated. The true density, which is the density of the cell walls, is considered to be the same for different wood species [117], and accordingly the same true density was used for both hardwoods and softwoods. In Fig. 11, the porosities listed in some works were also plotted.

It is shown in Fig. 11 that porosity increases as density decreases, which fits with the theoretical understanding of the wood structure, containing a solid matrix and pores filled with gas (in case of oven-dry wood). A higher porosity indicates a higher volume filled with gas phase, which leads to a reduction in apparent density. As stated earlier, by discussing the agreement of chosen apparent densities in models with literature data, it was found that porosities also agree well with what can theoretically be expected for certain wood species. It was also found that the applied porosities, given in a limited number of works, agreed well with what would have been theoretically expected. When it comes to finding values for densities of different wood species, a broad range of values is available in the open literature. Accordingly, less uncertainties are expected to be introduced to models, by the choice of wood densities.

4.6.5. Thermal conductivity

The characteristics of wood vary along, across and tangential to the grains, which also affects heat and mass transfer. Thermal conductivity across- and tangential to the fiber direction is approximately one-third of the thermal conductivity along the grains [39]. The effective thermal conductivity of green wood is defined as [22]

$$k_{\text{eff,s}} = k_{\text{cond}} + k_{\text{rad}} \tag{43}$$

where k_{cond} and k_{rad} are the conductive and radiative contributions, respectively. The conductive part is a function of the thermal properties of the fibers, bound and liquid free water and gas [22]

$$k_{\text{cond}} = f(k_{\text{fiber}}, k_{\text{bound, liquid free water}}, k_{\text{gas}}). \tag{44}$$

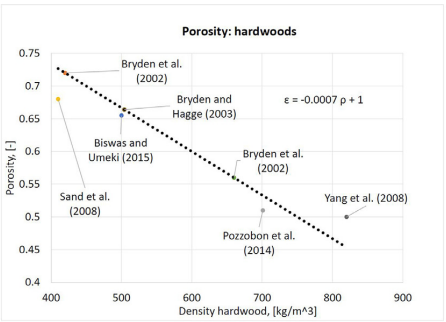

(a) Porosities of hardwoods. The plot shows the calculated porosities, obtained when using the apparent densities listed in models and a certain true density taken from the literature [117]. Given values for porosities found in literature were also added to the plot (single dots).

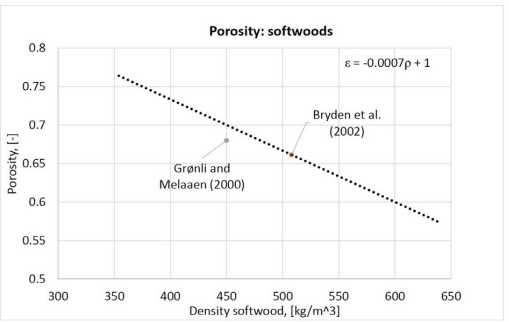

(b) Porosities of softwoods. The plot shows the calculated porosities obtained when using the apparent densities listed in models and a certain true density taken from literature [117]. Given values for porosities found in literature were also added to the plot (single dots).

Fig. 11. Porosities of different wood species plotted against the typical wood species density. (The calculated porosities are illustrated by the corresponding trendline (blue line)). (For interpretation of the references to color in this figure legend, the reader is referred to the web version of this article.)

The radiative term in the effective thermal conductivity is less important in green wood but becomes more influential as pore size increases, which is the case in the char layer. Furthermore, the radiative term in the effective thermal conductivity definition is influenced by the temperature to the power of three, and accordingly in the stage of char conversion, and for conditions where higher temperatures are expected, this term becomes significant.

Biswas and Umeki [1] use high conductivity values, but these values are given for cell walls. Multiplication with porosity leads to the actual thermal conductivity of dry wood

$$k_{\text{wood}} = k_{\text{cell wall}}(1-\epsilon_g). \tag{45}$$

It is also relatively common to combine the parallel and perpendicular thermal conductivities into one effective thermal conductivity, which is based on a fraction term that indicates the amount of material perpendicular to the heat flow (1-ξ) and parallel to the heat flow (ξ). Here, ξ is often referred to as a bridge factor. This modeling approach has already been discussed when discussing anisotropy modeling in 1D. The mathematical expression for this correlation is given as [22]

$$k_{\text{eff,s}} = \xi k_{\text{parallel}} + (1-\xi)k_{\text{perpendicular}}. \tag{46}$$

One of the weaknesses of the bridge factor is that it is actually often only used to fit modeling results to experimental results.

The choice of bridge factor has a significant influence on the temperature profile and conversion time, as shown in Fig. 12.

The bridge factor weights the actual thermal conductivity between a maximum value (parallel to the fiber direction, ξ = 1) and a minimum value (perpendicular to the fiber direction, ξ = 0). The faster heating related to pure thermal conductivity along the grains leads to faster conversion times and a lower residual solid mass. This significant influence highlights that not only does the value chosen for thermal conductivities have an influence on model accuracy, but also that the corresponding direction (parallel and perpendicular) influence heating to a certain extent. The bridge factor is a value that is found to fit model results to experiments, and a broad range of values is actually found in the literature [22]. Moreover, the bridge factor does not provide a detailed description of anisotropy, and is therefore considered a less complex method that can still provide reasonable predictions for temperature profiles and mass losses. Concerning a velocity field this bridge factor is however assumed to result in errors.

The most common dependencies of thermal conductivities are discussed hereafter, which includes the influence of densities and therefore wood species and temperature

As suggested by Simpson and TenWolde [33], it can be seen in Fig. 13 that the thermal conductivity (across the grain) increases with the wood density, which is the case for both softwood and hardwood. This correlates well with the general understanding that an increasing density is related to decreasing porosity, and accordingly the influence of the cell wall thermal conductivity increases, which as such is higher than the thermal conductivity of the apparent wood. Furthermore, one can clearly see that the dependency of the thermal conductivity on wood density is similar for hardwoods and softwoods. When comparing thermal conductivities across the grain used in models (listed in Table 3, plotted in Fig. 13 in dark blue diamonds) with values found for oven-dry wood in the reference literature [33] (light blue rectangles), the overall agreement was acceptable. Even though, especially at higher densities, the values deviate significantly, they were found to be acceptable, as it was claimed in the reference data [33] that the actual thermal conductivities can deviate by about 20% from the listed values ($k_{\text{ref, perp}}$ plotted in Fig. 13 (light blue rectangles)). The brownish line presents the trend line for thermal conductivities along the grain commonly used in models. One can clearly see that those values are significantly higher than the thermal conductivity across the grain [33]. The effective thermal conductivities applied in 1D models (see Table 3; marked by orange triangles in Fig. 13), mostly has a value between the thermal conductivity across and the thermal conductivity along the grain.

However, because there is no clear trend visible on how the thermal conductivities in the modeling works were chosen, it is suggested that they were chosen in such a way that modeling results fitted well with the experimental data.

Only a limited number of works [36,39,55,62] is available in which the anisotropy of wood was considered by setting different values for the thermal conductivity of wood and char, depending on the actual direction of heat flow with respect to the fiber structure in a multi-dimensional model.

The difference between perpendicular and parallel values is significant, as shown in Fig. 14.

2D models, e.g. [62], are based on the simplifying assumption that the radial and tangential values for thermal conductivity do not differ significantly. Accordingly, it was said that a 2D model will yield an acceptable accuracy. This difference in thermal conductivity depending on the direction in the wood log, suggests that accurate consideration of this property can only be done by multi-dimensional models.

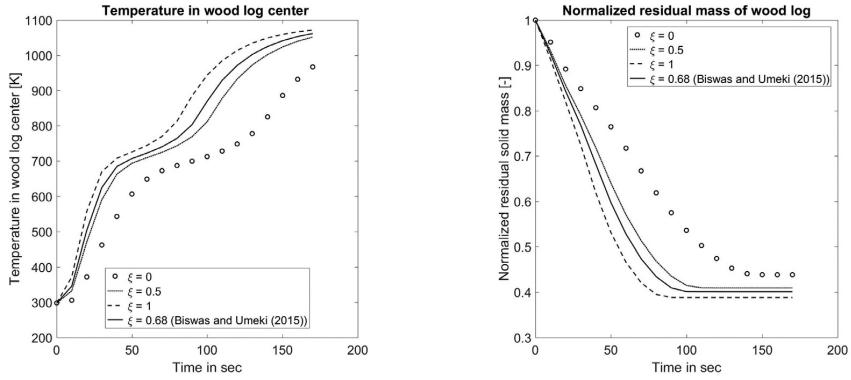

(a) Influence of bridge factor on core temperature profile.

(b) Influence of bridge factor on normalized residual mass and overall conversion time.

Fig. 12. Influence of different bridge factors on temperature and normalized residual mass. Different bridge factors were chosen to outline that the choice of bridge factor can significantly influence the accuracy of a model. The tested model was developed by the authors.

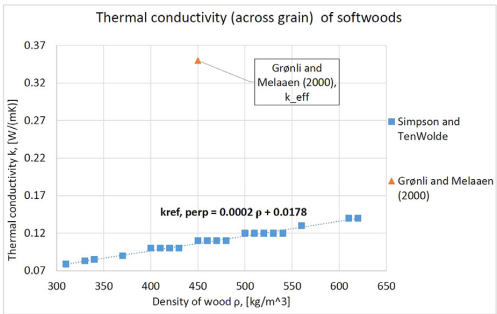

(a) Thermal conductivity of softwoods. Comparison of $k_{\text{eff.}}, k_{\text{perp.}}, k_{\text{parall.}}$

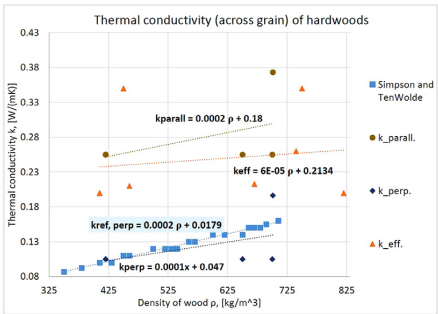

(b) Thermal conductivity of hardwoods. Comparison of $k_{\text{eff.}}, k_{\text{perp.}}, k_{\text{parall.}}$

Fig. 13. Thermal conductivity dependency on wood density for hardwood and softwood. The reference data used in this figure has been taken from Simpson and TenWolde [33] ($k_{\text{ref, perp}}$, light blue rectangles and trend-line). The residual data has been collected from models where it was given together with a wood species, listed in Table 3. If the wood species was not given, or no constant value of thermal conductivity of virgin wood was used, the value was not added to the figure. The thermal conductivities used in models plotted here were taken from [22,36,37,39–41,46,50,51,55–57,60,62,64]. (For interpretation of the references to color in this figure legend, the reader is referred to the web version of this article.)

The thermal conductivity of wood has quite often been described as a function of temperature, while other dependencies are neglected. Density dependencies have only been added by Bryden et al. [42,47] and Hagge and Bryden [43]. It has, however, not been modeled how this relation between thermal conductivity and wood density changes as wood density changes due to thermochemical degradation. Still, it can be assumed that it is a fair enough approximation in that case to model the change of thermal conductivity, as a linear interpolation between the thermal conductivity of wood and char such that the actual value is only defined by the degree of conversion. Further dependencies of the thermal conductivity of wood on either extractives or structural irregularities, which have been found for wood material [33], have not been included in any of the applied thermal conductivities for wood used in models listed in Table 3. Future research could therefore investigate how extractives and structural irregularities influence the modeling results, and whether the increased complexity due to their incorporation is balanced by the enhanced accuracy.

Furthermore, little information is given on the thermal conductivity of the pyrolysis gas. In [37,40,48,52,53], a thermal conductivity of 0.026 W/mK for the gas phase was used. In contrast to this, Sand et al. [56] used the thermal conductivity of propane (0.0176 W/mK) for modeling the gas phase. Reviewing a number of modeling works has shown that the thermal conductivity is commonly not adjusted based on the chemical composition of the gas phase. However, this simplifying assumption is reasonable, as the influence of the gas

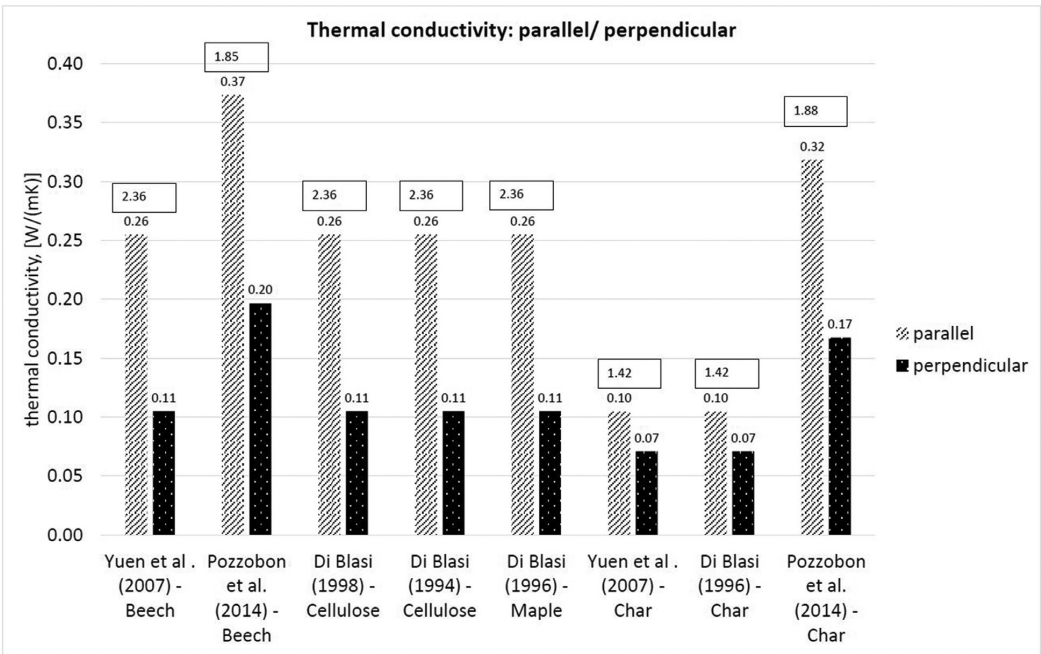

Fig. 14. Thermal conductivities parallel and perpendicular to the fiber direction. The numbers in the boxes represent the ratio between the two thermal conductivities.

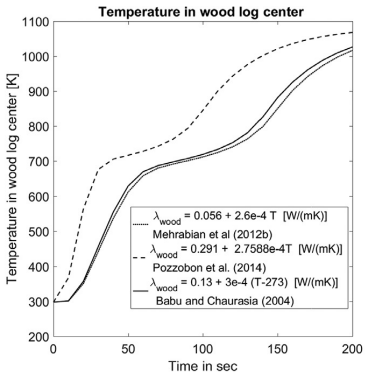

(a) Influence of thermal conductivity of wood on core temperature profile.

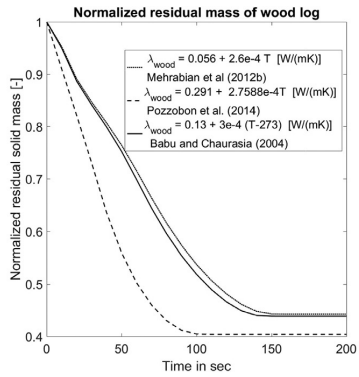

(b) Influence of thermal conductivity of wood on normalized residual mass and overall conversion time.

Fig. 15. Different temperature functions of thermal conductivity are compared. Their influence on normalized residual mass, conversion time and core temperature are compared. The thermal conductivity changed from the one for wood to the one for char as a linear function of the degree of conversion.

phase conductivity in relation to the influence of the solid phase conductivity on the temperature history in the wood log is less important.

In Fig. 15, the temperature function for the thermal conductivity of wood has been modeled as linearly conversion-dependent. The dashed line in Fig. 15 corresponds to the thermal conductivity of Pozzobon et al. [62], who modeled beech. Babu and Chaurasia [48] did not explicitly mention which wood species was modeled, but compared with the results by Scott et al. [118] and Pyle and Zaror [119], who were using maple and pine, respectively. Their thermal conductivity is presented by the solid line. Again, the weakness in their model is that they used the same properties for comparing hardwood and softwood experiments. The dotted line corresponds to the thermal conductivity used by Mehrabian et al. [10], who modeled poplar. In all three cases, hardwood was modeled, although the applied values differed quite a bit. One can also clearly see that by considering the increasing influence of formed char, permanent gas and tar, the heat transfer inwards slows done, as all these products have lower thermal conductivities compared to wood. A very reasonable finding is also that the residual solid mass is lowest at the highest heating rate (dashed line). In this case, the char yield decreases as the produced gaseous products increase. It is therefore clear that the thermal conductivity has a significant influence on the prediction of product yields, as well as the overall devolatilization time, ranging from approximately 100 s (dashed) to 140 s (dotted) for beech wood modeling when the thermal conductivity is a function of temperature and degree of conversion. After having reached the temperature plateau at roughly 680 to 700 K, the residual heating-up seems to be slower than the initial one (from start until the plateau). The reason for this is that the second increase is occurring after devolatilization has proceeded, so therefore only char, permanent gas and tar are left, all of which have lower thermal conductivities than wood. Accordingly, by only looking at the temperature increase, one can clearly identify three different stages: the first stage is related to the pre-devolatilization heating of the wood, as the thermal conductivity of wood dominates the heat transfer; in the second stage, the actual devolatilization, the endothermic reactions of primary devolatilization, dominate the temperature profile, and the plateau is formed. The third stage in the temperature increase is slower than the initial temperature increase, which is due to the lower thermal conductivities of char, tar and permanent gas, which dominate the post-devolatilization heating process.

In Fig. 16, it is shown how the temperature-dependent thermal conductivities of char influence the temperature history in the center of a wood log, in addition to the overall conversion time.

A low thermal conductivity (line marked with × in Fig. 16) yields a significantly larger amount of residual solid, which seems reasonable as the temperature increases very slowly and remains at around typical pyrolysis temperatures (< 500 °C) for longer times (compare line marked with × and line marked with +). Such a slower heating enhances char formation instead of the formation of permanent gas and tar. It can also be seen that initially neither the temperature profile nor the mass loss vary significantly by choosing different thermal conductivities of char. This seems reasonable, as at earlier conversion times the degree of thermal conversion is limited; thus, the influence of the thermal conductivity of wood dominates over the influence of the thermal conductivity of char. In this comparison, the thermal conductivity of wood has been the same for all four test cases.

It is shown in Fig. 16 that the applied thermal conductivities of char used in current models differ significantly. It is interesting that two temperature-dependent descriptions of thermal conductivity of char actually predict that thermal conductivity decreases as temperature increases [35,48,58]. As can be seen, this temperature dependency gives high discrepancy compared to what is obtained by a constant thermal conductivity or when increasing the thermal conductivity of char with increasing temperature.

After devolatilization reactions have been enhanced significantly at temperatures at approximately 700 K, the difference in the evolution of temperature and residual mass increases, thereby highlighting that the increased presence of char makes an accurate prediction of its thermal conductivity necessary.

Pozzobon et al. [62] were the only ones modeling thermal conductivity of char as a function of T^4. However, the overall validity of this function describing the thermal conductivity of wood has only been tested in a temperature range of 20 to 600 °C [120], which is rather low for gasification and combustion conditions. This significant change in thermal conductivity with respect to temperature is also the reason why it is found that using constant values, commonly around 0.1 W/(mK) [40–43,46,47,52–56,59,61] is yielding false prediction of the temperature history within the wood log, which can consequently affect product yield predictions.

4.6.6. Heat capacity

A wide range of different specific heat capacities of wood, char, ash and pyrolysis gases are used in the literature. The figures below

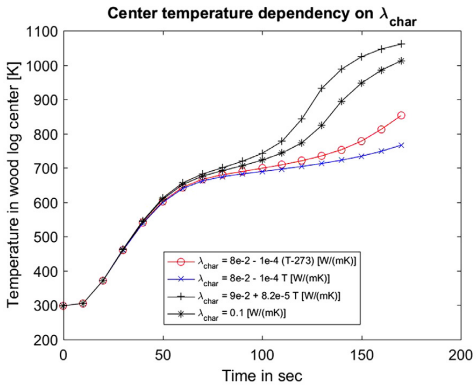

(a) Influence of thermal conductivity of char on core temperature profile.

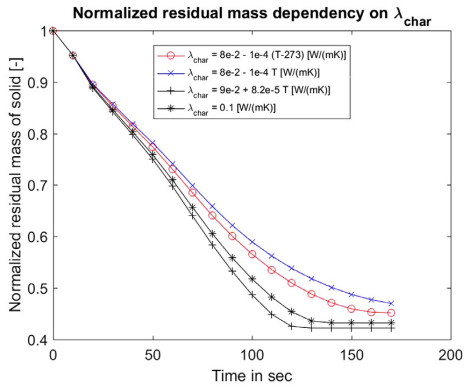

(b) Influence of thermal conductivity of char on normalized residual mass and overall conversion time.

Fig. 16. Different temperature functions of thermal conductivity of char are compared. Their influence on normalized residual mass, conversion time and core temperature are compared. The thermal conductivities were taken from what is used in current models [34,35,48,58]. Furthermore, it was modeled how a commonly chosen constant value for the thermal conductivity of char differs from temperature-dependent thermal conductivities. Again the authors' model was applied.

aim to illustrate the values used, not only for different wood species, but also for char and gases.

The following plots highlight that the choice of wood species is expected to have a significant impact on the choice of specific heat capacity, but only a limited amount of different values is commonly used in models.

Based on Fig. 17, it is suggested that a linear temperature dependency is a common modeling approach for describing the changing specific heat capacity of the virgin wood. It was found that the linear correlation applied by Bryden et al. [42] for oak wood leads to a significant increase of specific heat capacity as temperature increases. Devolatilization is expected to be finished at < 500 °C, and in such a range the values for specific heat capacity can still increase up to approximately 3000 J/kgK, which is considered very high. A higher specific heat capacity of approximately 3500 J/kgK for modeling oak has also been used [59]. This value exceeds all the other data found in literature and seems non-physically high. It is also expected that by pre-defining constant values for specific heat capacity, errors in the modeling results are significant, because in Fig. 17 it is obvious that constant values are commonly well below what is predicted from temperature dependencies. It is also concluded that the choice of specific heat capacity for wood species is ambiguous, in some modeling works [42] the same temperature dependency for both softwood and hardwood is used.

Furthermore, the same linear dependency applied by Mehrabian et al. [7,10] for poplar modeling has been used by Grønli and Melaaen [22,40] for modeling Norwegian spruce. Biswas and Umeki [1] have also used the same correlation when modeling the Katsura tree, which is classified as hardwood. As far as models based on pine wood are concerned, the choice of specific heat capacities is very random, since the specific heat capacity has been set to 1255.5 J/kgK [42] or 1150 J/kgK [59] in some works, which is significantly lower than other values, such as 1950 J/kgK [34].

From Fig. 18, it can be seen that the influence of specific heat capacity of wood on the temperature evolution and mass loss curve is less significant than the influence of thermal conductivity. It seems that the product yields with respect to solid residue are not significantly affected, even though the conversion time deviates, being shortest by choosing a lower constant value for the specific heat capacity of wood. Both temperature dependencies increase linearly, and there is hardly any difference between the two with respect to the modeling of the wood log center temperature and mass loss behavior. It is therefore concluded that the choice of a specific heat of wood is not the most sensitive parameter affecting accuracy of a model. A similar behavior is also expected for the specific heat of char.

It is obvious that a broad range of specific heat capacities of char is used in current models, having a maximum value of 2870 J/kgK at 890 K and a minimum value of 1225 J/kgK at the same temperature. Commonly linear temperature dependencies for specific heat capacities are modeled, which is assumed to be mainly due to their simplicity with respect to implementation in numerical codes. The inconsistency in the chosen value for specific heat capacity of char leads to the conclusion that this property is considered a main source of error in current models.

It has to be pointed out that the produced char yield, its composition and therefore also its properties are expected to vary depending on operational conditions. Accordingly, one expects a broad range of values. It also has to be pointed out that the parent fuel can also affect the composition of the produced char; hence, one expects that this leads to a broad variation in values for specific heat capacities for char. Nevertheless, the main reason for such an ambiguous choice of values as shown in Fig. 19 is expected to be due to the general lack of data based on a detailed analysis of the char produced from different wood species. Therefore, future research should focus more on collecting detailed data on specific heat capacities of char, depending on varying operational conditions and parent fuels.

Larfeldt et al. [41] provided the only model where specific heat capacities for wood and char were calculated from thermal diffusivity. The relation between thermal diffusivity and specific heat capacity was such that

$$\alpha = \frac{k_{\text{eff}}}{c_{\text{P,s}}\rho_{\text{s}} + \epsilon_{\text{g}} c_{\text{P,g}} \rho_{\text{g}}^{\text{g}}} \approx \frac{k_{\text{eff}}}{c_{\text{P,s}}\rho_{\text{s}}}. \tag{47}$$

The final approximation suggests that the influence of the gas phase can be neglected in the definition of the thermal diffusivity since the solid phase dominates over the contribution of the gas phase. We have shown that applying constant values in a model affects the accuracy of the modeling results. Still setting constant values for specific heat capacity for wood species, char and gases is a common modeling approach [34,37,39,51–53,56,60,61,64].

When analyzing the specific heat capacities of gases, the span of values is significant. Moreover, it is also shown in Fig. 20 that the influence of increasing temperature on the specific heat capacity is

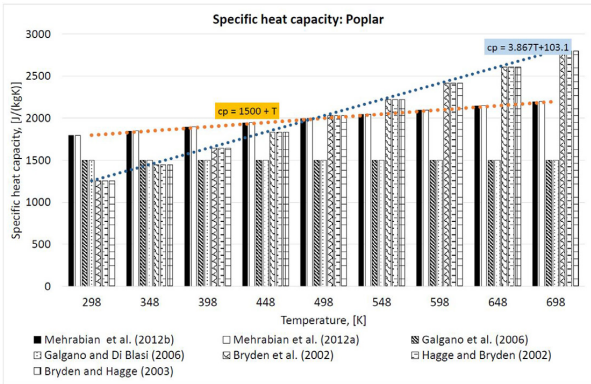

(a) Specific heat capacities for poplar wood.

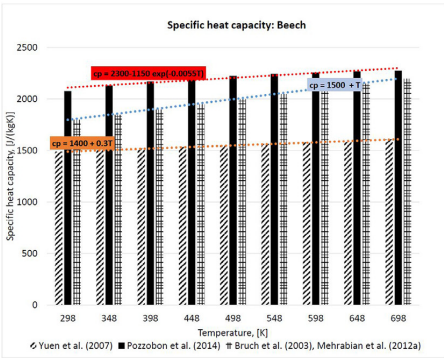

(b) Specific heat capacities for beech wood.

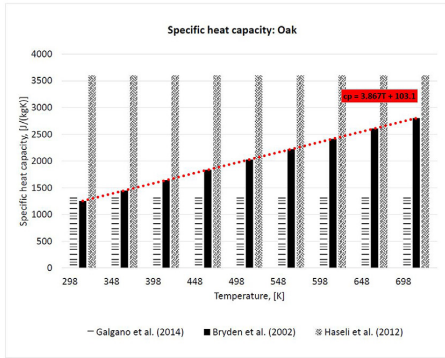

(c) Specific heat capacities for oak wood.

Fig. 17. Specific heat capacities for commonly applied wood species. These figures aim to show that the specific heat capacities of wood are expected to vary depending on the wood species, and that modeling specific heat capacities as temperature-dependent or constant, can have influence on the modeling results.

hardly considered in any model. The highest constant value applied, 2400 J/kgK [42,43,47,54] exceeds the lowest constant value by 1300 J/kgK [37–39,41,49,52,53,56] so it is also assumed that the modeling results are affected by the choice of specific heat capacities. Yet, the overall influence of the specific heat capacity of gases is negligible compared to the influence of specific heat capacities of solids, since the effective specific heat capacity influencing the heat equation is mass-averaged. For this reason, the higher mass

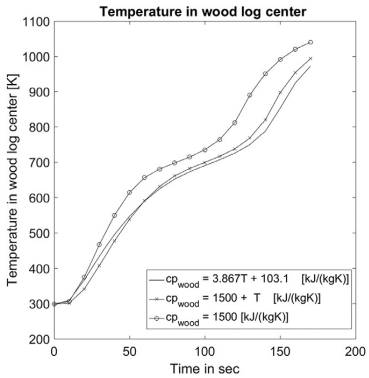

(a) Influence of specific heat capacity of wood on core temperature evolution.

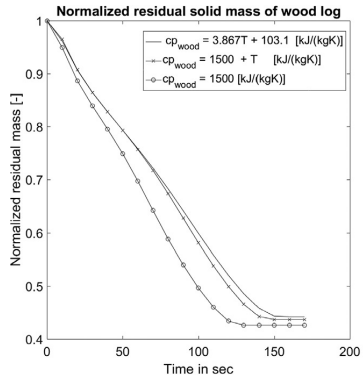

(b) Influence of specific heat capacity of wood on normalized residual solid mass.

Fig. 18. Different temperature functions for the specific heat capacity of wood are compared. Their influence on normalized residual solid mass, conversion time and core temperature are also compared. The values of specific heat capacity have been taken from reference literature [33] and models [10,37].

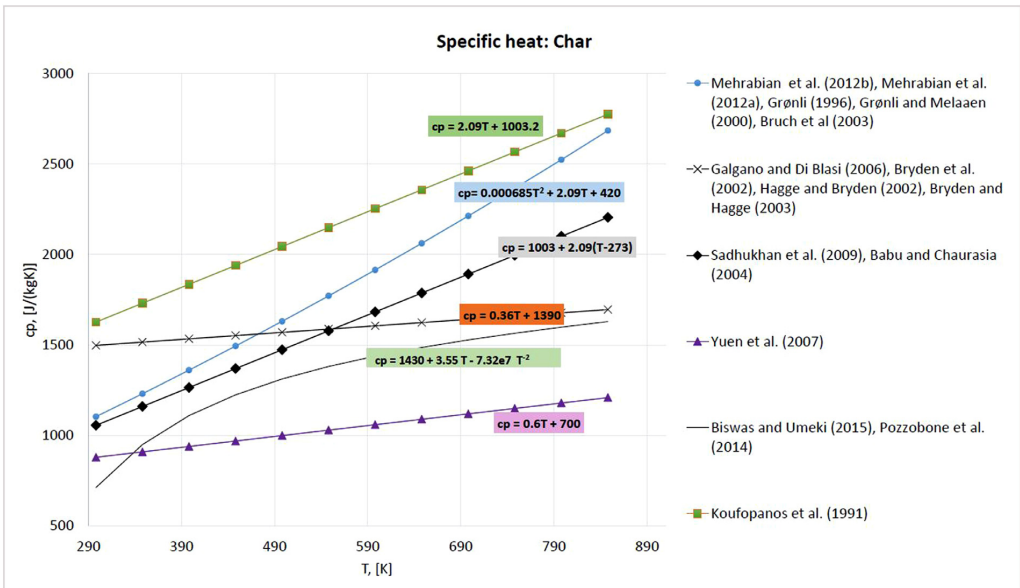

Fig. 19. Specific heat capacities of char. The applied specific heat capacities of char of different models are compared here. Temperature-dependent values are shown.

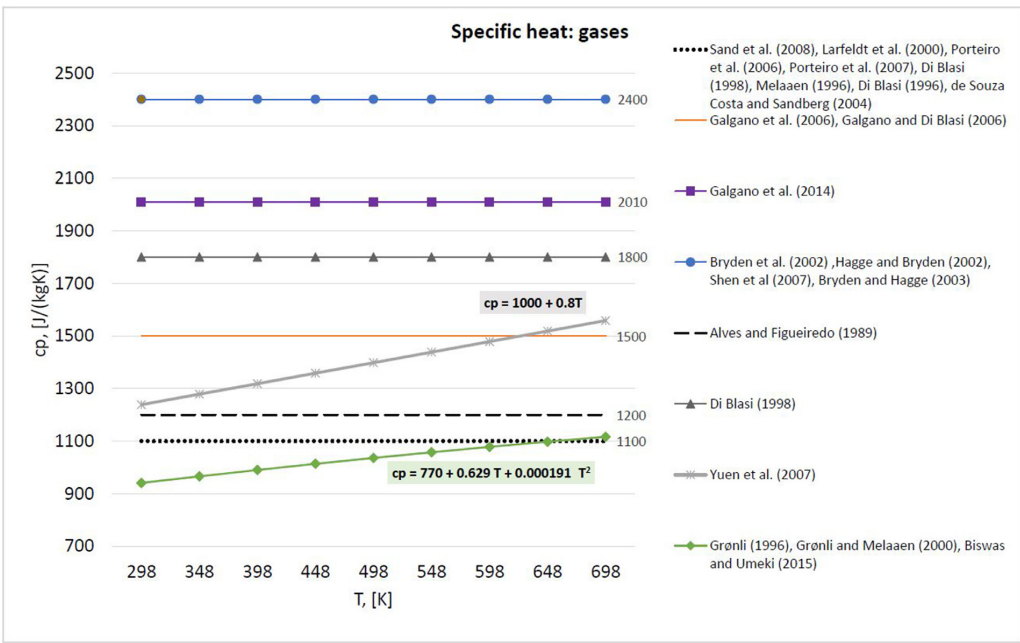

Fig. 20. Specific heat capacity of gases. The applied specific heat capacities used in different models are compared here. Constant values are compared against temperature-dependent values.

of the solids leads to a higher influence on the specific heat capacities.

Furthermore, the specific heat capacity of gases should consider the composition of the gas phase. Detailed knowledge of this composition cannot be easily acquired, since the reacting wood already includes a broad range of chemical compounds. As detailed knowledge on gas phase composition is commonly not included in current numerical models, a corresponding value for specific heat capacity of the gas mixture is also related to approximations.

4.6.7. Permeability

The gas flow inside the wood particle is strongly affected by the wood structure, which consists of a large number of small pores. The pore walls act as a barrier for the bulk flow moving from one neighboring pore to another [56]. The permeability is much lower in radial and tangential directions than along the wood grain.

One expects differences in permeability, not only between virgin wood and char, but also between hardwood and softwood. It can be seen from Fig. 2 that softwoods have slightly lower densities, as the plotted range is from 330 - 620 kg/m^3, while hardwoods have higher densities, ranging from 370 to 770 kg/m^3. It has to be pointed out that some wood species within these two groups can be either below or above the range limits mentioned here, though most of the species will have densities within these limits. Accordingly, it can be assumed that softwoods have either more pores or a larger pore size, since both would contribute to lower apparent wood densities. Thus, one would assume that the permeabilities of softwood are higher than the permeabilities of hardwoods.

As can be seen from Fig. 21 only limited conclusions can be drawn in case of softwoods, as very few models were based on softwoods and included the influence of convection on heat and mass transfer; and thus had to provide information on permeabilities. As previously mentioned, it is concluded that the choice of permeability is still related to a high uncertainty, which can also be seen from the large spread of data points in Fig. 21. Bryden et al. [42] used the same permeabilities for softwood and hardwood. One reason for this might be that the overall availability of data on wood permeabilities is rather limited. However, it can still be seen that the lowest permeability for hardwood is as low as approximately 10^{-17} m^2, which is much lower than what has been used for modeling softwoods. This agrees with a previous theoretical conclusion, that flow is more facilitated in softwoods. With respect to char permeabilities, however, no significant differentiation between hardwood and softwood derived chars can be found in the literature. Still, it can clearly be seen that due to an increasing porosity in char compared to wood, the permeability of char is much higher than the permeability of virgin woods.

A reasonable choice of permeability is needed in order to correctly compute the pressure field in the interior of the wood particle. Furthermore, it has to be pointed out that due to the anisotropy of wood, it is recommended to at least develop a 2D model, because different values for permeability with respect to the fiber direction can then be applied. It is consequently assumed that the pressure in the interior of the wood particle can be predicted more accurately and consequently also the velocity field. This has not been a primary concern in past research, even though it is assumed that the correct prediction of the pressure results in a good prediction of crack formation. Such an accurate prediction of the physical change of the wood particle can affect the modeling results of overall conversion times and product compositions as well as temperature history.

However, it has been found that the choice of permeability is a major uncertainty of thermal degradation and combustion models for wood particles. It has also been the case in a number of works [39] that the permeability was simply defined by fitting the modeling results to the experiments. If so, the physical validity of the used permeability cannot be taken for granted.

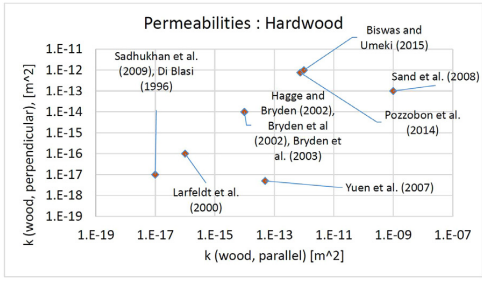

(a) Permeabilities for hardwoods, parallel and perpendicular to the fiber direction.

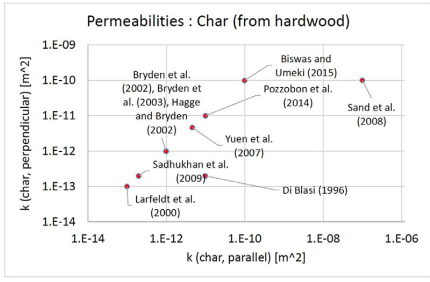

(b) Permeabilities for chars derived from hardwoods, parallel and perpendicular to the fiber direction.

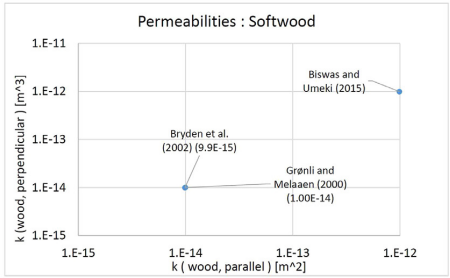

(c) Permeabilities for softwoods, parallel and perpendicular to the fiber direction.

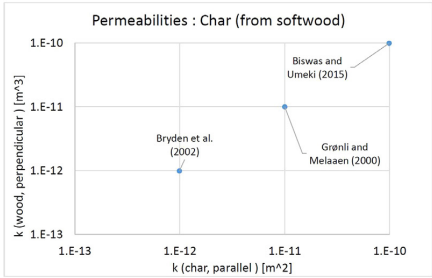

(d) Permeabilities for chars derived from softwoods, parallel and perpendicular to the fiber direction.

Fig. 21. Different permeabilities applied for modeling convection within the porous structure of wood and the char layer that is forming around it due to ongoing devolatilization.

4.6.8. Shrinkage modeling

The ratio between the decreased dimension and the initial dimension is what is defined as shrinkage [43]. Shrinkage during devolatilization varies with respect to the direction in the wood log. Because of this, shrinkage can only be accurately replicated in a 3D model, while 1D models instead focus on shrinkage in only one preferential direction, e.g. commonly radially in the case of cylindrical wood logs or particles. Such a simplifying assumption is commonly done in a number of 1D models, e.g. [1,43,61]. Then again, none of these works focuses explicitly on the distortion of a wood particle during volumetric shrinkage. Therefore, future research is recommended to focus on such physical changes in wood particles to help identify the extent to which they affect heat and mass transfer and the structure and shape of wood logs.

There are two different and broadly used approaches for modeling the shrinkage of a particle during devolatilization. The first shrinkage model was introduced by Di Blasi [37], and is based on three parameters. The main assumption of this model is that the volume first occupied by the solid is linearly reduced with the wood mass, while it is increased by the increasing char mass. The correlation describing to what extent the volumetric shrinkage is increasing linearly with the char mass is described by the first shrinkage factor, α. Also, the gas volume contribution to the entire volume changes during devolatilization. The gas phase volume includes two contributions by itself, which are the initial gas phase volume and the fraction β, describing which amount of the solid volume is added to the gas phase volume due to conversion reactions. The third parameter of the shrinkage model, γ, accounts for internal structural changes, such as a porosity increase as devolatilization proceeds [20]. Accordingly, these three parameters are not related to the common definition of shrinkage factors as described by Hagge and Bryden [43]. A significant uncertainty of this three-parameter model is that the choice of values for the three parameters is rather ambiguous. They are not derived from any experiments, but are chosen to fit the model to the experimental data. Additionally, it is not yet known whether these three parameters are affected by intra-dependencies or not, even though the current version of the shrinkage model assumes that α, β and γ are independent from each other [18].

Hagge and Bryden [43] used a one-parameter approach for modeling shrinkage. The basic idea of this model is the constant intrinsic densities of char and wood, and shrinkage is assumed to linearly depend on the degree of conversion of the solid. This does not entirely agree with experiments, in which it was shown that shrinkage commences later than the mass loss during devolatilization reactions [121,122]. In order to express this correlation, the shrinkage factor is introduced, which can mathematically be expressed as [43]

$$f = \frac{\text{current dimension}}{\text{original dimension}} = \frac{\Delta y}{\Delta y_0}. \tag{48}$$

However, this equation outlines that cracking is commonly not considered when discussing shrinkage factors, and it further highlights that in most works such shrinkage factors are related to a certain direction, e.g. radial or longitudinal. For example, Eq. (48) only considers shrinkage across the grains, since Δx and Δz remain unchanged. A disadvantage of this shrinkage consideration is actually that the shrinkage factors have been experimentally obtained by Bryden and Hagge [47]. The factors were related to the final char dimensions, which are provided in the final shrinkage values. A simplifying assumption for deriving a suitable mathematical expression for shrinkage from measured values is therefore obtained by assuming that the char dimensions decrease, but that there is no fragmentation [47]. Accordingly, one can conclude that for the restricted modeling of shrinkage during devolatilization, the mentioned simplifying assumption yields an acceptable mathematical description of shrinkage. Even though the mathematical derivation of shrinkage is acceptable, the validity of the overall description of shrinkage is restricted because of the experimentally derived values for shrinkage factors, suggesting that these are only valid in a limited range of operational conditions.

The one-parameter model has been applied in many different works [1,5,8,43,44,47,52,53,58,62]. Sadhukhan et al. [58] found that particle shrinkage during devolatilization led to a reduced heat transfer area. As a result, it was found that more heat, mainly obtained from exothermic secondary tar reactions, was kept inside the particle, resulting in a higher center temperature of the particle than the temperature at the surface.

The most simplifying assumption, however, is that shrinkage can be neglected, and that the particle volume therefore stays constant during drying and devolatilization [22,36,39,40,63]. Nonetheless, it is assumed that this assumption is not very realistic, since wood loses roughly 80% of its organic mass during devolatilization; hence, such a significant conversion of the solid to gas phase is assumed to have a significant influence on the physical structure of a wood particle. A critical aspect of neglecting shrinkage in the model is that the validation of the model against experiments is highly inaccurate, as shrinkage will always occur in an experimental investigation on the thermal conversion of wood samples. However, a suitable assumption for an acceptable validation was presented by Grønli and Melaaen [40], as they neglected shrinkage in their devolatilization model, but compared the results against experiments of spruce wood, which was heated in parallel with the grain. The reasoning is that in the axial direction only, a low shrinkage is expected, and it is most reasonable to compare the obtained experimental results with a non-shrinkage model.

Shrinkage modeling is usually highly dependent on pre-defined shrinkage parameters. The derivation of those parameters, commonly either experimental or based on assumptions, is a main weakness of current models, as it cannot be easily and flexibly changed to different operational conditions and wood species.

5. Homogeneous gas phase reactions

The released permanent gases, including released combustible gases obtained from char conversion, enter into the freeboard (which is the gas phase area above the wood log), where they are eventually oxidized. The consideration of this homogeneous gas phase reaction is very significant, as the temperature increase resulting from the oxidation further heats up the wood log, so that drying, devolatilization and char conversion reactions can proceed. Accordingly, a discussion of those reactions is required in connection with a discussion of the thermal degradation of a solid wood particle in a combustion unit. Please note that gas phase combustion is also discussed in connection with a relevant application in the chapter on small-scale furnace modeling, where particularly turbulence and combustion models are discussed.

The relevant reactions of homogeneous gas phase reactions are [23]

$$CO + 0.5O_2 \rightarrow CO_2, \tag{R6}$$

which is commonly considered in the freeboard of current domestic wood heating appliances [50,51,123–126]. In some cases, the complexity of the homogeneous reaction model is further enhanced by also considering CO_2 dissociation [124]. This reaction is only relevant at very high temperatures though. Hydrogen oxidation;

$$H_2 + 0.5O_2 \rightarrow H_2O \tag{R7}$$

has also been modeled in small-scale wood heating appliances [50,51,124–127], since it is expected that hydrogen is one of the main compounds of the volatiles released during the devolatilization of a wood particle. The increasing importance of H_2 with respect to increasing temperature has been discussed earlier [19], and as such,

it seems reasonable that a high temperature conversion processes, such as that occurring in e.g. wood stoves, requires the explicit consideration of this homogeneous gas phase reaction.

Regarding combustion of methane it can be modeled in two different ways, either as a full oxidation [50,51,127];

$$CH_4 + 2O_2 \rightarrow CO_2 + 2H_2O \quad (R8)$$

or as a partial oxidation, as is done by Porteiro et al. [124];

$$CH_4 + \frac{3}{2}\ O_2 \rightarrow CO + 2\ H_2O. \quad (R9)$$

Huttunen et al. [126] also described incomplete oxidation of methane to carbon monoxide, similar to what is shown in equation (R9).

In addition to modeling light hydrocarbon oxidation, such as the oxidation of methane, more complex hydrocarbon structures than methane can also be included in homogeneous gas phase modeling, e.g. [124]

$$C_6H_6 + \frac{15}{2}\ O_2 \rightarrow 6\ CO_2 + 3\ H_2O, \quad (R10)$$

which is modeling the combustion of heavy hydrocarbons released from a wood particle undergoing thermal conversion.

In addition to the previous reactions, the water-gas-shift reaction

$$CO + H_2O \rightarrow CO_2 + H_2 \quad (R11)$$

is also of interest [50,51,126], as it can be important for staged combustion units that have more gasifier-like conditions in the primary stage.

Only in a limited number of works has a differentiation in homogeneous gas phase modeling been done by modeling saturated and unsaturated hydrocarbons. Saturated hydrocarbons contain only single bonds, while unsaturated hydrocarbons can also contain double or triple bonds. Tabet et al. [128] assumed that the released saturated hydrocarbons (CH_{X_1}) decompose to unsaturated hydrocarbons (CH_{X_2}), which then react to CO. This CO is then combusted to CO_2. In addition, nitrogen containing species are released from the degrading wood particle, and consequently, NO_x formation has to be modeled.

5.1. NO_x formation

So far, none of the described reactions consider the influence of nitrogen-containing gas phase species. The influence of fuel-bound nitrogen is relevant when modeling thermal wood degradation and combustion, as the parent fuel contains a certain amount of nitrogen. The nitrogen released from the wood during devolatilization and char conversion is not considered in any of the single particle models. Not even the detailed Ranzi scheme [27] can describe the release rate of either NH_3 or HCN from wood, which will be the main precursors for NO_x (from fuel-bound nitrogen). Some researchers developed post-processing [129] models for NO_x formation. This simplification can be justified because NO_x reactions have very little influence on the combustion nor the fluid itself.

Due to the relatively complicated formation mechanisms of NO_x, it is generally required to use detailed reaction kinetics in order to obtain reasonably accurate predictions of the NO_x formation. With respect to modeling of detailed gas phase reactions, it is, however, a common approach to reduce the actual number of reactions and species. This reduction has to be based on the relevant conditions and accuracy requirements. This reduction of a detailed mechanism to a skeletal mechanism can be a very efficient approach to reduce complexity and computational cost of a model, but still obtain a high enough accuracy when it comes to model predictions. Bugge et al. [13,130] compared a detailed reaction mechanism including 81 species and 1401 reactions with more simplified skeletal mechanisms, developed by Løvås et al. [131], with only 49 species and 36 species. The detailed mechanism fully describes the interaction between nitrogen species and hydrocarbons. One main finding was that the results of the skeletal mechanism including 49 species was close to the results of the detailed mechanism including 81 species, whereas the mechanism including 36 species deviated significantly from the results of the other two reaction mechanisms. In the case of 36 species, the formation of NO_2, HCN, NO, NH_3 and N_2O was over-predicted [13]. In fact, the skeletal mechanism including 36 species agreed with the detailed mechanism including 81 species only at very high temperatures (about 1073 K), while at lower temperatures (about 873 K) NO_x was over-predicted. In previous work, where Bugge et al. [132] only tested a mechanism with 36 species, they found that the prediction of prompt NO_x was overestimated by 20 times with this skeletal mechanism. Thermal NO_x was entirely negligible since the temperatures in the stove were below 1700 K which indicates that the Zeldovich mechanism does not significantly contribute to the NO_x formation.

However, there are also other modeling approaches on how NO_x prediction originating from fuel-bound nitrogen can be modeled, without requiring a detailed reaction scheme. Huttunen et al. [126] assumed that half the nitrogen in the permanent gas phase is NH_3, which is a precursor for NO_x, originating from fuel-bound nitrogen. The rest is assumed to be N_2. Furthermore, it is assumed that the nitrogen in pyrolysis gases and char is proportional to the amount of char and volatiles in wood and therefore also their ratio. However, basing NO predictions on this approximation resulted in predicted emission levels that where five to ten times smaller compared to what was found in experiments. Accordingly, such a gross simplification of the evolution path for nitric oxides, cannot yield accurate results, even though it has not been tested if better results can be obtained when modeling HCN and NH_3 as NO precursors [126].

Reviewing homogeneous gas phase modeling has clearly shown that simplifications are not only required for chemical and physical processes in the interior of the wood log, but are also a significant aspect for the development of efficient gas phase models. This highlights that a computationally efficient simulation tool for wood heating appliances does not solely rely on a numerically efficient and accurate solid phase model, but also highly depends on the numerical efficiency of the gas phase model. The complexity of a model can for example be reduced by reducing the number of homogeneous gas phase reactions by lumping heavy and light hydrocarbons into two representative species. A higher number of homogeneous gas phase reactions is expected to result in a stiffer system of equations. For a numerically efficient simulation tool, it is required to reduce the number of stiff equations, such that the computational cost is balanced with accuracy. This principle accounts for the devolatilization modeling of wood, as well as the homogeneous reactions of the released volatiles species.

5.2. Theory of soot formation and its modeling

There is only a limited amount of works available that discuss soot formation from biomass conversion processes, either experimentally or by modeling. Yet, it is clear that soot formation is a key aspect of an accurate wood heating appliances simulation tool, as soot in the flame intensifies radiant heat transfer between gases and wall such that the gas temperature decreases [126]. The parent fuel will have a significant influence on the soot production; therefore, soot formation models for liquid and gaseous hydrocarbon fuels are not applicable for biomass.

Wood smoke which is responsible for a high number of deaths per year, has soot as a primary contributor, and further includes ash and volatiles. Soot is built up by two components; organic and black soot. Black soot contains furthermore two components; elemental soot and condensed organic compounds [133–135].

The most common description of soot formation is with acetylene as a precursor. Acetylene (C_2H_2) enhances the formation of

increasingly larger ring structures. The process starts with the abstraction of H from the ring structure by a free H. The products of the initial step are therefore H_2 and an aromatic radical. The aromatic radical will then react with C_2H_2. An additional C_2H_2 will then react, and the reaction will lead to cyclization and the formation of more connected aromatic ring structures [21]. This reaction sequence is commonly shortened to "hydrogen-abstraction-carbon-addition"-route (HACA) . The reaction products will be PAH, which contains one to four-aromatic-ring-structures. According to the Frenklach model, the soot precursors subsequently start to nucleate and size growth occurs, which suggests that nucleation occurs through an association of four-aromatic-ring species. First soot precursors are formed, and this initializing stage is followed by nucleation and surface growth. Larger spherical particles are formed, which then cluster together and by agglomeration form chains [136]. However, as the particle grows, the forming particles are also affected by oxidation reactions [21]. Accordingly, both formation and consumption are relevant and define the final soot yield.

However, with respect to soot formation from degrading wood, soot can be synthesized via an additional reaction pathway [137,138], in which it is suggested that biomass devolatilization fragments react further. This formation mechanism of soot has been found relevant for species adsorbed onto the soot particle, as they seem to be intermediates between small oxygenated biomass devolatilization compounds and the large structures of soot.

It is suggested that cyclopentadiene (CPD) can be a precursor for an additional PAH formation route [136]. Cyclopentadiene is formed via primary reactions of phenols (therefore lignin compounds), in which CO is eliminated from the initial chemical structures in wood, such that CPD is formed, as well as its methyl derivatives [139–141]. Further pyrolysis of CPD then leads to the formation of benzene, toluene, indene and naphtalene [142–145]. In a more simplified explanation, one can mention the following steps as part of the second soot-formation route; wood degrades into decomposition products (mostly from lignin), that can then continue reacting according to the traditional HACA-soot-formation root, or form oxygen-containing aromatic species and char. The oxygen-containing aromatic species can further react and form soot.

Most interesting is that the original formation pathway of HACA does not consider oxygen-containing PAH, as it only considers PAH based on four-aromatic-ring structures. When modeling the second reaction pathway, one can also accurately consider C/O ratios in the soot. It was also generally found that PAH formation and destruction is very sensitive to the C/O ratio in the parent fuel and the temperatures of the thermal conversion processes. Furthermore, with respect to common temperatures in combustion units (1220 K), it was also found that such high temperatures, as well as the time during which the temperature remains at such a high level, influence the PAH/soot formation [146]. An additional influence on soot formation is the ratio of O_2 / CO_2 in the combustion atmosphere, since this ratio has a significant influence on the temperature profile of the particle, which can then affect the amount of soot formed [147]. Most interesting, however, is that Wijayanta et al. [148] claimed that biomass soot formation modeling can be based on previous modeling work done on soot formation from coal. One would not expect this, since there is a significant difference in the composition of wood and coal; hence, C/O and C/H ratios are assumed to be different, which is expected to have some effect on soot formation. Wijayanta et al. [148] developed a soot formation model for biomass, in which 276 species were involved, and 2158 conventional gas phase reactions were modeled, in addition to 1635 heterogeneous surface reactions. They based their soot model on previous work done by Ergut et al. [149] on soot formation from coal conversion. Ergut et al. [149] assumed an atmospheric pressure, which would make the model suitable for modeling soot formation in domestic wood heating appliances, where no significant pressure increase is expected. In their model, pyrene, naphtalene, methylnaphtalene and phenol are present in negligible amounts, while most of the species that can react and form soot are CO, CO_2, CH_4, acetylene, ethylene and C_2, in addition to C_3 alkanes. To some reduced extent benzene and toluene are considered, but much less significant compared to the previously mentioned species. To a certain degree, it can therefore be concluded that the influence of biomass fragments on soot formation and the influence of CO elimination from phenol compounds is not considered at all in their model, which again highlights that it might be suitable for coal, but one expects it to exhibit higher discrepancies for wood soot formation modeling. By considering such a detailed description of soot formation, as done by Wijayanta et al. [148], they were able to identify the influence of temperature on soot formation. It was found that PAHs formation increases as the temperature rises from (1073–1473 K), but again decreases at higher temperatures (1678–1873 K). Within the first temperature range, it is assumed that the temperature influences the conversion kinetics of hydrocarbon polymerization for PAH formation. It is interesting to note that no soot was found at temperatures below 1473 K, because at these temperatures the oxidation reactions of soot and PAH are faster than soot growth. Within the second temperature range, temperatures are high enough to enhance PAH oxidation reactions, this is due to enhanced OH radial formation at these temperatures. It was also found that the pressure in a reactor system has an insignificant influence on soot formation reactions.

With respect to furnace modeling, primarily small-scale heating appliances, soot formation has only been considered very limitedly in current models. Bugge et al. [13,130,132] used the Moss and Brookes soot model [150], in which the primary precursors for soot formation are acetylene and ethylene. Brookes and Moss [150] focused on jet diffusion flames burning methane at elevated or atmospheric pressure. The purpose was to discuss how flame radiative heat losses and soot production rate are linked. Their modeling followed the conventional HACA pathway of soot formation. Because this work is not linked to detailed information on soot formation from biomass, it is considered to go beyond the scope of this work, and is therefore not discussed in more detail here.

Huttunen et al. [126] modeled soot formation according to two different models, whereby one was developed by Magnussen and Hjertager [151] and Tesner et al. [152], while the other one was developed at Brigham Young University [153]. However, Huttunen et al. [126] stated that for solid fuel combustion, the Brigham Young University model is more suitable, and was consequently linked in their model to the TULISIJA code. Magnussen and Hjertager [151] also did not focus on soot formation from the thermal conversion of wood, but predicted soot formation from C_2H_2 diffusion flames. Soot formation in this work occurred stepwise, in which the first stage was the formation of radical nuclei, while the second stage was soot formation from these nuclei. Soot combustion in their work was modeled in regions, where the local mean soot concentration dropped below the concentration of oxygen. Because the focus of this work is again gaseous fuels, it is concluded that a detailed discussion of this soot formation model goes beyond the scope of this review paper, and the same reason for neglecting a detailed discussion can be applied to the model by Tesner et al. [152]. They also discussed soot formation from a C_2H_2 diffusion flame. It was claimed that soot particles are formed due to branched-chain processes and the destruction of active particles on the surface of the formed soot particle [152].

Due to the limited number of works currently available in the open literature, it is not yet clear how soot and PAH formation are influenced by different wood species. Most of the works are on liquid or gaseous fuels, while wood has not been investigated intensively. So far, most of the available works concerning soot formed during thermal conversion of wood have been performed on pine wood [136,148]. Furthermore, none of the works focused on soot

formation from large wood logs. Nevertheless, it is expected that the size of the woody particle has an influence on soot formation, as it has been pointed out by Liu et al. [147] that the temperature history of the particle influences soot formation. Since entirely different temperature histories are expected for large and small particles, it is clear that the particle size has an influence. It is also expected that particle shape has an impact on soot formation, as the external surface area of the particle exposed to heat also has an influence on the heating history of the wood particle. Future research is therefore recommended to confront these unknown components of soot formation occurring during thermal wood conversion in small-scale wood heating appliances.

6. Small-scale furnace modeling

Only a limited amount of works has been done on small-scale furnace modeling [13,14,50,51,123,125–128,130,132,154,155]. The most challenging difficulty of current works is the enormous computational effort of common CFD models, since a very fine mesh is required, where steep gradients can be expected and very detailed reaction mechanisms are needed to model combustion chemistry sufficiently well [124]. In the following chapter, the current state-of-the-art of small-scale heating appliances modeling is reviewed in order to identify the most important features of small-scale furnace simulation tools, and to discuss the most common approximations and assumptions current models are based on. Furthermore, the most important modeling results are outlined. However, one has to acknowledge that both the development of precise models, as well as the accurate performance of experiments, is difficult. With respect to experiments, it has to be emphasized that due to the mostly discontinuous feeding system of small-scale boilers or stoves, a stable reaction environment can not be obtained. For example, by opening the heating unit during discontinuous feeding, the air-fuel ratio, which has to be controlled in well-defined experiments, can vary significantly [124]. Furthermore, 100% constant feed rates can hardly be managed, even in automatically fed pellet boilers. Accordingly, even with respect to the validation of modeling results, it has to be considered that errors can arise on both the experimental and modeling side.

Table 6 outlines that a simulation tool for real-world small-scale heating appliances has to include certain modeling aspects in order to accurately model a given reactor configuration. First, a model has to include a description of the solid bed, which will be thermally converted to gaseous products and ash. The solid phase conversion defines the volatiles release rate to the gas phase. The solid bed model describes the drying of moist wood, together with wood devolatilization, where most of the combustible gases are released, as well as char conversion. The char can be converted through gasification, oxidation, or a combination of the two. The extent to which these two reaction paths occur is dependent on the operational conditions of the furnace. As outlined in the previous section on particle degradation modeling (Section 4), also with respect to the bed model in domestic combustion units, chemical processes related to the thermal conversion of wood have to be simplified significantly in order to be used in an efficient simulation tool for engineering applications, such as optimization and design of heating appliances. Not only is the thermal conversion of a single particle a model requirement, but also the accurate description of the influence of various wood particles on each other is needed for a detailed bed model. It should also be mentioned that another requirement for the accurate modeling of heating appliances is the ability of the bed model to account for the wood species of interest. A flexible bed model, which allows for a detailed characterization of the parent fuel, is mostly achieved by splitting wood into its pseudo-components.

Also presented in Table 6 is the second chief feature of a domestic heating unit model is the gas phase model, which must contain a

Table 6
Chief features required for model development of small-scale heating appliances. This table lists the most important features of a model.[a] implies that the bed model was decoupled from the gas phase model, as the temperature at the boundaries of the wood log were set to constant values. [b] RSM refers to Reynolds-Stress Model, [c] refers to the Eddy Dissipation Model (EDM), [d] refers to the Eddy Break-Up model (EBU), [e] refers to the Eddy Dissipation Concept (EDC), [f] refers to probability density function modeling approach. The references refer to current state-of-the-art models, that included certain key aspects of a specific feature. "*Theoretical model*" implies that model development was based on theoretical knowledge of the processes and was purely mathematically modeled. This required that transport equations were solved. "*Empirical model*" models have been derived mainly from data obtained from experiments. "*Semi-empirical model*" is used to categorize models that are not based on solving transport equations, but are related to simplified mathematical expressions that are commonly related to measurements.

Chief features	Key aspects of the features
Bed model	1) Detailed characterization of wood species (hemicellulose, cellulose, lignin) 2) Dimensionality 2.1) 1D, e.g. [14,50,51,124,126,127,154] 2.2) 2D 2.3) 3D 3) Shape of wood particle 4) Drying model 4.1) Empirical model, e.g. [14,154] 4.2) Theoretical model, e.g. [50,51,123,124,127,128] 4.3) Semi-empirical model, e.g. [126,127] 5) Devolatilization model 5.1) Empirical model, e.g. [14,154] 5.2) Theoretical model, e.g. [50,51,123,124,127,128] 5.3) Semi-empirical model, e.g. [126,127] 6) Char conversion model 6.1) Empirical model, e.g. [14,154] 6.2) Theoretical model, e.g. [50,51,123,124,127,128] 6.3) Semi-empirical model, e.g. [126] 7) Particle-particle-contact 7.1) Heat transfer 7.2) Mass transfer
Bed model boundary conditions	1) Heat and mass transfer coefficients 1.1) Blowing effect of leaving gases 2) Emissivity of wood particle 3) Structural changes affecting gas release and heat transfer 4) Coupling gas-phase and solid-phase: 4.1) Coupled, e.g. [14,50,51,124,127,128,154] 4.1) Decoupled [a], e.g. [123,126]
Gas phase model	1) Turbulence model 1.1) Standard k-ϵ, e.g. [123–126,128] 1.2) Realizable k-ϵ, e.g. [13,14,130,132,154] 1.3) RSM [b], e.g. [125] 1.4) Low-Reynolds-number-model, e.g. [50,51,125,127] 1.5) RNG k-ϵ model, e.g. [126,127] 2) Combustion model 2.1) EDM [c], e.g. [154] 2.2) EBU [d] 2.3) EDC [e], e.g. [13,50,51,125,127,130,132] 2.4) PDF [f], e.g. [128] 2.5) Finite-Rate-Eddy-Dissipation, e.g. [14,124] 3) Radiation model 3.1) Discrete ordinate model (DOM), e.g[13,14,123–125,127, 128,130,132,154]. 3.2) Discrete transfer method by Lockwood and Shah, also referred to as DTRM, e.g. [50,51,126] 4) Gas phase kinetics

(*continued*)

Table 6 (*Continued*)

Chief features	Key aspects of the features
	4.1) Detailed mechanism, e.g. [13,130,132]
	4.2) Simplified mechanism, e.g. [14,50,51,123–128,154]
	5) Soot modeling, e.g. [13,126,132]
	6) Particle entrainment, e.g. [124]
	7) Ash deposit formation, e.g. [154]
Furnace boundary conditions	1) Furnace wall emissivity
	2) Heat storage in the furnace wall
	3) Heat transfer to the surrounding room
	4) Primary air supply / Secondary air supply
	5) Glass window: radiation losses
	6) Furnace geometry

detailed descriptions of homogeneous gas phase reactions, see Section 5, turbulence, turbulent combustion and radiation. Gas phase kinetics are subject to gross simplifications, since not all chemical species released from the wood log can be modeled due to efficiency requirements of the simulation tool. Furthermore, not all evolution paths of all emissions are yet fully understood.

A third chief feature in the modeling of a small-scale combustion unit, also listed in Table 6, is an accurate coupling between the solid and gas phases, as the two phases significantly interact. Accordingly, heat and mass transfer from one phase to the other need to be accounted for in great detail. Blowing effects of leaving volatiles from the wood particle will reduce the heat and mass transfer of the gas phase back to the solid phase, see Section 4.1.1, which can affect conversion times and product yields.

A fourth main feature listed in Table 6 is an accurate description of furnace geometry and furnace wall material properties, both of which have a significant effect on temperature history within a combustion chamber. The material properties of furnace walls, which are also recommended to include the presence of any glass windows, significantly affect the temperature in the combustion chamber, as well as heat transfer into the room surrounding the heating unit. Moreover, an accurate description of flow fields entering and leaving a computational domain is required to precisely model emission products and quantities.

Based on the above, one can conclude that a number of different features must be included in a model in order to yield an accurate real-world simulation tool. In the following sub-sections, this will be discussed in more detailed for the particular application of boilers or stoves.

6.1. Boiler

6.1.1. Bed model

Empirical bed models [154] are a well-established concepts for fixed bed modeling of wood log-fired boilers and wood pellet boilers. The release of volatiles in these models is based on the main compounds of wood, which are C, H and O. This means that the presence of S, N and Cl, initially found in the wood material, is commonly neglected.

Accordingly, such a simplified bed model cannot account for the formation of either NO_x or ash vapor precursors. There is a number of works in which these minor constituents of wood are neglected, e.g. [123,127]. Typical volatile species that are included in the models are; CH_4, CO, CO_2, H_2 and H_2O [154], with the release rate depending on the local fuel composition and stoichiometric air ratio. Furthermore, char can react (gasification) with CO_2 to form CO, and with O_2 (oxidation) to form CO_2 or CO, that reacts with O_2 in the gas phase to form CO_2. The main problem with this model, which is also applied in [14], is that the temperature dependency of the CO/CO_2 is neglected. Another weakness of such empirical models is that the accuracy of the modeling results are totally dependent on the accuracy and applicability of the experimental data used to build the empirical model. One should therefore be very cautious not to use an empirical model for cases that are different from the experimental setup for which the model was designed. If used for the right conditions, however, empirical bed models may yield high accuracy results at an affordable cost.

In comparison to the empirical model approach discussed above, there are other bed models based on a theoretical understanding of the chemical and physical processes occurring during the thermal conversion of wood and the mathematical description of those processes. Porteiro et al. [124] developed a 1D transient particle model and applied it to the simulation of a domestic wood pellet boiler. More information on this model can be found elsewhere [52,53] (also in Section 4 of this review paper), and is not repeated here. In the following we will describe how their bed model interacts with the gas phase above the bed. They modeled pellets [124], and as the pellets became very small, they leave the bed and get entrained into the gas phase, where a Lagrangian particle approach is used to track the particle transport. The Damköhler number is defined as the ratio between the time scales for chemical reactions and convective transport. For a pellet boiler, the Damköhler number is large, and hence, the bed can be approximated as a well-stirred reactor. This means that all particles can be assumed to be surrounded by the same gas species concentrations [124]. This is not the case, however, for wood logs, where the Damköhler number is much smaller.

Another bed modeling approach is based on the approximation of constant load operation, which indicates that wood and oxidizer flow rates and compositions are not allowed to change during the entire model scenario [123]. It is accentuated that this simulated test case can hardly be maintained in the entire transient thermal conversion cycle in a combustion unit due to inevitable fluctuations. However, if the purpose of the model is to gain fundamental understanding of the processes in the combustion chamber, the effect of this assumption is negligible.

Splitting the wood log in constant layers in which the three conversion stages, drying, devolatilization and char conversion occur is another simplifying assumption [123]. The thickness of the different layers is set based on the ultimate analysis of wood, the need to maintain a constant burnout of the wood log and the motivation to predict a reasonable temperature in the combustion zone, as a large amount of char is assumed to lead to too high temperatures. Accordingly, it is suggested that the bed model is consequently somewhat fitted to what has been observed in experiments and what can theoretically be expected from the combustion of wood logs in combustion units. Even when splitting the wood log into three layers, the wood log was not fully resolved for [123] and no mass transfer phenomena of the volatiles within the wood log were modeled. As a result, the volumetric mass sources entering the CFD simulation are only kinetically controlled, and thus only the temperature at the wood log surface defines the mass release rate of volatiles. In this work,was CO_2 also considered to be the only oxidation product, which is another simplifying assumption of that solid phase model [123] that is considered a weakness. Considering that the formation of CO from char would lead to a different heat release rate, a different temperature profile and gas species concentrations entering the CFD gas phase model via boundary conditions can be expected. The deviation between the experimental results and the modeling results [123] highlights that this consideration of CO formation does not yield accurate predictions of CO levels.

A common simplifying assumption of the solid phase model of a wood heating appliances simulation is the decoupling of the bed model from the results of the gas phase model [123]. This setting suggests that there is only a forward coupling between the bed model and the gas phase model. However, this approximation

entirely neglects that the temperature in the combustion zone is fluctuating and accordingly, a varying heat transfer to the wood log surface is assumed to also affect the thermal conversion of the wood log and therefore the volatiles release- and char conversion rates. For this reason, it is considered to be one of the main error sources in the simulation of wood fired combustion units. It is recommended to base the coupling on a dynamic interaction between results of the gas phase model and results of the bed model [124]. In such a case, the bed model is also influenced by variations of the operational conditions of the combustion unit.

6.1.2. Gas phase model

In this section, the most relevant aspects of the gas phase model are discussed. This includes the turbulence model, the combustion model and the radiation model. Gas phase kinetics have already been discussed in the chapter on homogeneous gas phase modeling, Section 5.

Turbulence model

The realizable k-ϵ model is used in some boiler simulations [154], but the standard k-ϵ model is more common [123,124].

The motivation for choosing the standard k-ϵ turbulence model is its robustness, the fact that it is computationally efficient, and that it still leads to a reasonable accuracy. Near the walls of the furnace, standard wall functions are applied [123]. Since computational cost is a primary aspect of the applicability of a simulation tool, the choice of the standard k-ϵ model seems reasonable, but the realizable version is recommended due to better accuracy for more complicated flow patterns.

Combustion model

Some researchers [154] coupled turbulence and combustion with the Eddy Dissipation Model (EDM). Buchmayr et al. [156] claim that EDM with a two-step methane combustion mechanism is used quite frequently, despite the disadvantage that the EDM (also valid for the Eddy Break-Up model, EBU) cannot consider detailed chemistry. On the other hand, they are very fast, which makes them attractive for engineering applications. The EDM (and EBU) will result in elevated reaction rates, since the reaction rates only depend on turbulent mixing [156].

The effect of neglecting detailed chemistry is that the gas temperature tends to be over-predicted. This is due to the fact that for global chemical reactions there are no radicals in the gas phase, where the radicals carry chemical energy that could otherwise be converted to heat. Furthermore, multi-step chemistry such as that relevant in the evolution path of nitric oxides cannot be accounted for.

The Finite-Rate-Eddy-Dissipation modeling approach, which was used by Porteiro et al. [124], calculates the Arrhenius expression as well as the Eddy dissipation rate, and the smaller of the two is chosen to model the reaction rates in the species equations. It is assumed that this combustion modeling approach can predict what happens in a combustion chamber in great detail. Close to the bed, where the flame is located and very high temperatures can be measured (about 1000 °C), the reaction kinetics are very fast, and accordingly, the mixing between volatiles and oxygen will control combustion reactions. Close to the water pipes and the furnace wall, temperatures will be significantly lower, so the kinetics will be the controlling factor for combustion reactions. More general information on various turbulent combustion models can be found elsewhere [157]. One can conclude that the choice of combustion model depends significantly on the purpose of the simulation tool, with either being a fast tool or a more accurate one.

Radiation model

Most commonly, the discrete ordinate model (DOM) is used for modeling the radiative heat transfer in boilers [123,124,154]. When modeling the DOM, the radiative transfer equation is solved for a limited number of distinct solid angles. One thereby models the transport of radiative intensity in a sector that is defined by the solid angle. The value of the intensity is influenced by both the position vector and the direction vector [123]. DOM is commonly used since it can be applied over the full range of optical thicknesses [158], which can also be done by the Discrete Transfer Radiation Model (DTRM) [159]. The DTRM is based on the assumption that radiation exiting a surface element within a range of certain solid angles can be clustered together and modeled as a single ray. Nonetheless, one needs to take into consideration that both DOM and DTRM are computationally more expensive than other radiation models, such as the P–1 model and the Rosseland model, with the latter being the most computationally effective [158]. DTRM becomes disproportionately expensive, if there are too many surfaces that rays must be traced from. This implies that especially for boilers with complex installations in the interior of the combustion chamber, a denser grid has to be used and the DTRM is considered too computationally expensive, as tracing the rays through a large number of control volumes increases the computational effort.

When applying a less expensive radiation model, other restrictions become important. The P–1 model is restricted to an optical thickness larger than 1, while the Rosseland model is restricted to an optical thickness larger than 3 [158]. In the P–1 model, the radiative heat flux vector in a gray medium is approximated [160,161], whereas in the Rosseland radiation model, intensity is assumed to be the intensity of a black body at the gas temperature [160]. One advantage of the Rosseland model is its efficiency, while a main disadvantage is that it cannot account for particle effects. For a pellet-fired furnace, where particles may be entrained in the gas flow during the last phases of burnout, or where the nucleation of ash vapors in the cooler furnace regions can lead to particle formation, the influence of the radiation exchange between particles and gases may be significant. This highlights that particularly the P–1 model and the DOM are relevant for wood heating appliance modeling due to their ability to handle embedded particles. However, even though the DOM is computationally more expensive, it is able to consider semi-transparent walls, e.g. glass, which makes it suitable for a furnace modeling where the radiant heat losses via the glass window have a significant effect on the temperature within the combustion chamber [158]. The potential of considering the glass window in a radiation model can be a criterion of exclusion for other less expensive models. Considering all these aspects, it is concluded that the DOM considers most of the key aspects of a suitable radiation model, which belongs to one of the chief features of a realistic simulation tool. This discussion of radiation modeling does not only apply to domestic boiler modeling, but is also valid for the domestic stove modeling discussed in the following section. Most commonly, the properties of the gases (absorption/ emissivity) are modeled by the Weighted-Sum-Of-Gray-Gases (WSGG) model, e.g. [124]. However, no simulation tool for domestic boilers included the absorption and emissivity characteristics of soot, even though the influence of most of the volatile species products is considered by implementing the WSGG model. A future field of research is therefore the full and accurate consideration of the role of soot in combustion units, which therefore also requires the accurate adjustment of the properties of gas including soot.

6.1.3. Boundary conditions of boiler

To reduce the computational cost of a simulation, it is a common approximation to not simulate the entire boiler [124]. The water side of the boiler can be modeled by convective heat transfer, with a constant heat transfer coefficient. This simplification reduces the

computational cost significantly and it yields good results. At the boundaries of the furnace modeling domain, where heat is transferred to the heat exchanger surfaces, the grid has to be refined in order to be able to handle the steep temperature gradients [123]. Furnace wall emissivities are normally set to constant values, such as 0.8 [124] or 0.9 [123]. There is currently no model available that considers the change of emissivity and heat transfer of the furnace walls, due to ash vapor condensation and particle deposition. This is therefore recommended to be investigated further in future research.

6.1.4. Most important modeling results

Scharler et al. [154] found that an optimization of the secondary air nozzles, in addition to a reduction in the number of installed air nozzles yield an improved mixing between flue gas and secondary air, which resulted in a significantly better burnout of CO. Porteiro et al. [124] were able to detect a strong recirculation zone with their model. The recirculation zone is essential, since it stabilizes the flame. In their prediction, the flame occupied two-thirds of the combustion chamber. Another advantage of their model is that a very good prediction of NO_x and an overall good agreement of the CO prediction between the model and measured values [162,163] was achieved. Furthermore, they found that the operational conditions of the furnace had negligible effects on NO_x formation, and all modeled cases resulted in a more or less constant NO_x yield [124].

In other works, the predicted CO deviated significantly from what had been experimentally measured. As pointed out earlier, the choice of kinetics of homogeneous and heterogeneous reactions is assumed to be one main source of error [123] with respect to these predictions.

Overall, the number of works on small-scale-boiler modeling (scale of smaller 30 kW), is very limited. Future research is therefore encouraged to increase the focus on such small-scale boiler units, since those small units are related to high emission levels.

6.2. Stoves

6.2.1. Bed model

Empirical models are also commonly used for wood log modeling in domestic wood stoves [14]. Details on the model of Scharler et al. [14] have been discussed in the boiler section, and the same model has been used for wood log modeling in stoves where a bed of two non-touching wood logs was modeled. Touching wood logs imply that heat and mass transfer from and to the wood log surface were hindered. However, such a blockade to transport phenomena has not been modeled in any of the reviewed works.

When modeling small-scale wood stoves fired by wood logs, it is also a common approach to derive volumetric mass source terms entering the gas phase model without actually fully discretizing and solving a bed model [13,132]. The volatiles release of six non-touching wood logs in the combustion chamber was modeled in these specific cases. The released gas composition was either based on Norwegian spruce [13,132] or demolition wood pellets [130]. The wood consumption rate has to be obtained experimentally for the model, and accordingly, the wood consumption rate is given under fixed operational conditions of the furnace, which therefore limits the applicability of the model to one specific time of a particular test case. Furthermore, the consumption rate depends on the wood species tested. If the wood consumption rates are only known for a limited number of test cases and wood species, the flexibility of the bed model is restricted. However, since the main purpose of the work of Bugge et al. [13,132], was to gain a fundamental understanding of NO_x formation mechanisms from fuel-bound nitrogen, it is assumed that relevant knowledge can be gained from this model, even though no detailed bed model has been developed.

Another bed model discussed in the available open-literature restricts the active area to the external surface of the wood log, while the interior of the wood log was not discretized and modeled [127]. Devolatilization was modeled with a one-step global reaction mechanism, which was based on literature data [51,164] linking the composition of the gaseous mixture to the wood consumption. Char gasification was treated in a similar manner. Coupling between the gas phase model and the bed model was done with mass and heat source terms at the interface between them.

In some works, the solid phase model was assumed to be quasi-steady-state [126–128]. These models are based on the assumption that only one specific stage of combustion can be described by the model, where a constant burning rate is given and the stage is related to a slow shrinkage of the wood log. It is said that the time scale for wood degradation can be expressed with the time of shrinkage, which is in the range of minutes. This is very long compared to gas phase reactions, which have time scales in the order of seconds, so the solid degradation process can hence be assumed to be steady state [127]. The model can be considered as a computationally efficient modeling approach, but does entirely neglect secondary reactions of the leaving tar, as well as the cooling of exiting water vapor or volatiles. The assumption of immediately leaving gaseous products of wood conversion is assumed to be related to significant errors as far as emission predictions are concerned.

Tabet et al. [128] modeled a bed composed of a single wood log. They described the solid bed by three layers that represent drying, devolatilization and char conversion. The wood log was 50 cm long, and each layer had a height of 4 cm. This suggests that the sizes of the layers do not change, suggesting that they maintain the exact same thickness throughout the conversion. Accordingly, this assumption is limited to a conversion stage where conversion can be considered to be a quasi-steady-state. Furthermore, this assumption restricts its application to a specific stage in thermal conversion, making it unsuitable to model an entire combustion cycle.

Steady-state assumptions were also performed by Huttunen et al. [126], though that overall approach for the bed model was slightly different from previous modeling approaches. Huttunen et al. [126,155] developed a model for wood log drying, devolatilization and char conversion, and coupled it to a CFD model by using the TULISIJA-code (more background information on the code itself can be found elsewhere [165,166]). Huttunen et al. [126,155] developed their solid bed model in two steps, in which the first stage was only discussing the volatile composition and release rate, whereas the second stage focused on char conversion modeling. They made two different models (the first-generation pyrolysis model and the second-generation pyrolysis model) for devolatilization and drying. In the first-generation pyrolysis model, the drying and devolatilization rates were based on the energy equation describing heat storage, conduction and convection in the interior of the wood log, and in addition also energy sources originating from drying and devolatilization. The equations were based on a radiative heat flux to the surface of the wood log, which in their model was defined to be uniform. The disadvantage of this model is that it is not time-dependent, which is a problem if e.g. ignition is supposed to be considered. In the second-generation pyrolysis model, the drying and devolatilization rates were modeled differently and were said to depend on the penetration velocity of the temperature zone into the wood log. Limitations of the second-generation pyrolysis model are that it is only applicable in a certain range of radiation temperatures and log diameters. The rate of evaporation and devolatilization is proportional to the penetration velocity of a certain temperature zone, where the penetration velocity includes the influences of a constant and $1/\sqrt{t}$, with t being time [126]. Huttunen et al. [126] coupled the pyrolysis model to the flow model by inserting its results (mass, energy fluxes, etc.) in the evolution equations as source terms.

For wood log modeling in wood stoves, there are also more comprehensive models available in open-literature. These models include models with fully discretized wood logs that also contain a detailed description of chemical and physical processes related to thermal wood conversion [50,51]. These models have been discussed in detail with respect to single particle models (Section 4). Galgano et al. [50,51] show that the flow field is closely connected to the temperature and the species distribution released from the wood.

6.2.2. Turbulence model

Knaus et al. [125] implemented the standard k-ϵ model, the Reynolds stress model (RSM) and the low Reynolds number k-ϵ model suggested by Lam and Bremhost [167]. They tested two cases, whereof one was an isothermal case (no combustion) and the second one was the combustion case. In the isothermal case, they investigated the prediction of recirculation zones by the different turbulence models and found that the standard k-ϵ model correctly predicts location and strength of the recirculation zone, whereas the RSM gives more accurate results. However, these two previously mentioned models are only applicable at high Reynolds numbers. It was found that there might also be zones of low Reynolds numbers. This justifies use of the low Reynolds number k-ϵ model. Another problem is the influence of the walls on the free flow. It was found that it cannot be adequately modeled with standard wall functions applied in the k-ϵ model and RSM in such narrow geometries. This underlines the fact that the low Reynolds number k-ϵ has some significant advantages [125].

Comparing the standard k-ϵ model and the RNG-k-ϵ model show that the choice of turbulence models has a significant effect on predictions of both temperature and emission levels [126]. The RNG k-ϵ model predicts lower turbulent viscosity and a longer turbulent time scale than the standard k-ϵ model.

For high Reynolds numbers, the RSM is known to yield more accurate results than any k-ϵ model. This does, however, come at the cost of more CPU load. In wood stoves, the Reynolds number is typically rather low, and the extra CPU cost of the RSM model will therefore not necessarily pay off. The RNG k-ϵ model has not been proven to perform significantly better than the standard k-ϵ model, maybe with the exception of rotational flows. A better choice is then to use the realizable k-ϵ model, which lately has shown to yield improved results for a large number of different flows. Unless one really feels that a low Reynolds number k-ϵ model is required, the realizable model seems to be the preferred option for wood stove simulations.

By using the RNG k-ϵ model instead of the low Reynolds number model of Chien it was found that the flame ignite earlier, leading to higher temperatures in front of the wood log [127].

Due to its impact on the level of temperature fluctuations, the choice of turbulence model can have a significant effect on modeling of NOx emissions. Hill [168] studied the effect of either considering or neglecting fluctuations of temperature and species and found that this could yield differences in NOx emissions up to 600%. The relevance of the turbulence model for the accuracy of the predictions of NOx emissions has so far only been studied for pulverized coal combustion, where entrainment of converting fuel particles is significant [168], which means that the turbulence is of significance not only for homogeneous gas phase reactions, but also for particle-gas heat transfer and therefore particle conversion. It has not yet been studied how important the turbulence model is for large wood log conversion, where turbulence is mainly influencing homogeneous burnout of combustible gases.

6.2.3. Combustion model

Knaus et al. [125] as well as many other researchers [13,50,51,127,132] coupled turbulence and combustion modeling via EDC. Very few models [128] used a pre-assumed probability density function approach. With respect to wood stove applications also the Eddy Dissipation / Finite Rates Kinetics Combustion Model has been applied [14]. This approach will yield relatively accurate results with global chemical kinetics as it accounts for both kinetically and mixing controlled combustion. If detailed chemistry is required, the EDC model is the more appropriate choice. The increased accuracy does come at the expense of somewhat higher computations costs. All wood stove models focusing on NO_x are based on the EDC.

6.2.4. Radiation model

In case of wood stove modeling, the Discrete Ordinates Method (DOM) is commonly applied [13,14,125,127,128,132], as it is also for boiler modeling. Some researchers [50,51,126] used a discrete transfer model, originally suggested by Lockwood and Shah [169] for modeling radiation, which is previously discussed but referred to as DTRM. In work by Huttunen et al. [126], the local absorption coefficient of the gas phase was calculated based on the Weighted Sum of Grey Gases (WSGG) approach while the absorption of the soot was added on top of this. A similar approach has also been used by others [170,171]. The detailed discussion on advantages and disadvantages of various radiation models presented with respect to the boiler model, Section 6.1.2, can be applied to stove modeling as well, due to similarities between these two heating appliances.

6.2.5. Boundary conditions of the wood stove

The importance of the consideration of the glass window of a wood stove as part of the boundary conditions of the stove on temperature predictions has been outlined in a number of works [13,132]. However, the influence of a glass window and the radiative heat loss due to it, are not captured by current models, since the glass window, like any other furnace wall, is commonly assigned the same constant temperature as any other furnace wall [13,127,132]. Some works define stove boundary conditions based on purely experimentally derived values [126,165,166]. There is clearly room for significant improvements here. This should be done by including the transparency of the window and by accounting for heat transfer to the surroundings through all furnace walls. In addition, the air inlets should not be placed at the inlet to the furnace, but rather at the position where the air enters the stove itself. This means that the air transport channels leading to the furnace must be meshed and simulated. A reasonable pressure difference should then be applied between the inlet and the outlet to drive the draft. In this way, the total airflow to the furnace and distribution between the different inlets would automatically be correct.

6.3. Detailed comparison of wood stove models

In addition to the models discussed in the previous sub-sections, also more case specific models may be included to yield more accurate wood stove simulations. In the current section, a number of such case specific models for wood log combustion will be discussed. Important aspects of a reliable simulation tool for wood stoves are explained in more detail in Table 7.

Table 7 outlines which aspects are considered by the currently available models. The aim is to identify the completeness of current models in order to understand which aspects of furnace modeling cannot yet be described. Reviewing the current state-of-the-art has shown that modeling CO and to some extent also NO_x emissions is a main feature of current models. Even though a deeper understanding of the evolution paths of different gas phase species is recommended in order to optimize gas phase kinetics, the principle implementation of the gas phase reactions and the corresponding predictions of emission levels are rather well-established. In contrary, many aspects related to the bed model are either entirely neglected or not accurately accounted for in current models.

The first aspect 1) refers to models that include detailed descriptions of chemical and physical processes related to thermal

Table 7
Aspects for a real world simulation tool for wood stoves. The table marks which aspects of an advanced simulation tool have or have not been considered in current models.

No. in Fig. 6	Aspect								
	Ref.	[132]	[13]	[14]	[154]	[128]	[127]	[50,51]	[126]
1)	Detailed solid phase model	–	–	–	–	–	–	✓	–
2)	Bark layer	–	–	–	–	–	–	–	–
3)	Stack of logs	✓	✓	✓	✓	–	–	–	✓
4)	Logs in contact	–	–	–	–	–	–	–	–
5)	Transient log model	–	–	✓	✓	–	–	✓	–
6)	Log shape	brick	brick	irrr.	irr.	irr.	cyl.	cyl.	brick
7)	Log size	NA	NA	NA	NA	NA	ø 12–21 cm 1.5 m long	ø 12–21 cm 1.5 m long	5 x 5 x 30 cm
8)	Modeling of pseudo-components	–	–	–	–	–	–	–	–
9)	Ignition principle	–	–	–	–	–	–	–	–
10)	Multi–cycles	–	–	–	–	–	–	–	–
11)	Soot modeling	✓	✓	–	–	–	–	–	✓
12)	Prediction of recirculation zones	NA	NA	NA	NA	✓	✓	✓	NA
13)	Radiation loss through glass	–	–	–	–	–	–	–	–
14)	Air flushing of glass window	✓	✓	✓	✓	✓	–	–	–
15)	Stove walls modeled	–	–	✓	✓	–	–	–	–
16)	Heat transfer to room	–	–	✓	✓	–	–	–	–

"irr." is the abbreviation for irregular, "cyl." is the abbreviation for cylindrical and "brick" is the abbreviation for brick–shaped. "NA" means not announced. If "Prediction of recirculation zones" is marked as "NA", this indicates that this aspect might have been modeled, but was not discussed in the paper at all.

conversion of wood and that include evolution equations for wood mass, char mass, gas species and temperature. It also implies that the interior of the wood log has been fully discretized. As can be seen from Table 7, only a limited number of works includes such a detailed description of the solid fuel. The main reason for this is the increased computational cost that results from a comprehensive bed model.

The second aspect 2) clearly shows that none of the currently available models considers the influence of bark. The elemental composition of bark, however, differs significantly from the elemental composition of the wood. This may have a significant effect on conversion reactions, since the bark contains a higher amount of inorganics that can catalytically influence the conversion reactions. Especially, when ash formation is a major concern of a model, bark has to be considered, as it contains a significantly higher ash content than the inner wood [172].

Modeling stacks of logs (point 3) is a more realistic assumption, even though it is not assumed to have a significant influence on the modeling results if the wood logs are not touching. If the stacked wood logs in the combustion unit touch (point 4 in Table 7), which has not been modeled so far, there will be a reduction of mass and heat transfer to and from the blocked wood surfaces. Accordingly, depending on the position in a wood stack and depending on the degree of contact between wood logs, different boundary conditions for the wood log models have to be used. This is expected to influence conversion times, and product release rates. So far none of the wood stove models, has taken the complexity of in-contact stacking of wood logs into consideration. A transient log model (point 5) can be applied for the entire thermal conversion process, also including initial heating and ignition of the wood logs, the stage of more or less stable devolatilization and char conversion rates, as well as the final stage where only residual char is converted to ash. Some of the models available in the current literature only focus on one specific stage in the thermal conversion of the wood log, where constant thermochemical degradation and combustion can be assumed [126–128]. The aspect of transient log models is furthermore closely linked to modeling of ignition principle (aspect 9). It was found that unless a dynamic coupling between gas phase and bed model, considering the influence of a higher heat flux back to the bed model to due flame establishment, was done, the ignition principle was not fully accounted for. Furthermore, if the aim is to model a multi-cycle, ignition modeling is essential. However, as can be seen from Table 7 also none of the current models was extended over more than a single combustion cycle.

When pseudo-components are modeled (point 8), wood is split into hemicellulose, cellulose and lignin and therefore enables the user to adjust the corresponding mass fractions with respect to the applied wood species. If only wood (the mixture of all main pseudo-components) is simulated, the aspect is marked as "not considered (–)" in Table 7. Splitting the wood into its pseudo-components, which results in a higher flexibility of the model since different wood species can easily be modeled, is not common for wood log conversion modeling in wood stoves.

Only Bugge et al. [13,132] explicitly mentioned the relevance of glass windows on the energy equations of the stove, since the glass window can be linked to significant heat losses. Still, even in their work, the glass was treated as an optically thick isothermal wall. Expanding the computational domain to also including the stove walls in an energy balance, such that the heat transfer to the surrounding room can be modeled, has only been done by Scharler et al. [14,154].

Soot is only considered in models developed by Bugge et al. [13,132] as well as Huttunen et al. [126]. Furthermore, the validity of the soot models and chemical kinetics used in these works, and their ability to accurately predict the correct level of soot, still has to be proven.

This discussion outlines that with respect to wood stove modeling, a significant number of chief aspects required for a realistic simulation tool, have not yet been considered in current models.

7. Bed models in grate furnace modeling

This section focuses on fuel bed modeling in large-scale grate furnaces. Yin et al. [173] stated in their review paper that there are two common approaches to modeling biomass conversion in a large-scale grate furnace fuel bed. These approaches are listed and briefly described in Table 8.

The main challenges for current bed models are the inhomogeneity and complexity of the wood bed, and the fact that this demands detailed multi-dimensional models. In order to capture the

Table 8
General modeling approaches used for woody biomass conversion in the fuel bed in grate furnaces.

Approach	Short description
Approach 1	The bed model is measurement-based as well as experience-based. The inlet conditions for the freeboard model are taken from measurements. The prescribed combustion rate is dependent on the position on the grate and can be obtained from heat and mass balances of fuel and primary air. Outputs of the bed model are temperature, species concentration and velocity profiles, which enter the freeboard [a] model [173].
Approach 2	Separate models for solid bed and gas phase are developed. In the most advanced case the bed models deliver the inlet conditions for the CFD model and radiative heat transfer from the freeboard back to the fuel bed model is also modeled, resulting in a dynamic coupling between the two models [174]. In a more simplified approach, the two models can also be decoupled, and therefore the degree of coupling can vary.

[a] Freeboard refers to the gas phase above the fuel bed.

structural changes of the bed due to thermal conversion, as well as phenomena occurring in connection to those changes, such as channeling, multi-dimensional models are more accurate. But, multi-dimensional simulations are also associated with higher computational costs. For efficient large-scale grate furnace simulation tools, simplifications of the fuel bed are therefore required. These simplifying assumptions are the primary difference between single particle modeling and fuel-bed modeling in large-scale grate furnaces.

The main disadvantage of today's independent modeling approaches for the solid bed and freeboard is that in order to describe flow, turbulence and heat transfer in two separate submodels, a number of simplifications are required (e.g. for temperature and velocity profiles at the interface between the gas phase and bed model) [174]. The bed shape is also usually geometrically simplified, e.g. evened out. Due to these simplifications, no overall valid model is commonly developed, but rather models that only apply to certain furnace types. This is due to the fact that a lot of simplifying assumptions are based on measurements in specific plants with different grates. Furthermore, experiments for validation of the output from the bed, which enters the gas phase, can hardly be done, because experiments at the interface between the two phases are very challenging [174]. Fig. 22 shows the theoretical coupling between the freeboard and fuel bed that is required for an accurate CFD simulation of the grate furnace.

Table 9 outlines the current state-of-the-art of solid bed models applied in large-scale grate furnace simulations. Only grate furnace bed models using woody biomass have been included. Biomass types other than wood have not been considered.

Ash-related problems are vast, and can range from affecting particulate emissions, to causing internal plant problems related to slagging, deposit formation and corrosion. The enhanced ash melting behavior of a fuel in particular can lead to problems in a grate furnace [172]. Wood has a rather low ash content, while herbaceous biomass has a high ash content that can affect the furnace operation. It is expected that it is crucial to account for the ash for accurate modeling predictions if herbaceous biomass is converted, while it is less relevant for wood conversion. The modeling of fine particulate formation and ash deposit formation, with a special focus on grate furnaces, is not frequently done in current models [154]. Because a biomass is thermally converted on the grate, ash-forming vapors are released [154]. As the flue gas containing ash vapors cools, fine particles can be formed due to nucleation or condensation processes. Ash vapors can condense on these particles. However, in addition to condensation on the particles, ash vapors can also condense on the boiler walls [154]. These ash vapors contain sulfur and chlorine, which means that condensation on the furnace walls can lead to corrosion. One can clearly see that depending on operational conditions, and therefore temperatures in the furnace, as well as the biomass type, the importance of ash vapor condensation varies significantly.

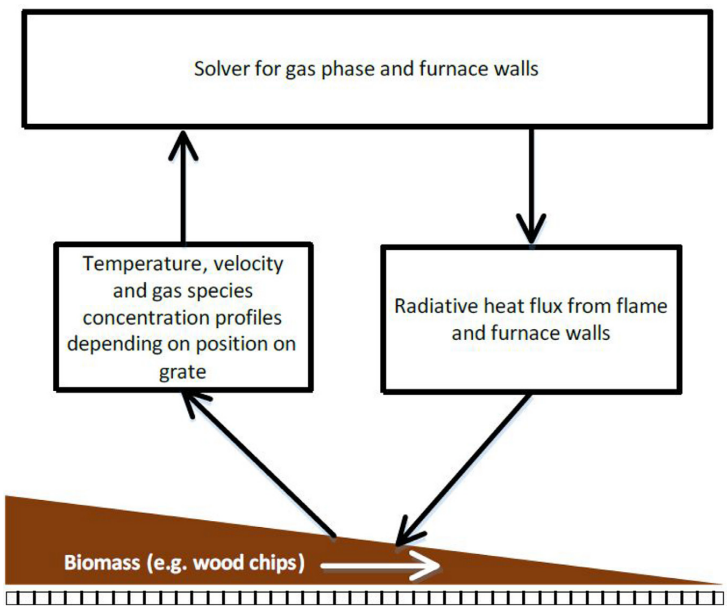

Fig. 22. Coupling between gas phase and solid phase. The brown triangle illustrates the fuel bed on the grate. The bed height decreases along the grate as the degree of conversion increases. The combustion gas exits the solid phase and enters the freeboard, while the radiative heat fluxes emitted by the flame and the furnace walls heat up the biomass on the grate.

Table 9
Bed models applied in current woody-biomass-grate-fired furnace models. The bed models are sorted by increasing complexity. The models are categorized by the "Approach type" listen in Table 8. "Empirical" indicates that main data entering the model has been taken from experiments. The fourth column lists the literature, parameters have been taken from. "Separate sub-models" outlines that a model has been developed for the bed model and another model has been developed for the gas phase. "Conversion from literature" indicates that conversion parameters were required in the model and those were taken from literature.

Author & year	Ref.	Bed model type	Empirical	Conversion from literature	Separate sub-models	Approach type
Griselin and Bai (2000)	[175]	Empirical B.M.	✓	NA	–	1
Klason & Bai (2006)	[16]	Empirical B.M.	✓	[176]	–	1
Scharler et al. (2000)	[177]	Empirical B.M.	✓	[178]	–	1
Scharler and Obernberger (2000)	[17]	Empirical B.M.	✓	[178–180]	–	1
Scharler and Obernberger (2002)	[181]	Empirical B.M.	✓	[178]	–	1
Scharler et al. (2004)	[182]	Empirical B.M.	✓	[178,183]	–	1
Costa et al. (2014)	[184]	Empirical B.M.	✓	[185]	–	1
Rajh et al. (2016)	[186]	Empirical B.M.	✓	NA	–	1
Wurzenberger et al. (2002)	[45]	Transport equations	–	–	✓	2
Bruch et al. (2003)	[46]	Transport equations	–	–	✓	2
Huttunen et al. (2004)	[187]	Three zone B.M.	–	–	✓	2
Zhang et al. (2010)	[3]	FLIC [b]	–	–	✓	2
Boriouchkine et al. (2012)	[188]	Transport equations	–	–	✓	2
Kurz et al. (2012)	[174]	One single 3D CFD code	–	[189]	✓	2
Chen et al. (2015)	[190]	FLIC [c]	–	–	✓	2

[a] FLIC is the abbreviation for "FLuid dynamic Incinerator code".

One of the most detailed bed models available today solves a 3D CFD code for both the solid and gas phase by only adjusting the transport equations with respect to the volume fraction occupied by the solid matrix [174]. This highlights the fact that the bed model and the gas phase model are closely linked, and that the interaction between these two phases is dynamic. The model is steady-state and accounts for freeboard and bed modeling based on a multiphase approach. The principle of the multi-phase approach is that the physics and the reactions of both the solid and gas phase are considered simultaneously. Drying is based on a pure thermal model. Detailed reactions describing devolatilization and char conversion are included in the model. A simplifying approximation of the model is that the detailed gas phase composition is not fully modeled, instead, volatile species mass fractions are approximated based on experimentally defined relations. Experimental relations suggested by Thunman et al. [189] were then used, in addition to the elemental mass balance in order to calculate the mass fractions of a total of five different volatile species. The particle mixing model accounts for the influence of grate movement, which is causing a stronger mixing in the bed. The corresponding particle mixing coefficient is experimentally obtained [191], and it is affected by the physical properties of the biomass in the fuel bed, the type of grate installed in the furnace and the operation conditions of the furnace. The simulation results gave too high temperatures compared to experiments. This deviation is most likely due to the wall boundary conditions, which are set to be adiabatic. Another reason for over-predictions of temperatures was found to be the inaccurate prediction of secondary air penetration. The model under-predicted the penetration depth of the air from the secondary air nozzles [174].

The FLuid dynamic Incinerator Code (FLIC), where transport equations are solved in 2D [3,190], is less complex than the 3D model discussed above. Two sub-models, where one accounts for the fuel bed (FLIC) while the other handles the gas flow in the freeboard above the bed, are the basis of this model. The two sub-models are dynamically coupled via the boundary conditions, but the fuel bed is only heated by radiation from the gas phase. Devolatilization is described with a one-step global model, and the permanent gas phase is composed of C_2H_4, CO_2 and H_2O. As products of char conversion, CO as well as CO_2, are formed [3].

FLIC is based on solving transport equations for both the entire bed and the freeboard [191]. The equations in the bed are solved in 2D. The solid fuel conversion is split into four sub-processes, namely drying, devolatilization, combustion of the volatiles in the gaseous phase and char gasification. The model is steady-state, and it is assumed that the conversion front moves downward from the top of the bed at the same constant speed. During drying, the fuel is heated by radiation, but also the dry primary air flow from below the grate drives moisture out of the bed. Gas combustion is considered to take place in the voids of the bed. The burning of the volatiles is dependent on kinetics, as well as the mixing rate with the under-fire air. One current restriction to the FLIC model is that it is not possible to solve the velocities of the bed, but instead a horizontal movement of the bed is predefined. The vertical component of movement is obtained from the solid-phase continuity equation [191].

Due to channeling, the temperature profile across the bed is highly non-uniform. It is assumed that channeling inhibits mixing between combustible gases and air, and results in a lower combustion efficiency of hydrocarbons, thus increasing the C_xH_y emissions. Only a limited amount of work has yet been done concerning

modeling of channeling. Hermansson and Thunman [192] modeled channeling and the shrinkage of a bed in a grate furnace. However, they only discussed char conversion in the bed model (excluding drying and devolatilization), their model was therefore not included in Table 9. It was found that the shrinking of the bed is not smooth. The reasons for this are uneven fuel consumption across the bed and the influence of the moving grate, as well as the non-spherical particle shape. The particles have a rough surface; therefore, particles will not smoothly slide down in the bed as the thermal conversion of the bed proceeds. Hermansson and Thunman [192] recommended describing shrinkage as a combination of continuous bed shrinkage and occasional collapses due to porosity growth.

Using the FLIC model for simulating a wood chip boiler predicted that char conversion starts in the middle of the moving grate [3]. High CO contents were found next to the bed, and CO levels were reduced significantly as mixing with secondary air increased. Experiments showed that volume fractions of CO and NO in the flue gas experienced significant fluctuations, ranging from 313 to 781 mg/m^3 and 27.8 to 65.1 ppmv, respectively. Modeling results were within these ranges, being 403.5 mg/m^3 and 40.6 ppmv, respectively [3]. For validation, one has to keep in mind that near the bed, detailed measurements cannot be obtained mainly due to unavoidable unsteady phenomena, mostly due to the riddling of the fuel on the grate, which is enhanced by grate movement and sudden collapses of channel-structures in the bed, thus leading to fluctuations in measurements [174].

The influence of flue gas recirculation can also be captured with this simulation tool, built up by a combination of FLIC and Fluent [190]. The CO reduction when modeling a test case without flue gas recirculation has been shown to be significant compared to a test case considering flue gas recirculation. This behavior can also be replicated by the model [190]. As a rather cold flue gas was recirculated, this flue gas also reduced the flame temperature, resulting in lower peak flame temperatures and higher gas volumes being transported through the combustion chamber, resulting in an enhanced CO formation. However, the advantage of such a recirculation is that the temperature reduction leads to less NO_x formation as the thermal NO_x formation route is decelerated. However, the reduction potential found in experiments and simulation was small, as the main source of NO_x is not the thermal formation route, but rather fuel-bound nitrogen [190].

It is concluded that the 2D-FLIC code in connection with Fluent for free board handling is able to correctly simulate the combined phenomena of heat transfer, homogeneous and heterogeneous kinetics and fluid flue for a moving grate-boiler.

A 1D bed model solving for governing equations for energy of solid and gas phase and gas species was developed for a biomass boiler, where the fuel enters a conical grate from below [188]. The fuel is then transported outwards, with rings that rotate either clockwise or counterclockwise. The fuel bed of biomass in grate furnaces is highly heterogeneous. Even though detailed evolution equations were solved [188], devolatilization was simplified compared to what has been found in single particle modeling. Devolatilization was based on earlier single particle modeling work by Alves and Figueiredo [34]. In comparison to their work, only the devolatilization reactions of cellulose and hemicellulose were modeled [188] instead of modeling six independent parallel reactions as suggested by Alves and Figueiredo [34]. In order to compensate for the higher computational cost of solving a higher number of transport equations, the model was reduced to 1D. Since transport equations for the bed and the gas phase are modeled, they dynamically interact [188]. The model was able to clearly identify the influence of the particle size on the overall conversion process [188]. Smaller particles ignite faster and absorb radiative heat more efficiently. However, the simulations also gave temperature oscillations, which can be explained by an easier cooling of smaller particles compared to large particles. As reactions in the solid particle are enhanced, heat release starts and the temperature of the particle rises, which enhances the temperature difference between the solid phase and the gas phase. Consequently, re-radiation losses of the particle will be enhanced, cooling the particle and resulting in the observed temperature oscillation [188].

The bed modeling of grate furnaces is also done by developing single particle models and coupling them to a bed model. Most of these bed models, based on explicit particle models, are based on thermally thin particles [108,193–195], while it is assumed that for wood chips or pellets forming the bed, the intraparticle temperature gradient also has to be considered. Models based on the assumption of thermally thick particles in beds [45,46] were already discussed in Section 4. The bed models were 1D, assuming that only the gradients in the direction of the bed height were relevant. This is also the direction of the primary air flow. Next, the gas phase in the bed was solved in Cartesian coordinates, whereas the single particles were described by 1D spherical coordinates [45,46]. Therefore, the bed model is discretized by the so-called "1D + 1D"-grid [45]. One of these particle models [45] is based on the assumption of constant operational conditions, which as a consequence lead to the simplification of a pseudo-steady-state. Another simplifying assumption of the model is that one assumes the bed surface temperature to be constant over the entire length of the grate. This is considered to be a gross simplification, since it is well known that the temperature of the bed drops as the degree of conversion proceeds, and that the temperature of the ash near the ash outlet is lower. The reason for this simplification is that the bed model and the gas phase model were not modeled as dynamically coupled, and therefore independent boundary conditions for the bed model are set that do not vary depending on the gas phase modeling results. This is a gross simplification, since the interaction between the two phases influenced by the operational conditions of the furnace are entirely neglected [45].

A rather intermediately complex bed model splits the bed into three zones, in which drying, devolatilization and char conversion, respectively, are described [187]. The bed model is 1D, leading to reduced computational costs. The surface layer of the bed in the drying zone is affected by radiative heat, while the length of the drying zone is made dependent on the temperature. As long as the temperature is below the ignition temperature, the drying layer is still present. As soon as the temperature increases over this critical ignition temperature, the devolatilization zone is reached. The ignition temperature is user-defined, thereby suggesting that the geometrical dependencies of different conversion layers and the propagation speeds of these layers are solely dependent on a fixed temperature defined by the user of the model [187]. This is clearly a gross simplification of the model, thus reducing its flexibility to certain wood species and operation conditions. The ignition velocity influencing the bed conversion and gas release from the bed has been taken from literature data found for batch combustion, and is a function of particle diameter, moisture content (dry basis), ignition temperature, initial temperature, particle density and specific heat [196]. This is assumed to introduce some error to the model, since a grate furnace does not have an exact counter-flow of ignition front and airflow, as in the batch case. It is assumed that by using this literature data, the ignition velocity will be under-predicted, but then again the length of the devolatilization zone is made dependent on the ignition velocity [196], hence influencing the prediction of the volatiles release rate. An advantage over most other models is that this model allows for volatile consumption within the bed. This is assumed to affect the fractions of released gases from the bed model entering the free board.

The models of lowest complexity are empirical models, which have the primary advantage of being related to low computational costs, since they do not solve a high number of governing transport equations. A well-established empirical 1D bed model has been developed by Scharler et al. [17,177,181,182]. The model is based on

experimental results that showed that linear correlations between the release rates of H_2O, C, H, N and O from the woody fuel can be found. This leads to the simplification that only a single parameter (e.g. the release of C) has to be known to mathematically describe fuel consumption. This parameter is obtained from test runs where samples are taken at different locations on the grate. Furthermore, conversion parameters have to be known, which are required to model the concentration of gas phase species at a certain location. These conversion parameters are either taken from literature or based on experience/ assumptions. When modeling NO_x formation in a biomass grate furnace, the empirical bed model is recommended to be improved by a more fundamental model based on transport equations [182], even though such a development has to be balanced with the computational effort.

It is not common for empirical models to include a dynamic coupling between the bed and the free board. It is very often only forward coupling that is done [177,181,182]. Such a decoupling of bed and gas phase models [16,17,175,177,181,182] is clearly a gross simplification, since changes in operating conditions will affect conversion in the fuel bed and therefore also conditions in the freeboard, which is not accounted for if decoupling is done.

Some empirical 1D bed models do, however, include a dynamic coupling between the bed and the gas phase [186]. The dynamic coupling is then done with the radiative heat flux emitted by the flame and the furnace walls, which heats up the fuel bed, as well as the mass flux of combustible gases from the fuel bed into the gas phase. Yet, the fuel conversion, being influenced by these radiative heat fluxes, as well as the primary air flow and recycled flue gas flow through the bed, is only described with an empirical 1D bed model. The output of this model entering the gas phase includes temperature and velocity profiles of the exiting volatiles, in addition to species concentration profiles.

The model of lowest complexity is the zero dimensional time-independent scheme [184] that splits the bed into two zones [197]. This model has not been added to Table 9, since it cannot be categorized by one of the approaches listed in Table 8. The furnace operates under steady conditions. The two zones are drying and conversion (devolatilization and char conversion), and in each of these zones mass and energy balances have to be solved. In the conversion section, it is assumed that a mixture of 11 species is present in the gas phase and the species exiting the fuel bed are in a thermochemical equilibrium. The empirical bed model, as well as the zero dimensional time-independent scheme, are acceptable engineering tools if the focus of the studies lies in an analysis of the freeboard processes and optimization in the freeboard region. These models, however, might not be suitable for primary air zone optimization [184].

It was found that a major part of the bed models in large-scale grate furnaces is empirical [16,17,175,177,181,182,184,186]. This finding was confirmed by Yin et al. [173], claiming that such experience- and measurement- based models are attractive due to their robustness. Due to their reduced computational time, these models are still important for engineering applications.

In conclusion, it can be stated that detailed thermal degradation and the combustion of single particles forming the bed are not commonly done with respect to grate furnace modeling. This was also found by Hajek and Jurena [198], who stated that current works model a homogeneous isotropic packed bed rather than individual particles of fuel.

8. Conclusion and recommendation

Single particle degradation models, simulations of small-scale heating appliances and bed models of large-scale grate furnaces have been reviewed in this work. A short introduction to wood chemistry is given. This is considered to be essential in order to understand the complexity of the challenges related to devolatilization and the char conversion modeling of wood. Physical differences of wood logs, pellets and briquettes are subsequently mentioned to outline the diversity of the reacting wood type. Following this introduction, particle degradation modeling with interface or mesh-based models is discussed and the main assumptions and simulation results are outlined. Interface-based models are commonly used if reduced computational cost is essential while mesh-based models are more detailed and include more physics, such as the gas phase flow and pressure solutions inside the wood particle. Secondary tar reactions are also commonly implemented in mesh-based models. For engineering applications, the interface-based models provid accurate predictions of mass and energy fluxes, which are the main coupling to gas phase modeling. An emphasis was also placed on discussing the complexity of the models with respect to dimensionality, outlining that mainly 1D models have been developed so far.

Different drying models were discussed in this paper, and it was found that a combination of the equilibrium model and the thermal drying model is a suitable choice for accurately describing drying in both low and high-temperature conditions, thus covering a broad temperature range. Kinetic rate drying models are typically found to be significantly less CPU intensive though.

Especially with respect to the quantitative determination for the heat of reactions of devolatilization, no common consensus exists. The same kinetic data for gasification and oxidation reactions are often used, since limited data can be found in the literature. The available kinetic data for heterogeneous reactions is therefore not able to account for the varying char reactivity dependent on the operational conditions the char has been formed in, and the wood species the char has been derived from.

The second part of the paper focuses on small-scale heating appliances. The chief features and their main aspects were listed and it is not surprising that an accurate bed model and its coupling to the gas phase can have a significant influence on the accuracy of the gas phase simulations.

The third part of the paper focuses on the bed model of large-scale grate furnaces. It was found that a number of simplifications are necessary to keep the model numerically efficient. The complexity of the bed model covers a broad span, ranging from purely empirical models, to advanced 3D CFD codes based on multi-phase approaches.

A list of the 11 most relevant recommendations for future development is presented below. These recommendations will yield more reliable simulation tools for both single particle degradation and small- and large-scale furnaces:

1. When using the thermal drying model, the evaporation temperature is recommended to be modeled as pressure-dependent, since it is expected that the internal wood particle pressure will significantly exceed atmospheric pressure, such that the assumption of drying at 373 K can result in false predictions.
2. Determine the influence of inorganics on the conversion of the solid phase.
3. Determine the volatile species composition for different wood species and conversion rates. As a consequence it is also possible to model ash deposit formation more accurately and predict ash-related internal furnace problems, and influence of ash deposit formation on the thermal efficiency of a furnace.
4. Define reaction pathways and determine precisely the products and reaction kinetics for gasification and oxidation reactions of char derived from wood devolatilization. In addition it is recommended to model char conversion as pressure dependent. This will result in a more accurate description of heat release as well as a more detailed modeling of reaction products that enter the gas phase model.

5. Development of multi-dimensional single particle models such that the diversity of wood particles can accurately be replicated. Multi-dimensional models would also account for anisotropy of the solid and non-homogeneous boundary conditions of a large particle, such as a wood log.
6. Development of a comprehensive, but numerically efficient single particle model that can accurately describe gas phase movement in the interior of the particle, therefore also accounting for internal pressure-related structural changes of the particle. Accurate internal pressure predictions require detailed knowledge of permeabilities of different wood species. Therefore, the database of experimentally defined permeabilities needs to be enlarged in the future.
7. Determination of soot formation reactions related to wood conversion processes, since significant influences on soot formation are expected, dependent on whether liquid, solid or gaseous hydrocarbons are reacting.
8. Develop a detailed model accounting for the NO_x formation, mainly due to fuel-bound nitrogen in large-scale grate furnaces as well as boilers and stoves, which balances a detailed description of the multi-step chemical evolution path and computational cost.
9. Development of a more realistic description of the wood log bed model in a small-scale heating appliance, accounting for touching of wood logs, bark-containing wood and the transient character of thermal wood conversion, which also includes initial heat-up and ignition. This is assumed to lead to a more accurate description of CO and unburnt hydrocarbon emissions.
10. Expand the computational domain of small-scale heating appliances, such that radiative and convective heat transfer into the surrounding room can be accurately modeled. This is assumed to be necessary if the purpose of the simulation tool is the optimization of small-scale heating appliances, since a stable heat release to the room is a chief feature.
11. Consideration of the influence of different materials used in the furnace on radiative heat losses, e.g. glass windows. Only in this case can the small-scale heating unit be fully optimized.

Acknowledgements

This work has been done within two projects: Firstly, the WoodCFD (243752/E20) project, which is funded by: Dovre AS, Norsk Kleber AS, Jøtulgruppen and Morsø AS together with the Research Council of Norway through the ENERGIX program. Secondly, the GrateCFD (267957/E20) project, which is funded by: LOGE AB, Statkraft Varme AS, EGE Oslo, Vattenfall AB, Hitachi Zosen Inova AG and Returkraft AS together with the Research Council of Norway through the ENERGIX program.

References

[1] Biswas AK, Umeki K. Simplification of devolatilization models for thermally-thick 1 particles: Differences between wood logs and pellets. Chemical Engineering Journal 2015;274:181–91.
[2] Basu P. Chapter 1 - Introduction. In: Basu P, editor. Biomass Gasification, Pyrolysis and Torrefaction. Second ed., Boston: Academic Press; 2013. p. 1–27.
[3] Zhang X, Chen Q, Bradford R, Sharifi V, Swithenbank J. Experimental investigation and mathematical modelling of wood combustion in a moving grate boiler. Fuel Processing Technology 2010;91(11):1491–9.
[4] Sousa N, Azevedo JLT. Model simplifications on biomass particle combustion. Fuel 2016;184:948–56.
[5] Ström H, Thunman H. A computationally efficient particle submodel for CFD-simulations of fixed-bed conversion. Applied Energy 2013;112:808–17.
[6] Daouk E, Van de Steene L, Paviet F, Salvador S. Thick wood particle pyrolysis in an oxidative atmosphere. Chemical Engineering Science 2015;126:608–15.
[7] Mehrabian R, Scharler R, Obernberger I. Effects of pyrolysis conditions on the heating rate in biomass particles and applicability of TGA kinetic parameters in particle thermal conversion modelling. Fuel 2012;93:567–75.
[8] Ström H, Thunman H. CFD simulations of biofuel bed conversion: A submodel for the drying and devolatilization of thermally thick wood particles. Combustion and Flame 2013;160(2):417–31.
[9] Gómez MA, Porteiro J, Patiño D, Míguez JL. Fast-solving thermally thick model of biomass particles embedded in a CFD code for the simulation of fixed-bed burners. Energy Conversion and Management 2015;105:30–44.
[10] Mehrabian R, Zahirovic S, Scharler R, Obernberger I, Kleditzsch S, Wirtz S, et al. A CFD model for thermal conversion of thermally thick biomass particles. Fuel Processing Technology 2012;95:96–108.
[11] Buczyński R, Weber R, Szlek A. Innovative design solutions for small-scale domestic boilers: Combustion improvements using a CFD-based mathematical model. Journal of the Energy Institute 2015;88(1):53–63.
[12] Skreiberg Ø, Seljeskog M, Georges L. The process of batch combustion of logs in wood stoves - transient modelling for generation of input to CFD modelling of stoves and thermal comfort simulations. Chemical Engineering Transactions 2015;43:433–8.
[13] Bugge M, Skreiberg Ø, Haugen NEL, Carlsson P, Seljeskog M. Predicting NO_x emissions from wood stoves using detailed chemistry and computational fluid dynamics. Energy Procedia 2015;75:1740–5.
[14] Scharler R, Benesch C, Neubeck A, Obernberger I. CFD based design and optimisation of wood log fired stoves. In: Proceedings of 17th European Biomass Conference and Exhibition. Hamburg, Germany; 2009. p. 1361–7.
[15] Chaney J, Liu H, Li J. An overview of CFD modelling of small-scale fixed-bed biomass pellet boilers with preliminary results from a simplified approach. Energy Conversion and Management 2012;63:149–56.
[16] Klason T, Bai XS. Combustion process in a biomass grate fired industry furnace: a cfd study. Progress in Computational Fluid Dynamics, An International Journal 2006;6(4-5):278–86.
[17] Scharler R, Obernberger I. Numerical modelling of biomass grate furnaces. In: Proceedings of the 5th European Conference on Industrial Furnaces and Boilers. Porto, Portugal: Rio Tinto, Portugal; April 2000. p. 1–17.
[18] Anca-Couce A. Reaction mechanisms and multi-scale modelling of lignocellulosic biomass pyrolysis. Progress in Energy and Combustion Science 2016;53:41–79.
[19] Neves D, Thunman H, Matos A, Tarelho L, Gómez-Barea A. Characterization and prediction of biomass pyrolysis products. Progress in Energy and Combustion Science 2011;37(5):611–30.
[20] Di Blasi C. Modeling chemical and physical processes of wood and biomass pyrolysis. Progress in Energy and Combustion Science 2008;34(1):47–90.
[21] Borman GL, Ragland KW. Combustion Engineering. McGraw-Hill series in mechanical engineering. First ed., Singapore: McGraw-Hill; 1998.
[22] Grønli MG. A theoretical and experimental study of thermal degradation of biomass [PhD thesis]. Trondheim: Norwegian University of Science and Technology; 1996.
[23] Kaltschmitt M, Hartmann H, Hofbauer H. Energie aus Biomasse: Grundlagen, Techniken und Verfahren. Second ed., Berlin: Springer; 2009.
[24] Patil RA. Cleavage of acetyl groups for acetic acid production in kraft pulp mills. Maine: University of Maine; 2012 Electronic theses and dissertations paper 1857 (2012).
[25] Adam M, Ocone R, Mohammad J, Berruti F, Briens C. Kinetic Investigations of Kraft Lignin Pyrolysis. Industrial & Engineering Chemistry Research 2013;52(26):8645–54.
[26] Anca-Couce A, Obernberger I. Application of a detailed biomass pyrolysis kinetic scheme to hardwood and softwood torrefaction. Fuel 2016;167:158–67.
[27] Ranzi E, Cuoci A, Faravelli T, Frassoldati A, Migliavacca G, Pierucci S, et al. Chemical kinetics of biomass pyrolysis. Energy & Fuels 2008;22(6):4292–300.
[28] Mohanty AK, Misra M, Hinrichsen G. Biofibres, biodegradable polymers and biocomposites: An overview. Macromolecular Materials and Engineering 2000;276-277(1):1–24.
[29] Spiridon I, Popa VI. Chapter 13 - Hemicelluloses: Major Sources, Properties and Applications. In: Belgacem MN, Gandini A, editors. Monomers, Polymers and Composites from Renewable Resources. 1st ed. Amsterdam: Elsevier; 2008. p. 289–304.
[30] Obernberger I, Thek G. Physical characterisation and chemical composition of densified biomass fuels with regard to their combustion behaviour. Biomass and Bioenergy 2004;27(6):653–69.
[31] Döring S. Chapter 2: Biomass types for pellet production. In: Power from Pellets: Technology and Applications. -ed Berlin, Heidelberg: Springer Berlin Heidelberg; 2013. p. 13–30.
[32] NS 4414. Ns 4414 - ved til brensel i husholdninger. 1997.
[33] Simpson W, TenWolde A. Wood Handbook - Wood as an Engineering Material. General technical report FPL–GTR–113. Physical properties and moisture relations of wood. Forest Products Laboratory, U.S. Department of Agriculture; 1999. p. 3.1–3.24.
[34] Alves SS, Figueiredo JL. A model for pyrolysis of wet wood. Chemical Engineering Science 1989;44(12):2861–9.
[35] Koufopanos C, Papayannakos N, Maschio G, Lucchesi A. Modelling of the pyrolysis of biomass particles. studies on kinetics, thermal and heat transfer effects. The Canadian Journal of Chemical Engineering 1991;69:907–15.
[36] Di Blasi C. On the influence of physical processes on the transient pyrolysis of cellulosic samples. Fire Safety Science 4 1994: 229–40.
[37] Di Blasi C. Heat, momentum and mass transport through a shrinking biomass particle exposed to thermal radiation. Chemical Engineering Science 1996;51(7):1121–32.
[38] Melaaen MC. Numerical analysis of heat and mass transfer in drying and pyrolysis of porous media. Numerical Heat Transfer, Part A: Applications 1996;29(4):331–55.

[39] Di Blasi C. Physico-chemical processes occurring inside a degrading two-dimensional anisotropic porous medium. International Journal of Heat and Mass Transfer 1998;41(24):4139–50.
[40] Grønli MG, Melaaen MC. Mathematical Model for Wood Pyrolysis - Comparison of Experimental Measurements with Model Predictions. Energy & Fuels 2000;14(4):791–800.
[41] Larfeldt J, Leckner B, Melaaen MC. Modelling and measurements of the pyrolysis of large wood particles. Fuel 2000;79(13):1637–43.
[42] Bryden KM, Ragland KW, Rutland CJ. Modeling thermally thick pyrolysis of wood. Biomass and Bioenergy 2002;22(1):41–53.
[43] Hagge MJ, Bryden KM. Modeling the impact of shrinkage on the pyrolysis of dry biomass. Chemical Engineering Science 2002;57(14):2811–23.
[44] Thunman H, Leckner B, Niklasson F, Johnsson F. Combustion of wood particles - A particle model for Eulerian calculations. Combustion and Flame 2002;129(1-2):30–46.
[45] Wurzenberger J, Wallner S, Raupenstrauch H, Khinast J. Thermal conversion of biomass: comprehensive reactor and particle modeling. AIChE J 2002;48:2398–411.
[46] Bruch C, Peters B, Nussbaumer T. Modelling wood combustion under fixed bed conditions. Fuel 2003;82(6):729–38.
[47] Bryden KM, Hagge MJ. Modeling the combined impact of moisture and char shrinkage on the pyrolysis of a biomass particle. Fuel 2003;82(13):1633–44.
[48] Babu BV, Chaurasia AS. Heat transfer and kinetics in the pyrolysis of shrinking biomass particle. Chemical Engineering Science 2004;59:1999–2012.
[49] de Souza Costa F, Sandberg D. Mathematical model of a smoldering log. Combustion and Flame 2004;139(3):227–38.
[50] Galgano A, Di Blasi C. Coupling a CFD code with a solid-phase combustion model. Progress in Computational Fluid Dynamics 2006;6:287–302.
[51] Galgano A, Di Blasi C, Horvat A, Sinai Y. Experimental validation of a coupled solid- and gas-phase model for combustion and gasification of wood logs. Energy & Fuels 2006;20(5):2223–32.
[52] Porteiro J, Míguez JL, Granada E, Moran JC. Mathematical modelling of the combustion of a single wood particle. Fuel Processing Technology 2006;87(2):169–75.
[53] Porteiro J, Granada E, Collazo J, Patiño D, Morán JC. A Model for the Combustion of Large Particles of Densified Wood. Energy & Fuels 2007;21(6):3151–9.
[54] Shen DK, Fang MX, Luo ZY, Cen KF. Modeling pyrolysis of wet wood under external heat flux. Fire Safety Journal 2007;42(3):210–7.
[55] Yuen RKK, Yeoh GH, de Vahl Davis G, Leonardi E. Modelling the pyrolysis of wet wood I. three-dimensional formulation and analysis. International Journal of Heat and Mass Transfer 2007;50(21–22):4371–86.
[56] Sand U, Sandberg J, Larfeldt J, Bel Fdhila R. Numerical prediction of the transport and pyrolysis in the interior and surrounding of dry and wet wood log. Applied Energy 2008;85(12):1208–24.
[57] Yang YB, Sharifi VN, Swithenbank J, Ma L, Darvell LI, Jones JM, et al. Combustion of a single particle of biomass. Energy& Fuel 2008;22:306–16.
[58] Sadhukhan AK, Gupta P, Saha RK. Modelling of pyrolysis of large wood particles. Bioresource technology 2009;100(12):3134–9.
[59] Haseli Y, van Oijen JA, de Goey LPH. A simplified pyrolysis model of a biomass particle based on infinitesimally thin reaction front approximation. Energy & Fuels 2012;26(6):3230–43.
[60] Galgano A, Di Blasi C, Ritondale S, Todisco A. Numerical simulation of the glowing combustion of moist wood by means of a front-based model. Fire and Materials 2014;38(6):639–58.
[61] Kwiatkowski K, Bajer K, Celińska A, Dudyński M, Korotko J, Sosnowska M. Pyrolysis and gasification of a thermally thick wood particle - Effect of fragmentation. Fuel 2014;132:125–34.
[62] Pozzobon V, Salvador S, Bézian JJ, El-Hafi M, Maoult YL, Flamant G. Radiative pyrolysis of wet wood under intermediate heat flux: Experiments and modelling. Fuel Processing Technology 2014;128:319–30.
[63] Seljeskog M, Skreiberg Ø. Batch combustion of logs in wood stoves - Transient fuel models and modelling of the fuel decomposition and products composition as input to CFD gas phase calculation. First International workshop on CFD and Biomass Thermochemical conversion. Leipzig, Germany; 2014. p. 39–44.
[64] Ding Y, Wang C, Lu S. Modeling the pyrolysis of wet wood using FireFOAM. Energy Conversion and Management 2015;98:500–6.
[65] Basu P. Chapter 5 - pyrolysis. In: Basu P, editor. Biomass Gasification, Pyrolysis and Torrefaction. 2nd ed., Boston: Academic Press; 2013. p. 147–76.
[66] Plötze M, Niemz P. Porosity and pore size distribution of different wood types as determined by mercury intrusion porosimetry. European Journal of Wood and Wood Products 2011;69(4):649–57.
[67] Kansa EJ, Perlee HE, Chaiken RF. Mathematical model of wood pyrolysis including internal forced convection. Combustion and Flame 1977;29:311–24.
[68] Galgano A, Di Blasi C. Modeling wood degradation by the unreacted-core-shrinking approximation. Industrial & Engineering Chemistry Research 2003;42(10):2101–11.
[69] Galgano A, Di Blasi C. Modeling the propagation of drying and decomposition fronts in wood. Combustion and Flame 2004;139(12):16–27.
[70] Spolek GA, Plumb OA. Capillary pressure in softwoods. Wood Science and Technology 1981;15(3):189–99.
[71] Perre P, Degiovanni A. Control-volume formulation of simultaneous transfer in anisotropic porous-media - simulations of softwood drying at low and high temperature. International Journal of Heat and Mass Transfer 1990;33:2463–78.
[72] Fogler HS. Elements of Chemical Reaction Engineering. New Jersey: Prentice Hall International Editions; 1986.
[73] Bear J, Buchlin JM. Modelling and applications of transport phenomena in porous media. In: Bear J, Buchlin JM, editors. Dordrecht: Kluwer Academic Publishers Dordrecht; 1991.
[74] Park WC, Atreya A, Baum HR. Experimental and theoretical investigation of heat and mass transfer processes during wood pyrolysis. Combustion and Flame 2010;157(3):481–94.
[75] Demirbas A. Hydrocarbons from pyrolysis and hydrolysis processes of biomass. Energy Sources 2003;25(1):67–75.
[76] Moffat RJ, Kays WM. The turbulent boundary layer on a porous plate: Experimental heat transfer with uniform blowing and suction. International Journal of Heat and Mass Transfer 1968;11(10):1547–66.
[77] Fatehi H, Bai XS. A comprehensive mathematical model for biomass combustion. Combustion Science and Technology 2014;186(4-5):574–93.
[78] Lu H, Robert W, Peirce G, Ripa B, Baxter LL. Comprehensive study of biomass particle combustion. Energy & Fuels 2008;22(4):2826–39.
[79] Saastamoinen J, Richard JR. Simultaneous drying and pyrolysis of solid fuel particles. Combustion and Flame 1996;106(3):288–300.
[80] Font R, Marcilla A, Verdu E, Devesa J. Kinetics of the pyrolysis of almond shells and almond shells impregnated with CoCl2 in a fluidized bed reactor and in a Pyroprobe 100. Industrial and Engineering Chemistry Research 1990;29(9):1846–55.
[81] Chan WCR, Kelbon M, Krieger BB. Modelling and experimental verification of physical and chemical processes during pyrolysis of a large biomass particle. Fuel 1985;64(11):1505–13.
[82] Di Blasi C. Modeling and simulation of combustion processes of charring and non-charring solid fuels. Progress in Energy and Combustion Science 1993;19(1):71–104.
[83] Sharma A, Pareek V, Zhang D. Biomass pyrolysis - A review of modelling, process parameters and catalytic studies. Renewable and Sustainable Energy Reviews 2015;50:1081–96.
[84] Di Blasi C. Comparison of semi-global mechanisms for primary pyrolysis of lignocellulosic fuels. Journal of Analytical and Applied Pyrolysis 1998;47(1):43–64.
[85] Ranzi E, Pierucci S, Aliprandi PC, Stringa S. Comprehensive and detailed kinetic model of a traveling grate combustor of biomass. Energy & Fuels 2011;25(9):4195–205.
[86] Hashimoto K, Hasegawa I, Hayashi J, Mae K. Correlations of kinetic parameters in biomass pyrolysis with solid residue yield and lignin content. Fuel 2011;90(1):104–12.
[87] Miller RS, Bellan J. A generalized biomass pyrolysis model based on superimposed cellulose, hemicelluloseand liqnin kinetics. Combustion Science and Technology 1997;126(1-6):97–137.
[88] Wichman IS, Oladipo AB. Examination of three pyrolytic reaction schemes for cellulosic materials. Fire safety science 4 1994: 313–23.
[89] Thurner F, Mann U. Kinetic investigation of wood pyrolysis. Industrial & Engineering Chemistry Process Design and Development 1981;20(3):482–8.
[90] Hajaligol MR, Howard JB, Longwell JP, Peters WA. Product compositions and kinetics for rapid pyrolysis of cellulose. Industrial & Engineering Chemistry Process Design and Development 1982;21(3):457–65.
[91] Di Blasi C. Analysis of convection and secondary reaction effects within porous solid fuels undergoing pyrolysis. Combustion Science and Technology 1993;90(5-6):315–40.
[92] Di Blasi C, Branca C. Kinetics of primary product formation from wood pyrolysis. Industrial & Engineering Chemistry Research 2001;40(23):5547–56.
[93] Nunn TR, Howard JB, Longwell JP, Peters WA. Product compositions and kinetics in the rapid pyrolysis of sweet gum hardwood. Industrial & Engineering Chemistry Process Design and Development 1985;24(3):836–44.
[94] Papari S, Hawboldt K. A review on the pyrolysis of woody biomass to bio-oil: Focus on kinetic models. Renewable and Sustainable Energy Reviews 2015;52:1580–95.
[95] Rath J, Wolfinger MG, Steiner G, Krammer G, Barontini F, Cozzani V. Heat of wood pyrolysis. Fuel 2003;82(1):81–91.
[96] van de Velden M, Baeyens J, Brems A, Janssens B, Dewil R. Fundamentals, kinetics and endothermicity of the biomass pyrolysis reaction. Renewable Energy 2010;35(1):232–42.
[97] Branca C, Albano A, Di Blasi C. Critical evaluation of global mechanisms of wood devolatilization. Thermochimica Acta 2005;429(2):133–41.
[98] Orfão JJM, Antunes FJA, Figueiredo JL. Pyrolysis kinetics of lignocellulosic material - three independent reactions model. Fuel 1999;78(3):349–58.
[99] Manyà JJ, Velo E, Puigjaner L. Kinetics of Biomass Pyrolysis: A Reformulated Three-Parallel-Reactions Model. Industrial & Engineering Chemistry Research 2003;42(3):434–41.
[100] Turner I, Rousset P, Remond R, Perre P. An experimental and theoretical investigation of the thermal treatment of wood (Fagus sylvatica L.) in the range 200 - 260 °C. International Journal of Heat and Mass Transfer 2010;53(4):715–25.
[101] Hosoya T, Kawamoto H, Saka S. Cellulose-hemicellulose and cellulose-lignin interactions in wood pyrolysis at gasification temperature. Journal of Analytical and Applied Pyrolysis 2007;80(1):118–25.
[102] Shafizadeh F. Introduction to pyrolysis of biomass. Journal of Analytical and Applied Pyrolysis 1982;3(4):283–305.
[103] Mamleev V, Bourbigot S, Yvon J. Kinetic analysis of the thermal decomposition of cellulose: The main step of mass loss. Journal of Analytical and Applied Pyrolysis 2007;80(1):151–65.
[104] Seebauer V. Experimentelle untersuchungen zur pyrolyse von kohle und holz. [PhD thesis], Graz: Graz University of Technology; 1999.

[105] Glaister DS. The prediction of chemical kinetic, heat, and mass transfer processes during the one- and two-dimensional pyrolysis of a large wood pellet. Seattle: University of Washington; 1987 Master's thesis.
[106] Levenspiel O. Chapter 25: Fluid-Particle reactions: Kinetics. In: Santor K, editor. Chemical reaction engineering. 3rd ed. New York: John Wiley and Sons, Inc.; 1972. p. 566–88.
[107] Septien S, Valin S, Peyrot M, Dupont C, Salvador S. Characterization of char and soot from millimetric wood particles pyrolysis in a drop tube reactor between 800 °C and 1400 °C. Fuel 2014;121:216–24.
[108] Shin D, Choi S. The combustion of simulated waste particles in a fixed bed. Combustion and Flame 2000;121(1-2):167–80.
[109] Dasappa S, Sridhar H, Paul P, Mukunda H, Shrinivasa U. On the combustion of wood-char spheres in O_2/N_2 mixtures-experiments and analysis. Symposium (International) on Combustion 1994;25(1):569–76.
[110] Fatehi H, Bai XS. Effect of pore size on the gasification of biomass char. Energy Procedia 2015;75:779–85.
[111] Hurt RH, Sarofim AF, Longwell JP. The role of microporous surface area in the gasification of chars from a sub-bituminous coal. Fuel 1991;70(9):1079–82.
[112] Ballal G, Zygourakis K. Evolution of pore surface area during noncatalytic gas-solid reactions. 2. experimental results and model validation. Industrial & Engineering Chemistry Research 1987;26(9):1787–96.
[113] Chi WK, Perlmutter DD. The effect of pore structure on the char-steam reaction. AIChE Journal 1989;35(11):1791–802.
[114] Dutta S, Wen CY. Reactivity of coal and char. 2. in oxygen-nitrogen atmosphere. Industrial & Engineering Chemistry Process Design and Development 1977;16(1):31–7.
[115] Di Blasi C, Buonanno F, Branca C. Reactivities of some biomass chars in air. Carbon 1999;37(8):1227–38.
[116] Lu H. Experimental and modelling investigation of biomass particle combustion [PhD thesis]. Provo, Utah: Brigham Young University; 2006.
[117] Forest Products Laboratory. Wood Handbook - Wood as an Engineering Material. General Technical Report FPL–GTR–190. Madison, Wisconsin: U.S. Department of Agriculture; 1999.
[118] Scott DS, Piskorz J, Bergougnou MA, Graham R, Overend RP. The role of temperature in the fast pyrolysis of cellulose and wood. Industrial & Engineering Chemistry Research 1988;27(1):8–15.
[119] Pyle DL, Zaror CA. Heat transfer and kinetics in the low temperature pyrolysis of solids. Chemical Engineering Science 1984;39:147–58.
[120] Gauthier G. Synthèse de biocarburants de deuxième génération: étude de la pyrolyse à haute température de particules de bois centimétriques. Thèse de doctorat dirigée, Ecole nationale des Mines d'Albi-Carmaux; 2013.
[121] Bellais M, Davidsson KO, Liliedahl T, Sjöström K, Pettersson JBC. Pyrolysis of large wood particles: a study of shrinkage importance in simulations. Fuel 2003;82(12):1541–8.
[122] Paulauskas R, Džiugys A, Striūgas N. Experimental investigation of wood pellet swelling and shrinking during pyrolysis. Fuel 2015;142:145–51.
[123] Athanasios N, Nikolopoulos N, Nikolaos M, Panagiotis G, Kakaras E. Optimization of a log wood boiler through CFD simulation methods. Fuel Processing Technology 2015;137:75–92.
[124] Porteiro J, Collazo J, Patiño D, Granada E, Gonzalez JCM, Míguez JL. Numerical modeling of a biomass pellet domestic boiler. Energy & Fuels 2009;23:1067–75.
[125] Knaus H, Richter S, Unterberger S, Schnell U, Maier H, Hein KRG. On the application of different turbulence models for the computation of fluid flow and combustion processes in small scale wood heaters. Experimental Thermal and Fluid Science 2000;21(1-3):99–108.
[126] Huttunen M, Saastamoinen J, Kilpinen P, Kjäldman L, Oravainen H, Boström S. Emission formation during wood log combustion in fireplaces - part I: volatile combustion stage. Progress in Computational Fluid Dynamics 2006;6(4–5):200–8.
[127] Menghini D, Marra FS. A model of wood logs combustion for CFD simulations. In: Proceedings of 16th European Biomass Conference and Exhibition. Valencia, Spain; 2008. p. 1407–14.
[128] Tabet F, Fichet V, Plion P. A comprehensive CFD based model for domestic biomass heating systems. Journal of the Energy Institute 2016;89(2):199–214.
[129] Zahirovic S. CFD analysis of gas phase combustion and NO_x formation in biomass packed-bed furnaces: a contribution towards quantitative prediction of CO and NO_x emissions [Dissertation]. Graz, Austria: Institut für Prozess- und Partikeltechnik, Graz Univeristy of Technology, Austria; 2008.
[130] Bugge M, Skreiberg Ø, Haugen NEL, Carlsson P, Houshfar E, Løvås T. Numerical simulations of staged biomass grate fired combustion with an emphasis on NO_x emissions. Energy Procedia 2015;75:156–61.
[131] Løvås T, Houshfar E, Bugge M, Skreiberg Ø. Automatic generation of kinetic skeletal mechanisms for biomass combustion. Energy & Fuels 2013;27(11):6979–91.
[132] Bugge M, Haugen NEL, Skreiberg Ø. NO_x emission from wood stoves - a CFD modelling approach. In: Proceedings of 22nd European Biomass Conference and Exhibition. Hamburg, Germany; 2014. p. 676–9.
[133] Penner JE, Chuang CC, Grant K. Climate forcing by carbonaceous and sulfate aerosols. Climate Dynamics 1998;14(12):839–51.
[134] Grant KE, Chuang CC, Grossman AS, Penner JE. Modeling the spectral optical properties of ammonium sulfate and biomass burning aerosols: parameterization of relative humidity effects and model results. Atmospheric Environment 1999;33(17):2603–20.
[135] Cooke WF, Liousse C, Cachier H, Feichter J. Construction of a 1° x 1° fossil fuel emission data set for carbonaceous aerosol and implementation and radiative impact in the echam4 model. Journal of Geophysical Research: Atmospheres 1999;104(D18):22137–62.
[136] Fitzpatrick EM, Jones JM, Pourkashanian M, Ross AB, Williams A, Bartle KD. Mechanistic aspects of soot formation from the combustion of pine wood. Energy & Fuels 2008;22(6):3771–8.
[137] Fitzpatrick EM, Ross A, Jones JM, Willians A. Formation of soot and oxygenated species from wood combustion. European Combustion Meeting 2007. Chania, Greece; 2007.
[138] Fitzpatrick EM, Ross A, Jones JM, Willians A. Smoke produced from combustion of biomass. 15th Biomass Conference and Exhibition. Berlin, Germany; 2007.
[139] Cypres R, Bettens B. Mecanismes de fragmentation pyrolytique du phenol et des cresols. Tetrahedron 1974;30(10):1253–60.
[140] Cypres R, Bettens B. Pyrolyse thermique des [^{14}C] et [^{3}H] ortho et para-cresols. Tetrahedron 1975;31(4):353–7.
[141] Cypres R, Bettens B. La formation de la plupart des composes aromatiques produits lors de la pyrolyse du phenol, ne fait pas intervenir le carbone porteur de la fonction hydroxyle. Tetrahedron 1975;31(4):359–65.
[142] Spielmann R, Cramers CA. Cyclopentadienic compounds as intermediates in the thermal degradation of phenols. kinetics of the thermal decomposition of cyclopentadiene. Chromatographia 1972;5(12):295–300.
[143] Mulholland JA, Lu M, Kim D-H. Pyrolytic growth of polycyclic aromatic hydrocarbons by cyclopentadienyl moieties. Proceedings of the Combustion Institute 2000;28(2):2593–9.
[144] Lu M, Mulholland JA. PAH growth from the pyrolysis of CPD, indene and naphthalene mixture. Chemosphere 2004;55(4):605–10.
[145] Melius CF, Colvin ME, Marinov NM, Pit WJ, Senkan SM. Reaction mechanisms in aromatic hydrocarbon formation involving the C_5H_5 cyclopentadienyl moiety. Symposium (International) on Combustion 1996;26(1):685–92.
[146] Koziński J, Saade R. Effect of biomass burning on the formation of soot particles and heavy hydrocarbons. an experimental study. Fuel 1998;77(4):225–37.
[147] Liu F, Guo H, Smallwood G, Gülder O. The chemical effects of carbon dioxide as an additive in an ethylene diffusion flame: Implications for soot and NO_x formation. Combustion and Flame 2001;125(1-2):778–87.
[148] Wijayanta AT, Alam MS, Nakaso K, Fukai J, Shimizu M. Optimized combustion of biomass volatiles by varying O_2 and CO_2 levels: A numerical simulation using a highly detailed soot formation reaction mechanism. Bioresource Technology 2012;110:645–51.
[149] Ergut A, Granata S, Jordan J, Carlson J, Howard JB, Richter H, et al. PAH formation in one-dimensional premixed fuel-rich atmospheric pressure ethylbenzene and ethyl alcohol flames. Combustion and Flame 2006;144(4):757–72.
[150] Brookes SJ, Moss JB. Predictions of soot and thermal radiation properties in confined turbulent jet diffusion flames. Combustion and Flame 1999;116(4):486–503.
[151] Magnussen BF, Hjertager BH. On mathematical modeling of turbulent combustion with special emphasis on soot formation and combustion. Symposium (International) on Combustion 1977;16(1):719–29.
[152] Tesner PA, Smegiriova TD, Knorre VG. Kinetics of dispersed carbon formation. Combustion and Flame 1971;17(2):253–60.
[153] Brown AL, Fletcher TH. Modeling soot derived from pulverized coal. Energy & Fuels 1998;12(4):745–57.
[154] Scharler R, Benesch C, Schulze K, Obernberger I. CFD simulations as efficient tool for the development and optimization of small-scale biomass furnaces and stoves. In: Proceedings of 19th European Biomass Conference and Exhibition. Berlin, Germany; 2011. p. 4–12.
[155] Huttunen M, Saastamoinen J, Kilpinen P, Kjäldman L, Oravainen H, Boström S. Emission formation during wood log combustion in fireplaces - part II: char combustion stage. Progress in Computational Fluid Dynamics 2006;6(4–5):209–16.
[156] Buchmayr M, Gruber J, Hargassner M, Hochenauer C. A computationally inexpensive CFD approach for small-scale biomass burners equipped with enhanced air staging. Energy Conversion and Management 2016;115:32–42.
[157] Veynante D, Vervisch L. Turbulent combustion modeling. Progress in Energy and Combustion Science 2002;28(3):193–266.
[158] Fluent Inc. Choosing a radiation model. https://www.sharcnet.ca/Software/Fluent6/html/ug/node583.htm; 2006 [accessed: March 2, 2017].
[159] Fluent Inc. Discrete transfer radiation model (DTRM) theory. https://www.sharcnet.ca/Software/Fluent6/html/ug/node579.htm; 2006 [accessed: March 2, 2017].
[160] Fluent Inc. Rosseland radiation model theory. https://www.sharcnet.ca/Software/Fluent6/html/ug/node578.htm; 2006 [accessed: March 2, 2017].
[161] Fluent Inc. P-1 radiation model theory. https://www.sharcnet.ca/Software/Fluent6/html/ug/node577.htm; 2006 [accessed: March 2, 2017].
[162] Granada E, Lareo G, Míguez JL, Moran J, Porteiro J, Ortiz L. Feasibility study of forest residue use as fuel through co-firing with pellet. Biomass and Bioenergy 2006;30(3):238–46.
[163] Patiño D, Moran J, Porteiro J, Collazo J, Granada E, Míguez JL. Improving the cofiring process of wood pellet and refuse derived fuel in a small-scale boiler plant. Energy & Fuels 2008;22(3):2121–8.
[164] Bryden KM, Ragland KW. Numerical modeling of a deep, fixed bed combustor. Energy & Fuels 1996;10(2):269–75.
[165] Kilpinen P, Ljung M, Bostrom S, Hupa M. Final report of the tulisija programme 1997 -1999. Tech. Rep. Abo Akademi Unversity, Tulisija Coordination; 2000.
[166] Kilpinen P, Ljung M, Bostrom S, Hupa M. TULISIJA technical review, 1997 - 1999. Tech. Rep. Abo Akademi Unversity, Tulisija Coordination; 2000.
[167] Lam CKG, Bremhorst K. A modified form of the k-epsilon model for predicting wall turbulence. ASME Transactions Journal of Fluids Engineering 1981;103:456–60.

[168] Hill S, Smoot L, Smith P. Prediction of nitrogen oxide formation in turbulent coal flames. Proceedings of the Combustion Institute 1985;20(1):1391–400.
[169] Lockwood FC, Shah NG. A new radiation solution method for incorporation in general combustion prediction procedures. Symposium (International) on Combustion 1981;18(1):1405–14.
[170] Coppalle A, Vervisch P. The total emissivities of high-temperature flames. Combustion and Flame 1983;49(1):101–8.
[171] Taylor PB, Foster PJ. Some gray gas weighting coefficients for CO_2-H_2O-soot mixtures. International Journal of Heat and Mass Transfer 1975;18(11):1331–2.
[172] Biedermann F, Obernberger I. Ash-related problems during biomass combustion and possibilities for a sustainable ash utilisation. In: Proceedings of the International Conference 'World Renewable Energy Congress (WREC)'. Aberdeen, Scottland: Elsevier Ltd., Oxford, UK; May 2005.
[173] Yin C, Rosendahl LA, Kær SK. Grate-firing of biomass for heat and power production. Progress in Energy and Combustion Science 2008;34(6):725–54.
[174] Kurz D, Schnell U, Scheffknecht G. CFD simulation of wood chip combustion on a grate using an Euler-Euler approach. Combustion Theory and Modelling 2012;16(2):251–73.
[175] Griselin N, Bai XS. Particle dynamics in a biomass fired furnace predictions of solid residence changes with operation. IFRF Combustion Journal 2000 (October).
[176] Lindsjö H, Bai XS, Fuchs L. Numerical and experimental studies of NO_x emissions in a biomass furnace. International Journal on Environmental Combustion Technologies 2001(2):93–113.
[177] Scharler R, Obernberger I, Längle G, Heinzle J. CFD analysis of air staging and flue gas recirculation in biomass grate furnaces. In: Proceedings of the 1st World Conference on Biomass for Energy and Industry. Sevilla, Spain; June 2000. p. 1935–9.
[178] Keller R. Primärmaßnahmen zur NO_x Minderung bei der Holzverbrennung mit dem Schwerpunkt der Luftstufung. forschungsbericht nr. 18. Tech. Rep. ETH Zürich, Switzerland: Laboratorium für Energiesysteme; 1994.
[179] Weissinger A, Obernberger I. NO_x reduction by primary measures on a travelling - grate furnace for biomass fuels and waste wood. In: Proceedings of the 4th Biomass Conference of the Americas. Oakland, USA: Elsevier Science Ltd., Oxford, UK; September 1999. p. 1417–25.
[180] Skreiberg Ø. Theoretical and experimental studies on emissions from wood combustion. Tech. Rep. ITEV Report 97:03. Trondheim, Norway: The Norwegian University of Science and Technology; 1997.
[181] Scharler R, Obernberger I. Deriving guidelines for the design of biomass grate furnaces with CFD analysis - a few mutlifuel-low-NO_x furnace as example. In: Proceedings of 6th European conference on industrial furnaces and boilers. Portugal; April 2002. p. 227–41.
[182] Scharler R, Widmann E, Obernberger I. CFD modelling of NO_x formation in biomass grate furnaces with detailed chemistry. In: Proc. of the Internat. Conf. Science in Thermal and Chemical Biomass Conversion. Victoria, Vancouver Island, BC, Canada; 2004. p. 284–300.
[183] Obernberger I, Widmann E, Scharler R. Entwicklung eines Abbrandmodells und eines NO_x-Postprozessors zur Verbesserung der CFD-simulation von Biomasse-Festbettfeuerungen. berichte aus energie-und umweltforschung no. 31/(2003). Tech. Rep. Vienna, Austria: Ministry for Transport, Innovation and Technology; 2003.
[184] Costa M, Massarotti N, Indrizzi V, Rajh B, Yin C, Samec N. Engineering bed models for solid fuel conversion process in grate-fired boilers. Energy 2014;77:244–53.
[185] Yin C, Rosendahl L, Clausen S, Hvid SL. Characterizing and modeling of an 88 mw grate-fired boiler burning wheat straw: Experience and lessons. Energy 2012;41(1):473–82.
[186] Rajh B, Yin C, Samec N, Hriberšek M, Zadravec M. Advanced modelling and testing of a 13 MW_{th} waste wood-fired grate boiler with recycled flue gas. Energy Conversion and Management 2016;125:230–41.
[187] Huttunen M, Kjäldman L, Saastamoinen J. Analysis of grate firing of wood with numerical flow simulation. IFRF Combustion Journal 2004 (Article no. 200401).
[188] Boriouchkine A, Zakharov A, Jämsä-Jounela SL. Dynamic modeling of combustion in a biograte furnace: The effect of operation parameters on biomass firing. Chemical Engineering Science 2012;69(1):669–78.
[189] Thunman H, Niklasson F, Johnsson F, Leckner B. Composition of volatile gases and thermochemical properties of wood for modeling of fixed or fluidized beds. Energy & Fuels 2001;15(6):1488–97.
[190] Chen Q, Zhang X, Zhou J, Sharifi VN, Swithenbank J. Effects of flue gas recirculation on emissions from a small scale wood chip fired boiler. Energy Procedia 2015;66:65–8.
[191] Yang YB, Goh YR, Zakaria R, Nasserzadeh V, Swithenbank J. Mathematical modelling of MSW incineration on a travelling bed. Waste Management 2002;22(4):369–80.
[192] Hermansson S, Thunman H. CFD modelling of bed shrinkage and channelling in fixed-bed combustion. Combustion and Flame 2011;158(5):988–99.
[193] Liu S-I, Amundson NR. Stability of adiabatic packed bed reactors. an elementary treatment. Industrial & Engineering Chemistry Fundamentals 1962;1(3):200–8.
[194] Eigenberger G. On the dynamic behavior of the catalytic fixed-bed reactor in the region of multiple steady states -i. the influence of heat conduction in two phase models. Chemical Engineering Science 1972;27(11):1909–15.
[195] Di Blasi C. Dynamic behaviour of stratified downdraft gasifiers. Chemical Engineering Science 2000;55(15):2931–44.
[196] Saastamoinen J, Taipale R, Horttanainen M, Sarkomaa P. Propagation of the ignition front in beds of wood particles. Combustion and Flame 2000;123(1–2):214–26.
[197] Deydier A, Marias F, Bernada P, Couture F, Michon U. Equilibrium model for a travelling bed gasifier. Biomass and Bioenergy 2011;35(1):133–45.
[198] Hajek J, Jurena T. Modelling of 1 MW solid biomass combustor: Simplified balance-based bed model coupled with freeboard CFD simulation. Chemical Engineering Transactions 2012;29:745–50.

Paper II

Reproduced with permission from

Inge Haberle, Nils Erland L. Haugen, and Øyvind Skreiberg, Drying of Thermally Thick Wood Particles: A Study of the Numerical Efficiency, Accuracy, and Stability of Common Drying Models, Energy & Fuels 2017, 31, 13743 - 13760.

---

energy&fuels

Article

Cite This: Energy Fuels 2017, 31, 13743−13760

pubs.acs.org/EF

Drying of Thermally Thick Wood Particles: A Study of the Numerical Efficiency, Accuracy, and Stability of Common Drying Models

Inge Haberle,*[,†] Nils Erland L. Haugen,[†,‡] and Øyvind Skreiberg[‡]

[†]Department of Energy and Process Engineering, Norwegian University of Science and Technology, Kolbjørn Hejes vei 1 B, 7491 Trondheim, Norway

[‡]Department of Thermal Energy, SINTEF Energy Research, Kolbjørn Hejes vei 1 A, 7491 Trondheim, Norway

ABSTRACT: The primary focus of this paper is on studying different numerical models for drying of wet wood particles. More specifically, the advantages and disadvantages of the models, with respect to numerical efficiency, stability, and accuracy, are investigated. The two basic models that are studied in detail are the thermal drying model and the kinetic rate drying model. The drying models have been implemented in an in-house simulation tool that solves for drying and devolatilization of a one-dimensional cylindrical wood log. It is found that the choice of drying model can significantly influence the computational time associated with the thermal conversion. Furthermore, the occurrence of numerical pressure oscillations in the thermal drying model has been found and investigated. The numerical oscillations are reduced by introducing an evaporation fraction, f_{evap}. When the thermal drying model is applied, the drying zone is very thin, commonly only including one grid point, which can result in numerical instabilities. The evaporation fraction allows the smearing of the drying zone by reducing the heat flux used for evaporation of liquid water and using the residual heat flux for heating the grid points. Reducing the evaporation fraction also resulted in reduced CPU times. It was found that model accuracy was not significantly influenced by the choice of drying model.

1. INTRODUCTION

Even though a significant amount of research has been focused toward numerical modeling of the thermal conversion of thermally thick wet wood particles over the last decades,[1−7] little work has been done on the numerical efficiency and accuracy of different drying models. The different drying models commonly applied when modeling the drying of thermally thick wet wood particles, are the thermal model, the kinetic rate model, and the equilibrium model. The kinetic rate model handles evaporation as a heterogeneous reaction that is described as an Arrhenius expression, while the thermal model assumes drying to occur at 373 K and no further temperature increase in a grid cell is allowed unless all the water in a cell has been evaporated. The equilibrium model assumes that liquid water and water vapor are in thermodynamic equilibrium. As a consequence, the evaporation rate is a function of the difference of equilibrium concentration and the actual water vapor concentration.[4] A focus on those drying models and their numerical efficiency is needed, since this can support the development of a low-computational-cost simulation tool for describing the thermal conversion of wood. The purpose of such a numerical model, describing thermal conversion of thermally thick wood particles and logs, can be its coupling to gas-phase modeling (and, therefore, a CFD platform), such that the combined model can be used as a simulation tool for wood stove design and optimization.

Such an optimization of current wood stoves is needed because of stricter demands toward emissions, efficiency, and user-friendliness in the future. So far, improvements have mainly been achieved via experiments, while, in contrast to this, a combination of experiments and modeling can result in cost-efficient design developments for future wood stoves or other combustion units.[8] This highlights the need for detailed but also numerically efficient models that describe the thermal conversion of wood, which need to grant a high degree of flexibility, as both input fuel in a wood stove as well as boundary conditions of the solid phase model can vary significantly. This flexibility can only be achieved by multi-dimensional models, and in order to keep those models numerically efficient, one must know which stage of the thermal conversion of wood is related to the highest computational cost and how this can be optimized. Studying numerical efficiency on a one-dimensional (1D) model is a good basis for the extension of this model to a numerical efficient multidimensional model.

Besides the studies on numerical efficiency and accuracy, it is also important to develop a model that is not affected by numerical instabilities. Numerical oscillations related to the thermal drying model have already been observed but have only been discussed in a few papers, e.g., by Fatehi and Bai.[9] This lack of information on numerical instabilities of drying models leads to the motivation that more research within this field is needed such that the authors have added an additional discussion on numerical instabilities of drying models.

The progress in numerical modeling of these two stages of thermal conversion of wood is fast and a significant range of models and modeling approaches has been presented over the last years. A detailed discussion of those models for thermally thick particles is presented by Haberle et al.[10] Even though there are many works available discussing model development for drying and devolatilization, only very limited work has been

Received: September 15, 2017
Revised: November 15, 2017
Published: December 7, 2017

DOI: 10.1021/acs.energyfuels.7b02771
Energy Fuels 2017, 31, 13743−13760

done on studying the numerical efficiency, accuracy, and stability of drying models in detail.

2. NUMERICAL MODELING

A 1D mesh-based simulation tool for drying and devolatilization of an infinitely long wet cylindrical wood log was developed. The model solves for the solid phase, as well as the gas and liquid phases. The involved gas species are water vapor, noncondensable gases, and tar. Intraparticle transportation of the gas phase was taken into account, while the intraparticle transportation of liquid water was neglected, even though it also can theoretically be activated in the model. Intraparticle transportation of liquid free water was activated and deactivated in two test cases, and it was found that the influence of intraparticle transportation of liquid water is negligible. As shown in the subsequent section, only one temperature equation is solved in the model. This is based on the assumption of thermal equilibrium between the phases. In earlier works regarding thermally thick particles, it has been found that this assumption predicts conversion times to be ~20% longer,[11,12] compared to models based on individual temperature equations for the gas, solid, and liquid phases. Still, a local thermal equilibrium was assumed in this model, since it is assumed that, by this simplification of the temperature equations, the efficiency of the model can be significantly increased while the accuracy is still acceptable. Drying was modeled by the thermal model and the kinetic drying model. In addition, the equilibrium model was also partly tested. Devolatilization was described by a scheme that involves three independent competitive reactions and secondary tar reactions (see Figure 1).

$$\text{Dry wood}\begin{cases}\xrightarrow{k1}\text{Non}-\text{condensable gases}\\ \xrightarrow{k2}\text{Tar}\\ \xrightarrow{k3}\text{Char}\end{cases}$$

$$\text{Tar}\begin{cases}\xrightarrow{k4}\text{Non}-\text{condensable gases}\\ \xrightarrow{k5}\text{Char}\end{cases}$$

Figure 1. Three independent competitive reactions scheme in combination with the secondary tar reactions.

The governing equations require simplifications in order to be able to simultaneously describe all chemical reactions and physical phenomena related to thermal wood conversion at reasonable computational cost.

The applied simplifying assumptions are as follows:

(1) Darcy's law can be used for modeling the gas-phase flow in the wood particle. Hereby, one is not required to solve the momentum equation, which reduces the computational cost of the model. The accuracy is assumed to not be affected by this assumption, as it is known that, with respect to increasing particle sizes, the convective term in the transport equations becomes less important.[13] In this work, only thermally thick particles are modeled, which, as such, are related to larger particle sizes.

(2) The gases in the solid matrix are assumed to be ideal. As reviewing of several models has shown, such an assumption is common practice in thermal wood particle conversion modeling.[10]

(3) The blowing effect of the leaving volatiles on heat and mass transfer to the particle is neglected. It is assumed that radiation dominates over convection, with respect to heat transfer to the particle, which makes the effect of blowing on the heat transfer negligible. Furthermore, since char conversion is not included, the mass transfer of gas species to the particle surface from the surrounding gas is irrelevant.

(4) During drying, shrinkage is neglected, since it is small, compared to shrinkage during devolatilization.[4] Shrinkage during devolatilization is considered by a three-parameter model, which is based on constant shrinkage parameters (α, β, and γ). A more-detailed description of this shrinkage model and a detailed discussion of the three different shrinkage parameters can be found elsewhere.[14] This simplifies the complexity of the shrinkage modeling and reduces computational cost.

(5) Cracking and fragmentation are neglected. This results in reduced computational cost. Neglecting these structural changes might affect model accuracy, as they will affect the permeability of the particle and, therefore, the flow of the exiting gas phase.

(6) The model is 1D, which reduces the computational cost significantly. For investigation of fundamental processes, it is assumed that this is a valid approach. Furthermore, it is assumed that an optimized 1D model is a good starting point for extension to two-dimensional (2D) or three-dimensional (3D).

(7) A bridge-factor is implemented to account for anisotropy, since this is the only way anisotropy can be considered in 1D models. However, a bridge-factor consideration of the anisotropic wood simplifies anisotropy significantly. For accurate anisotropy consideration, multidimensional models are required.

(8) Most of the thermophysical properties are modeled as being linearly dependent on the degree of conversion and/or temperature, e.g., permeability, thermal conductivity, and specific heat capacity; commonly, a temperature increase is related to an increase of those values. This consideration is assumed to lead to higher accuracy of the model, compared to the assumption of constant thermophysical properties. Furthermore, the implementation of linear functions of the properties is assumed to not significantly contribute to an increasing complexity of the model.

(9) Tar recondensation reactions have been neglected. It is assumed that these reactions occur only to a negligible extent.

The model validation was done against experimental work by Lu et al.[5] Good agreement between the modeling predictions and the experiments was found.

2.1. Governing Equations. The gas-phase continuity equation is given by[15]

$$\frac{\partial \epsilon_g \rho_g^g}{\partial t} + \frac{1}{r}\frac{\partial (r \rho_g^g \epsilon_g u_r)}{\partial r} = \dot{\omega}_{gas} - \frac{\rho_g^g \epsilon_g}{V}\frac{\partial V}{\partial t} \quad (1)$$

where ρ_g^g is the intrinsic phase average of the total gas-phase density, ϵ_g is the volume fraction occupied by the gas phase, u_r is the superficial gas phase velocity in radial direction, r is the radius, V is the cell volume related to one grid point in the 1D mesh. and $\dot{\omega}_{gas}$ is the reaction rate due to evaporation and devolatilization. The volume fraction occupied by the gas phase can be calulated from the porosity (ϵ_{pore}), according to

$$\epsilon_g = \epsilon_{pore}(1 - \phi) \quad (2)$$

DOI: 10.1021/acs.energyfuels.7b02771
Energy Fuels 2017, 31, 13743−13760

with ϕ being the fraction of pores that is filled with liquid water and $\epsilon_{pore} = V_{pore}/V$. The gas phase contains water vapor, tar, noncondensable gases, and air. A simplified consideration of air, instead of explicit modeling of nitrogen and oxygen, is valid as long as oxygen-consuming reactions are not relevant. The last term in eq 1 represents the shrinkage, and similar expressions in eqs 7, 8, and 9 refer to the same structural change. In the case of wood drying and devolatilization, $\dot{\omega}_{gas}$ is expressed as

$$\dot{\omega}_{gas} = (k_1 + k_2)\rho_{wood} - k_3\rho_{tar}^{g}\epsilon_g + \dot{\omega}_{evap} - \dot{\omega}_{recond,l} \quad (3)$$

where $\dot{\omega}_{evap}$ is the source term due to evaporation of liquid free water and bound water, while $\dot{\omega}_{recond,l}$ models the recondensation of water vapor to liquid free water.

The reaction rate constants in eq 3 are calculated according to the Arrhenius expression

$$k_i = A_i \exp\left(\frac{-E_{a,i}}{RT}\right) \quad (4)$$

for devolatilization reactions with R being the ideal gas constant and T the temperature. The superficial gas phase velocity (u_r) is described by Darcy's law,[15]

$$u_r = \frac{-\kappa}{\mu_g}\frac{\partial P_g}{\partial r} \quad (5)$$

where μ_g is the dynamic viscosity of the gas phase and κ is the permeability of the solid.

The gas-phase pressure can be obtained from the gas-phase density by using the ideal equation of state,

$$P_g = \frac{\rho_g^{g} RT}{MW_{mix,total}} \quad (6)$$

with $MW_{mix,total}$ being the total mixed molecular weight.

The gas species evolution equation is given by[15]

$$\frac{\partial(\epsilon_g\rho_g^{g}Y_k)}{\partial t} + \frac{1}{r}\frac{\partial(r\rho_g^{g}\epsilon_g Y_k u_r)}{\partial r} = \frac{1}{r}\frac{\partial}{\partial r}\left(r\epsilon_g\rho_g^{g}D_{eff}\frac{\partial Y_k}{\partial r}\right) - \frac{\epsilon_g\rho_g^{g}Y_k}{V}\frac{\partial V}{\partial t} + \dot{\omega}_k \quad (7)$$

where D_{eff} is the effective diffusivity and Y_k is the mass fraction of species k, which could be either tar, noncondensable gases, or water vapor, since the mass fraction of air is calculated by difference. The evolution of the mass density of wood reads[15]

$$\frac{\partial\rho_{wood}}{\partial t} = -(k_1 + k_2 + k_3)\rho_{wood} - \frac{\rho_{wood}}{V}\frac{\partial V}{\partial t} \quad (8)$$

and the evolution equation for char mass density is given as

$$\frac{\partial\rho_{char}}{\partial t} = k_3\rho_{wood} + \epsilon_g k_3\rho_{tar}^{g} - \frac{\rho_{char}}{V}\frac{\partial V}{\partial t} \quad (9)$$

The temperature equation reads[16]

$$(\rho_{wood}c_{P,wood} + \rho_{char}c_{P,char} + \rho_l c_{P,l} + \rho_b c_{P,b} + \epsilon_g\rho_g^{g}c_{P,g})\frac{\partial T}{\partial t} + (\rho_l c_{P,l}u_l + \rho_b c_{P,b}u_b + \rho_g^{g}\epsilon_g c_{P,g}u_r)\frac{\partial T}{\partial r} = \frac{1}{r}\frac{\partial}{\partial r}\left(r\lambda_{eff}\left(\frac{\partial T}{\partial r}\right)\right) - \Phi_{evap} - \Phi_{devol,1} + \Phi_{devol,2} \quad (10)$$

where the source term Φ_{evap} refers to the endothermicity of evaporation reactions, $\Phi_{devol,1}$ represents the source terms related to primary devolatilization reactions (commonly modeled as endothermic), and $\Phi_{devol,2}$ are exothermic secondary tar reactions. However, the definition of the heat of reaction for primary and secondary devolatilization reactions is still a challenge, since the experimental determination is difficult.[17−20] Furthermore, note that ρ_g^{g} refers to the intrinsic gas-phase average, while ρ_g refers to the gas-phase average. The relationship between the two densities is given by

$$\rho_g = \rho_g^{g}\epsilon_{pore}(1 - \phi) \quad (11)$$

The particle surface temperature is dependent on the radiative influx from the wall and the convective heat transfer to the particle surface, such that the heat flux to the surface is given by

$$\lambda_{eff}\frac{\partial T}{\partial r} = \sigma\epsilon_{particle}({T_{wall}}^4 - {T_{surf}}^4) + h_{conv}(T_{gas} - T_{surf}) \quad (12)$$

where σ is the Stefan−Boltzmann constant, h_{conv} is the heat-transfer coefficient, $\epsilon_{particle}$ is the emissivity of the particle, and λ_{eff} is the effective thermal conductivity of the outer part of the particle.

Mass conservation of liquid free water is calculated as[21]

$$\frac{\partial\rho_l}{\partial t} + \frac{1}{r}\frac{\partial(r\rho_l u_l)}{\partial r} = -\dot{\omega}_{evap,l} + \dot{\omega}_{recond,l} \quad (13)$$

where the velocity of the liquid free water is calculated according to

$$u_l = -\frac{\kappa_l}{\mu_l}\frac{\partial P_l}{\partial r} \quad (14)$$

where μ_l is the dynamic viscosity of the liquid phase, κ_l is the permeability of the liquid water, and ρ_l is defined as

$$\rho_l = \rho_l^{l}\phi\epsilon_{pore} \quad (15)$$

with ϕ being the volume fraction of pores filled with water and ρ_l^{l} is the intrinsic density of water (ρ_l^{l} = 1000 kg m^{-3}). The pressure of the liquid phase (P_l) is calculated as[21]

$$P_l = P_g - P_c \quad (16)$$

and the capillary pressure P_c is calculated according to[22]

$$P_c = 10\,000\left(\frac{\rho_{wood,0}M_l}{\epsilon_{pore}\rho_l}\right)^{-0.61} \quad (17)$$

where M_l is the mass fraction of liquid free water (dry basis). This correlation and the applied coefficients were suggested by Spolek and Plumb,[23] who presented this equation after having measured the capillarity pressure of pine wood. Regarding the water vapor recondensation reactions, it is assumed that the water vapor recondensation reactions ($\dot{\omega}_{recond,l}$) can be modeled by an equilibrium assumption[5]

$$\dot{\omega}_{recond,l} = S_{C,wood}\frac{\rho_l}{\rho_{l,0}}h_{m,pore}\epsilon_g(\rho_v^{sat} - Y_{vap}\rho_g^{g}) \quad (18)$$

with $S_{C,wood}$ being the specific surface area of wood and $\rho_{l,0}$ is the initial liquid free water density. The initial liquid free water density is defined as the water density in the wood log before

DOI: 10.1021/acs.energyfuels.7b02771
Energy Fuels 2017, 31, 13743−13760

drying has started. The mass-transfer coefficient of vapor in the pore ($h_{m,pore}$) is defined as[5]

$$h_{m,pore} = 3.66\left(\frac{D_{eff,fw}}{d_{pore,hydraulic}}\right) \quad (19)$$

while the hydraulic pore diameter is[5]

$$d_{pore,hydraulic} = \frac{4\epsilon_{pore}}{S_{C,wood}(1-\epsilon_{pore})} \quad (20)$$

and the effective liquid free water diffusivity is[5]

$$D_{eff,fw} = 6.1\times10^{3}\left(\frac{\kappa_l}{\mu_l}\right)\epsilon_{pore}^{0.61}\left(\frac{\rho_{wood}M_l}{\rho_l}\right) \quad (21)$$

The liquid permeability (κ_l) is given as[5]

$$\kappa_l = \begin{cases} 0 & \text{if } \left(\frac{\rho_{wood}M_l}{\epsilon_{pore}\rho_l}\right) \le S_{ir} \\ \kappa_l^{\Phi}\left[1-\cos\left(\frac{\pi}{2}\left(\frac{\frac{\rho_{wood}M_l}{\epsilon_{pore}\rho_l}-S_{ir}}{1-S_{ir}}\right)\right)\right] & \text{if } \left(\frac{\rho_{wood}M_l}{\epsilon_{pore}\rho_l}\right) > S_{ir} \end{cases}$$

with S_{ir} = 0.1 being the irreducible saturation and κ_l^{Φ} = 3×10^{-15} m^2.[5] The equation for κ_l was used by de Paiva Souza,[22] who referred to the experimental work by Tesoro et al.[24] The coefficients in eq 21 can be traced back to the previously mentioned definition of capillary pressure. The diffusivity that is required here is defined by expressing the liquid free water flux using Darcy's law and reformulating this flux and expressing it using Fick's law.

The liquid viscosity (μ_l) is defined as[22]

$$\log(\mu_l) = -13.73 + \frac{1828}{T} + 1.966\times10^{-2}T - 1.466\times10^{-5}T^2 \quad (22)$$

in order to correctly describe the temperature dependency of liquid viscosity. The saturated vapor pressure is calculated as[21]

$$P_{vap}^{sat} = \exp\left(24.1201 - \frac{4671.3545}{T}\right) \quad (23)$$

and the corresponding water vapor density is calculated according to

$$\rho_v^{sat} = \frac{P_{vap}^{sat}MW_{water}}{RT} \quad (24)$$

The equation for saturated water vapor pressure has been obtained from fitting the expression to water vapor data over a flat plate.[25]

Mass conservation of bound water (ρ_b) is calculated according to[21]

$$\frac{\partial\rho_b}{\partial t} = \frac{1}{r}\frac{\partial}{\partial r}\left(rD_b\frac{\partial\rho_b}{\partial r}\right) - \dot{\omega}_{evap,b} \quad (25)$$

when the density of dry wood is assumed to be constant, since no organic mass is converted during drying. In the equation above, D_b is the bound water diffusivity. The bound water diffusivity in the tangential direction is calculated based on the equation discussed by Grønli,[21]

$$D_b = 7\times10^{-6}\exp\left(\frac{-4633 + 3523\frac{\rho_b}{\rho_{wood}}}{T}\right) \quad (26)$$

and the bound water diffusivity in the radial direction is obtained by multiplying the tangential one by a factor of 2/3, as suggested by Grønli.[21] This expression for bound water diffusivity, including all the coefficients, has been derived by Siau[26] and is based on experimental work by Stamm.[27]

Based on all the previously discussed equations, the time integrator must be able to handle a system of differential and algebraic equations.[21] Therefore, the IDA solver, included in SUNDIALS,[28] was applied. It uses a backward differentiation formula.

2.2. Drying. There are three different drying models that are commonly discussed in the literature; the thermal model, the kinetic rate drying model, and the equilibrium model.[4] In this work, only the thermal model, the kinetic rate model, or a combination of the two drying models are tested in detail. The equilibrium model is not included in the discussion of numerical efficiency and stability, because it is commonly applied only for low-temperature drying processes.[4,29] However, it was also implemented to determine if its results are more similar to the results of the kinetic rate model or the thermal model.

For implementation of the equilibrium model, the mass fraction of water vapor ($Y_{vap,corr}$) that is due to the change in saturated vapor pressure is calculated according to

$$Y_{vap,corr} = \frac{P_{vap}^{sat}}{P_g}\left(\frac{MW_{water}}{MW_{mix,total}}\right) \quad (27)$$

where P_{vap}^{sat} is defined in eq 23 and the evaporation rate is then calculated as

$$\dot{\omega}_{evap} = \frac{\epsilon_{pore}(1-\phi)\rho_g^g(Y_{vap,corr}-Y_{vap})}{dt} \quad (28)$$

where dt is the time step size, ϵ_{pore} is, again, the porosity, and Y_{vap} is the mass fraction of water vapor at the old time step.

The thermal drying model is based on the concept of switching the evaporation in a grid cell on and off. Mathematically, this relationship can be expressed as[9]

$$\dot{\omega}_{evap} = \begin{cases} f_{evap}\dfrac{F_{heat}}{\Delta h_{evap}} & T \ge T_{evap},\ \rho_l > 0 \\ 0 & \text{otherwise} \end{cases} \quad (29)$$

where $\dot{\omega}_{evap}$ is the evaporation rate, and f_{evap} is the evaporation fraction. The heat flux (F_{heat}) is given by

$$F_{heat} = \frac{1}{r}\frac{\partial}{\partial r}\left(r\epsilon_{pore}(1-\phi)\rho_g^g u_r c_{p,g}T - r\lambda_{eff}\frac{\partial T}{\partial r}\right) \quad (30)$$

The thermal drying model is commonly based on the assumption that drying occurs at a fixed boiling temperature of 373 K.[4] In this work, evaporation temperature and boiling temperature are used interchangeably. However, during drying, a significant amount of water suddenly evaporates and enters the gas phase as water vapor, which results in an increase in pressure. Therefore, the pressure in the interior of the wood particle may significantly differ from atmospheric pressure. Such a higher internal pressure results in increased evaporation temperatures, which yield liquid free water evaporation above

DOI: 10.1021/acs.energyfuels.7b02771
Energy Fuels 2017, 31, 13743−13760

373 K. In order to account for this, the evaporation temperature is modeled as a function of the internal pressure, according to

$$T_{evap} = T_A \log\left(\frac{P_g}{P_{1\,atm}}\right) + T_0 \quad (31)$$

when T_A = 32.7 K, T_0 = 373 K, and $P_{1\,atm}$ = 101 325 Pa. The coefficients within this equation have been determined by calculating the temperature from a given internal saturated water vapor pressure and fitting a mathematical expression to this correlation.

This pressure-dependent boiling temperature can only be applied in a model that accurately monitors pressure evolution inside the wood particle.

The kinetic rate drying model describes drying as a chemical reaction, which can be expressed by an Arrhenius term,

$$\dot{\omega}_{evap} = k_{evap}\rho_{water} \quad (32)$$

where ρ_{water} is the density of the liquid water. In this work, only bound water evaporates according to the kinetic rate drying model, such that bound water density substitutes for liquid water density in the previous equation. The evaporation rate constant is expressed as[30]

$$k_{evap} = A_{evap}\exp\left(\frac{-E_{a,evap}}{RT}\right) \quad (33)$$

In the literature, a broad range of different kinetics is used to describe evaporation, with the most common ones listed in Table 1.

Table 1. Kinetic Data for the Kinetic Rate Drying Model

activation energy [kJ mol^{-1}]	pre-exponential factor [s^{-1}]	ref
88	5.13 × 10^{10}	9, 30
24/120[a]	5.13 × 10^{6}	31
88	5.60 × 10^{8}	32
88	5.13 × 10^{6}	33

[a]The first value is used for liquid free water evaporation modeling, and the second term is used for bound water evaporation modeling.

The wide range of different kinetic data used to model drying suggests that the drying model is commonly tuned in order to fit experimental data. In this model, the first and the third set of kinetic data have been tested. The main advantage of the kinetic rate drying model is that it is more numerically stable[4] than the thermal drying model.

It is also possible to model drying with a combination of the thermal model and the kinetic rate model. In such a case, the evaporation of the liquid free water is modeled with the thermal model and the evaporation of the bound water is described by the kinetic rate model. The critical moisture content, which defines whether liquid free water or bound water need to be modeled, is the fiber saturation point (M_{fsp}), which is commonly set to 30 wt % on an oven-dry basis.

2.3. Devolatilization. Devolatilization (see Table 2) is described by a scheme of three independent competitive reactions, where wood degrades to the main products: tar, char, and noncondensable gases.[21] After the primary devolatilization, tar reacts further, commonly via intraparticle cracking and repolymerization reactions, and forms noncondensable gases and char, respectively.[15] The kinetic data for primary and secondary devolatilization reactions was taken from Lu et al.[5]

Devolatilization is a complex process where both chemical and physical processes influence each other and, therefore, must be considered simultaneously. The influence of extractives on chemical reactions has not been explicitly considered, since wood is already modeled as a mixture of compounds.

3. NUMERICAL SETUP

In the cases presented in this paper, the following case-specific boundary conditions and additional settings of the 1D simulation tool were used:

(1) The furnace wall and gas phase temperatures were set to 1276 and 1050 K, respectively.[5]
(2) The pressure at the particle surface was set equal to the ambient pressure.
(3) The boundary condition for the species mass fractions was a zero-gradient condition.
(4) The 1D mesh includes 55 grid points along the entire particle diameter. Therefore, the particle radius is devided into an equidistant grid by 27 grid points.
(5) The convective terms were discretized by first-order upwinding.
(6) Diffusive terms were discretized by central differencing.
(7) The maximum time step was 10^{-5} s.
(8) Mass conservation was checked for 55, as well as 111, grid points. For the test run with 55 grid points, the relative error was 2.6%, whereas for 111 grid points, the relative error was 2.15%.

It was found that, with 55 grid points, a grid-independent solution is obtained. The wood properties used in the model are listed in Table 3.

The apparent wood density deviates slightly from what Lu et al.[5] and Mehrabian et al.[4] used, which is due to the fact that we chose the porosity such that the apparent wood density can be derived from the true wood density, according to

$$\rho_{wood,apparent} = \rho_{wood,true}(1 - \epsilon_{pore}) \quad (34)$$

However, this density difference is minor.

Table 2. Kinetic Data Used for Modeling Devolatilization, Which Are the Same as That Described in the Work of Lu et al.[5]

reaction rate constant	reaction	pre-exponential factor [s^{-1}]	activation energy [kJ mol^{-1}]	ref	heat of reaction [kJ kg^{-1}]	ref
k_1	wood → gases[a]	1.11 × 10^{11}	177	34	−207[b]	18
k_2	wood → tar	9.28 × 10^{9}	149	34	−207[b]	18
k_3	wood → char	3.05 × 10^{7}	125	34	−207[b]	18
k_4	tar → gases[a]	4.28 × 10^{6}	107.5	35	42	36
k_5	tar → char	1 × 10^{5}	107.5	37	42	36

[a]The term "gases" in this table refers to noncondensable gases. [b]The heat of reaction for primary devolatilization reactions was taken specifically for poplar and, therefore, was not taken from Lu et al.[5]

DOI: 10.1021/acs.energyfuels.7b02771
Energy Fuels 2017, 31, 13743−13760

Table 3. Properties Used as Input Values for the Drying and Devolatilization Model[a]

property	units	value	ref
apparent wood density, ρ_{wood}	kg m^{-3}	570	*b*
true wood density, $\rho_{wood,\,true}$	kg m^{-3}	1500	38
porosity, $\epsilon_{pore,0}$		0.62	*b*
thermal conductivity (wood), $\lambda_{wood,\,\parallel}$	W m^{-1} K^{-1}	$0.291 + 2.7588 \times 10^{-4}T$	39
thermal conductivity (wood), $\lambda_{wood,\,\perp}$	W m^{-1} K^{-1}	$\frac{\lambda_{wood,\,\parallel}}{1.9}$	39
thermal conductivity (char), $\lambda_{char,\,\parallel,\,\perp}$	W m^{-1} K^{-1}	0.071	5
thermal conductivity (gases), λ_g	W m^{-1} K^{-1}	25.77×10^{-3}	5
bridge factor, ξ		0.68	15
specific heat capacity			
for wood, $c_{P,wood}$	J kg^{-1} K^{-1}	$1500 + T$	4
for char, $c_{P,char}$	J kg^{-1} K^{-1}	$420 + 2.09T + 6.85 \times 10^{-4}T^2$	4
for gases, $c_{P,g}$	J kg^{-1} K^{-1}	1100	14
dynamic viscosity (gases), μ_{gases}	kg m^{-1} s^{-1}	3×10^{-5}	14
diffusivity, D_{eff}	m^2 s^{-1}	1×10^{-8}	*c*
permeability of wood, $\kappa_{wood\ \perp,\,\parallel}$	m^2	1×10^{-14}	40
permeability of char, $\kappa_{char\perp,\,\parallel}$	m^2	1×10^{-13}	41
permeability for liquid phase, κ_l	m^2	0	*d*
shrinkage parameters			
α		1	*e*
β		0.75	*e*
γ		1	*e*
latent heat of evaporation, Δh_{evap}	J kg^{-1}	2.44×10^6	5
particle emissivity $\epsilon_{particle}$		0.7	*d*
particle diameter, d_p	m	9.5×10^{-3}	5
aspect ratio		4	5
moisture content	wt % (wet basis)	40	5
specific surface area of wood	m^2 m^{-3}	9.04×10^4	5

[a]The data are applied for poplar wood (hardwood). [b]This value was calculated based on knowing the apparent density and the true density. [c]This value was assumed to avoid tar diffusion and, therefore, recondensation in interior grid points. [d]This value was assumed by the authors. [e]The shrinkage parameters were assumed by the authors for fitting modeling results.

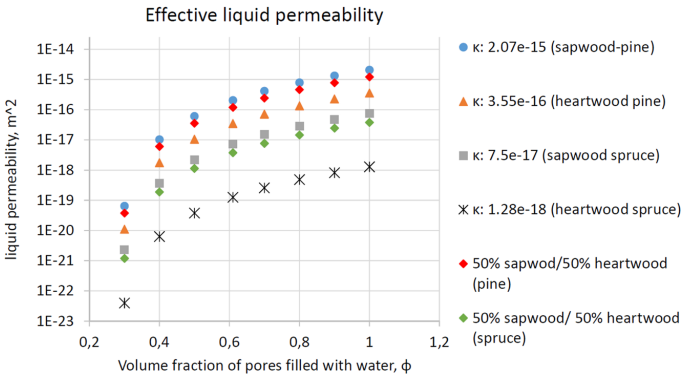

Figure 2. Comparison of effective liquid permeabilities for spruce and pine. The effective liquid permeability is plotted against the volume fraction of pores filled with water. The effective liquid permeability is defined as $\kappa_{l,eff} = \kappa_{l,relative}\kappa_{l,intrinsic}$, where the definitions of $\kappa_{l,relative}$ and $\kappa_{l,intrinsic}$ (mentioned as κ in the plot) have been taken from Grønli.[21] For the definition of the relative permeability the initial porosity, $\epsilon_{pore,0} = 0.62$ (as assumed in this work) and, therefore, a dry wood density of 570 kg m^{-3} were used.

4. RESULTS AND DISCUSSION

Different permeabilities of the liquid water were tested. The effective permeability, which was obtained via

$$\kappa_{l,eff} = \kappa_{l,relative}\kappa_{l,intrinsic} \quad (35)$$

where $\kappa_{l,intrinsic}$ is the intrinsic liquid permeability, which is defined as[21]

$$\kappa_{l,intrinsic} = \kappa_{g,drywood} \quad (36)$$

This suggests that the intrinsic permeability of liquid water is equal to that for the gas mixture. The effective permeability of the liquid phase is plotted in Figure 2.

The water saturation (S) is defined as[21]

DOI: 10.1021/acs.energyfuels.7b02771
Energy Fuels 2017, 31, 13743−13760

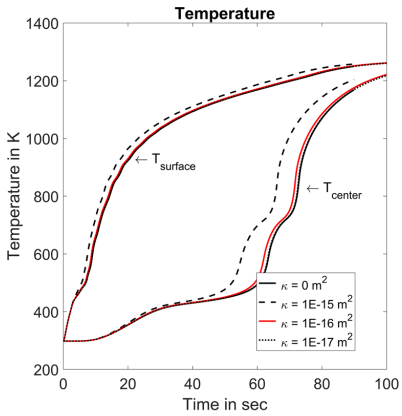

(a) Influence of choice of liquid permeability on center and surface temperature predictions.

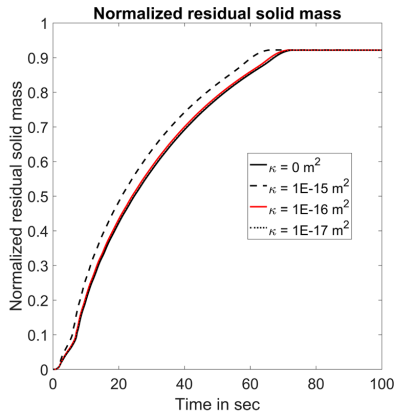

(b) Influence of choice of liquid permeability on normalized residual solid mass predictions.

Figure 3. Determination of the relevance of liquid water convection modeling. Liquid water convection is fully neglected when the liquid permeability is set to 0 m^2. The orders of magnitude of the other tested liquid permeabilities have been taken from the literature.[21] (For distinct differentiation of the plotted lines, see the online version of this article.)

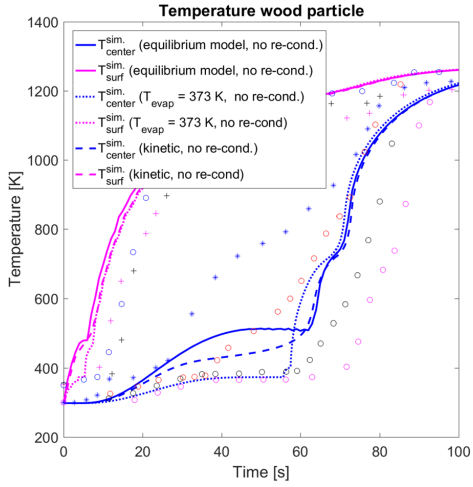

(a) Comparison of the center and surface temperature predicted with the thermal, the kinetic rate and the equilibrium model.

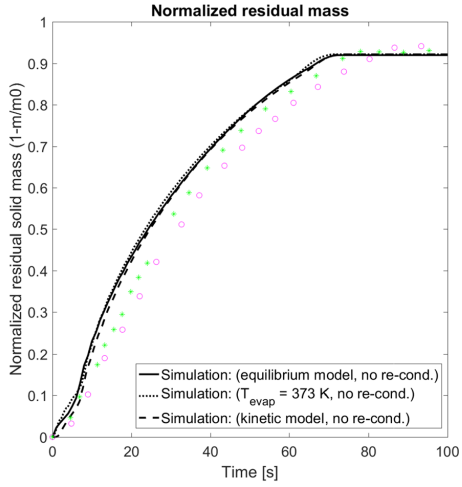

(b) Comparison of the normalized residual solid mass predicted with the thermal, the kinetic rate and the equilibrium model.

Figure 4. Comparison of the results of the thermal model, the kinetic rate model, and the equilibrium model. The kinetic rate model was used with the kinetic data being $A = 5.6 \times 10^8$ s^{-1} and $E_{a,evap} = 88$ kJ mol^{-1}. For distinct interpretation of the surface and center temperatures in panel (a), the online version of this article is recommended to be viewed. All experimental data used for validation has been taken from Lu et al.[5] [Legend in panel (a): purple and black cross symbols (+) and blue open circle (○) represent the experimentally determined particle surface temperatures; black, red, and purple open circles (○), as well as blue asterisks (*), represent the particle center temperatures. Legend in panel (b): green asterisks (*) and purple open circles (○) represent the experimentally measured normalized residual solid masses.]

$$S = \frac{M - M_{fsp}}{M_{sat} - M_{fsp}} \tag{37}$$

where M_{fsp}, M, and M_{sat} are the fiber saturation point (set to 0.3), the actual liquid water fraction, and the water fraction at saturation, respectively. The water saturation must be known to define the relative permeability in the longitudinal direction, such that

$$\kappa_{l,relative,long} = S^8 \tag{38}$$

and

$$\kappa_{l,relative,tang} = S^3 \tag{39}$$

DOI: 10.1021/acs.energyfuels.7b02771
Energy Fuels 2017, 31, 13743−13760

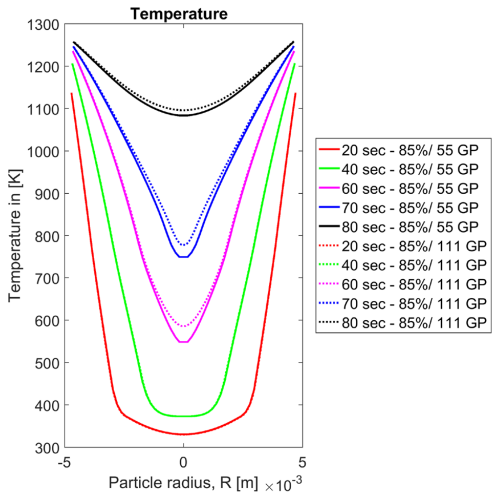

(a) Temperature prediction (thermal drying model with f_{evap}=0.85) with 55 and 111 grid points.

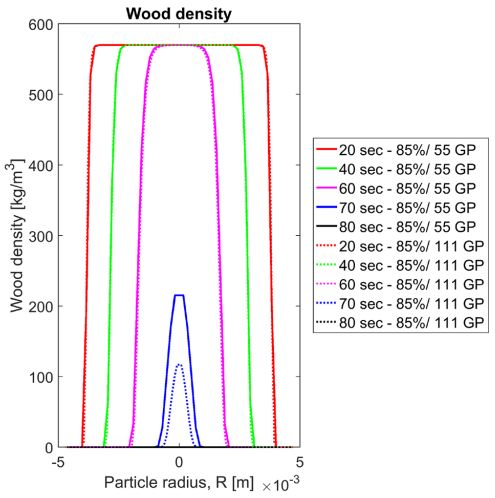

(b) Wood density prediction (thermal drying model with f_{evap}=0.85) with 55 and 111 grid points.

Figure 5. Results of the grid independence study of the thermal drying model with f_{evap} = 0.85, with 55 and 111 grid points. Recondensation of water vapor to liquid free water has been considered.

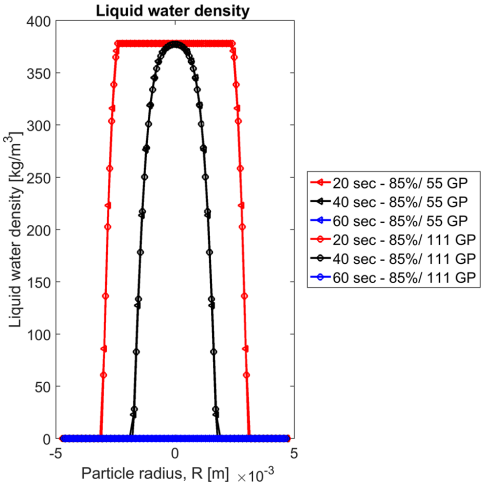

Figure 6. Mesh-independent prediction of drying fronts with the evaporation fraction f_{evap} = 0.85. The tested grid point numbers were 55 and 111.

if the permeability in tangential direction is to be defined.[21]

Since there is commonly very little difference between radial and tangential directions, the authors assumed that

$$\kappa_{l,relative,tang} = \kappa_{l,relative,rad} \quad (40)$$

with $\kappa_{l,relative,rad}$ being the relative liquid permeability in the radial direction. In Figure 2 it is shown that, for volume fractions of pores filled with water of <0.5, which are within a typical range for wood burned in wood stoves, the liquid permeability is commonly below 1×10^{-16} m^2. The liquid permeabilities plotted in Figure 2 are valid for softwoods. Because of the lower porosities (and, consequently, the higher dry virgin wood densities) of hardwood species, such as poplar, which is modeled in this work, hardwood species will have even lower liquid permeabilities, compared to the softwood species.

The influence of the liquid permeability on the modeling results is plotted in Figures 3a and 3b.

It was found that only a liquid permeability as high as 10^{-15} m^2 yielded significantly different results, compared to fully neglecting the liquid water convection. Liquid permeabilities of the order of 10^{-16} m^2 and 10^{-17} m^2 did not significantly differ from the assumption of fully negligible liquid water convection.

Based on Figure 3, one can justify that a typical effective liquid permeability of 10^{-16} m^2 (or smaller) can be used for modeling liquid water convection in wood particles or logs burning in wood stoves. Since the corresponding results are very similar to the results of a model that is fully neglecting liquid water convection, one can also simplify the thermal conversion model of a wood particle by fully neglecting liquid water convection.

The focus on permeability of liquid water, with respect to its influence on the model, was due to the numerical instabilities a nonzero and comparably large permeability can result in when applied together with the thermal drying model. These instabilities are due to continuous on- and off-switching of evaporation reactions in cells where drying has already been fully accomplished at an earlier time. This reactivation of drying is due to some liquid water transportation outward to dry cells and the requirement that whatever water that is present there must be gone if temperatures shall exceed the boiling temperature.

DOI: 10.1021/acs.energyfuels.7b02771
Energy Fuels 2017, 31, 13743−13760

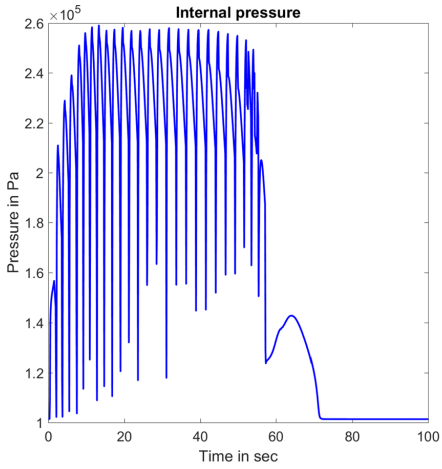

(a) Pressure prediction in the wood particle center (f_{evap}=1).

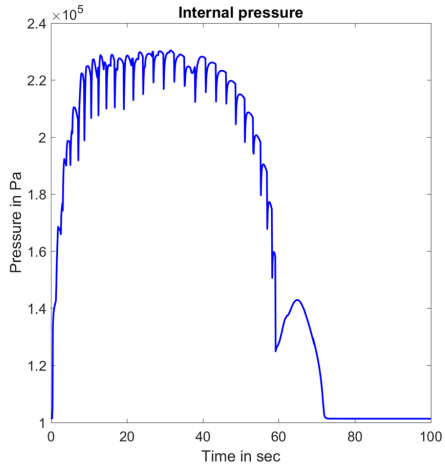

(b) Pressure prediction in the wood particle center (f_{evap}=0.85).

Figure 7. Internal pressure prediction obtained when applying the thermal drying model without and with correction (f_{evap} = 1 or f_{evap} = 0.85, respectively). Correction is required to reduce numerical oscillations. Recondensation of water vapor to liquid free water has been considered.

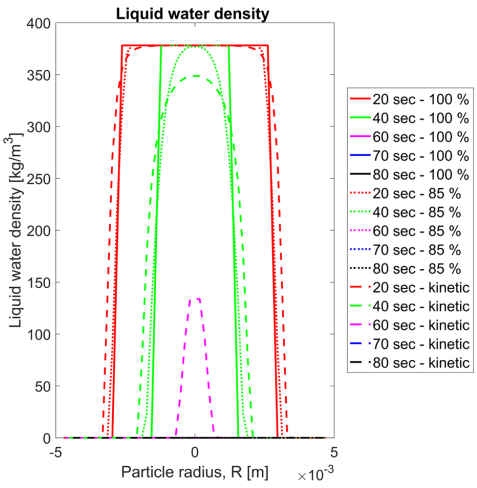

(a) Drying-front at different times for f_{evap}=0.85.

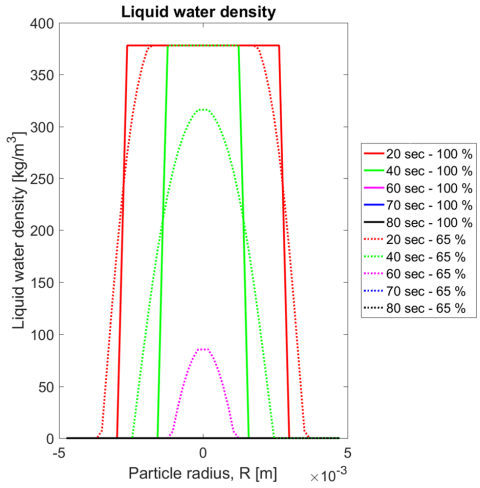

(b) Drying-front at different times for f_{evap}= 0.65.

Figure 8. Comparison of the smearing of the drying front for f_{evap} = 0.85 and f_{evap} = 0.65. Both fractions were compared against the noncorrected drying front, with f_{evap} = 1. Recondensation of water vapor to liquid free water has been considered.

Therefore, the authors' conclusion was that liquid permeability can be set to zero and convective liquid free water transportation can be neglected, since this does not affect modeling results, while, at the same time, it can stop the numerical instabilities.

As mentioned earlier, the authors have also tested the equilibrium model to determine whether its results were more similar to predictions obtained from the thermal drying model or the kinetic rate drying model. It was found that the equilibrium model would predict a significantly different center temperature, compared to the thermal drying model and the kinetic rate drying model with a lower pre-exponential factor (see Figure 4).

One can clearly see that the equilibrium model predicts very different center temperatures, compared to both the kinetic rate model and the thermal drying model. The surface temperature and the residual solid mass do not differ significantly. However, the results of the equilibrium model differ most significantly

DOI: 10.1021/acs.energyfuels.7b02771
Energy Fuels 2017, 31, 13743−13760

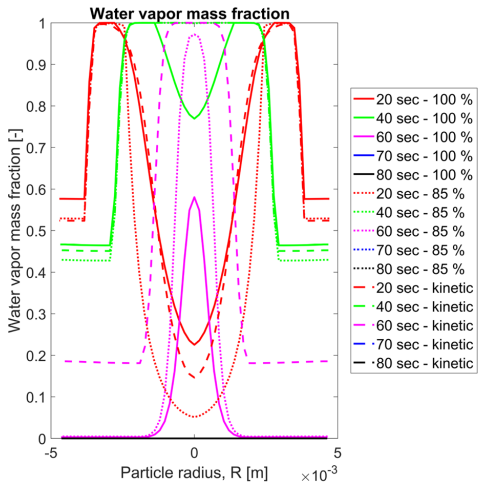

(a) Model results of water vapor mass fraction.

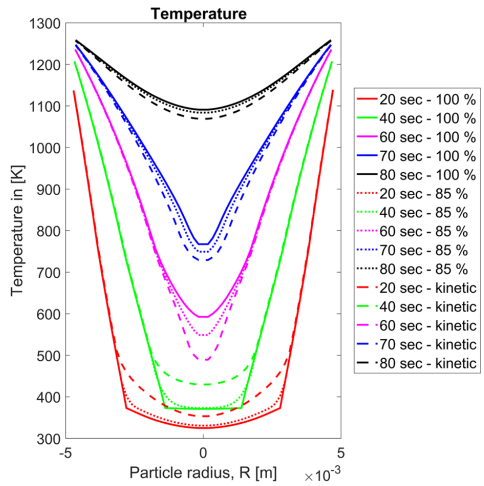

(b) Model results of temperature.

Figure 9. Comparison of water vapor mass fractions and temperature predictions for f_{evap} = 0.85 and f_{evap} = 1 and the kinetic rate drying model. The initial moisture content was 40 wt % (wet basis), and the boiling temperature was fixed to 373 K. Recondensation of water vapor to liquid free water has been considered.

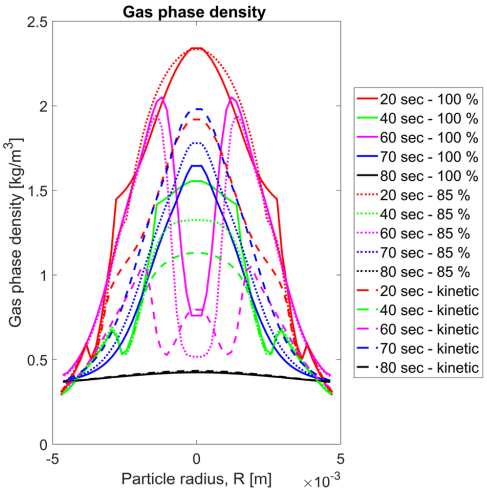

(a) Gas phase density predictions.

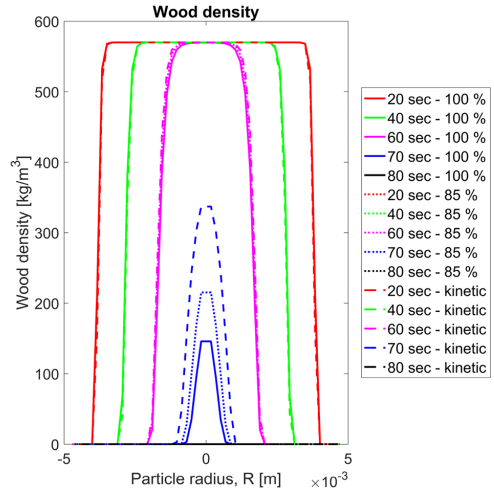

(b) Wood density predictions.

Figure 10. Model predictions of total gas density and wood density for f_{evap} = 0.85 and f_{evap} = 1 and the kinetic rate drying model. The initial moisture content was 40 wt % (wet basis), and the boiling temperature was fixed to 373 K. Recondensation of water vapor to liquid free water has been considered.

from the experiments; therefore, further discussion of model accuracy, stability, and efficiency is only done with the more suitable thermal and kinetic rate models, whose results are closer to what has been experimentally observed. The main reason for the difference between the equilibrium model and the two other drying models is most likely that the equilibirum model is developed for low-temperature drying, which is different from the case that we tested in this model (see numerical setup).

4.1. Grid Independence Study. Different numbers of grid points have been tested in order to identify the number of grid points that are required to ensure grid-independent results. Initially, the model was tested with 55 grid points along the entire wood particle diameter, and, subsequently, 111 grid points were used to generate the 1D mesh. It was found that the model describing drying and devolatilization yields grid-independent solutions already with 55 grid points (see Figures 5a and 5b).

DOI: 10.1021/acs.energyfuels.7b02771
Energy Fuels 2017, 31, 13743−13760

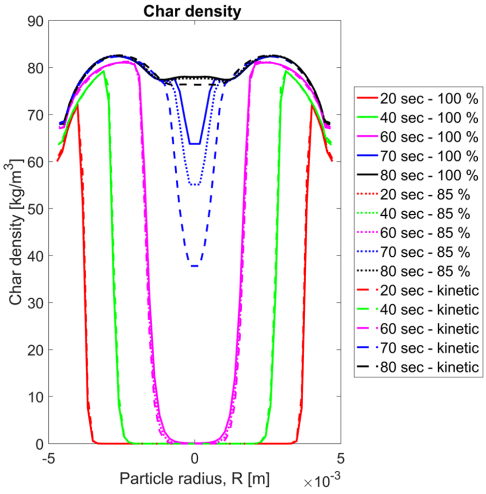

(a) Char density modeling results.

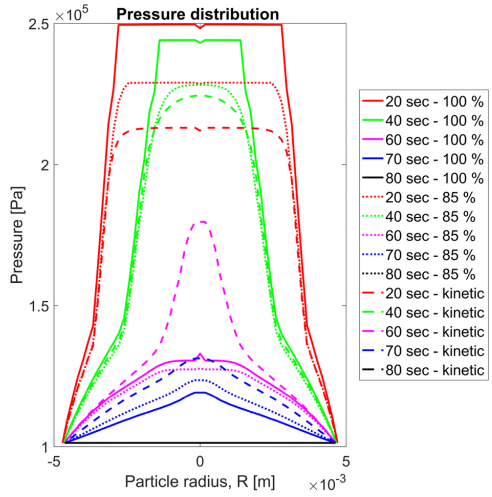

(b) Pressure modeling results.

Figure 11. Model predictions of char density and internal pressure for f_{evap} = 0.85 and f_{evap} = 1 and the kinetic rate drying model. The initial moisture content was 40 wt % (wet basis), and the boiling temperature was fixed to 373 K. Recondensation of water vapor to liquid free water has been considered.

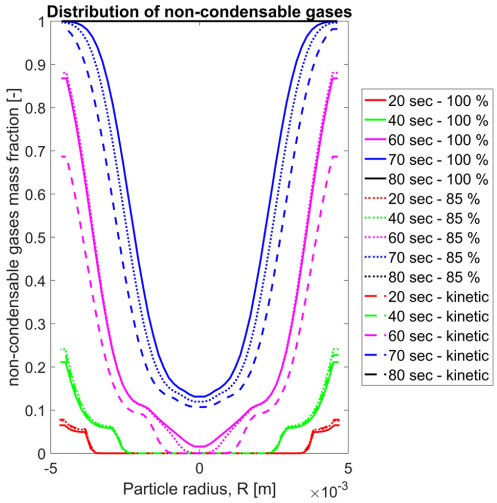

(a) Non-condensable gas species mass fraction modeling results.

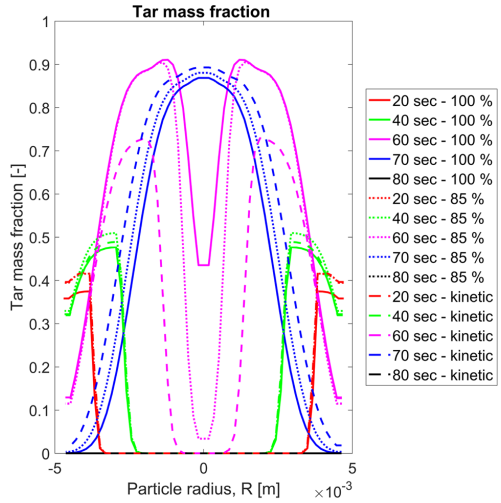

(b) Tar mass fraction modeling results.

Figure 12. Comparison of noncondensable gas-species mass fraction and tar mass fraction predictions for f_{evap} = 0.85 and f_{evap} = 1 and the kinetic rate drying model. The initial moisture content was 40 wt % (wet basis), and the boiling temperature was fixed to 373 K. Recondensation of water vapor to liquid free water has been considered.

Only the plots for temperature and wood density are shown here. Even though there are some small deviations in the center of the wood particle, the differences are rather minor and do not affect the predicted conversion time. Since predicted values near the particle surface agree well when comparing the coarse and the fine mesh, it is recommended to use the smaller grid point number, since by halving the grid points, the computer processing unit (CPU) time of the drying and devolatilization model can be significantly decreased. In case of the thermal drying model with f_{evap} = 0.85, the model with 111 grid points results in a CPU time of 15 412 s, which is significantly larger, compared to the same numerical setup with 55 grid points, where the CPU time is 5045 s.

DOI: 10.1021/acs.energyfuels.7b02771
Energy Fuels 2017, 31, 13743−13760

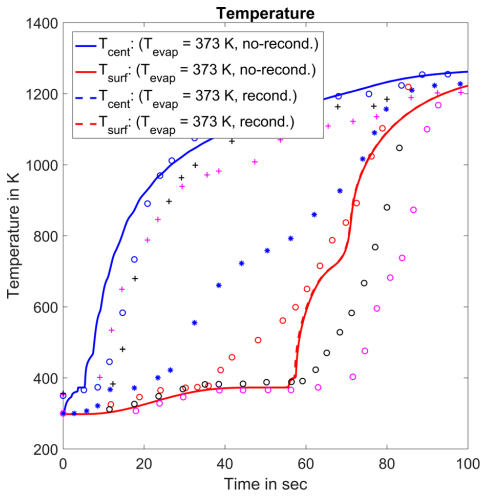

(a) Surface and center temperature modeling results with re-condensation of water vapor and without re-condensation reactions.

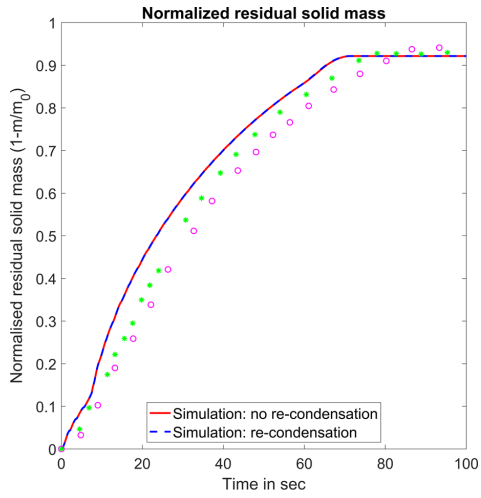

(b) Normalized residual solid mass modeling results with re-condensation of water vapor and without re-condensation reactions.

Figure 13. Comparison of temperature and normalized residual solid mass predictions, with and without water vapor recondensation. The thermal drying model, with an evaporation fraction of 1 and a fixed boiling temperature, was applied. The initial moisture content was 40 wt % (wet basis). All experimental data used for validation has been taken from Lu et al.[5] [Legend in panel (a): purple and black cross symbols (+) and blue open circle (○) represent the experimentally determined particle surface temperatures; black, red, and purple open circles (○), as well as blue asterisks (*), represent the particle center temperatures. Legend in panel (b): green asterisks (*) and purple open circles (○) represent the experimentally measured normalized residual solid masses.]

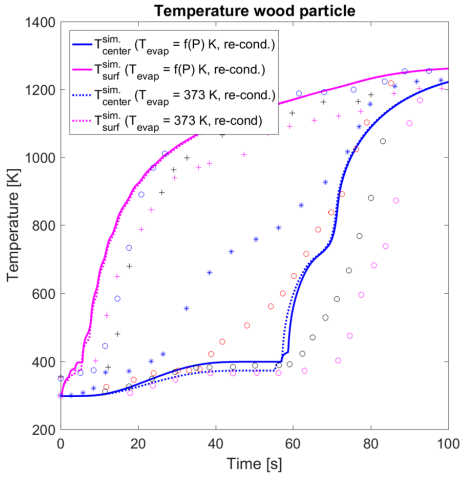

(a) Predicted center and surface temperature (T_{evap} being 373 K and pressure-dependent).

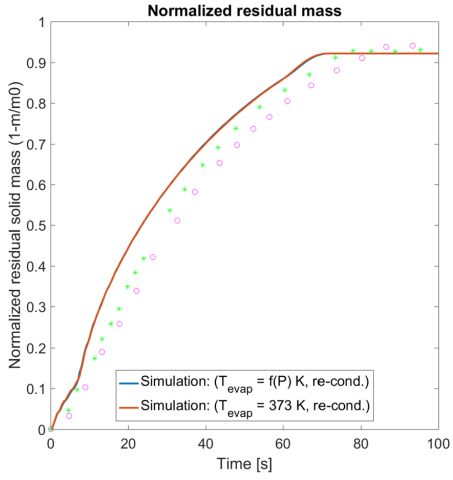

(b) Normalized residual solid mass predicted (T_{evap} being 373 K and pressure-dependent).

Figure 14. Comparison of predictions of normalized residual solid mass and temperatures at the particle surface and in the particle center by first assuming the thermal drying model with a fixed boiling temperature of 373 K and by second assuming the thermal drying model with a pressure-dependent boiling temperature. The evaporation fraction was 1 and the initial moisture content was 40 wt % (wet basis). All experimental data used for validation has been taken from Lu et al.[5] [Legend in panel (a): purple and black cross symbols (+) and blue open circle (○) represent the experimentally determined particle surface temperatures; black, red, and purple open circles (○), as well as blue asterisks (*), represent the particle center temperatures. Legend in panel (b): green asterisks (*) and purple open circles (○) represent the experimentally measured normalized residual solid masses.] Recondensation of water vapor to liquid free water has been considered.

DOI: 10.1021/acs.energyfuels.7b02771
Energy Fuels 2017, 31, 13743−13760

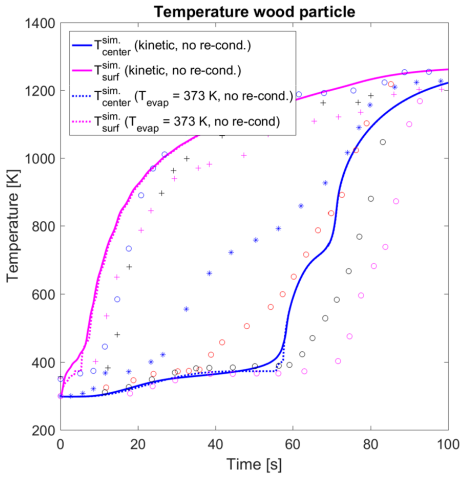

(a) Predicted center and surface temperature predicted when applying the kinetic rate drying model compared to the thermal model.

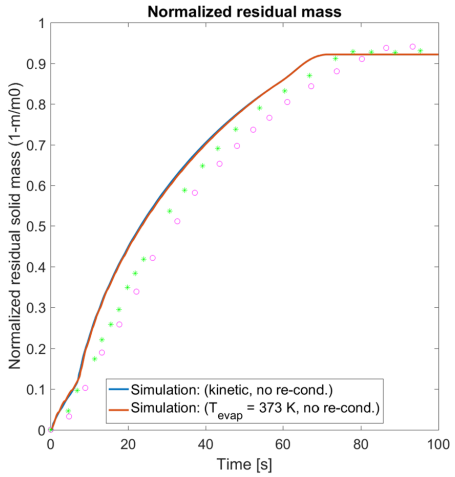

(b) Normalized residual solid mass predicted when applying the kinetic rate drying model compared to the thermal model.

Figure 15. Comparison of predictions of normalized residual solid mass and temperatures at the particle surface and in the particle center by assuming the thermal drying model with a fixed boiling temperature or by assuming the kinetic rate drying model with a high pre-exponential factor ($A = 5.13 \times 10^{10}$ s^{-1} and $E_a = 88$ kJ mol^{-1}). The kinetic drying model was compared against the thermal drying model with the evaporation fraction being 1. Recondensation of water vapor to liquid free water has not been considered when describing evaporation via the thermal drying model (denoted as dotted lines). The initial moisture content of 40 wt % (wet basis). All experimental data used for validation has been taken from Lu et al.[5] [Legend in panel (a): purple and black cross symbols (+) and blue open circle (○) represent the experimentally determined particle surface temperatures; black, red, and purple open circles (○), as well as blue asterisks (*), represent the particle center temperatures. Legend in panel (b): green asterisks (*) and purple open circles (○) represent the experimentally measured normalized residual solid masses.]

The grid independence study also showed that the evaporation fraction introduced in this paper, which is smearing the drying fronts predicted with the thermal drying model, is a mesh-independent correction approach for numerical oscillations. Figure 6 shows that the drying fronts of the model run with 55 and 111 grid points overlay each other very nicely, suggesting that the drying front has the same thickness with both the coarse mesh and the fine mesh.

4.2. Numerical Instabilities of the Thermal Drying Model. A disadvantage of the thermal drying model is that it tends to give oscillatory numerical results,[9] which can be observed in Figure 7a. The reason behind the oscillations is that as soon as a grid cell that contains water is heated to the evaporation temperature, the entire heat flux to this grid cell is used to evaporate the water. The result of this is that the cell is not heated above the evaporation temperature, which consequently means that the neighboring cell on the cold (and humid) side maintains a temperature *below* the evaporation temperature. When all the water in the evaporating cell is gone, it will therefore take some time before the interior cell reaches the evaporation temperature. In this period, there is suddenly no evaporation going on. This means that the pressure will be reduced significantly, until the evaporation in the new cell starts and a pressure increase can be observed. However, this behavior is purely numerical (see Figures 7a and 7b), such that corrections are required.

Yang et al.[6] suggested to overcome these numerical oscillations by multiplying the evaporation rate with a corrective factor. Their correction setup is the same as that used in this model, but the assigned corrective factor differs. Yang et al. set the corrective factor equal to 1 if no adjustment of the evaporation term was done, while by setting the corrective factor equal to the initial moisture content (dry basis), the numerical instabilities were reduced.[6] However, we found that if lower moisture contents are to be modeled, this assumption would result in significantly slower drying at one specific location in the wood log or particle, since only a very small fraction of the entire energy theoretically available for drying is then effectively used for evaporation. Consequently, the theoretically thin evaporation zone is significantly smeared out in the model. Therefore, the choice of a more-independent corrective factor should result in better agreement with the concept of a sharp drying front upon which the thermal drying model is based.

The correction approach applied in this work was to extend the drying zone over more than one grid point and hereby smear the sharp drying front, such that the fluctuation between maximum evaporation rate and minimum evaporation rate (being zero) is avoided. This was achieved by defining the fraction that is reducing the heat flux to a grid cell that could theoretically be used for evaporation in that particular grid cell. The rest of the heat flux is used to heat the cell. A portion of this heat will then be conducted further inward, such that, eventually, a few of the neighboring grid cells also will exceed the evaporation temperature and the evaporation of water there will continue simultaneously (see the mathematical explanation in eq 29). A higher fraction of heat flux used for heating the evaporating grid cells, and therefore a lower fraction of heat flux used for evaporation, leads to a larger number of grid points where evaporation occurs simultaneously. This fraction is

DOI: 10.1021/acs.energyfuels.7b02771
Energy Fuels 2017, 31, 13743−13760

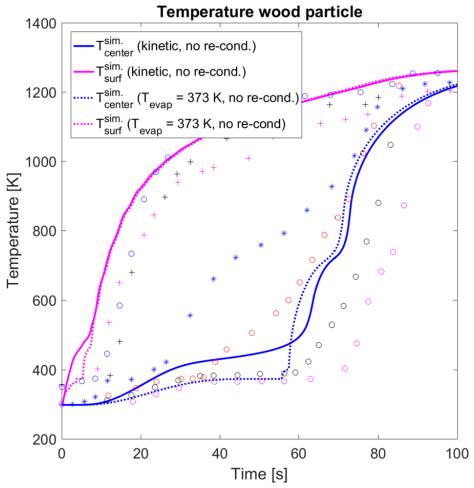

Figure 16. Predicted temperatures at the particle surface and in the particle center by assuming the kinetic rate drying model with a lower pre-exponential factor (A = 5.6 × 10^8 s^{-1} and E_a = 88 kJ mol^{-1}). The kinetic drying model was compared against the thermal drying model results, with the evaporation fraction being 1. Recondensation of water vapor to liquid free water has not been considered when using the thermal drying model (denoted by dashed lines). The initial moisture content was 40 wt % (wet basis). Experimental results for validation were taken from Lu et al.[5] [Legend regarding the experimental data: open blue circles (○), and black and purple crosses (+) represent $T_{surface}$ data; purple, black, and red open circles (○), as well as blue asterisk (*) represent T_{center} data.]

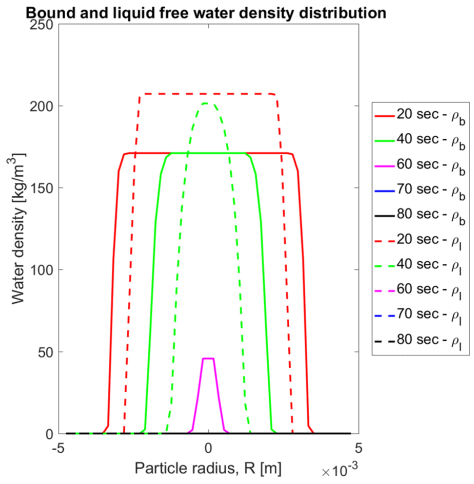

Figure 17. Water densities of liquid free water (ρ_l) and bound water (ρ_b) along the wood particle diameter plotted at different times.

referenced as the evaporation fraction, f_{evap}, in this work. Figure 7b shows how the pressure fluctuations were reduced when applying f_{evap} = 0.85.

With f_{evap} = 0.85, which expresses that 85% of the incoming heat flux is used for evaporation, the pressure oscillations are significantly reduced, compared to what is seen when applying f_{evap} = 1. In the case of f_{evap} = 0.85, the drying front reached over 4 grid points (given at 20 s) (Figure 8a). Therefore, the smearing was still limited, such that the assumption of a sharp drying front is still valid. In comparison to f_{evap} = 0.85, a lower evaporation fraction (f_{evap} = 0.65) led to a more significant smearing over 9 grid points (given at 20 s), as shown in Figure 8b.

It was found that a smearing of the drying front over 9 grid points was too significant, with respect to a total number of 27 points along the radius of the wood particle. Such an extensive smearing results in a significant deviation from the modeling concept of a sharp drying front moving inward, which is the fundamental idea of the thermal drying model. Therefore, this assumption is considered to be inaccurate for the thermal drying model. It was found that applying a value of f_{evap} = 0.85 yields more accurate results. Comparing the results of a noncorrected drying front and a drying front smeared out by f_{evap} = 0.85 showed that, overall, the two predictions agree well (see Figures 9−12). This confirmed the assumption that f_{evap} = 0.85 can significantly correct the internal pressure fluctuations, while, at the same time, not affecting the model predictions too much. In Figures 8−12 the term "kinetic" refers to a pre-exponential factor of 5.6 × 10^8 s^{-1} and an activation energy of 88 kJ mol^{-1}. Transportation of liquid free water was set to zero, when the thermal model was used.

Significant deviations occur between the corrected thermal drying model (f_{evap} = 0.85) and the uncorrected thermal drying model (f_{evap} = 1), as well as the kinetic rate model, when the water vapor mass fraction is modeled (see Figure 9a). The kinetic rate model results in different modeling results, compared to the thermal model, since it models enhanced drying reactions at temperatures higher than 373 K, such that more time is required to terminate the pre-drying heating. Meanwhile, the thermal drying model has proceeded slightly further than the kinetic rate drying model at the same time and, based on these less-enhanced evaporation reactions, the behavior of the water vapor mass fraction (predicted by the kinetic rate model) follows the behavior of the mass fraction of water vapor predicted by the thermal drying model but is retarded. At 60 s, the water vapor mass fractions at the boundaries differ significantly, which is assumed to be due to less-enhanced devolatilization reactions in the wood log, when the kinetic rate model is used. This is due to still ongoing evaporation reactions. In contrast to this, the thermal drying model models evaporation reactions to be finished, such that post-drying heating starts earlier, and temperatures where enhanced devolatilization reactions occur are reached earlier. However, at 70 s, the water vapor mass fractions predicted by the two drying models result in the same results. At the boundaries, the uncorrected and the corrected thermal drying models do not differ significantly. They predict different results in the particle center, as can be seen at 20 s, where the deviation is obvious, and it is assumed that this is due to enhanced inward transportation due to diffusion. The uncorrected thermal drying model predicts a high water vapor mass fraction at one specific location, while the interior grid cell has no evaporation reactions and, therefore, low water vapor mass fractions. However, the corrected thermal drying model predicts evaporation reactions at a limited number of neighboring cells, and, therefore, it is assumed that the difference between the mass fractions of water vapor at two neighboring points is lower, such that reduced inward diffusion occurs. Therefore, the mass fraction of water vapor predicted by the uncorrected

DOI: 10.1021/acs.energyfuels.7b02771
Energy Fuels 2017, 31, 13743−13760

Table 4. CPU Times of Different Drying Models[a]

drying model	T_{evap} [K]	A_{evap} [s^{-1}]	$E_{a,evap}$ [kJ mol^{-1}]	evaporation fraction, f_{evap}	M_{water} [wt % (wet basis)]	CPU time [s]
TDM[b]	373			0.65	40	3415
TDM[b]	373			0.85	40	3685
TDM[b]	373			1	40	5045
TDM[b]	$f(P)$			0.85	40	3334
TDM[b]	$f(P)$			1	40	4309
KRDM		5.6×10^8	88		40	3467
KRDM		5.13×10^{10}	88		40	2930
TDM[b] and KRDM	f(P)	5.6×10^8	88	0.85	40	3947

[a]"TDM" is the abbreviation for the "Thermal drying model" and "KRDM" is the abbreviation for the "Kinetic rate drying model". $f(P)$ indicates that the boiling temperature was modeled as a function of the internal pressure. [b]The thermal drying model is considering recondensation reactions of water vapor to liquid free water. The final time used in these test cases was always 100 s.

thermal drying model is highest in the center, which is due to inward transportation, rather than evaporation reactions. At 60 s, it is assumed that reversed effects of diffusion affecting the distribution of water vapor mass fractions cause the discrepancy in modeling results.

The temperature predictions were not significantly affected by the choice of drying model or the application of an evaporation fraction. Deviations can only be detected in the particle center, where both the kinetic rate drying model, as well as the corrected thermal drying model (f_{evap} = 0.85), resulted in a smoother temperature transition between the dry and wet wood zones. However, in the outer particle zones, the same temperatures were predicted by all models.

The outer peaks of the gas-phase density (Figure 10a) are due to devolatilization reactions. When comparing Figures 10a and 10b, one can clearly see that the peaks in gas phase density overlap with the zones of decreasing wood density. This indicates that the peaks in the gas phase are due to primary devolatilization reactions. Figure 10b shows that the wood density—and, therefore, also the primary devolatilization modeling results—were not significantly affected by the different drying models, since the deviation between the predictions, which was clearly visible at 60 s, vanished after 70 s. The difference in gas phase at 60 s is assumed to be primarily due to retarded drying, which was obtained when modeling drying with the kinetic rate drying model. While the kinetic rate drying model still has a peak of gas-phase density in the center of the wood particle, which indicates ongoing evaporation reactions, the thermal drying model showed lower values in the center of the particle, compared to the devolatilization fronts. This outlines that evaporation reactions have been terminated in the uncorrected as well as the corrected thermal drying model.

The differences in wood density (Figure 10b) in the center of the particle are rather minor, and are only due to slight differences in evaporation time predictions. This outlines that drying and devolatilization are closely linked and therefore an accurate thermal conversion model must describe all stages of thermal conversion very well.

The internal pressure seems to be affected by the numerical oscillations of the thermal drying model (see Figure 11b). One can clearly see in Figure 11b that a smaller pressure gradient occurs in the zones where the stage of devolatilization has been accomplished. This flattening is due to the increased permeability of the char layer, which enhances the outward flow of the gas. Here, pressure cannot build up as significantly as in the dry or wet wood areas of the particle, where a lower permeability is given. One can also clearly see that the assumption of different drying models does not affect char densities significantly (see Figure 11a).

Little deviation is seen for the noncondensable gases and tar. The highest deviation was observed at 60 s for the tar. However, this deviation is again fully balanced at 80 s and is at least slightly less significant at 70 s. The differences in tar and noncondensable gases are assumed to be due to the difference in temperature which most likely is due to the retarded drying stage modeled by the kinetic rate drying model and the corrected thermal drying model, compared to the uncorrected thermal drying model. It is also interesting to see that, between 70 s and 80 s, ongoing secondary tar reactions lead to complete consumption of tar and a significant increase in noncondensable gases.

The most important finding of this section is that both thermal drying models, corrected by f_{evap} = 0.85 or f_{evap} = 1, resulted in more or less similar modeling results, especially near the particle surface. The same total conversion times were obtained (meaning similar predictions of normalized residual solid mass), which highlights that both models are accurate and f_{evap} = 0.85 does not introduce any significant errors to the model.

4.3. Importance of Water Vapor Recondensation. Even though it is assumed that water vapor recondensation only occurs to a limited extent, it is interesting to see how its consideration or negligence affect model accuracy. The water vapor was only allowed to recondense back to liquid free water. The evaporation fraction (f_{evap}) of the thermal drying model was set to unity. No bound water was considered.

It was found that, for this test case, the influence of recondensation reactions is limited, leading to the conclusion that recondensation reactions of water vapor can be neglected.

As can be seen from Figure 13, there is hardly any difference in modeling results. This suggests that the water vapor recondensation reactions also can be neglected. Consequently, it is valid to apply the simplifying assumption of negligible recondensation reactions, without hereby significantly affecting model accuracy.

4.4. Pressure-Dependent Boiling Temperature. The thermal drying model was also tested by using a boiling temperature that is modeled as a function of internal pressure. The accuracy of a pressure-dependent boiling temperature is closely linked to the assumed permeabilities of wood, since the permeabilities define the maximum internal pressure and, therefore, also the evaporation temperature.

Comparison of the modeling results of the two different thermal drying modeling approaches in Figures 14a and 14b shows that the differences in the model predictions are very

DOI: 10.1021/acs.energyfuels.7b02771
Energy Fuels 2017, 31, 13743−13760

small, even though one can clearly see that the temperature plateau, which is observed at 373 K for the common thermal drying model with fixed boiling temperature, increased to slightly higher temperature when the boiling temperature was made pressure-dependent (Figure 14a). The predicted surface temperatures are hardly affected. It was found that the predicted normalized residual solid mass was similar for both concepts of the thermal drying model.

One can conclude that assuming a pressure-dependent boiling temperature does not result in a significant increase of accuracy of the model but is rather superfluous for conditions similar to those tested in this model.

4.5. Combined Drying Model. Even though it has been found that applying the thermal drying model and the kinetic rate drying model separately results in accurate model predictions of drying (Figure 15), it is of interest to identify how model accuracy is affected if the two models are combined. If such a combination of the drying models is done, the kinetic rate model is used to describe bound water evaporation, while the thermal model is used to describe liquid free water evaporation. A combination of drying models is supposed to mimic that liquid free water and bound water evaporate differently.

The applied kinetic data in Figures 15a and 15b were based on a high pre-exponential factor and therefore a very fast drying process, which involves only a few grid points at the same time. One can see that there is hardly any difference in the predictions when using the thermal drying model and the kinetic rate drying model separately. The kinetic data with a lower pre-exponential factor ($A = 5.6 \times 10^8$ s^{-1} and $E_a = 88$ kJ mol^{-1}) showed significant deviation from thermal drying model predictions regarding the prediction of the center temperature, as shown in Figure 16.

When testing a combined drying model, a numerical setup with the total liquid water content being split into bound water and liquid free water by the fiber saturation point M_{fsp} (30 wt % moisture content (oven-dry basis)) was used. The evolution of these two types of liquid water can be seen in Figure 17. The boiling temperature was assumed to be 373 K. The applied kinetic rate drying model was based on a pre-exponential factor of 5.6×10^8 s^{-1} and an activation energy of 88 kJ mol^{-1}.

It was found that modeling the present liquid water as a combination of bound water and liquid free water did not increase the accuracy of the model. The accuracy of normalized residual solid mass and surface, as well as center temperature predictions, could not be increased.

It is assumed that the most important aspect of an accurate drying model is an accurate description of the evaporation, while the description of liquid water transportation does not significantly influence the modeling results. However, it must be mentioned that, in the test cases discussed in this paper, high-temperature drying conditions are given, such as in a wood stove. Liquid water transportation might become more important if low-temperature drying processes are modeled.

4.6. Numerical Efficiency of the Drying Models. In order to evaluate numerical efficiency of the drying models, the CPU times were compared (see Table 4).

It can clearly be seen that the model requires more time to reach convergence if the thermal drying model is used without the evaporation fraction. It is assumed that the reason is that, in the uncorrected drying model, significant fluctuations of the internal pressure must be modeled. When smearing the sharp drying front by an evaporation fraction of 0.65, the CPU time decreases from 5045 s to 3415 s, while the CPU time decreased slightly less (to 3685 s) when an evaporation fraction of 0.85 was applied. Hence, the evaporation fraction does not only reduce numerical oscillations but also affects numerical efficiency of the model. It was also found that modeling a pressure-dependent boiling temperature for the thermal drying model resulted in reduced CPU times. With a fixed boiling temperature, the CPU time was 5045 s, while it was 4309 s when modeling a pressure-dependent boiling temperature. In both cases, the drying front was not smeared (with the evaporation fraction being unity).

Kinetic rate drying models, which are considered more numerically stable, are more numerically efficient, compared to the thermal drying models. By increasing the pre-exponential factor of the Arrhenius term describing evaporation, enhanced evaporation is shifted to lower temperatures. For a pre-exponential factor on the order of 10^8 s^{-1}, the CPU time is as high as 3467 s and, therefore, it is faster than the uncorrected thermal drying model (5045 s). By further increasing the pre-exponential factor from 5.6×10^8 s^{-1} to 5.13×10^{10} s^{-1}, the CPU time decreased to 2930 s.

The combined drying model resulted in a CPU time that was in the range of the separate corrected thermal drying model ($f_{evap} = 0.85$), as can be seen from Table 4.

The numerical efficiency of the thermal drying model can be improved by applying evaporation fractions and hereby smearing the drying front. Nonetheless, note that the choice of evaporation fraction cannot be done arbitrarily, with the sole purpose of reducing oscillatory numerical results and CPU times. One must also consider that evaporation fractions cannot be chosen to be too small, since they will also have an effect on model accuracy.

5. CONCLUSIONS AND RECOMMENDATIONS

In this work, the numerical instabilities of the thermal drying model, the accuracy of the thermal drying model and the kinetic rate drying model, and the numerical efficiency of the two models were investigated. In order to accomplish this, a 1D mesh-based drying and devolatilization model was developed.

It was found that recondensation reactions do not have to be modeled, since they do not increase model accuracy. Neglecting recondensation of water vapor has proven to be a valid simplifying assumption.

The sensitivity of modeling results to the liquid permeability was investigated. It was shown that, with respect to thermal wood conversion applications similar to wood stoves, where lower moisture contents of wood are critical for the stove's operation, one can neglect the liquid free water convection. This is due to the rather low effective permeabilities of the liquid water, which lead to results similar to those of a model that is fully neglecting liquid free water convection.

It was found that the thermal drying model resulted in oscillatory numerical solutions that require correction. Therefore, an evaporation fraction was introduced, which smeared the drying front, such that evaporation was numerically allowed to occur at a limited number of neighboring grid points. Hereby, the oscillations, which were clearly visible when plotting the internal pressure evolution, were reduced and more physically reasonable results were obtained.

Furthermore, it was found that, at least for the small thermally thick wood particles tested in this work, there is no significant difference between assuming a fixed boiling temperature or a pressure-dependent boiling temperature.

DOI: 10.1021/acs.energyfuels.7b02771
Energy Fuels 2017, 31, 13743−13760

Applying a combined model did not improve model accuracy in comparison to separately applied kinetic rate drying models or thermal drying models.

Numerical efficiency tests showed that a corrected thermal drying model with an evaporation fraction of 0.85 operates at lower computational cost than the uncorrected thermal drying model. The pressure-dependent boiling temperature assumption also resulted in reduced CPU time. When applying the kinetic rate model with a higher pre-exponential factor, the CPU times were reduced, compared to the kinetic rate drying model with lower pre-exponential factors.

AUTHOR INFORMATION

Corresponding Author

*Tel.: +47 73 593697. E-mail: inge.haberle@ntnu.no.

ORCID

Inge Haberle: 0000-0002-3945-3627

Notes

The authors declare no competing financial interest.

ACKNOWLEDGMENTS

This work has been carried out within the WoodCFD (243752/E20) project, which is funded by Dovre AS, Norsk Kleber AS, Jøtulgruppen, and Morsø AS, together with the Research Council of Norway, through the ENERGIX program.

NOMENCLATURE

A = pre-exponential factor [s^{-1}]
c_P = specific heat capacity [J kg^{-1} K^{-1}]
D_b = bound water diffusivity [m^2 s^{-1}]
D_{eff} = effective mass diffusivity [m^2 s^{-1}]
d_p = particle diameter [m]
$d_{pore,hydraulic}$ = hydraulic pore diameter [m]
E_a = activation energy [kJ mol^{-1}]
f_{evap} = evaporation fraction [−]
Δh = heat of reaction [kJ kg^{-1}]
h_{conv} = heat-transfer coefficient [W m^{-2} K^{-1}]
$h_{m,pore}$ = mass-transfer coefficient of vapor in pores [m s^{-1}]
k = reaction rate constant [s^{-1}]
M_{fsp} = moisture content at fiber saturation point; dry basis [kg kg^{-1}]
M_l = moisture content (liquid free water); dry basis [kg kg^{-1}]
MW = molecular weight [kg mol^{-1}]
P_c = capillary pressure [Pa]
P_g = gas pressure [Pa]
P_l = liquid phase pressure [Pa]
R = ideal gas constant [kJ mol^{-1} K^{-1}]
r = radius [m]
T = temperature [K]
$S_{C,wood}$ = specific surface area of wood [m^2 m^{-3}]
t = time [s]
T_{evap} = boiling (evaporation) temperature [K]
u_r = gas-phase velocity in the radial direction [m s^{-1}]
u_l = liquid free water velocity in radial direction [m s^{-1}]
V = control volume [m^3]
Y = mass fraction [−]

Greek Letters

α, β, γ = shrinkage parameters [−]
ϵ_g = gas-phase volume fraction [−]
ϵ_{pore} = porosity [−]
$\epsilon_{particle}$ = particle emissivity [−]
κ = permeability [m^2]
λ = thermal conductivity [W m^{-1} K^{-1}]
μ = dynamic viscosity [kg m^{-1} s^{-1}]
ρ = density [kg m^{-3}]
σ = Stefan−Boltzmann constant [W m^{-2} K^{-4}]
ϕ = volume fraction of pores filled with water [−]
Φ = endothermic/exothermic heat of reaction terms [J m^{-3} s^{-1}]
$\dot{\omega}$ = reaction rate [kg m^{-3} s^{-1}]

Subscripts

b = bound water
char = char
devol,1 = primary devolatilization
devol,2 = secondary devolatilization
eff = effective
i = reaction
ir = irreducible saturation
evap = evaporation
vap, corr = saturated water vapor mass fraction after recondensation reactions
fsp = fiber saturation point
g, gas = total gas phase
k = gas species
l = liquid free water
mix, total = mixed gas phase
recond = water vapor recondensation reactions
surf = particle surface
tar = tar
wall = furnace wall
wood = dry wood
wood,0 = dry wood initial
$\parallel$ = parallel to fiber direction
$\perp$ = perpendicular to fiber direction
0 = initial

Superscripts

g = gas phase
sat = saturation

REFERENCES

(1) Porteiro, J.; Granada, E.; Collazo, J.; Patiño, D.; Morán, J. C. *Energy Fuels* **2007**, *21*, 3151−3159.
(2) Porteiro, J.; Míguez, J. L.; Granada, E.; Moran, J. C. *Fuel Process. Technol.* **2006**, *87*, 169−175.
(3) Thunman, H.; Leckner, B.; Niklasson, F.; Johnsson, F. *Combust. Flame* **2002**, *129*, 30−46.
(4) Mehrabian, R.; Zahirovic, S.; Scharler, R.; Obernberger, I.; Kleditzsch, S.; Wirtz, S.; Scherer, V.; Lu, H.; Baxter, L. L. *Fuel Process. Technol.* **2012**, *95*, 96−108.
(5) Lu, H.; Robert, W.; Peirce, G.; Ripa, B.; Baxter, L. L. *Energy Fuels* **2008**, *22*, 2826−2839.
(6) Yang, Y. B.; Sharifi, V. N.; Swithenbank, J.; Ma, L.; Darvell, L. I.; Jones, J. M.; Pourkashanian, M.; Williams, A. *Energy Fuels* **2008**, *22*, 306−316.
(7) Kwiatkowski, K.; Bajer, K.; Celińska, A.; Dudyński, M.; Korotko, J.; Sosnowska, M. *Fuel* **2014**, *132*, 125−134.
(8) Skreiberg, Ø.; Seljeskog, M.; Georges, L. *Chem. Eng. Trans.* **2015**, *43*, 433−438.
(9) Fatehi, H.; Bai, X. S. *Combust. Sci. Technol.* **2014**, *186*, 574−593.
(10) Haberle, I.; Skreiberg, Ø.; Łazar, J.; Haugen, N. E. L. *Prog. Energy Combust. Sci.* **2017**, *63*, 204−252.
(11) Galgano, A.; Di Blasi, C. *Combust. Flame* **2004**, *139*, 16−27.
(12) Galgano, A.; Di Blasi, C. *Ind. Eng. Chem. Res.* **2003**, *42*, 2101−2111.
(13) Di Blasi, C. *Int. J. Heat Mass Transfer* **1998**, *41*, 4139−4150.
(14) Di Blasi, C. *Chem. Eng. Sci.* **1996**, *51*, 1121−1132.

DOI: 10.1021/acs.energyfuels.7b02771
Energy Fuels 2017, 31, 13743−13760

(15) Biswas, A. K.; Umeki, K. *Chem. Eng. J.* **2015**, *274*, 181−191.
(16) Larfeldt, J.; Leckner, B.; Melaaen, M. C. *Fuel* **2000**, *79*, 1637−1643.
(17) Ström, H.; Thunman, H. *Combust. Flame* **2013**, *160*, 417−431.
(18) Van de Velden, M.; Baeyens, J.; Brems, A.; Janssens, B.; Dewil, R. *Renewable Energy* **2010**, *35*, 232−242.
(19) Neves, D.; Thunman, H.; Matos, A.; Tarelho, L.; Gómez-Barea, A. *Prog. Energy Combust. Sci.* **2011**, *37*, 611−630.
(20) Rath, J.; Wolfinger, M.; Steiner, G.; Krammer, G.; Barontini, F.; Cozzani, V. *Fuel* **2003**, *82*, 81−91.
(21) Grønli, M. G. A theoretical and experimental study of thermal degradation of biomass. Ph.D. Thesis, Norwegian University of Science and Technology, Trondheim, Norway, 1996.
(22) de Paiva Souza, M. E.; Nebra, S. A. *Wood Fiber Sci.* **2000**, *32*, 153−163.
(23) Spolek, G. A.; Plumb, O. A. *Wood Sci. Technol.* **1981**, *15*, 189−199.
(24) Tesoro, F. O.; Choong, E. T.; Kimbler, O. K. *Wood Fiber Sci.* **1974**, *6*, 226−236.
(25) Ražnjević, K. *Handbook of Thermodynamic Tables and Charts*; Hemisphere Publishing Corporation: Washington, DC, 1976; pp 1−392.
(26) Siau, J. F. *Wood Sci.* **1980**, *13*, 11−13.
(27) Stamm, A. J. *Wood and Cellulose Science*; Ronald Press: New York, 1964; pp 1−549.
(28) National Laboratory Lawrence Livermore, SUNDIALS: SUite of Nonlinear and DIfferential/ALgebraic Equation Solvers—IDA. 2016; available via the Internet at: http://computation.llnl.gov/projects/sundials/ida [accessed April 28, 2017].
(29) Ouelhazi, N.; Arnaud, G.; Fohr, J. P. *Transp. Porous Media* **1992**, *7*, 39−61.
(30) Bryden, K. M.; Hagge, M. *Fuel* **2003**, *82*, 1633−1644.
(31) Peters, B.; Bruch, C. J. *J. Anal. Appl. Pyrolysis* **2003**, *70*, 233−250.
(32) Di Blasi, C.; Branca, C.; Sparano, S.; La Mantia, B. *Biomass Bioenergy* **2003**, *25*, 45−58.
(33) Chan, W.-C. R.; Kelbon, M.; Krieger, B. B. *Fuel* **1985**, *64*, 1505−1513.
(34) Wagenaar, B.; Prins, W.; van Swaaij, W. *Fuel Process. Technol.* **1993**, *36*, 291−298.
(35) Liden, A.; Berruti, F.; Scott, D. *Chem. Eng. Commun.* **1988**, *65*, 207−221.
(36) Koufopanos, C.; Papayannakos, N.; Maschio, G.; Lucchesi, A. *Can. J. Chem. Eng.* **1991**, *69*, 907−915.
(37) Di Blasi, C. *Combust. Sci. Technol.* **1993**, *90*, 315−340.
(38) Forest Products Laboratory. *Wood Handbook—Wood as an Engineering Material*; General Technical Report No. FPL-GTR-190; U.S. Department of Agriculture: Madison, WI, 1999.
(39) Pozzobon, V.; Salvador, S.; Bézian, J. J.; El-Hafi, M.; Le Maoult, Y.; Flamant, G. *Fuel Process. Technol.* **2014**, *128*, 319−330.
(40) Hagge, M. J.; Bryden, K. M. *Chem. Eng. Sci.* **2002**, *57*, 2811−2823.
(41) Park, W. C.; Atreya, A.; Baum, H. R. *Combust. Flame* **2010**, *157*, 481−494.

DOI: 10.1021/acs.energyfuels.7b02771
Energy Fuels 2017, 31, 13743−13760

Errata for Paper II

This document lists errors found in Paper II. Only errors that matter from a mathematical viewpoint are listed.

Location	Original text	Correction
pp. 13744, Eq. (1)	$\frac{\partial \varepsilon_g \rho_g^g}{\partial t} + \frac{1}{r}\frac{\partial (r \rho_g^g \varepsilon_g u_r)}{\partial r} = \dot{\omega}_{gas} - \frac{\rho_g^g \varepsilon_g}{V}\frac{\partial V}{\partial t}$	$\frac{\partial \varepsilon_g \rho_g^g}{\partial t} + \frac{1}{r}\frac{\partial (r \rho_g^g u_r)}{\partial r} = \dot{\omega}_{gas} - \frac{\rho_g^g \varepsilon_g}{V}\frac{\partial V}{\partial t}$
pp. 13745, Eq.(7)	$\frac{\partial (\varepsilon_g \rho_g^g Y_k)}{\partial t} + \frac{1}{r}\frac{\partial (r \rho_g^g \varepsilon_g Y_k u_r)}{\partial r} = \frac{1}{r}\frac{\partial}{\partial r}\left(r \varepsilon_g \rho_g^g D_{eff}\frac{\partial Y_k}{\partial r}\right) - \frac{\varepsilon_g \rho_g^g Y_k}{V}\frac{\partial V}{\partial t} + \dot{\omega}_k$	$\frac{\partial (\varepsilon_g \rho_g^g Y_k)}{\partial t} + \frac{1}{r}\frac{\partial (r \rho_g^g Y_k u_r)}{\partial r} = \frac{1}{r}\frac{\partial}{\partial r}\left(r \rho_g^g D_{eff}\frac{\partial Y_k}{\partial r}\right) - \frac{\varepsilon_g \rho_g^g Y_k}{V}\frac{\partial V}{\partial t} + \dot{\omega}_k$
pp. 13745, Eq.(10)	$\left(\rho_{wood} c_{P,wood} + \rho_{char} c_{P,char} + \rho_l c_{P,l} + \rho_b c_{P,b} + \varepsilon_g \rho_g^g c_{P,g}\right)\frac{\partial T}{\partial t} + \left(\rho_l c_{P,l} u_l + \rho_b c_{P,b} u_b + \rho_g^g \varepsilon_g c_{P,g} u_r\right)\frac{\partial T}{\partial r} = \frac{1}{r}\frac{\partial}{\partial r}\left(r \lambda_{eff}\left(\frac{\partial T}{\partial r}\right)\right) - \Phi_{evap} - \Phi_{devol,1} + \Phi_{devol,2}$	$\left(\rho_{wood} c_{P,wood} + \rho_{char} c_{P,char} + \rho_l c_{P,l} + \rho_b c_{P,b} + \varepsilon_g \rho_g^g c_{P,g}\right)\frac{\partial T}{\partial t} + \left(\rho_l c_{P,l} u_l + \rho_b c_{P,b} u_b + \rho_g^g c_{P,g} u_r\right)\frac{\partial T}{\partial r} = \frac{1}{r}\frac{\partial}{\partial r}\left(r \lambda_{eff}\left(\frac{\partial T}{\partial r}\right)\right) - \Phi_{evap} - \Phi_{devol,1} + \Phi_{devol,2}$

Paper III

Inge Haberle, Nils Erland L. Haugen and Øyvind Skreiberg, Combustion of Thermally Thick Wood Particles: A Study on the Influence of Wood Particle Size on the Combustion Behavior, Energy & Fuels 2018, 32, 6847 - 6862.

---

energy&fuels

Article

Cite This: Energy Fuels 2018, 32, 6847−6862

pubs.acs.org/EF

Combustion of Thermally Thick Wood Particles: A Study on the Influence of Wood Particle Size on the Combustion Behavior

Inge Haberle,*[,†] Nils Erland L. Haugen,[†,‡] and Øyvind Skreiberg[‡]

[†]Department of Energy and Process Engineering, Norwegian University of Science and Technology, Kolbjørn Hejes vei 1 B, 7491 Trondheim, Norway

[‡]Department of Thermal Energy, SINTEF Energy Research, Kolbjørn Hejes vei 1 A, 7491 Trondheim, Norway

ABSTRACT: A one-dimensional (1D) comprehensive combustion model for thermally thick wet wood particles, which is also applicable for studying large wood logs, is developed. The model describes drying, devolatilization, and char gasification as well as char oxidation. Furthermore, CO oxidation is modeled, in order to account for the fact that exiting gas products can be oxidized and therefore limit the oxygen transportation to the active sites. The challenges for model validation are outlined. Model validation was done against experimental data for combustion of near-spherical wood particles. Furthermore, the validated model was up-scaled and the effect of wood log diameter on the thermal conversion time, the extent as well as the position of drying, devolatilization, and char conversion zones were studied. The upscaling was done for cylindrical wood logs with an aspect ratio of 4. The thermal conversion time significantly increased with the size. It was also found that the relative extent of the drying, devolatilization, and char conversion zones decreased as wood log size increased. The paper concludes with recommendations for future work.

1. INTRODUCTION

Wood has caught the attention of numerous researchers due to its important role as a renewable energy source. Its applications are broad with an enhanced usage within the field of thermal conversion, where a wide range of particle sizes is used.[1] Over the last decades, the designs of the combustion units used to thermochemically convert wood, e.g., wood stoves, were improved based on experimental studies. However, a more cost-efficient optimization route is the combination of modeling and experiments.[2] Therefore, it is of interest to focus on model development describing thermochemical conversion of wood. However, if a wood combustion model shall be embedded in a simulation tool that is used for design and optimization purposes of wood combustion units, an accurate description of the char conversion stage, in addition to the implementation of detailed drying and devolatilization models, is crucial. The reason why char conversion is considered a key part of an accurate solid phase model is that the char conversion stage is significantly slower than drying and devolatilization and hereby influences the total thermal conversion time. Consequently, the char burnout time has a significant effect on the design of a combustion unit. In addition, a significant amount of the thermal energy is stored in the char.

There is already a number of combustion models available.[1,3−11] Two different modeling concepts are used: the layer (or interface) approach[3,4,7,9−11] and the mesh-based approach.[1,5,6,8] A more detailed analysis of currently available thermal wood conversion models is presented by Haberle et al.[12] Still, compared to modeling work related to thermal coal conversion, the literature on wood particles is limited.

Even though numerous studies on coal combustion are available in the open literature these studies are not directly relevant for wood combustion modeling since wood and coal are very different fuels, with wood having a higher volatile content and a lower energy density.[13] The volatile content in biomass is around 80% compared to only around 30% for coal.[14] In addition, while the pore structure of coal is isotropic, the pore structure of biomass is non-isotropic.

Due to the significantly higher volatile content of biomass, biomass has a longer devolatilization stage compared to coal. In fact these two fuels differ significantly in ignition temperature, ignition delay and burnout times. For biomass conversion, volatiles can more easily exit the particle through its porous structure. In coal particles on the other hand, the internal pressure increases more, due to its lower porosity and if the pressure becomes high enough, the walls in the particle break while suddenly releasing the volatiles in jets.[15] This different behavior in volatile release affects the volatiles combustion time. While the combustion time of volatile matter of biomass takes 40−50% of the total combustion time, it only takes 10−20% of the total combustion time of coal particles.[15] All these aspects highlight that wood combustion models are not simply compatible with coal combustion models and wood combustion models therefore have to be considered as an independent area of research where further development is needed.

Yang et al.[1] studied the combustion characteristics of biomass, with a special focus on the particle size range from 10 μm to 20 mm. This was done both experimentally and with a two-dimensional (2D) mesh-based model. Their char conversion model does not explicitly consider the diffusion of oxygen to the active sites and also only considers oxidation reactions, while fully neglecting both steam and CO_2 gasification.[1] However, it has been reported by other

Received: March 6, 2018
Revised: May 3, 2018
Published: June 6, 2018

DOI: 10.1021/acs.energyfuels.8b00777
Energy Fuels 2018, 32, 6847−6862

Table 1. List of Evolution Equations That Have to Be Implemented for the Drying and Devolatilization Model[a]

evolution equation		ref
wood density[b]	$\frac{\partial \rho_{\text{wood}}}{\partial t} = -(k_1 + k_2 + k_3)\rho_{\text{wood}} - \frac{\rho_{\text{wood}}}{V_j}\frac{\partial V_j}{\partial t}$	19
ash density	$\frac{\partial \rho_{\text{ash}}}{\partial t} = -\frac{\rho_{\text{ash}}}{V_j}\frac{\partial V_j}{\partial t}$	5
gas phase continuity equation	$\frac{\partial \epsilon_g \rho_g^g}{\partial t} + \frac{1}{r}\frac{\partial\left(r\epsilon_g \rho_g^g u_r\right)}{\partial r} = \dot{\omega}_g$	5
species mass fraction	$\frac{\partial\left(\epsilon_g \rho_g^g Y_k\right)}{\partial t} + \frac{1}{r}\frac{\partial\left(r\epsilon_g \rho_g^g Y_k u_r\right)}{\partial r} = \frac{1}{r}\frac{\partial}{\partial r}\left(r\epsilon_g \rho_g^g D_{\text{eff}}\frac{\partial Y_k}{\partial r}\right) + \dot{\omega}_k$	5
char density[c]	$\frac{\partial \rho_{\text{char}}}{\partial t} = k_3 \rho_{\text{wood}} + \epsilon_g k_5 \rho_{\text{tar}}^g - \frac{\rho_{\text{char}}}{V_j}\frac{\partial V_j}{\partial t}$	19
temperature	$\left(\rho_{\text{wood}} c_{P,\text{wood}} + \rho_{\text{char}} c_{P,\text{char}} + \rho_l c_{P,l} + \rho_b c_{P,b} + \epsilon_g \rho_g^g c_{P,g}\right)\frac{\partial T}{\partial t} + \left(\rho_l c_{P,l} u_l + \rho_b c_{P,b} u_b + \epsilon_g \rho_g^g c_{P,g} u_r\right)\frac{\partial T}{\partial r} = \frac{1}{r}\frac{\partial}{\partial r}\left(r\lambda_{\text{eff}}\left(\frac{\partial T}{\partial r}\right)\right) - \Phi_{\text{evap}} - \Phi_{\text{devol},1} + \Phi_{\text{devol},2}$	20
liquid free water	$\frac{\partial \rho_l}{\partial t} + \frac{1}{r}\frac{\partial(r\rho_l u_l)}{\partial r} = -\dot{\omega}_{\text{evap},l}$	21
bound water	$\frac{\partial \rho_b}{\partial t} = \frac{1}{r}\frac{\partial}{\partial r}\left(rD_b\frac{\partial \rho_b}{\partial r}\right) - \dot{\omega}_{\text{evap},b}$	21

[a]The last column gives the relevant references. [b]The reaction rates of wood to noncondensable gases, tar, and char are given by k_1, k_2, and k_3, respectively. [c]k_5 marks the reaction of tar to char.

researchers that in the case of significantly wet particles being thermally converted, the available water vapor leaving the inner parts of the particle where drying and devolatilization still occur passes through the hot char zones, where it can act as gasifying agent.[16] Yang et al.[1] used a simplified one-step global devolatilization model, which requires a predefined ratio between produced char and gases. This means that the char content does not automatically change depending on the heating rate. This behavior can be accurately predicted with more advanced devolatilization models, e.g., with three independent competitive reactions. Yang et al.[1] found that the influence of particle shape on the particle's combustion behavior is crucial. They also found that due to the ignition of the released volatiles, the particle temperature increased. As a consequence, also the volatile release and the char burning rate were accelerated. This trend was observed for all particle sizes tested. The time until this volatile gas ignition occurred, increased as particle size increased.

Lu et al.[5] developed a one-dimensional (1D) model describing wood combustion and presented experimental data as well as modeling results of combustion characteristics of differently sized particles, within a size range of 3 to 15 mm. Furthermore, they studied different shapes of particles, with their model being able to describe combustion of cylinders, spheres, and flat plates. Due to the nonisotropic nature of biomass, it is not clear, however, how well multidimensional physics is reproduced by the use of simple bridge factors in a 1D model.

Besides the more obvious influence of particle size and shape on combustion behavior, there is also current research effort on identifying the influence of thermal pretreatment of wood on its combustion behavior.[17] These studies were performed with spherical particles with a size range of 3 to 5 mm. The combustion behavior of torrefied particles was studied and it was found that for such particles the devolatilization time was linearly dependent on the mass of the tested sample. It was also shown that for raw biomass particles, within the same particle size range, the char burnout time also increased linearly with increasing biomass mass.[17]

The current paper presents a study on how particle size affects the combustion of large thermally thick wood particles and logs by means of a 1D mesh-based model. Therefore, the paper first presents the validation of the model. Experimental data was available for a thermally thick, near-spherical particle (aspect ratio of 1), and validation was done for such wood particles. After validation, the model was up-scaled to larger cylindrical wood logs. This was done because the model will be used for simulating the thermochemical degradation and char conversion in typical wood stoves. Here, we define a wood log as a thermally thick wood particle that has a size in the cm-range and typically an aspect ratio larger than 4.

Even though there are works available studying the combustion characteristics of differently sized wood particles, none of those works focused on wood particles of sizes close to wood logs used for combustion in wood stoves. The influence of particle size is expected to be very important when modeling thermal biomass conversion, as it involves a closely coupled interaction between chemistry and heat and mass transfer processes with emphasis on the fact that the mentioned transfer phenomena are affected by particle size.[1] Furthermore, the

DOI: 10.1021/acs.energyfuels.8b00777
Energy Fuels 2018, 32, 6847−6862

Table 2. List of Additional Equations That Are Required for a Drying and Devolatilization Model[a]

additional equation		ref
radial gas phase velocity	$u_r = -\frac{\kappa}{\mu_g}\frac{\partial P_g}{\partial r}$	5
ideal equation of state	$P_g = \frac{\rho_g^g RT}{MW_{mix,total}}$	5
reaction rates of devolatilization	$k_i = A_i \exp\left(\frac{-E_{a,i}}{RT}\right)$	5
liquid free water velocity	$u_l = -\frac{\kappa_l}{\mu_l}\frac{\partial P_l}{\partial r}$	21
liquid pressure[b]	$P_l = P_g - P_c$	21
fraction of residual wood	$\eta = \frac{\rho_{wood}}{\rho_{wood,0}}$	
effective thermal conductivity[f]	$\lambda_{eff} = \epsilon_{pore}(1-\phi)\lambda_g + \epsilon_{pore}\phi\lambda_l + (1-\epsilon_{pore})(\lambda_{wood}\frac{\rho_{wood}}{\rho_{wood}+\rho_{char}+\rho_{ash}} + \lambda_{char}\frac{\rho_{char}}{\rho_{wood}+\rho_{char}+\rho_{ash}} + \lambda_{ash}\frac{\rho_{ash}}{\rho_{wood}+\rho_{char}+\rho_{ash}}) + \frac{\epsilon_g\sigma T^3 d_{pore}}{\omega_{pore}}$	
effective permeability[c]	$\kappa_{eff} = \xi(\eta\kappa_{ll,wood} + (1-\eta)\kappa_{ll,char}) + (1-\xi)(\eta\kappa_{\perp,wood} + (1-\eta)\kappa_{\perp,char})$	
bound water diffusivity	$D_b = 7\times10^{-6}\exp\left(\frac{-4633 + 3523\frac{\rho_b}{\rho_{wood}}}{T}\right)$	21
Knudsen diffusivity, $D_{Knudsen}$	$D_{Knudsen} = \frac{2r_{pore}}{3}\sqrt{(8RT/\pi MW_i)}$	8
effective diffusivity, D_{eff}	$D_{eff} = \left(1/(\frac{1}{D_{AB}} + \frac{1}{D_{Knudsen}})\right)\epsilon_{pore}^2$	8
evaporation bound water	$\dot{\omega}_{evap,b} = A_{evap}\exp\left(\frac{-E_{a,evap}}{RT}\right)\rho_b$	
evaporation liquid free water[d]	$\dot{\omega}_{evap,l} = f_{evap}\frac{F_{heat}}{\Delta h_{evap}}$, with $F_{heat} = \frac{1}{r}\frac{\partial}{\partial r}\left(r\epsilon_g\rho_g^g u_r c_{p,g} T - r\lambda_{eff}\frac{\partial T}{\partial r}\right)$	8
gas phase volume fraction	$\epsilon_g = \epsilon_{pore}(1-\phi) = \frac{V_g}{V}$	21
porosity	$\epsilon_{pore} = \frac{V_{pore}}{V}$	21
phase average liquid free density[e]	$\rho_l = \rho_l^l \phi \epsilon_{pore}$	21
phase average gas phase[e]	$\rho_g = \rho_g^g(1-\phi)\epsilon_{pore}$	21

[a]The last column gives the relevant references. [b]P_c is the capillary pressure, which is commonly described by expressions obtained from experimental observations. In this model we used

$$P_c = 10000\left(\frac{\rho_{wood,0}M_l}{\epsilon_{pore}\rho_l}\right)^{-0.61}$$

also used by de Paiva Souza and Nebra[22]. [c]ξ is the bridge factor. [d]The latent heat of vaporization, Δh_{evap}, was 2.44×10^6 J/kg[5]. [e]ρ_l^l and ρ_g^g are the intrinsic phase averages of liquid and gas phase, respectively, while ϕ is the volume fraction of pores filled with liquid free water. [f]The effective thermal conductivity for wood and char in the solid phase has been taken from Fatehi and Bai[8] and extended to also include the influence of ash and liquid free water and bound water.

DOI: 10.1021/acs.energyfuels.8b00777
Energy Fuels 2018, 32, 6847−6862

paper also includes a detailed discussion on grid-independence and the requirements for the 1D-mesh to obtain a grid-independent solution. In addition, the challenges for model validation of a thermal conversion model, with focus on char conversion modeling validation are discussed.

Finally, it should be noted that for highly detailed simulation models, like the ones being used here, a number of input data are required in order for the simulation tool to yield reliable results. These input data, such as permeability, internal surface area, or thermal conductivity, are typically determined for different wood species in specially designed experiments. As part of the model development and validation, we therefore also aimed for testing and running the model with the best available key input data that can be found in current literature.

2. NUMERICAL MODELING

A 1D mesh-based model for drying, devolatilization, and char conversion of a wet thermally thick cylindrical wood particle was developed. The differentiation between particle and log was done, based on the shape that was tested. Near-spherical particles were considered as particles, while wood particles with an aspect ratio larger than 1, and consequently considered cylindrical, were referred to as wood logs in this work.

Mesh-based models are comprehensive models that divide the particle into a large number of shells (in the case of a cylindrical or spherical particle). At every grid point, solid, liquid, and gas phases are present and the gas phase consists of a number of gas species. The model includes the evolution equations for wood density, char density, ash density, total gas phase, gas phase species, temperature, and liquid free water as well as bound water. The water content exceeding the fiber saturation point (for most wood species 30 wt %, dry basis) is classified as liquid free water, while the water content below the fiber saturation point is classified as bound water. The convective and diffusive transport of the gas phase within the porous structure is modeled. Furthermore, the liquid phase can be transported by diffusion (if defined as bound water) or by convection (if defined as liquid free water). However, the transport of liquid free water has been found to be negligible during high temperature drying,[18] and it has therefore been deactivated in the current model. Drying is modeled either by the kinetic rate model or the thermal drying model. Devolatilization is described by a three independent competitive reactions scheme in the primary devolatilization stage and subsequent secondary tar reactions. More details on the scheme can be found in earlier works.[18] In the following subsection, the applied governing equations are discussed in more detail.

2.1. Governing Equations. A detailed discussion of the governing equations relevant for drying and devolatilization has been presented in an earlier work by Haberle et al.[18] Nonetheless, the most relevant equations are given in Table 1 and Table 2.

The numerical model describing char conversion includes oxidation of char

$$\mathrm{C} + x\mathrm{O}_2 \rightarrow a\mathrm{CO} + b\mathrm{CO}_2 \tag{R1}$$

as well as steam gasification

$$\mathrm{C} + \mathrm{H}_2\mathrm{O} \rightarrow \mathrm{H}_2 + \mathrm{CO} \tag{R2}$$

and CO_2 gasification

$$\mathrm{C} + \mathrm{CO}_2 \rightarrow 2\mathrm{CO} \tag{R3}$$

Compared to the pure drying and devolatilization model, the source term in the gas phase continuity equation, $\dot{\omega}_g$, (see Table 1) has to be changed in order to also consider char oxidation and gasification reactions such that

$$\dot{\omega}_g = \dot{\omega}_{k_1,k_2} - \dot{\omega}_{k_5} + \dot{\omega}_{\mathrm{evap}} + \dot{\omega}_{\mathrm{oxid}}\Omega_1\frac{\mathrm{MW_C}}{\mathrm{MW_{O_2}}} + \dot{\omega}_{\mathrm{H_2O,gasif}}\Omega_2 \frac{\mathrm{MW_C}}{\mathrm{MW_{H_2O}}} + \dot{\omega}_{\mathrm{CO_2,gasif}}\Omega_3\frac{\mathrm{MW_C}}{\mathrm{MW_{CO_2}}} \tag{1}$$

where $\dot{\omega}_{\mathrm{oxid}}$ is the reaction rate due to char oxidation while $\dot{\omega}_{\mathrm{H2O,gasif}}$ and $\dot{\omega}_{\mathrm{CO2,gasif}}$ are the reaction rates due to steam and CO_2 gasification, respectively. The first three terms on the right-hand side of eq 1 are due to primary devolatilization reactions of wood to noncondensable gases and tar, respectively, $\dot{\omega}_{k1,k2}$, secondary tar reactions to char, $\dot{\omega}_{k5}$, and evaporation, $\dot{\omega}_{\mathrm{evap}}$, respectively. The stoichiometric coefficients of the different char consumption reactions are given by Ω_2 (= 1) and Ω_3 (= 1), respectively, corresponding to the coefficients in reactions R2 and R3. Reaction R1 has been taken from Evan and Emmons[23] with the following definitions of coefficients

$$a + b = 1 \tag{2}$$

and

$$x = \frac{a}{2} + b \tag{3}$$

Their modeling assumption of a temperature-dependent ratio between CO/CO_2[23]

$$\frac{a}{b} = 4.3\exp(-3390/T) \tag{4}$$

has been simplified by setting a = 1 and therefore neglecting the temperature-dependency. As a consequence Ω_1 = 2 in Reaction R1. This simplification was done, since the model developed in this work was partly also compared against previous modeling results by Fatehi and Bai[8] and Lu et al.,[5] both only assuming heterogeneous char reactions to form CO. Despite the fact that a temperature-dependent CO/CO_2 ratio is more accurate, it has not been considered in the current work in order to ease validation against other modeling works.

The primary devolatilization reactions describe the formation of noncondensable gases, k_1, and tar, k_2, from wood, such that

$$\dot{\omega}_{k_1,k_2} = (k_1 + k_2)\rho_{\mathrm{wood}} \tag{5}$$

In eq 5, ρ_{wood} refers to the apparent wood density. The secondary tar cracking reaction, $\dot{\omega}_{k_5}$, describe the reaction of tar to char such that

$$\dot{\omega}_{k_5} = k_5\rho^{\mathrm{g}}_{\mathrm{tar}}\epsilon_{\mathrm{g}} \tag{6}$$

where $\rho^{\mathrm{g}}_{\mathrm{tar}}$ is the intrinsic tar density and k_5 is the reaction rate constant of tar to char. The third term on the right-hand side of eq 1 refers to water vapor formation due to drying, which can be modeled either by the kinetic rate drying model or the thermal drying model (see Table 2). More information on the drying stage can be found in an earlier work by Haberle et al.[18]

Besides the gas phase continuity equation, also char mass evolution and gas phase species equations have to be modified when char conversion is included in the model. The char mass evolution is described by

$$\frac{\partial\rho_{\mathrm{char}}}{\partial t} = \dot{\omega}_{k_3} + \dot{\omega}_{k_5} - \dot{\omega}_{\mathrm{oxid}}\Omega_1\frac{\mathrm{MW_C}}{\mathrm{MW_{O_2}}} - \dot{\omega}_{\mathrm{H_2O,gasif}}\Omega_2\frac{\mathrm{MW_C}}{\mathrm{MW_{H_2O}}} - \dot{\omega}_{\mathrm{CO_2,gasif}}\Omega_3\frac{\mathrm{MW_C}}{\mathrm{MW_{CO_2}}} \tag{7}$$

where

$$\dot{\omega}_{k_3} = k_3\rho_{\mathrm{wood}} \tag{8}$$

includes the reactions of wood to char due to primary devolatilization reactions, while k_3 is the corresponding reaction rate constant.

The heterogeneous char conversion reactions describing char conversion can be implemented in the model as[5]

$$\dot{\omega}_i = s_{\mathrm{a,char}}\frac{\rho_{\mathrm{char}}}{\rho_{\mathrm{char}} + \rho_{\mathrm{wood}} + \rho_{\mathrm{ash}}}k_i\epsilon_{\mathrm{g}}\rho^{\mathrm{g}}_{\mathrm{g}}Y_k \tag{9}$$

DOI: 10.1021/acs.energyfuels.8b00777
Energy Fuels 2018, 32, 6847−6862

where the reaction rate constants of reactions R1−R3, k_i, are described by a temperature-dependent Arrhenius expression such that[5]

$$k_i = A_i T \exp\left(\frac{-E_{a,i}}{RT}\right) \tag{10}$$

with A_i being the pre-exponential factor, $E_{a,i}$ the activation energy, R the ideal gas constant, and T the temperature. The subscript i, in eq 9 and eq 10, refers to the different char conversion reactions mentioned in reactions R1−R3. Furthermore, the term $\frac{\rho_{char}}{\rho_{char}+\rho_{wood}+\rho_{ash}}$ is included in eq 9 to account for the decreasing fraction of surface area occupied by char due to ongoing char conversion. This is a valid assumption, as it has also been shown by Wornat et al.[24] that the reactivity of two different biomass chars was reduced during char conversion. The reason herefore was stated to be an ongoing depletion of more reactive carbon, and the physical and chemical alteration of available inorganic compounds, which caused them to be less catalytically active.[24]

Metal release during biomass combustion was not considered in this work and therefore also the catalytic effect of potassium was neglected. This is a valid assumption since for large thermally thick wood particles, as those studied here, the conversion is dominated by transport phenomena and not by reaction kinetics.[1]

Spruce has an initial oxygen content of 43.5% while for birch the value is 44.3%. Consequently, hardwoods and softwoods both have a high oxygen content, and the resulting chars also still contain oxygen within the range of 5.1 to 6.4% for birch char and spruce char, respectively.[7] For simplicity, this oxygen content is not considered while modeling char oxidation.

In eq 9 the reaction order is set to unity. Char reactivity depends on the solid feedstock as well as the devolatilization conditions, which affect the pore structure of the char and the elemental composition. It has been suggested that the differences in the char reactivity derived from wood species can be taken into consideration by adjusting the pre-exponential factor as well as the reaction order.[25] However, in this work, the reaction order was set to unity, which is a common modeling approach, see, e.g., Fatehi and Bai[8] or Lu et al.[5]

One main difference of a comprehensive numerical model including all three stages of thermal conversion and a model that is focusing solely on drying and devolatilization is an increase in the number of considered gas phase species. While a pure drying and devolatilization model does not require an explicit consideration of H_2O, CO_2, H_2, CO, and O_2, the evolution of these species has to be modeled in a char conversion model to predict accurate char conversion rates. The governing equation for gas phase species is listed in Table 1. The corresponding source terms due to char conversion are

$$\dot{\omega}_{CO} = 2\dot{\omega}_{oxid}\frac{MW_{CO}}{MW_{O_2}} + f_{CO}\dot{\omega}_{k_1} + g_{CO}\dot{\omega}_{k_4} + \dot{\omega}_{H_2O,gasif}\frac{MW_{CO}}{MW_{H_2O}} + 2\dot{\omega}_{CO_2,gasif}\frac{MW_{CO}}{MW_{CO_2}} - \dot{\omega}_{CO,oxid} \tag{11}$$

$$\dot{\omega}_{O_2} = -\dot{\omega}_{oxid} - \dot{\omega}_{CO,oxid}\frac{1MW_{O_2}}{2MW_{CO}} \tag{12}$$

$$\dot{\omega}_{H_2} = f_{H_2}\dot{\omega}_{k_1} + g_{H_2}\dot{\omega}_{k_4} + \dot{\omega}_{H_2O,gasif}\frac{MW_{H_2}}{MW_{H_2O}} \tag{13}$$

$$\dot{\omega}_{H_2O,g} = \dot{\omega}_{evap} - \dot{\omega}_{H_2O,gasif} + f_{H_2O}\dot{\omega}_{k_1} + g_{H_2O}\dot{\omega}_{k_4} \tag{14}$$

$$\dot{\omega}_{CO_2} = f_{CO_2}\dot{\omega}_{k_1} + g_{CO_2}\dot{\omega}_{k_4} - \dot{\omega}_{CO_2,gasif} + \dot{\omega}_{CO,oxid}\frac{MW_{CO_2}}{MW_{CO}} \tag{15}$$

$$\dot{\omega}_{tar} = \dot{\omega}_{k_2} - \dot{\omega}_{k_4} - \dot{\omega}_{k_5} \tag{16}$$

where $\dot{\omega}_{k4}$ represents reaction rates due to the tar cracking to noncondensable gases,

$$\dot{\omega}_{k_4} = k_4\rho_{tar}^{g}\epsilon_g \tag{17}$$

The fractions f_{CO2}, f_{CO}, f_{H2}, and f_{H2O} define how much carbon dioxide, carbon monoxide, hydrogen, and water vapor are produced from primary devolatilization reactions, and the fractions g_{CO2}, g_{CO}, g_{H2}, and g_{H2O} define how much of the corresponding species are formed from tar reactions.

Homogeneous gas phase reactions are partly considered in this model, where carbon monoxide reactions occur inside the pores. This is a critical aspect that needs to be considered, since this reaction consumes oxygen and therefore even further restricts the oxygen transportation to the active sites. The corresponding reaction and kinetics that were used are listed in Table 4.

Finally, the temperature equation becomes

$$\begin{aligned}&(\rho_{wood}c_{P,wood} + \rho_{char}c_{P,char} + \rho_{ash}c_{P,ash} + \rho_l c_{P,l} + \rho_b c_{P,b} + \epsilon_g\rho_g^g c_{P,g})\frac{\partial T}{\partial t} + (\rho_l c_{P,l}u_l + \rho_b c_{P,b}u_b + \epsilon_g\rho_g^g c_{P,g}u_r)\frac{\partial T}{\partial r}\\ &= \frac{1}{r}\frac{\partial}{\partial r}\left(r\lambda_{eff}\left(\frac{\partial T}{\partial r}\right)\right) - \Phi_{heat}\end{aligned} \tag{18}$$

where

$$\begin{aligned}\Phi_{heat} &= \dot{\omega}_{k1,k2,k3}\Delta h_{devol,1} + \dot{\omega}_{k4,k5}\Delta h_{devol,2} + \dot{\omega}_{evap}\Delta h_{evap}\\ &+ \dot{\omega}_{oxid}\Omega_1\frac{MW_C}{MW_{O_2}}\Delta h_{oxid} + \dot{\omega}_{H_2O,gasif}\Omega_2\frac{MW_C}{MW_{H_2O}}\Delta h_{H_2O,gasif}\\ &+\dot{\omega}_{CO_2,gasif}\Omega_3\frac{MW_C}{MW_{CO_2}}\Delta h_{CO_2,gasif} + \dot{\omega}_{CO,oxid}\Delta h_{CO,oxid}\\ &+ \dot{\omega}_{k1}\left(\int_{T_0}^{T}(c_{P,wood} - c_{P,noncond.gases})dT\right)\\ &+ \dot{\omega}_{k2}\left(\int_{T_0}^{T}(c_{P,wood} - c_{P,tar})dT\right)\\ &+ \dot{\omega}_{k3}\int_{T_0}^{T}(c_{P,wood} - c_{P,char})dT\\ &+ \dot{\omega}_{evap}\left(\int_{T_0}^{T}(c_{P,water} - c_{P,vapor})dT\right)\\ &+(\dot{\omega}_{H_2O,gasif} + \dot{\omega}_{oxid} + \dot{\omega}_{CO_2,gasif})\left(\int_{T_0}^{T}(c_{P,char} - c_{P,noncond.gases})dT\right)\\ &+ \dot{\omega}_{k4}\left(\int_{T_0}^{T}(c_{P,tar} - c_{P,noncond.gases})dT\right)\\ &+ \dot{\omega}_{k5}\left(\int_{T_0}^{T}(c_{P,tar} - c_{P,char})dT\right)\end{aligned} \tag{19}$$

The the average bound water mass flux $\rho_b u_b$, entering eq 18 needs to be defined as suggested by Grønli[21]

$$\rho_b u_b = -D_b\frac{\partial \rho_b}{\partial r} \tag{20}$$

under the assumption that wood density remains more or less constant within the wet wood zone, where bound water transportation is of relevance.

The set of differential and algebraic equations has to be solved by a suitable solver. A complication is that homogeneous gas phase reactions, such as carbon monoxide oxidation, are very stiff, which has to be considered when a suitable solver is chosen. In the current work we use the IDA solver, which is a part of the SUNDIALS software package,[26] and time integration is done by a backward differentiation formula (order 1 to 5, which as well defines the temporal order of accuracy). The convective terms are discretized by first order upwinding, while the diffusion terms in the transport equations use a second order central difference. The spatial discretization is therefore of first order accuracy. In this work, the term combustion refers to the sum of all stages of thermal conversion, namely, drying, devolatilization, and char conversion.

DOI: 10.1021/acs.energyfuels.8b00777
Energy Fuels 2018, 32, 6847−6862

Table 3. Properties Used As Input Values for the Drying, Devolatilization, and Char Conversion Model[a]

property	unit	value	ref
apparent/true wood density, (ρ_{wood} and $\rho_{wood,true}$)	[kg/m^3]	570 and 1500 ($\rightarrow \epsilon_{pore,0} = 0.62$)	*b* and 29
thermal conductivity (wood), $\lambda_{wood,\parallel}/\lambda_{wood,\perp}$	[W/(m K)]	0.73/0.52	7
thermal conductivity (ash), $\lambda_{ash,\parallel,\perp}$	[W/(m K)]	1.03	27
thermal conductivity (char), $\lambda_{char,\parallel,\perp}$	[W/(m K)]	$1.47 + 1.1 \times 10^{-3}T$	27
thermal conductivity (gases), λ_g	[W/(m K)]	25.77×10^{-3}	19
thermal conductivity (water), λ_l	[W/(m K)]	$0.278 + 1.11 \times 10^{-3}T$	7
bridge factor, ξ	[−]	0.68	30
specific heat capacity (wood), $c_{P,wood}$	[J/(kg K)]	$1500 + T$	9
specific heat capacity (ash), $c_{P,ash}$	[J/(kg K)]	$754 + 0.586(T - 273)$	27
specific heat capacity (noncondensable gases), $c_{P,g}$	[J/(kg K)]	$770 + 0.624T - 1.91 \times 10^{-4}T^2$	21
specific heat capacity (char), $c_{P,char}$	[J/(kg K)]	$420 + 2.09T + 6.85 \times 10^{-4}T^2$	21
specific heat capacity (tar), $c_{P,tar}$	[J/(kg K)]	$-100 + 4.4T - 1.57 \times 10^{-3}T^2$	21
specific heat capacity (vapor), $c_{P,vapor}$	[J/(kg K)]	$1670 + 6.4 \times 10^{-1}T$	21
permeability, $\kappa_{solid\ \perp,\parallel}$	m^2	10^{-14}	31
particle emissivity, $\epsilon_{particle}$	[−]	0.85	9

[a]The data is applied for poplar wood (hardwood). [b]This value was calculated based on knowing the apparent density and the true density.

2.2. Boundary Conditions. The boundary conditions for temperature and species mass fractions are given by[8]

$$\lambda_{eff}\frac{\partial T}{\partial r} = \epsilon_{particle}\sigma(T_{wall}^4 - T_{surface}^4) + h_c(T_{gas} - T_{surface}) \quad (21)$$

and

$$\epsilon_g D_{eff}\frac{\partial Y_k}{\partial r} = h_m(Y_{\infty,k} - Y_{surface,k}) \quad (22)$$

The heat and mass transfer coefficients, h_c and h_m, entering these boundary conditions have to be corrected due to the influence of exiting gases. This influence is often called the blowing effect or the Stefan flow effect. It is only valid to set heat and mass transfer coefficients to their uncorrected values (marked by subscript $_{,0}$ in the following) if $\dot{M}_{total} \rightarrow 0$, i.e.,

$$h_{c,0} = \lim_{\dot{M}_{total}\rightarrow 0} h_c \quad (23)$$

and

$$h_{m,0} = \lim_{\dot{M}_{total}\rightarrow 0} h_m \quad (24)$$

where $\dot{M}_{total}$ is the total mass flux of gas species leaving the particle, being defined as

$$\dot{M}_{total} = \rho_g^g \epsilon_g u_r \quad (25)$$

The uncorrected mass transfer coefficient (without the influence of the Stefan flow) are found from

$$h_{m,0} = \frac{D_{AB}Sh}{d_p} \quad (26)$$

while the corresponding heat transfer coefficient is calculated as

$$h_{c,0} = \frac{Nu\lambda_g}{d_p} \quad (27)$$

Both Nu and Sh can be obtained from the Ranz-Marshall correlation[9]

$$Nu = 2 + 0.6\,Re^{0.5}\,Pr^{1/3} \quad (28)$$

and

$$Sh = 2 + 0.6\,Re^{0.5}\,Sc^{1/3} \quad (29)$$

for this specific test case, since a near-spherical particle is modeled. The diffusivity is calculated from the following equation[27]

$$D_{AB} = D_{AB,ref}\left(\frac{T}{T_{ref}}\right)^{1.75} \quad (30)$$

with the reference diffusivity, $D_{AB,ref} = 2 \times 10^{-5}$ m^2/s, being taken from Fatehi and Bai.[8] The thermal diffusivity of the gas phase (λ_g) is assumed constant and the value found in Table 3 is used.

The corrected heat and mass transfer coefficients are defined as[28]

$$h_m = \frac{\dot{M}_{total}}{\left(\exp\left(\frac{\dot{M}_{total}}{h_{m,0}}\right) - 1\right)} \quad (31)$$

Due to the analogy between heat and mass transfer, a similar expression can be defined for the corrected heat transfer coefficient[28]

$$h_c = \frac{\dot{M}_{total}\overline{c}_{P,g}}{\left(\exp\left(\frac{\dot{M}_{total}\overline{c}_{P,g}}{h_{c,0}}\right) - 1\right)} \quad (32)$$

where $\overline{c}_{P,g}$ is the mass averaged specific heat capacity of the gas phase.

For model validation, the surrounding gas phase temperature was set to 1050 K and the furnace wall temperature was set to 1276 K. The pressure at the particle surface was equal to ambient pressure.

The particle moisture content was 40% (wet basis), and a near-spherical particle with a diameter of 9.5 mm and an aspect ratio of 1 was tested. The authors emphasize that for more realistic combustion modeling of solid fuel conversion, a dynamic coupling between solid- and gas-phase is recommended. Only a dynamically coupled solid- and gas-phase model can accurately link for example a fluctuating radiative feedback of the flame to the solid and predict how this change in external heat source affects the heat-controlled phenomena occurring inside the wood particle during thermochemical wood degradation and combustion, e.g., the volatile release rate. For example, ANSYS Fluent, which has well-established gas phase models, lacks the ability to describe single wood particle or log combustion. This shortcoming therefore requires the implementation of a solid phase model via user-defined functions. Even though the authors aim for the CFD implementation of their solid phase model via user-defined functions, the current status is a model written as a stand-alone code. This is the first step in the development of the entire simulation tool (gas and solid phase). Before the user-defined functions can be developed, the authors, however, found that it is crucial to validate the chemical and physical phenomena considered and implemented in the stand-alone code. This is done in order to ensure that the solid phase model is a suitable modeling tool by itself, independent of whether it is linked to a gas phase model or not. Hence, it was not the scope of this work to develop the entire simulation tool but rather to present the solid phase combustion model.

DOI: 10.1021/acs.energyfuels.8b00777
Energy Fuels 2018, 32, 6847−6862

Table 4. Kinetic Data Used for Modeling Drying, Devolatilization, and Char Gasification and Oxidation[a]

reaction rate constant	reaction	pre-exponential factor [1/s]	activation energy [kJ/mol]	ref	heat of reaction [kJ/kg]	ref
k_1	wood → gases	1.11×10^{11}	177	32	−418	33
k_2	wood → tar	9.28×10^{9}	149	32	−418	33
k_3	wood → char	3.05×10^{7}	125	32	−418	33
k_4	tar → gases	4.28×10^{6}	107.5	34	42	35
k_5	tar → char	1×10^{5}	107.5	36	42	35
k_{evap}	$\rho_b \rightarrow \epsilon_g \rho_g^g Y_{vap}$	5.13×10^{10}	88	37	−2440	5
k_{oxid}	C + 0.5 O_2 → CO	$1.715T$	74.8	7	9212	b
$k_{H_2O,gasif}$	C + H_2O → CO + H_2	$3.42T$	130	5	−10940	b
$k_{CO2,gasif}$	C + CO_2 → 2 CO	$3.42T$	130	5	−14370	b
$k_{CO,oxid}$	CO + 0.5O → 2 CO_2	$10^{12.35}$	167	5	10110	5

[a]Gases in the following table refer to noncondensable gases. [b]The heat of reactions have been calculated by assuming char reacting as pure C.

3. NUMERICAL SETUP

The data given in Table 3 were used for the simulations presented in this paper, i.e., for modeling combustion of a single thermally thick poplar particle. For simulating the combustion of a poplar particle Mehrabian et al.[9] based their simulations on the following proximate analysis: 48.1 wt % d.b. C, 5.77 wt % d.b. H, 45.53 wt % d.b. O, and 0.1 wt % d.b. N. They furthermore assumed an ash content of 0.5 wt % d.b. which was also assumed in this work. This ash content outlines that wood in general contains little ash.

The pre-exponential factors, activation energies, and heat of reactions that were used for drying, devolatilization, and char conversion are presented in Table 4. The kinetic data for evaporation modeling is only relevant if the kinetic rate drying model is used.

Hydrogen oxidation reactions are deactivated in the presented test runs, since it is assumed that only minor amounts of hydrogen are formed from primary and secondary devolatilization. Since also steam gasification reactions are very slow compared to oxidation reactions, the source of hydrogen is limited, also limiting the homogeneous oxidation reactions.

In fact homogeneous oxidation reactions were only modeled for CO, neglecting that during devolatilization also other combustible gas products are formed. Theoretically all combustible gases formed during devolatilization, including CO, can contribute to homogeneous gas phase combustion within the pores. One expects CO, CO_2, H_2, CH_4, and some other short-chained hydrocarbons (C_xH_y) as main products. Neves et al.[38] found, based on reviewing literature data and developing a model to predict the gas product yields, that the amounts of CH_4 and C_xH_y are commonly negligible for devolatilization at primary devolatilization temperatures (commonly below 500 °C). For noncondensable gas formation occurring at these temperatures, CH_4 and C_xH_y mass fractions together form a contribution of 1% of the total noncondensable gas phase product yield. Only if the temperatures increase from 500 to 850 °C, the sum of the two species forms a significantly higher contribution of 10%. However, then again this implies, that this increased formation of CH_4 and C_xH_y at higher temperatures than 500 °C is due to secondary tar cracking reactions.[38] Other noncondensable gas phase products are even more restricted in their contribution to the total noncondensable gas phase yield (e.g., H_2 mass fraction only increased from 0.2% to less than 1% when temperature rose from 500 °C to about 850 °C).

Therefore the authors assumed that CO will be the main gas component that homogeneously consumes oxygen. Again emphasis is made that the detailed species composition of the product gas is not a modeling aim in the current work. The aim is the consideration of oxygen availability limitation for heterogeneous oxidation, not only by mass-transfer limitations but also chemical phenomena due to leaving gas products.

4. MODEL VALIDATION

The model was validated against experimental work by Lu et al.[5] These experimental data were for near-spherical particles with an aspect ratio of 1, and therefore also such particles were used for the model validation. However, their experimental results show a large spread. This indicates that the error-bars associated with the measurements, in particular of the temperature at the particle surface and in the particle center, were significant. This highlights how difficult it is to measure the temperature during char conversion, which is partly due to the ongoing size reduction of the particle during combustion.[5] Therefore, in order to validate the model, the modeling results of our 1D mesh-based model were not only compared against the experimental results but also against the modeling results by Lu et al.[5] and Fatehi and Bai.[8] Overall good agreement was found between our work and the work by Lu et al.[5] and Fatehi and Bai.[8] Small deviations are visible though, since some assumptions are different:

(1) The specific heat capacities of wood, char, ash and gases are different. The reason is that it is not clear from the paper of Lu et al.[5] how the specific heat capacities for wood and char were chosen.

(2) The porosity was allowed to change from wood (ϵ_g = 0.62) to char (ϵ_{char} = 0.9) to ash (ϵ_{ash} = 0.9, taken from Mehrabian et al.[9]). The authors assumed in this work that there is no change in porosity from char to ash (similar to what has been assumed by Fatehi and Bai[39]). When setting the initial wood porosity to 0.62, the true wood density has to be set to 1500 kg/m^3, in order to result in an apparent wood density of 570 kg/m^3. This is a reasonable assumption for true wood density of softwoods and hardwoods.[29] The assumed porosity by Lu et al.[5] (ϵ_g = 0.4) was considered too low, as it would require a true wood density of 950 kg/m^3, which is too low for most wood species. Therefore, different porosities were used in this work.

(3) The diffusivity of gases was assumed to be temperature-dependent as suggested by Hermansson and Thunman.[27] This is in contrast to the constant diffusivity, equal to the one at room temperature, that was used by Lu et al.[5]

(4) The model presented in this work is considering that liquid free water occupies part of the pore volume. This means that as long as liquid free water is present in the pores the volume fraction of the gas phase is lower than the porosity. This is not commonly done in other works, e.g., Fatehi and Bai[8] and Lu et al.,[5] where the simplifying assumption is made that all liquid water present in the particle is embedded in the solid matrix and is therefore not hindering the gas phase flow.

(5) Shrinkage is modeled based on the same concept as suggested by Lu et al.,[5] but shrinkage during drying was only considered if a change in bound water density occurred. A change in liquid free water density, due to liquid water evaporation, is not coupled to volumetric shrinkage. Therefore the empirical correlation describing shrinkage is given by[5]

$$\frac{V_{particle}}{V_{particle,0}} = 1 + (1 - \beta_{evap})\left(\frac{\rho_b}{\rho_{b,0}} - 1\right) + (1 - \beta_{devol})\left(\frac{\rho_{wood}}{\rho_{wood,0}} - 1\right) \quad (33)$$

with β_{evap} being 0.9 for modeling shrinkage during drying, β_{devol} being 0.9 for modeling shrinkage during devolatilization. Volumetric

DOI: 10.1021/acs.energyfuels.8b00777
Energy Fuels 2018, 32, 6847−6862

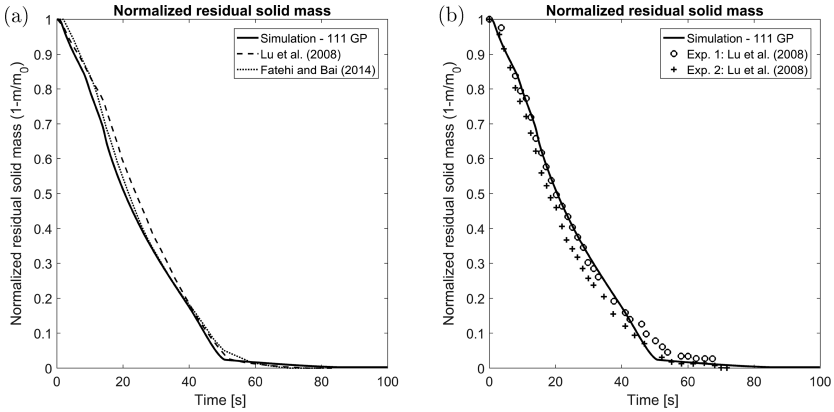

Figure 1. Validation of the normalized residual solid mass modeling results. (a) Normalized residual solid mass prediction validated against other modeling results (Fatehi and Bai,[8] Lu et al.[5]). (b) Normalized residual solid mass prediction validated against experimental results by Lu et al.[5]

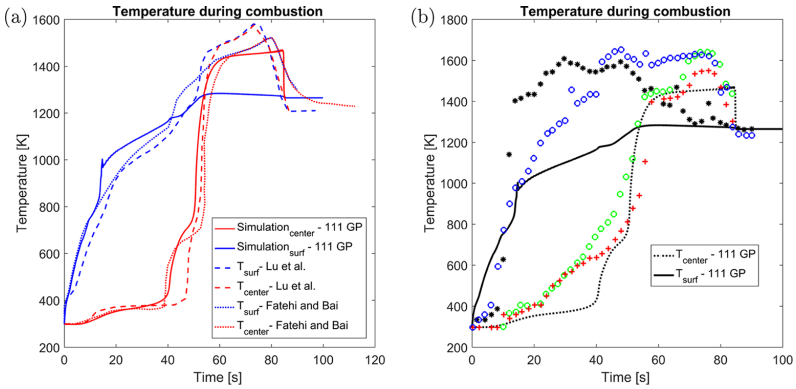

Figure 2. Validation of the surface and center temperature modeling results. The red lines in Figure 2a are the predicted center temperatures and the blue lines are the predicted surface temperatures. The following symbols are used in Figure 2b: $T_{surface}$, blue ○, *; T_{center}, green ○, red +. (a) Temperature modeling results validated against other modeling results (Fatehi and Bai,[8] Lu et al.[5]). (b) Temperature modeling results validated against experimental results by Lu et al.[5]

shrinkage during char conversion has not been modeled since we assumed that the particle size reduction during char conversion is due to char consumption reactions and not volumetric shrinkage. The char particle size reduction is instead accounted for by char being converted to ash at the outer part of the char layer.

(6) Due to numerical instabilities obtained with higher specific surface areas and therefore stiffer char oxidation reactions, the authors assumed a reduction in actual specific surface area as conversion proceeded. This was done for purely numerical reasons. The influence of such a reduction was tested to be minor, not affecting the mass loss trends, while only slightly affecting the predicted char layer thickness. The actual specific surface area was assumed to be in the range of 10^4 to 10^5 m^2/m^3.

Considering that some assumptions were different, the modeling results were compared against modeling results by Fatehi and Bai[8] as well as Lu et al.,[5] to see if the model developed by the authors predicted similar temperatures and mass losses.

The normalized residual solid mass is very well predicted by the model (see Figure 1). Small deviations from experiments (Figure 1b) are linked to modeling assumptions, but the difference is rather negligible. The small deviations from other modeling works (see Figure 1a) are related to different assumptions, as listed in the beginning of the chapter. The model predicts a slightly longer conversion time compared to what has been found in experiments or other modeling works, which highlights that other thermophysical properties could be tested as well, to see how significant their effect is on model accuracy and if other values are more suitable for describing poplar wood. When plotting the center and surface temperatures, more significant deviations became apparent (see Figure 2).

However, it needs to be pointed out that comparison of mass loss modeling results to experimental observations might be more reliable, since the measurement of temperature fields is more difficult than the continuous weighing of the residual particle.

Drying can be identified in all modeling results by the temperature plateau at ∼373 K (see Figure 2a). The plateau in this model is not as obvious as shown by modeling results by Lu et al.,[5] which is due to different drying models. In this work a pure kinetic rate drying model is used while Lu et al.[5] used a combination of the thermal drying model and the kinetic rate drying model. This difference in drying models is due to the numerical setup of this model, where liquid free water, evaporating by the thermal drying model, fills pores, while bound water, evaporating by the kinetic rate drying model, does not. Since Lu et al.[5] have not considered that liquid water as well occupies pore volume, even when using a combined thermal and kinetic rate drying model, it was found that the overall handling of the liquid phase is more similar to a pure bound water assumption in our model.

DOI: 10.1021/acs.energyfuels.8b00777
Energy Fuels 2018, 32, 6847−6862

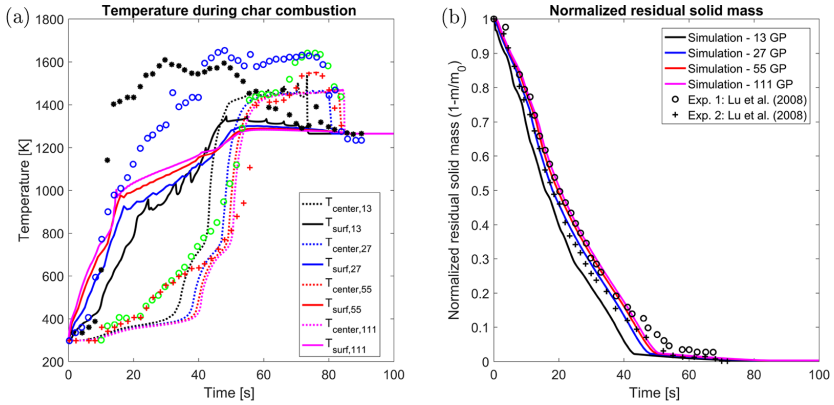

Figure 3. Effect of the grid point number on modeling results. (a) Temperature evolution obtained with a mesh of 13, 27, 55, and 111 grid points along the particle radius. The experimental data from Lu et al.[5] for surface and center temperatures are plotted and the corresponding symbols are $T_{surface}$, * and blue ○; T_{center}, red + and green ○. (b) Normalized residual solid mass evolution obtained with a mesh of 13, 27, 55, and 111 grid points along the particle radius.

The center temperature increases quickly as soon as drying has been accomplished and only between 600 and 800 K the influence of endothermic primary devolatilization reactions seems to slow down the temperature increase, before finally the char oxidation reactions start contributing to the temperature increase. The extent to which this second temperature plateau between 600 and 800 K is visible depends on the choice of heat of reaction of the primary devolatilization reactions.

The predicted surface temperature differs significantly from the experimental data (Figure 2b), but as mentioned earlier, the deviation between the two experimental series is also significant. Further validation against other experimental data is challenging since there is little information available in the open literature that covers experiments of single wood particles and logs converting under similar conditions, where the full thermal conversion is included. The predicted surface temperature also deviated from the predicted surface temperature by Lu et al.[5] and Fatehi and Bai.[8] It is assumed that this difference is due to assumed wood properties, such as, e.g., porosities, emissivity.

Overall, it was found that the modeling results of the wood combustion model differ from experimental results when it comes to center and surface temperature predictions. However, the mass loss predicted by the wood combustion model agrees well with what has been observed experimentally. Since temperature measurements are so challenging due to the size reduction of the char particle during char consumption and due to the intrusive nature of the measurements in the particle center, it is assumed that the deviation of modeling results from experimentally observed surface and center temperatures is mainly due to experimental artifacts. Measuring the mass loss, on the other hand, can still be accurately done, and with respect to that, the modeling results are very close to the experiments. This suggest that the model is of acceptable accuracy.

One expects that if the mass loss is accurate, also the gas release during drying, devolatilization, and char conversion is accurately predicted. This is an important input value for the gas phase model (= input data entering the CFD platform).

Due to the relatively large differences between numerical and experimental predictions, it is clear that the surface temperature prediction has to be interpreted with care. Since the temperature is coupled to the gas phase model, an error in the solid phase model with respect to this temperature profile could potentially affect the results of a simulation tool for wood stove design and optimization. However, then again one has to point out that validation of this surface temperature is very challenging, since experiments are obviously affected by significant errors. Furthermore, the wood particle surface is very much simplified (evened out and therefore assumed ideal). In addition, catalytic effects of minerals are entirely neglected, which can affect char conversion, and as a consequence, also char oxidation and corresponding heat release. Furthermore, the char is simply assumed to be pure C instead of also considering that it will contain fractions of H and O.

4.1. Grid-Independence Study. Compared to the pure drying and devolatilization model, it is expected that a finer mesh is required when char oxidation and gasification reactions are included in the model. One reason for this is that steep temperature gradients are expected in the particle, since exothermic char oxidation starts at the surface of the particle while evaporation still occurs in the particle center. Steep gradients are also expected for the oxygen concentration in the particle. Oxygen diffusion into the particle is limited by oxygen-involving reactions at the char surface or even by oxidation reactions of the exiting gases, such as CO. As a consequence, the oxygen cannot diffuse much into the particle, which means that the oxygen content is significant only in the vicinity of the char surface. Therefore, as part of the model development, the authors tested mesh refinement, to see how fine the mesh has to be to yield a grid-independent solution and how coarse it can be to yield numerically efficient modeling tools (see Figure 3).

It was found that a mesh with 13 grid points is not yielding grid-independent solutions. One can clearly see peaks in the surface temperature predictions, which are purely numerical and result from the rather coarse mesh. Furthermore, the thermochemical conversion is predicted too fast, since full conversion is achieved at earlier times compared to finer meshes with 27, 55, and 111 grid points. Therefore, further grid refinement was tested and meshes of 27, 55, and 111 grid points were studied. It was found that there was only a minor difference in modeling results between a mesh with 55 and with 111 grid points. Therefore, it is assumed that grid-independent results can already be obtained with a mesh of 55 grid points, which at the same time requires lower computational cost compared to a mesh with 111 grid points. The mesh with 27 grid points still resulted in some deviation in normalized mass prediction as well as temperature predictions compared to the very fine meshes of 55 and 111 grid points but the overall prediction of conversion trends and temperature trends was similar to what has been obtained from very fine meshes of 55 and 111 grid points. For qualitatively studying the conservation trends, a mesh with 27 grid points can as well be used.

The relative error in mass conservation for a mesh of 55 grid points was 1.93% and for a mesh of 111 grid points it was 1.94%. This highlights that since mass is well conserved with both meshes, a grid

DOI: 10.1021/acs.energyfuels.8b00777
Energy Fuels 2018, 32, 6847−6862

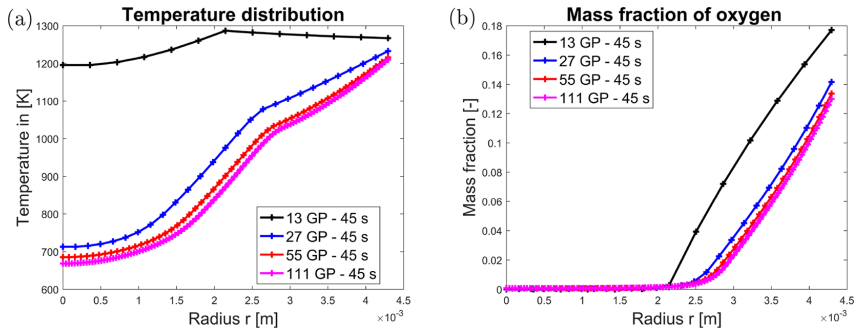

Figure 4. Effect of grid point number on the modeling results for temperature and oxygen mass fraction distribution within the reacting single particle. (a) Temperature distribution for meshes composed of 13, 27, 55, and 111 grid points. (b) Predicted oxygen mass fraction distribution for meshes composed of 13, 27, 55, and 111 grid points.

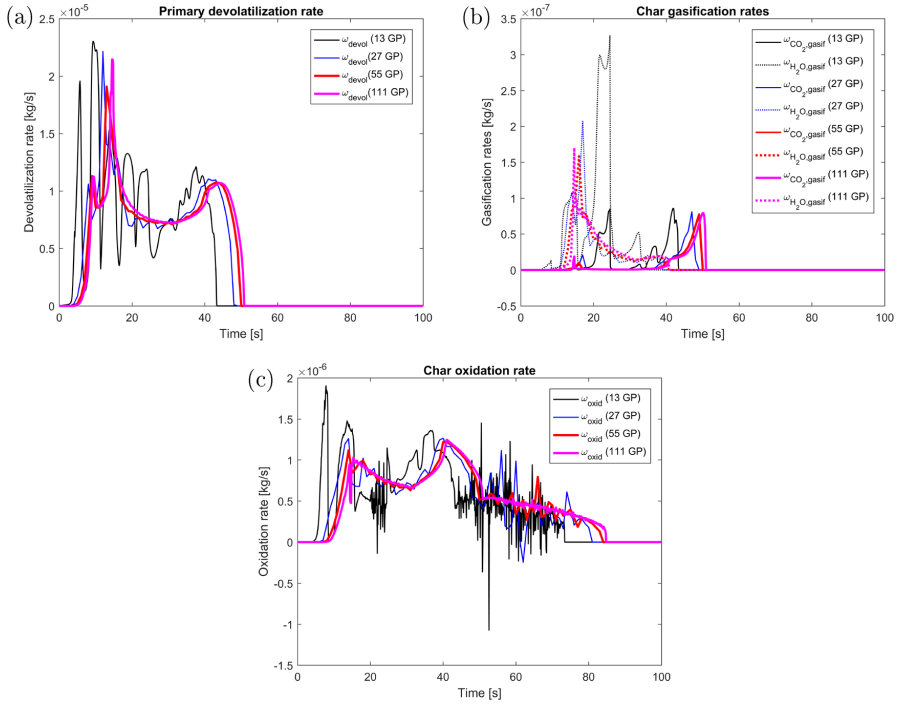

Figure 5. Grid-independence study with respect to reaction rates as a function of time during single wood particle combustion. Grid refinement was done from the originally coarse mesh of 13 grid points (spanning over the particle radius) to 27, 55, and 111 grid points. (a) Primary devolatilization rates as a function of time. (b) Gasification rates as a function of time. (c) Char oxidation rates as a function of time.

with 55 grid points can be used for studying the combustion behavior of the particle tested in this paper.

The conclusion that grid-independent results are obtained with 55 grid points is furthermore supported by the difference between temperature and oxygen mass fraction predictions (Figure 4). The differences obtained with meshes of 55 and 111 grid points are negligible. On the other hand one can clearly see that predictions obtained with a mesh of 13 grid points deviate significantly from predictions obtained from finer meshes.

It seems that the coarser meshes (13 and 27 grid points) predict slightly different times at which different stages of thermochemical conversion begin (Figure 5). Furthermore the char oxidation rate predicted with a mesh of 13 grid points does not show a realistic physical behavior. Significant numerical oscillations are visible and are only due to the coarse mesh. Reduced numerical oscillations can even still be observed with a grid of 27 mesh points. The differences between the reaction rates predicted with 55 and 111 grid points on the other hand are minor.

When comparing the reaction rates, one can identify that again the difference between the predicted reaction rates obtained with meshes of 55 and 111 grid points is minor, which again supports the

DOI: 10.1021/acs.energyfuels.8b00777
Energy Fuels 2018, 32, 6847−6862

conclusion that a mesh of 55 grid points is sufficient to yield grid-independent solutions.

5. RESULTS AND DISCUSSION

In this section we will first give a detailed presentation of the conversion process of a thermally thick wood particle. Then, we will discuss the effect of particle size on the thermal conversion and in particular on the position and extent of the conversion zones.

It has been stated in the literature that volatiles release from biomass occurs in three stages, with 10% of the volatiles being released between 200 and 300 °C, 70% between 300 and 400 °C, and the remaining 20% between 400 and 900 °C.[14] This, compared to the evaporation at about 100 °C implies that a very broad temperature range, and therefore a larger number of grid points is included in the primary devolatilization zone of wood.

Char conversion is the slowest stage of the entire thermal wood conversion, as oxygen diffusion to the active sites is limited. As oxygen cannot penetrate far into the particle, the char conversion occurs in a relatively thin zone.

One can identify the different conversion zones by the gradients of either liquid water, wood, or char. Figure 6 clearly shows that the theoretically narrow drying zone is smeared over some grid points in this model (see water density at 30 s). This smearing is due to the application of the kinetic rate drying model, which models drying over a broader temperature range than at exactly 100 °C.

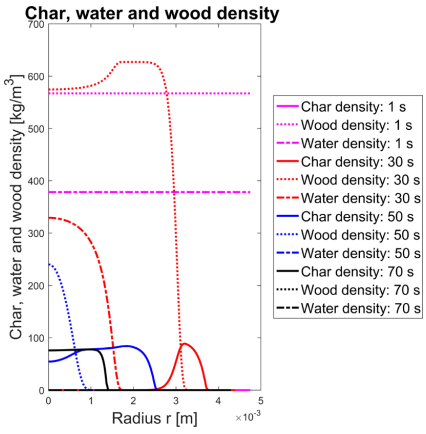

Figure 6. Char, wood, and liquid water density at different times during thermal conversion.

When studying the reaction rates in Figure 5 (for the 55 grid points test case), one can see that the reaction rates are enhanced at different times. The first peak of the devolatilization rate (at about 10 s) is due to very fast heating of the near surface areas of the particle. Since devolatilization is heat transfer controlled, the fast heating of the outer zones leads to a sudden and significant start of devolatilization. After this initial phase, the heat transfer further inward is slower due to the build-up of an insulating char layer outside the dry wood and due to the increased blowing effect that results from the production of volatile gases. This reduced heat transfer to the dry wood yields a slow-down of devolatilization. The second increase in the devolatilization rate (around 15 s) is due to enhanced heat release due to exothermic CO oxidation reactions as well as exothermic char oxidation reactions. Char gasification starts slightly after char oxidation reactions as well as CO oxidation, since gasification reactions are slower. The drop after the second increase is assumingly due to the decreasing heating contribution of char oxidation and CO oxidation reactions. The devolatilization zone moves further away from the char conversion zone and therefore a more limited influence of the heat release in the char conversion zone on the heat transfer controlled devolatilization zone occurs. In fact, it was found that a change in temperature gradient due to the enhanced contribution of exothermic reactions can have a significant influence on the devolatilization rate, since the reaction rates (especially for the reaction of wood to tar) increase significantly as soon as higher temperatures are reached.

It was found that CO oxidation reactions influence wood particle combustion in two ways. First, heterogeneous oxidation reactions slow down, since the oxygen diffusing inward is also consumed by the CO. Second, the heat release due to CO oxidation results in an acceleration of heat transfer controlled processes.

Compared to char oxidation (see Figure 5c), steam and CO_2 gasification are significantly slower (see Figure 5b). This was evaluated by comparing the maximum values for steam and CO_2 gasification and oxidation reaction rates.

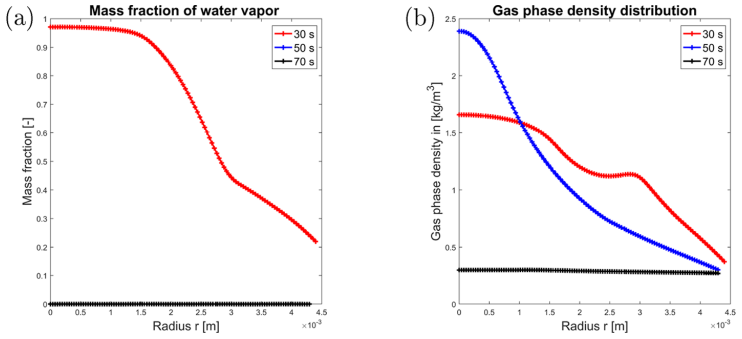

Figure 7. Water vapor mass fraction and gas phase density at different times during wood particle combustion. (a) Water vapor mass fraction at different times during wood particle combustion. (b) Gas phase density at different times during wood particle combustion.

DOI: 10.1021/acs.energyfuels.8b00777
Energy Fuels 2018, 32, 6847−6862

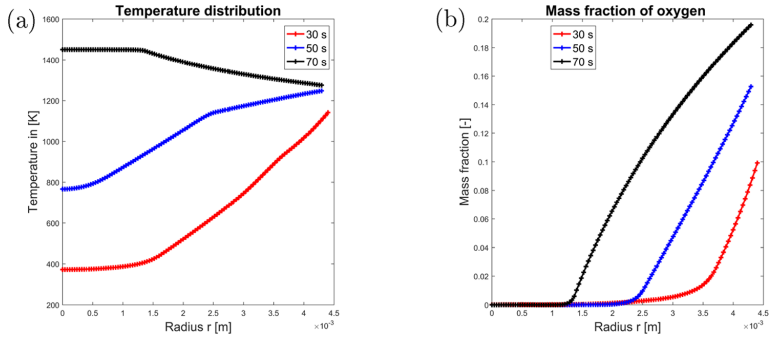

Figure 8. Temperature and oxygen mass fraction modeling results at different times during wood particle thermal conversion. (a) Temperature at different times during thermal conversion. (b) Oxygen mass fraction at different times during thermal conversion.

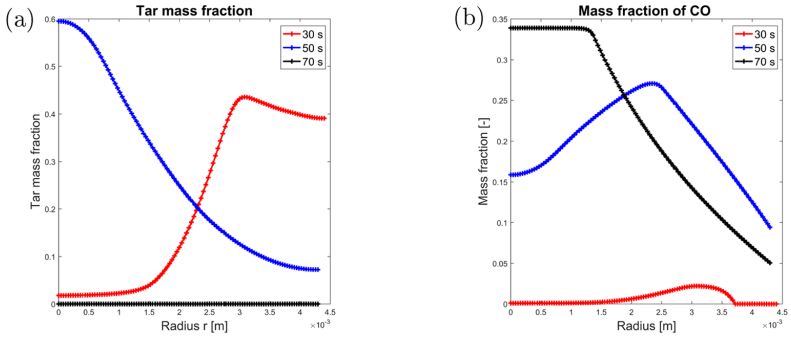

Figure 9. CO and tar mass fraction modeling results at different times during wood particle combustion.(a) Tar mass fraction at different times during combustion. (b) CO mass fraction at different times during combustion.

Figure 6 shows that the particle, with an initial diameter of 9.5 mm, decreases to about 8.58 mm in 70 s. This means that the model predicts only limited shrinkage. One can, however, see a very thick ash layer building up. At 70 s, the char core is only about 2.8 mm in diameter, while the full particle is still about 8.58 mm. This suggests that the current model cannot very well describe particle size reduction for wood, since for low-ash biomass, such as wood, one expects that the ash will immediately fall off the residual char core instead of building up an ash layer. A significant influence of ash seems more reasonable for high-ash content biomass, such as straw.

As long as drying is still occurring, the mass fraction of water vapor inside the porous wood particle is high (see 30 s in Figure 7a). After the drying is finalized in the wood particle center, the water vapor is quickly transported outward. During the thermal conversion it seems that only very little water vapor is consumed by steam gasification reactions, since these reactions are slow (see Figure 5b).

The gas density is rather high in the particle center during the drying and devolatilization phases (see Figure 7b). A significant amount of organic mass is entering the gas phase during wood devolatilization. Similarly, a lot of water vapor is quickly released to the gas phase during drying. Both phenomena result in higher gas density. The shown gas phase density profile leads to a pressure peak in the particle center. The pressure drops to ambient pressure at the particle surface. This gas phase pressure gradient is the driving force for gas phase convection.

In Figure 8a it is shown that after devolatilization is finalized, the oxidation of the residual char leads to a temperature increase (see temperature at 70 s), which is even exceeding the furnace temperature. This heat is then conducted outward through the ash-layer, while the temperature drops from more than 1400 K to a surface temperature slightly above the furnace temperature. Cooling of the particle at this stage of thermal conversion occurs via radiative losses.

Figure 8b shows that the oxygen mass fraction is more or less zero within the char core. In fact, oxygen diffusion into the char part of the particle is limited, as can be seen when comparing the size of the char core and the oxygen mass fraction at 70 s. The oxygen mass fraction at the outer particle surface quickly increases from 10% at 30 s to almost 20% at 70 s, which is due to reduced blowing factors. After devolatilization is over, the outwardly directed flow of gas is limited. This minimizes the blowing effect and, hence, increases the mass transfer coefficient.

Tar is produced during devolatilization, which can be seen from the tar mass fraction at 30 and 50 s in Figure 9a. The tar is then consumed by secondary tar reactions on its way through the surrounding char layer.

Figure 9b shows that the mass fraction of CO is low at early times, which is due to limited char oxidation reactions, while at 70 s, the CO mass fraction increases to a maximum of about

DOI: 10.1021/acs.energyfuels.8b00777
Energy Fuels 2018, 32, 6847−6862

Table 5. List of Tested Wood Log Diameters and Aspect Ratios As Well As Conversion Times[a]

$d_{particle}$ [mm]	$l_{particle}$ [mm]	V [mm^3]	t_{evap} [s]/%	t_{devol} [s]/%	t_{oxid} [s]/%	$t_{CO2,gasif}$ [s]/%	$t_{H2O,gasif}$ [s]/%	t_{total} [s]
10	40	3.14×10^{-6}	38/52.8	51/70.8	67/93.1	46/63.9	32/44.4	72
20	80	2.513×10^{-5}	145/48.8	182/61.3	292/98.3	178/60	143/48.1	297
40	160	2.01×10^{-4}	526/40.7	632/48.9	1285/99.5	610/47.2	520/40.2	1292

[a]The water content was 40 wt % wet basis in all test cases. The particle diameter is expressed by $d_{particle}$ and the wood log length is expressed by $l_{particle}$. The total thermal conversion time was defined as the time when 99% of the initial wet wood log mass had been converted.

33%, which indicates that mainly char is converting. This implies that most of the CO is formed during char oxidation rather than primary or secondary devolatilization reactions. The CO mass fraction drops to zero toward the particle surface at 30 s. This is due to CO oxidation reactions. The drop to lower values toward the surface at 50 and 70 s is due to inward diffusion of oxygen and nitrogen, since CO oxidation is negligible because of lack of water vapor due to the termination of the drying stage. Oxidation of CO requires OH radicals in order to occur sufficiently fast. The OH radicals are supplied in sufficient quantities by the water vapor leaving the evaporating inner sections of the particle. In fact, the need for OH radicals for sufficiently fast CO oxidation reactions can be seen from[6]

$$\dot{\omega}_{CO} = k_{CO}\left(\frac{\epsilon\rho_g^g Y_{CO}}{MW_{CO}}\right)\left(\frac{\epsilon\rho_g^g Y_{O_2}}{MW_{O_2}}\right)^{0.25}\left(\frac{\epsilon\rho_g^g Y_{H_2O}}{MW_{H_2O}}\right)^{0.5} MW_{CO} \quad (34)$$

5.1. Effect of Wood Particle Size. In the following, we study the influence of different wood particle diameters on their combustion behavior. The wood particles tested in this work have an aspect ratio of 4, and due to their large diameter and their cylindrical shape they can rather be referred to as wood logs. It is assumed that within the size range modeled in this work, the char burnout time is not affected by either increased or reduced char reactivity due to different internal heat transfer rates. Only within the range of high heating rates of, e.g., 10^4 °C/s one expects to see reduced char reactivity.[40−42]

The tested wood logs were of cylindrical shape with an aspect ratio of 4. The diameters and corresponding conversion times are listed in Table 5. The furnace wall temperature was 1276 K, with the surrounding gas phase temperature was kept at 1050 K.

Table 5 shows that wood log size and therefore also the wood log mass have a significant influence on the duration of all conversion stages of a full combustion process.

The start of a conversion stage, i.e. drying, devolatilization, or char conversion, is defined as the time when the reaction rates clearly start to increase. When the conversion rates drop to very small values again, the conversion stage is considered as being accomplished.

The corresponding plots have not been added to the paper, since they show the same trends as the reaction rates in Figure 5, and the most relevant information are summarized in Table 5.

It was observed that by increasing the wood log diameter by a factor of 2 (compared to the reference wood log diameter of 10 mm), the evaporation time increased by a factor of about 3.8 and the devolatilization time by a factor of 3.6. The char burnout time increased by a factor of 4.3. When comparing the time required for the full thermal conversion process, it is found that the full conversion time increased by a factor of 4.1. Even further increasing the particle size by increasing the wood log diameter by a factor of 4 (compared to the reference wood log diameter of 10 mm) prolonged the evaporation time by a factor of 13.8, while the devolatilization time was 12.4 times longer and the char burnout time was 19.2 times longer than in the reference case. The full thermal conversion process was prolonged by a factor of 17.9 compared to the thermal conversion time for a 10 mm wood log.

In order to compare the extents to which conversion zones are present at a given stage during thermal conversion, the authors compared the char, wood, and liquid water densities at the time of conversion where 50% of the initial wet wood mass have been converted. The results are found in Figure 10.

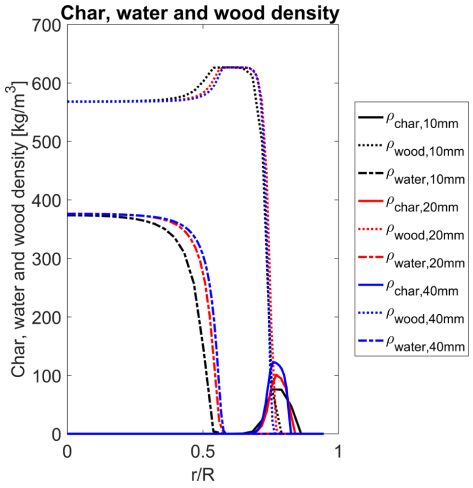

Figure 10. Conversion zones of cylindrical wood logs with diameters ranging from 10 mm to 40 mm and an aspect ratio of 4.

One can observe that for smaller particles, the peak of char density is lower than for larger particles, which is due to the different internal heat transfer rates. A lower internal heat transfer rate results in more char being formed. As a consequence, the wood log with a diameter of 10 mm has a maximum char density of 75 kg/m^3 at 50% thermal conversion, while the largest wood log (d_P = 40 mm) has a maximum char density of 120 kg/m^3 at the same degree of conversion. The char conversion zone is defined by the drop of char density, from its maximum value to zero. The char conversion zone spreads over 10.8% of the initial wood log radius for small wood logs (d_P = 10 mm), while it spreads over a zone of 6% of the initial radius for the large wood logs (d_P = 40 mm). In the wood log of intermediate size (d_P = 20 mm) the char conversion zone spread over 7% of the initial wood log radius.

The extent to which the devolatilization zone is present is decreasing as particle size increases. While the devolatilization zone spreads over 21.24% of the initial radius for the small

DOI: 10.1021/acs.energyfuels.8b00777
Energy Fuels 2018, 32, 6847−6862

wood log (d_p = 10 mm), it spreads over 11.5% of the radius of the large wood log (d_p = 40 mm).

For the drying zone, this analysis is more challenging due to the smearing effect of the kinetic rate drying model. Therefore, an analysis of the extent to which the drying zone is present in the wood logs of different sizes is rather rough. In order to avoid misinterpretation of the results, we defined the drying zone, as the zone where the liquid water density drop from 360 kg/m^3 to zero. By this, it was found that the extent to which the drying zone is present decreases as the wood log diameter increases. While the drying zone spreads over a range of 26% of the initial wood log radius for small logs (d_p = 10 mm), it only spreads over 17.5% for large logs (d_p = 40 mm).

The heat transfer controlled processes (drying and devolatilization) cover a larger domain of the particle than diffusion controlled char conversion. It is interesting to see that the model, validated against a rather small near-spherical particle, can be up-scaled to sinificantly larger particle dimensions (diameter in centimeter-range and aspect ratios larger than 1) and still replicate theoretically expected trends. This is a very promising observation, since only very limited literature is available on the thermochemical degradation of large wood logs, of sizes comparable to what is applied in wood stoves. Consequently, most of the model validation will have to be done against experiments done with small thermally thick particles. After validation, the particle must be up-scaled, if one aims to develop a solid phase model for wood log combustion in domestic heating appliances. The authors therefore conclude that this numerical model can be used to describe wood particle conversion as well as large wood log combustion.

6. CONCLUSIONS AND RECOMMENDATIONS

The 1D model has proven to be a good approach to fundamentally study the combustion behavior of wood particles. Nonetheless, obtained temperature data requires further validation, despite accurate mass loss predictions. Accurate surface temperature predictions are not possible with a stand-alone solid phase combustion model, since dynamic coupling between the gas phase and solid phase is required to accurately predict wood particle surface temperatures. The current solid phase model seems to capture the relevant chemical and physical phenomena very well, suggesting that coupling it to a gas phase model is a promising advancement for future research.

In this work, a combustion model for thermally thick wet near-spherical particles was validated and due to the assumption of thermally thick particles during validation, used for studying the combustion behavior of large wood logs. The model describes drying, devolatilization, and char oxidation and gasification as well as homogeneous oxidation reactions of CO. The model can describe oxygen diffusion into the particle, while accounting for a reduced mass transfer coefficient due to blowing of exiting gases. Volumetric shrinkage of the particle was considered during drying and devolatilization. Size reduction during char conversion was only considered by char conversion to pure ash at the outer char zone. Comparison to other modeling works and experimental data showed that the model is of acceptable accuracy and can be used for fundamental studies on combustion behavior of large thermally thick wood particles and logs.

It was shown that for a near-spherical particle (d_p = 9.5 mm) a mesh of 55 grid points (spanning over the particle radius) results in grid-independent solutions for the current conditions. Furthermore, it was found that due to challenges related to surface temperature measurements of combusting wood particles, validation of models is hard.

The wood log size does not influences the relative position of the conversion zones. The relative volume over which the three conversion zones were present decreased with increasing wood log diameter. The current shrinkage model cannot accurately describe the actual particle size of a near ash-free wood particle. For such wood species it is assumed that it is more accurate to assume inward moving boundaries, which means that no ash-layer builds up but that ash instead falls off immediately. With the current shrinkage model, a thick ash layer is allowed to build up. It is therefore recommended to compare the modeling results of a model with inward-moving boundary conditions, to the modeling results presented in this work and study which ash consideration is more appropriate for wood combustion modeling.

Furthermore, it needs to be mentioned that with respect to model input data, such as wood properties or even reaction kinetics as well as char reactivity, notable uncertainties do exist that will affect modeling results. Despite these potential sources of error, for the case studied here, the presented model has proven to capture physical and chemical phenomena related to combustion rather well. The sensitivity of the model to model input data should be studied in future works, in order to ensure that the model predicts combustion of single wood particles under different conditions equally well. However, such an extensive parametric study was not within the scope of this work dealing with model development.

AUTHOR INFORMATION

Corresponding Author

*E-mail: inge.haberle@ntnu.no.

ORCID

Inge Haberle: 0000-0002-3945-3627

Nils Erland L. Haugen: 0000-0002-9184-8722

Notes

The authors declare no competing financial interest.

ACKNOWLEDGMENTS

This work has been carried out within the WoodCFD (Grant 243752/E20) Project, which is funded by Dovre AS, Norsk Kleber AS, Jøtulgruppen, and Morsø AS together with the Research Council of Norway through the ENERGIX program.

NOMENCLATURE

A = pre-exponential factor [1/s]
AR = aspect ratio [−]
C = molar concentration (mol/m^3)
c_p = specific heat capacity [J/(kg K)]
D_{AB} = diffusivity [m^2/s]
D_b = bound water diffusivity [m^2/s]
D_{eff} = effective diffusivity [m^2/s]
$D_{Knudsen}$ = Knudsen diffusion [m^2/s]
d_p = particle diameter [m]
d_{pore} = pore diameter [m]
E_a = activation energy [kJ/mol]
f = gas species fraction from primary devolatilization [−]
f_{evap} = evaporation fraction [−]
F_{heat} = heat flux [J/(m^2 s)]
g = gas species fraction from secondary devolatilization [−]
Δh = heat of reaction [kJ/kg]

DOI: 10.1021/acs.energyfuels.8b00777
Energy Fuels 2018, 32, 6847−6862

$h_{c,0}$ = heat transfer coefficient [W/(m^2 K)] (without Stefan flow)
h_c = heat transfer coefficient [W/(m^2 K)] (with Stefan flow)
$h_{m,0}$ = mass transfer coefficient [m/s] (without Stefan flow)
h_m = mass transfer coefficient [m/s] (with Stefan flow)
k = reaction rate constant [1/s] or [m/s]
l = length of the cylinder
M_{fsp} = moisture content at fiber saturation point; dry basis [kg/kg]
$\dot{M}_{total}$ = total mass flow of exiting gases [kg/s]
M_l = moisture content (liquid free water); dry basis [kg/kg]
MW = molecular weight [kg/mol]
Nu = Nusselt number
P_c = capillary pressure [Pa]
P_g = gas pressure [Pa]
P_l = liquid phase pressure [Pa]
R = ideal gas constant [J/(mol K)]
r = radius [m]
T = temperature [K]
t = time [s]
$S_{a,char}$ = specific surface area of char [m^2/m^3]
Sh = Sherwood number
T_{gas} = surrounding gas phase temperature [K]
u_r = gas phase velocity in radial direction [m/s]
u_l = liquid free water velocity in radial direction [m/s]
V_j = control volume [m^3] (including shrinkage effect)
$V_{j,0}$ = initial control volume [m^3]
Y = mass fraction [−]

Greek Letters

β = shrinkage factors [−]
ϵ_g = gas phase volume fraction [−]
ϵ_{pore} = porosity [−]
$\epsilon_{particle}$ = particle emissivity [−]
η = fraction of residual wood [−]
θ = blowing factor [−]
κ = permeability [m^2]
λ = thermal conductivity [W/(m K)]
μ = dynamic viscosity [Pa s]
ξ = bridge factor [−]
ρ = density [kg/m^3]
σ = Stefan−Boltzmann constant [W/(m^2 K^4)]
ϕ = volume fraction of pores filled with water [−]
Φ = endothermic/exothermic heat of reaction terms [J/(m^3 s)]
$\dot{\omega}$ = reaction rate [kg/(m^3 s)]
ω_{pore} = pore emissivity [−]
Ω = stoichiometric factor

Subscript

ash = ash
b = bound water
C = carbon
char = char
CO_2,gasif = CO_2 gasification
devol,1 = primary devolatilization
devol,2 = secondary devolatilization
eff = effective
H_2O,g = water vapor
H_2O,gasif = H_2O gasification
i = reaction
evap = evaporation
fsp = fiber saturation point
g,gas = total gas phase
k = gas species
$k1$ = reaction: wood to noncondensable gases
$k2$ = reaction: wood to tar
$k3$ = reaction: wood to char
$k4$ = reaction: tar to noncondensable gases
$k5$ = reaction: tar to char
l = liquid free water
mix,total = mixed gas phase
oxid = char oxidation
ref = reference
surface = particle surface
tar = tar
wall = furnace wall
wood = dry wood
wood,0 = dry wood initial
$\parallel$ = parallel to fiber direction
$\perp$ = perpendicular to fiber direction
0 = initial
∞ = bulk

Superscript

g = gas phase
l = liquid phase

REFERENCES

(1) Yang, Y. B.; Sharifi, V. N.; Swithenbank, J.; Ma, L.; Darvell, L. I.; Jones, J. M.; Pourkashanian, M.; Williams, A. *Energy Fuels* **2008**, *22*, 306−316.
(2) Skreiberg, Ø.; Seljeskog, M.; Georges, L. *Chem. Eng. Trans.* **2015**, *43*, 433−438.
(3) Porteiro, J.; Granada, E.; Collazo, J.; Patiño, D.; Morán, J. C. *Energy Fuels* **2007**, *21*, 3151−3159.
(4) Porteiro, J.; Míguez, J. L.; Granada, E.; Moran, J. C. *Fuel Process. Technol.* **2006**, *87*, 169−175.
(5) Lu, H.; Robert, W.; Peirce, G.; Ripa, B.; Baxter, L. L. *Energy Fuels* **2008**, *22*, 2826−2839.
(6) Lu, H. *Experimental and modeling investigation of biomass particle combustion*. Ph.D. Thesis, Brigham Young University, Provo, UT, 2006.
(7) Thunman, H.; Leckner, B.; Niklasson, F.; Johnsson, F. *Combust. Flame* **2002**, *129*, 30−46.
(8) Fatehi, H.; Bai, X. S. *Combust. Sci. Technol.* **2014**, *186*, 574−593.
(9) Mehrabian, R.; Zahirovic, S.; Scharler, R.; Obernberger, I.; Kleditzsch, S.; Wirtz, S.; Scherer, V.; Lu, H.; Baxter, L. L. *Fuel Process. Technol.* **2012**, *95*, 96−108.
(10) Galgano, A.; Di Blasi, C.; Horvat, A.; Sinai, Y. *Energy Fuels* **2006**, *20*, 2223−2232.
(11) Galgano, A.; Di Blasi, C. *Prog. Comput. Fluid Dyn.* **2006**, *6*, 287−302.
(12) Haberle, I.; Skreiberg, Ø.; Łazar, J.; Haugen, N. E. L. *Prog. Energy Combust. Sci.* **2017**, *63*, 204−252.
(13) Li, J.; Paul, M. C.; Younger, P. L.; Watson, I.; Hossain, M.; Welch, S. *Appl. Energy* **2015**, *156*, 749−755.
(14) Saeed, M.; Andrews, G.; Phylaktou, H.; Gibbs, B. *Fuel* **2016**, *181*, 347−357.
(15) Riaza, J.; Gibbins, J.; Chalmers, H. *Fuel* **2017**, *202*, 650−655.
(16) Pozzobon, V.; Salvador, S.; Bézian, J. J.; El-Hafi, M.; Maoult, Y. L.; Flamant, G. *Fuel Process. Technol.* **2014**, *128*, 319−330.
(17) Lu, Z.; Jian, J.; Jensen, P. A.; Wu, H.; Glarborg, P. *Energy Fuels* **2016**, *30*, 5772−5778.
(18) Haberle, I.; Haugen, N. E. L.; Skreiberg, Ø. *Energy Fuels* **2017**, *31*, 13743−13760.
(19) Di Blasi, C. *Chem. Eng. Sci.* **1996**, *51*, 1121−1132.
(20) Larfeldt, J.; Leckner, B.; Melaaen, M. C. *Fuel* **2000**, *79*, 1637−1643.

DOI: 10.1021/acs.energyfuels.8b00777
Energy Fuels 2018, 32, 6847−6862

(21) Grønli, M. G. *A theoretical and experimental study of the thermal degradation of biomass*. Ph.D. Thesis, Norwegian University of Science and Technology, Trondheim, Norway, 1996.
(22) de Paiva Souza, M. E.; Nebra, S. A. *Wood Fiber Sci.* **2000**, *32*, 153−163.
(23) Evans, D.; Emmons, H. *Fire Saf. J.* **1977**, *1*, 57−66.
(24) Wornat, M. J.; Hurt, R. H.; Davis, K. A.; Yang, N. Y. *Symp. (Int.) Combust., [Proc.]* **1996**, *26*, 3075−3083.
(25) Branca, C.; Di Blasi, C. *Energy Fuels* **2003**, *17*, 1609−1615.
(26) National Laboratory Lawrence Livermore. *SUNDIALS: SUite of Nonlinear and DIfferential/ALgebraic Equation Solvers - IDA*, 2016; http://computation.llnl.gov/projects/sundials/ida (accessed April 7, 2017).
(27) Hermansson, S.; Thunman, H. *Combust. Flame* **2011**, *158*, 988−999.
(28) Bird, R. B.; Stewart, W. E.; Lightfoot, E. N. *Transport Phenomena*, 2nd ed.; John Wiley & Sons, Inc.: New York, 2002.
(29) Forest Products Laboratory. *Wood Handbook - Wood as an Engineering Material*. General Technical Report FPL-GTR-190; 2010.
(30) Biswas, A. K.; Umeki, K. *Chem. Eng. J.* **2015**, *274*, 181−191.
(31) Hagge, M. J.; Bryden, K. M. *Chem. Eng. Sci.* **2002**, *57*, 2811−2823.
(32) Wagenaar, B.; Prins, W.; van Swaaij, W. *Fuel Process. Technol.* **1993**, *36*, 291−298.
(33) Chan, W.-C. R.; Kelbon, M.; Krieger, B. B. *Fuel* **1985**, *64*, 1505−1513.
(34) Liden, A.; Berruti, F.; Scott, D. *Chem. Eng. Commun.* **1988**, *65*, 207−221.
(35) Koufopanos, C.; Papayannakos, N.; Maschio, G.; Lucchesi, A. *Can. J. Chem. Eng.* **1991**, *69*, 907−915.
(36) Di Blasi, C. *Combust. Sci. Technol.* **1993**, *90*, 315−340.
(37) Bryden, K. M.; Hagge, M. J. *Fuel* **2003**, *82*, 1633−1644.
(38) Neves, D.; Thunman, H.; Matos, A.; Tarelho, L.; Gomez-Barea, A. *Prog. Energy Combust. Sci.* **2011**, *37*, 611−630.
(39) Fatehi, H. *Numerical Simulation of Combustion and Gasification of Biomass Particles*. Ph.D. Thesis, LTH (Lund University), Lund, Sweden, 2014.
(40) Jones, J.; Bridgeman, T.; Darvell, L.; Gudka, B.; Saddawi, A.; Williams, A. *Fuel Process. Technol.* **2012**, *101*, 1−9.
(41) Fisher, E.; Dupont, C.; Darvell, L.; Commandré, J.-M.; Saddawi, A.; Jones, J.; Grateau, M.; Nocquet, T.; Salvador, S. *Bioresour. Technol.* **2012**, *119*, 157−165.
(42) McNamee, P.; Darvell, L.; Jones, J.; Williams, A. *Biomass Bioenergy* **2015**, *82*, 63−72.

DOI: 10.1021/acs.energyfuels.8b00777
Energy Fuels 2018, 32, 6847−6862

Errata for Paper III

This document lists errors found in Paper III. Only errors that matter from a mathematical viewpoint are listed.

Location	Original text	Correction
pp. 6852, Eq.(31)	$h_{\mathrm{m}} = \dfrac{\dot{M}_{\mathrm{total}}}{\left(\exp\left(\dfrac{\dot{M}_{\mathrm{total}}}{h_{\mathrm{m},0}}\right)-1\right)}$	$h_{\mathrm{m}} = \dfrac{\dot{M}_{\mathrm{total}}/\rho_{\mathrm{g}}^{\mathrm{g}}}{\left(\exp\left(\dfrac{\dot{M}_{\mathrm{total}}}{\rho_{\mathrm{g}}^{\mathrm{g}} h_{\mathrm{m},0}}\right)-1\right)}$
pp. 6848, Table 1 (gas phase continuity)	$\frac{\partial \varepsilon_{\mathrm{g}} \rho_{\mathrm{g}}^{\mathrm{g}}}{\partial t} + \frac{1}{r}\frac{\partial (r \varepsilon_{\mathrm{g}} \rho_{\mathrm{g}}^{\mathrm{g}} u_{\mathrm{r}})}{\partial r} = \dot{\omega}_{\mathrm{g}}$	$\frac{\partial \varepsilon_{\mathrm{g}} \rho_{\mathrm{g}}^{\mathrm{g}}}{\partial t} + \frac{1}{r}\frac{\partial}{\partial r}\left(r \rho_{\mathrm{g}}^{\mathrm{g}} u_{\mathrm{r}}\right) = \dot{\omega}_{\mathrm{g}}$
pp. 6848, Table 1 (species equation)	$\frac{\partial (\varepsilon_{\mathrm{g}} \rho_{\mathrm{g}}^{\mathrm{g}} Y_k)}{\partial t} + \frac{1}{r}\frac{\partial (r \varepsilon_{\mathrm{g}} \rho_{\mathrm{g}}^{\mathrm{g}} Y_{\mathrm{k}} u_{\mathrm{r}})}{\partial r} = \frac{1}{r}\frac{\partial}{\partial r}\left(r \varepsilon_{\mathrm{g}} \rho_{\mathrm{g}}^{\mathrm{g}} D_{\mathrm{eff}} \frac{\partial Y_{\mathrm{k}}}{\partial r}\right) + \dot{\omega}_k$	$\frac{\partial (\varepsilon_{\mathrm{g}} \rho_{\mathrm{g}}^{\mathrm{g}} Y_k)}{\partial t} + \frac{1}{r}\frac{\partial (r \rho_{\mathrm{g}}^{\mathrm{g}} Y_{\mathrm{k}} u_{\mathrm{r}})}{\partial r} = \frac{1}{r}\frac{\partial}{\partial r}\left(r \rho_{\mathrm{g}}^{\mathrm{g}} D_{\mathrm{eff}} \frac{\partial Y_{\mathrm{k}}}{\partial r}\right) + \dot{\omega}_k$
pp. 6848, Table 1 (Temperature)	$\left(\rho_{\mathrm{wood}} c_{P,\mathrm{wood}} + \rho_{\mathrm{char}} c_{P,\mathrm{char}} + \rho_{\mathrm{l}} c_{P,\mathrm{l}} + \rho_{\mathrm{b}} c_{P,\mathrm{b}} + \varepsilon_{\mathrm{g}} \rho_{\mathrm{g}}^{\mathrm{g}} c_{P,\mathrm{g}}\right)\frac{\partial T}{\partial t} + \left(\rho_{\mathrm{l}} c_{\mathrm{P,l}} u_{\mathrm{l}} + \rho_{\mathrm{b}} c_{\mathrm{P,b}} u_{\mathrm{b}} + \varepsilon_{\mathrm{g}} \rho_{\mathrm{g}}^{\mathrm{g}} c_{\mathrm{P,g}} u_{\mathrm{r}}\right)\frac{\partial T}{\partial r} = \frac{1}{r}\frac{\partial}{\partial r}\left(r \lambda_{\mathrm{eff}}\left(\frac{\partial T}{\partial r}\right)\right) - \Phi_{\mathrm{evap}} - \Phi_{\mathrm{devol,1}} + \Phi_{\mathrm{devol,2}}$	$\left(\rho_{\mathrm{wood}} c_{P,\mathrm{wood}} + \rho_{\mathrm{char}} c_{P,\mathrm{char}} + \rho_{\mathrm{l}} c_{P,\mathrm{l}} + \rho_{\mathrm{b}} c_{P,\mathrm{b}} + \varepsilon_{\mathrm{g}} \rho_{\mathrm{g}}^{\mathrm{g}} c_{P,\mathrm{g}}\right)\frac{\partial T}{\partial t} + \left(\rho_{\mathrm{l}} c_{\mathrm{P,l}} u_{\mathrm{l}} + \rho_{\mathrm{b}} c_{\mathrm{P,b}} u_{\mathrm{b}} + \rho_{\mathrm{g}}^{\mathrm{g}} c_{\mathrm{P,g}} u_{\mathrm{r}}\right)\frac{\partial T}{\partial r} = \frac{1}{r}\frac{\partial}{\partial r}\left(r \lambda_{\mathrm{eff}}\left(\frac{\partial T}{\partial r}\right)\right) - \Phi_{\mathrm{evap}} - \Phi_{\mathrm{devol,1}} + \Phi_{\mathrm{devol,2}}$

Paper IV

Reproduced with permission from Energy & Fuels, accepted for publication

Inge Haberle, Nils Erland L. Haugen and Øyvind Skreiberg, Simulating thermal wood particle conversion: Ash-layer modeling and parametric studies, Energy & Fuels (in press), 2018.

Simulating thermal wood particle conversion: Ash-layer modeling and parametric studies

Journal:	*Energy & Fuels*
Manuscript ID	ef-2018-02173b.R1
Manuscript Type:	Article
Date Submitted by the Author:	n/a
Complete List of Authors:	Haberle, Inge; NTNU Fakultet for ingeniorvitenskap og teknologi Trondheim, Energy and Process Engineering Haugen, Nils Erland L.; SINTEF Energy Research, Skreiberg, Øyvind; SINTEF Energy Research,

Simulating thermal wood particle conversion: Ash-layer modeling and parametric studies

Inge Haberle,*,† Nils Erland L. Haugen,*,†,‡ and Øyvind Skreiberg‡

†*Department of Energy and Process Engineering, Norwegian University of Science and Technology, Kolbjørn Hejes vei 1 B, 7491 Trondheim, Norway*

‡*Department of Thermal Energy, SINTEF Energy Research, Kolbjørn Hejes vei 1 A, 7491 Trondheim, Norway*

E-mail: inge.haberle@ntnu.no; nils.e.haugen@sintef.no

Abstract

In this work we study thermochemical degradation and char conversion of wet wood particle. The work is split in two main parts; 1) the effect of the ash layer handling approach and 2) a parametric study over different relevant parameters.

In the study of the ash layer handling, we investigate the effect of allowing the ash to remain on the surface of the particle when the char is converted (*Model A*) in contrast to removing the ash such that the reacting char layer is always exposed (*Model B*). It was found that the two modeling concepts yield significantly different mass losses and surface and center temperature predictions. *Model B* presents a faster thermal conversion while the results predicted by *Model A* are in better agreement with what has been observed experimentally.

A parametric study was also done, where the sensitivity to variations in thermal conductivity, specific surface area and gas permeability was studied. It was found that thermal conductivity influences the time when drying and devolatilization are accomplished. This is because these conversion stages are heat-transfer controlled. Char conversion is primarily affected by a shift to earlier times for the initialization of the final char conversion when higher thermal conductivities are used.

It is found that the specific surface area can significantly affect the final char conversion time. Since char conversion is a key stage of wood combustion, the full conversion time is also affected.

The gas permeability primarily affects mass diffusion into the particle. It was found that up until a critical effective gas permeability the modeling results are sensitive to assigned permeabilities.

Nomenclature

A	pre-exponential factor $[\frac{1}{\mathrm{s}}]$ / $[\frac{\mathrm{m}}{\mathrm{sK}}]$
AR	Aspect ratio
c_{P}	specific heat capacity $[\frac{\mathrm{J}}{\mathrm{kgK}}]$
D_{AB}	diffusivity $[\frac{\mathrm{m}^2}{\mathrm{s}}]$
D_{b}	bound water diffusivity $[\frac{\mathrm{m}^2}{\mathrm{s}}]$
D_{eff}	effective diffusivity $[\frac{\mathrm{m}^2}{\mathrm{s}}]$
D_{Knudsen}	Knudsen diffusion $[\frac{\mathrm{m}^2}{\mathrm{s}}]$
d_{P}	particle diameter [m]
d_{pore}	pore diameter [m]
E_a	activation energy $[\frac{\mathrm{J}}{\mathrm{mol}}]$
f	gas species fraction from primary devolatilization [-]
g	gas species fraction from secondary devolatilization [-]
$\triangle$h	heat of reaction $[\frac{\mathrm{J}}{\mathrm{kg}}]$
$h_{\mathrm{c,0}}$	heat transfer coefficient $[\frac{\mathrm{W}}{\mathrm{m^2K}}]$ (without Stefan flow)
h_{c}	heat transfer coefficient $[\frac{\mathrm{W}}{\mathrm{m^2K}}]$ (with Stefan flow)
$h_{\mathrm{m,0}}$	mass transfer coefficient $[\frac{\mathrm{m}}{\mathrm{s}}]$ (without Stefan flow)
h_{m}	mass transfer coefficient $[\frac{\mathrm{m}}{\mathrm{s}}]$ (with Stefan flow)
J_{diff}	diffusive mass flux [kg/(sm^2)]
k	reaction rate constant $[\frac{1}{\mathrm{s}}]$ or $[\frac{\mathrm{m}}{\mathrm{s}}]$
k_1	reaction: wood to non-condensable gases
k_2	reaction: wood to tar
k_3	reaction: wood to char
k_4	reaction: tar to non-condensable gases
k_5	reaction: tar to char
M_{liquid}	liquid moisture content [-]
$\dot{M}_{\mathrm{total}}$	total mass flux of exiting gases $[\frac{kg}{sm^2}]$
MW	molecular weight $[\frac{\mathrm{kg}}{\mathrm{mol}}]$
R	ideal gas constant $[\frac{\mathrm{J}}{\mathrm{molK}}]$

r	radius [m]		T	temperature [K]	
T	temperature [K]		$s_{\mathrm{a,char}}$	specific surface area of char $[\mathrm{m}^2/\mathrm{m}^3]$	
T_{gas}	surrounding gas phase temperature [K]		u_{b}	bound watere velocity in radial direction $[\frac{\mathrm{m}}{\mathrm{s}}]$	
T_{pyro}	pyrolysis temperature [K]		u_{r}	gas phase velocity in radial direction $[\frac{\mathrm{m}}{\mathrm{s}}]$	
T_{ref}	reference temperature [K] (298 K)		V_j	cell volume $[\mathrm{m}^3]$	
T_{wall}	furnace wall		Y	mass fraction [-]	

Greek letters

ϵ_{g}	gas phase volume fraction [-]		λ	thermal conductivity $[\frac{\mathrm{W}}{\mathrm{mK}}]$	
ϵ_{pore}	porosity [-]		ρ	density $[\frac{\mathrm{kg}}{\mathrm{m}^3}]$	
ω_{eff}	effective emissivity [-]		σ	Stefan-Boltzmann constant $[\frac{\mathrm{W}}{\mathrm{m}^2\mathrm{K}^4}]$	
Ω	stoichiometric coefficient [-]		θ	Shrinkage factor [-]	
Φ	heat source term $[\mathrm{J}/(\mathrm{sm}^3)]$		$\dot{\omega}$	reaction rate $[\frac{\mathrm{kg}}{\mathrm{m}^3\mathrm{s}}]$	
κ	permeability $[\mathrm{m}^2]$				

Subscript

ash	ash		$CO_{2,\mathrm{gasif}}$	CO_2 gasification	
b	bound water		$devol, 1$	primary devolatilization	
$char$	char		$devol, 2$	secondary devolatilization	

eff	effective
$evap$	evaporation
g	gas phase
H_2O, g	water vapor
i	reaction
k	gas species
$mix, total$	mixed gas phase
oxid	char oxidation
$pyro$	pyrolysis

Superscript

g	gas phase
ref	reference
$steam, gasif$	H_2O gasification
$surface$	particle surface
tar	tar
$wall$	furnace wall
$wood$	dry wood
$\perp$	perpendicular to fiber direction
∞	bulk

1 Introduction

Wood combustion is a main field of research nowadays. The increased focus on wood combustion is due to the renewable character of wood as an energy source. In order to understand chemical and physical phenomena related to wood combustion, numerical modeling has proven to be a useful tool. Hence, over the last decades, many fundamental studies on thermochemical wood degradation and combustion have been performed by the use of numerical simulation tools.[1]

Different models for wood combustion are available, with most of them being one-dimensional (1D).[2–8] One-dimensional (1D) models allow for fundamental studies of combustion related processes, while at the same time remaining numerically efficient.

One important element of a model describing drying, devolatilization and char conversion is the structural change due to volumetric shrinkage and char conversion occurring during thermochemical conversion. This change in particle size can have an influence on the thermochemical degradation of the particle.[9]

However, in general it must be pointed out that shrinkage is a multi-dimensional phenomenon that is always simplified in 1D models. The multi-dimensional character of shrinkage has been experimentally observed by Grønli.[10] While shrinkage during drying is commonly neglected, as it is only small compared to shrinkage during devolatilization,[2] the volumetric shrinkage during devolatilization must be accounted for due to significant organic mass loss during devolatilization. This volumetric shrinkage is often modeled by empirical shrinkage factors.[4] Most challenging, however, is the enormous size reduction the particle is affected by during char conversion. It is still studied how this size reduction can be accurately predicted by 1D models. As char is consumed by gasification and oxidation, the particle size is significantly decreasing. The final size of the particle can be predicted differently in models by either neglecting or considering residual ash in the model.

Wood is a biomass source with low ash content, which suggests that an ash layer could potentially be neglected in a combustion model due to its negligible influence on heat and mass transfer. However, reviewing earlier works on wood combustion modeling shows that a common modeling assumption is to consider an up-building ash layer and especially the effect of it on heat and mass transfer.[3,4] An advantage of this modeling assumption is that the boundaries are fixed to the same grid point during drying, devolatilization and char conversion. This implies that the char conversion front does not have to be tracked. This modeling assumption predicts the mass loss well, when validated against experiments. At the same time, it shows that the predicted surface and center temperatures are different from experimental measurements.[3,4] Even though the deviation between modeling results and experiments can also be due to inaccurate temperature measurements because of the significant size reduction of the particle during char conversion, it might as well be due to an

inadequate handling of the ash layer. The ash layer also affects the oxygen diffusion to the char surface which has an impact on the modeling results. This consideration of diffusion through an up-building ash layer can be conducted differently based on the choice of ash porosity. It can even be fully neglected by assuming the absence of the ash (i.e.; the ash is immediately removed from the surface after full char conversion at a distinct location). As was discussed, the suitability of the two modeling approaches is linked to the experimental conditions as well as the ash chemistry. The ash chemistry of a sample can affect the importance of the ash layer with respect to heat and mass transfer and also catalytic effects of the ash on conversion chemistry, as will be discussed in the following section. One migh expect that for agricultural biomass ash chemistry becomes crucial since the composition of ash can cause an encapsulation of the unreacted char, due to low ash melting temperatures. For those types of biomass one might expect that the consideration of the ash layer with respect to heat and mass transfer will significantly affect the char conversion time. On the other hand, for ash obtained when converting a woody fuel with low ash content, ash melting is not a major concern, and the ash structure is not altered by increasing temperatures, such that heat and mass transfer are not expected to be significantly altered. The ash maintains a porous structure.[11] For woody biomass, therefore, one would rather expect that by purely judging ash chemistry, the consideration of the ash layer is of negligible importance if the ash content is minor and the ash is highly porous. This is, indeed also what Strandberg et al.[11] stated who found that generally char conversion rates could be affected by dense ash layers (which themselves are often dominated by low-temperature melting alkali-silicates). However, such an inhibition is unlikely to occur for woody-type biomass, since woody biomass ash has a high content of calcium and low silicon content, resulting in higher ash melting temperatures.[11] It shall be pointed out, that the consideration of the presence or absence of an ash layer might also be a function of whether or not the bark layer surrounding the stem wood is modeled or not. Bark and stem wood have significantly different ash fractions and the ash chemistry can also differ signifcantly. Also experimental conditions can have an

impact on the validity of the two modeling approaches for certain test cases. Therefore, one can already observe that the motivations for the applicability of the two models is very vast and can be a field of research just by itself.

Therefore, this work focuses on how the different modeling concepts, with one considering an up-building ash layer and one neglecting it, affect the model predictions for thermal conversion times and particle temperatures. To the authors' knowledge, such a comparison of combustion models with fixed boundary conditions and inward-moving boundary conditions has not previously been done.

In addition, the model's sensitivity to the specific surface area of char and thermal conductivities of char and wood was also studied. The thermal conductivity is assumed to mainly affect drying and devolatilization, both being heat-transfer controlled conversion stages, while the specific surface area is assumed to affect the char conversion modeling results as it alters the reactivity of the char. Furthermore, the sensitivity of the model to gas permeability was also tested.

1.1 Ash contents of hard- and softwoods

Compared to other types of biomass, e.g. rice straw (ash fraction of 19.2 % dry basis),[12] wood has a very low ash content (see Table 1).

Table 1: Ash contents of different wood species given in wt.% dry basis. All original data has been taken from Pettersen[13] but averaging according to species has been done by the authors.

Wood species[*)]	**Hardwood**	**Softwood**	**Ash content (% dry basis)**
Maple	✓		0.3667
American Beech	✓		0.4
Hickory	✓		0.75
Oak	✓		0.6
Pine		✓	0.29
Birch	✓		0.5
Yellow Poplar	✓		1
Basswood	✓		0.4
Fir		✓	0.383
Hemlock		✓	0.467
Cedar		✓	0.367
Spruce		✓	0.267

[*)] marks that the wood species written in bold have been averaged since different sub-species of the wood species have been tested and different ash fractions were measured.

Table 1 shows that the majority of the wood species has an ash fraction smaller than 0.5wt.% (dry basis). Due to the very low ash content, the authors assumed that the development of a model where the ash *"falls off"* during char conversion, due to its negligible influence on heat and mass transfer, could be an alternative modeling approach compared to most of the already existing wood degradation models, e.g.[4,14] It is of interest to then study if the results of this modeling approach can get closer to experimental data. The *"falling off"* of the ash layer purely refers to the negligence of the ash layer in the numerical model, due to assumingly negligible influence of the ash layer on heat and mass transfer. In a numerical model, the *"falling off"* of the ash layer can be implemented by inward moving boundary conditions that are fixed to the outer char conversion front. An explicit consideration of the

ash layer is instead accounted for by fixed boundary conditions. In fact, making an inadequate assumption regarding heat and mass transfer may potentially affect model accuracy. This theoretical understanding of the influence of the ash layer on biomass combustion, has not previously been tested.

1.2 Theory of char reactivity

An accurate description of the char conversion stage is a key element of any simulation tool that will be used for design and optimization of combustion or gasification processes. The reason is that char conversion (oxidation and gasification) can be the limiting stage of the entire thermochemical conversion under certain conditions.[15]

The accuracy of a model is not only dependent on the modeling approach (fixed or inward-moving boundaries) but also on input data, such as specific surface area. Even though the char conversion of thermally thick wood particles is diffusion controlled, it is also of interest to study how sensitive the model accuracy is to the input data describing char reactivity. Char reactivity is influenced by the following properties:[15]

1. Surface area that can be accessed and is therefore available for surface reactions.
2. The inorganic compounds that are found in the carbon skeleton of the char and consequently also the concentration at which the inorganic matter is present.
3. The type of functional groups in the char and the concentration of those groups.

Those properties are influenced by the initial wood properties as well as the devolatilization process under which the char is formed.[15] In this work, the model's sensitivity to char reactivity is tested by means of specific surface area.

In Table 2 measured specific surface areas for wood chars are presented. It is obvious that observed values spread over a large range.

Table 2: Experimentally measured specific surface areas of different wood chars obtained under different conditions. Here, *d.b.* refers to the dry basis and T_{pyro} is the peak temperature the pyrolysis was accomplished at. The abbreviation *SSA* is used for specific surface area while *BET* refers to the "Brunauer-Emmett-Teller" testing method to define the total specific surface area. The specific surface area is given in m^2/m^3 (if the original data was given in m^2/g this has been converted by using an assumed apparent char density of 100 kg/m^3.)

Ref.	**Wood char species**	**Temperature,** T_{pyro}, °C	**Moisture** %	**Measurement**	**SSA** $[\frac{m^2}{m^3}]$
Lu et al.[4]	Poplar	NA	NA	BET	1×10^6
Grønli[10]	Birch	NA	NA	[1)]	4.1×10^7
Grønli[10]	Spruce	NA	NA	[1)]	4.59×10^7
Burhenne et al.[16]	Spruce	500	2.4 % w.b.	BET (N_2)	1.96×10^7
Burhenne et al.[16]	Spruce	500	16.4 % w.b.	BET (N_2)	3.97×10^7
Burhenne et al.[16]	Spruce	500	55.4 % w.b.	BET (N_2)	3.75×10^7
Burhenne et al.[16]	Spruce	800	2.4 % w.b.	BET (N_2)	5×10^2
Burhenne et al.[16]	Spruce	800	16.4 % w.b.	BET (N_2)	1.669×10^5
Burhenne et al.[16]	Spruce	800	55.4 % w.b.	BET (N_2)	1.066×10^5
Link et al.[17]	Douglas Fir	800	6.47 % d.b.	BET (N_2)	3.16×10^7
Link et al.[17]	Douglas Fir	800	6.47 % d.b.	BET (CO_2)	3.98×10^7
Link et al.[17]	Pine	800	8.6 % d.b.	BET (N_2)	4.85×10^7
Link et al.[17]	Pine	800	8.6 % d.b.	BET (CO_2)	5.36×10^7
Anca-Couce et al.[15]	Pine	500	NA [2)]	BET (N_2)	1.5176×10^6
Anca-Couce et al.[15]	Pine	500	NA [3)]	BET (N_2)	2.120×10^5
Anca-Couce et al.[15]	Pine	500	NA [3)]	BET (N_2)	1.06095×10^7

[1)] marks that *Coulter SA 3100 Surface Area Analyzer* has been used for measuring the specific surface area.
[2)] Anca-Couce et al.[15] produced the tested chars with TGA. More information regarding this can be found in their work.[15]
[3)] Anca-Couce et al.[15] produced the tested chars in a fixed-bed reactor. More information regarding this can be found in their work.[15]

Char formed under lower temperatures has a low specific surface area. However, the final surface area does not only depend on the temperature alone.[18]

By evaluating the data in Table 2 it turns out that there is a significant scattering in the measured char surface areas. One main reason for this is that the measurement methods can vary and based on this variation significantly different specific surface areas can be

determined for the same char (e.g. comparing the specific surface areas obtained with BET measurements with N_2 or CO_2 in Table 2).

Nitrogen is typically used for BET-measurements, but it has to be mentioned that the corresponding results can be affected by diffusion limitations of the gas into micropores. Based on this, the surface area might be underestimated. This limitation is the motivation for why some BET-measurements are performed with CO_2, as it diffuses more easily into fine pores and therefore predicts a higher specific surface area. The restrictions of BET-measurements performed with nitrogen have been reported to be as significant as to even not being able to measure the specific surface area of biochars generated at low-temperature conditions at all, while BET-measurements performed with CO_2 were able to measure specific surface areas in the range of hundreds of m^2/g.[18]

Furthermore, it needs to be mentioned that the measured specific surface area as such is not necessarily equal to the specific surface area accessible for heterogeneous char reactions. This is due to the distinct groups of pores, namely macro- (>50 nm diameter), meso- (2-50 nm diameter) and micropores (<2 nm diameter), which are affecting the measured inner specific surface area (of course the influence on micropores depends on the testing gas used in BET-measurements). However, heterogeneous char reactions occur primarily in macro- and mesopores, even though the micropores will significantly increase the measured surface area.

The influence of the total specific surface area, $s_{\mathrm{a,char}}$, in common comprehensive combustion models enters in a simplified manner[4]

$$\dot{\omega}_i = s_{\mathrm{a,char}} \frac{\rho_{\mathrm{char}}}{\rho_{\mathrm{char}} + \rho_{\mathrm{wood}} + \rho_{\mathrm{ash}}} k_i \rho_{\mathrm{g,k}} \tag{1}$$

with k_i being the reaction rate constant and $\rho_{\mathrm{g,k}}$ being the phase averaged species gas density of the reacting gas species k (either O_2, CO_2 or H_2O). The sensitivity of the model to the input data for $s_{\mathrm{a,char}}$ can be studied. The input data for specific surface area equals measured

BET surface data. The deactivation of active sites due to reduced char density is considered by the term $\frac{\rho_{\mathrm{char}}}{\rho_{\mathrm{char}}+\rho_{\mathrm{wood}}+\rho_{\mathrm{ash}}}$. Active sites refer to carbon edges, oxygen containing functional groups and inorganic impurities, onto which the reacting gas can chemisorb through electron transfer.[18] Based on the range of experimental data available for specific surface areas, it is of interest to investigate how much these variations can affect the modeling results.

1.3 Thermal conductivities of wood and char

In the same way as there is a significant scattering in existing data on specific surface area, a wide range of thermal conductivities for wood and char is also found in literature.[1] Since both drying and devolatilization are controlled by the internal heat transfer, the choice of char and wood thermal conductivity will affect the wood particle combustion time. The study of the significance of this influence is part of this work.

1.4 Gas permeabilities

Also modeling input data that can be directly linked to the gas phase flow such as gas permeabilities scatters significantly.[1] Values can differ significantly for different wood species.[10] Also, with respect to char permeability, different data can be found.[1] Char permeabilities are larger than wood permeabilities due to pore enlargement during conversion. Due to this scattering in data, the authors studied how the choice of gas permeability affects the temperature history and normalized residual mass.

2 Numerical model

A detailed discussion of the drying and devolatilization model for thermally thick wood particles that is applied here can also be found in earlier works.[19] There is literature available that discusses the applied governing equations for the entire wood particle combustion in

much detail, e.g.,[3,4,14,20] but for completeness we list them in Table 3. In this work, all the water (liquid + bound) is treated as bound water and drying is therefore modeled by the kinetic rate drying model. The reaction rates that appear in some of the governing equations in Table 3 are listed in Table 4.

Table 3: List of evolution equations for drying, devolatilization and char conversion. The last column gives the references the equations have been taken from.

Evolution equation		**Equation number**	**Ref.**
Wood density[1)]	$\frac{\partial \rho_{\mathrm{wood}}}{\partial t} = -(k_1 + k_2 + k_3)\rho_{\mathrm{wood}} - \frac{\rho_{\mathrm{wood}}}{V_j}\frac{\partial V_j}{\partial t}$	(2)	4
Ash density	$\frac{\partial \rho_{\mathrm{ash}}}{\partial t} = -\frac{\rho_{\mathrm{ash}}}{V_j}\frac{\partial V_j}{\partial t}$	(3)	4
Continuity equation	$\frac{\partial \epsilon_{\mathrm{g}} \rho_{\mathrm{g}}^{\mathrm{g}}}{\partial t} + \frac{1}{r}\frac{\partial}{\partial r}\left(r \rho_{\mathrm{g}}^{\mathrm{g}} u_{\mathrm{r}}\right) = \dot{\omega}_{\mathrm{g}}$	(4)	4
Species mass fraction	$\frac{\partial (\epsilon_{\mathrm{g}} \rho_{\mathrm{g}}^{\mathrm{g}} Y_{\mathrm{k}})}{\partial t} + \frac{1}{r}\frac{\partial (r \rho_{\mathrm{g}}^{\mathrm{g}} Y_{\mathrm{k}} u_{\mathrm{r}})}{\partial r} = \frac{1}{r}\frac{\partial}{\partial r}\left(r \rho_{\mathrm{g}}^{\mathrm{g}} D_{\mathrm{eff}} \frac{\partial Y_{\mathrm{k}}}{\partial r}\right) + \dot{\omega}_k$	(5)	4
Char density[2)]	$\frac{\partial \rho_{\mathrm{char}}}{\partial t} = k_3 \rho_{\mathrm{wood}} + \epsilon_{\mathrm{g}} k_5 \rho_{\mathrm{tar}}^{\mathrm{g}} - \frac{\rho_{\mathrm{char}}}{V_j}\frac{\partial V_j}{\partial t}$ $-\dot{\omega}_{\mathrm{oxid}}\frac{2MW_C}{MW_{O_2}} - \dot{\omega}_{\mathrm{steam,gasif}}\frac{MW_C}{MW_{H_2O}} - \dot{\omega}_{\mathrm{CO_2,gasif}}\frac{MW_C}{MW_{CO_2}}$	(6)	4
Temperature	$\left(\rho_{\mathrm{wood}} c_{P,\mathrm{wood}} + \rho_{\mathrm{ash}} c_{P,\mathrm{ash}} + \rho_{\mathrm{char}} c_{P,\mathrm{char}} + \rho_{\mathrm{b}} c_{P,\mathrm{b}} + \epsilon \rho_{\mathrm{g}}^{\mathrm{g}} c_{P,\mathrm{g}}\right)\frac{\partial T}{\partial t} + \left(\rho_{\mathrm{g}}^{\mathrm{g}} c_{\mathrm{P,g}} u_{\mathrm{r}}\right)\frac{\partial T}{\partial r} = \frac{1}{r}\frac{\partial}{\partial r}\left(r \lambda_{\mathrm{eff}}\left(\frac{\partial T}{\partial r}\right)\right) + \Phi_{\mathrm{Heat}}$	(7)	14
Bound water [3)]	$\frac{\partial \rho_{\mathrm{b}}}{\partial t} = \frac{1}{r}\frac{\partial}{\partial r}\left(r D_{\mathrm{b}}\frac{\partial \rho_{\mathrm{b}}}{\partial r}\right) - k_{\mathrm{evap,b}}\rho_{\mathrm{b}}$	(8)	10

[1)] The reaction rates of wood to non-condensable gases, tar and char are given by k_1, k_2 and k_3, respectively.

[2)] k_5 marks the reactions of tar to char.

[3)] $k_{\mathrm{evap,b}}$ is the kinetic evaporation rate for bound water.

The heat source term, Φ_{heat}, in Table 3 is defined as

$$\begin{aligned}\Phi_{\text{heat}} = \dot{\omega}_{k1,k2,k3}\triangle h_{\text{devol,1}} + \dot{\omega}_{k4,k5}\triangle h_{\text{devol,2}} + \dot{\omega}_{\text{evap}}\triangle h_{\text{evap}} \\ +\dot{\omega}_{\text{oxid}}\Omega_1\frac{MW_C}{MW_{O_2}}\triangle h_{\text{oxid}} + \dot{\omega}_{\text{steam,gasif}}\Omega_2\frac{MW_C}{MW_{H_2O}}\triangle h_{\text{steam,gasif}} \\ +\dot{\omega}_{\text{CO}_2\text{,gasif}}\Omega_3\frac{MW_C}{MW_{CO_2}}\triangle h_{\text{CO}_2\text{,gasif}} + \dot{\omega}_{\text{CO,oxid}}\triangle h_{\text{CO,oxid}} \\ +\dot{\omega}_{k1}\Big(\int_{T_0}^{T}(c_{\text{P,wood}} - c_{\text{P,non-cond. gases}})dT\Big) + \dot{\omega}_{k2}\Big(\int_{T_0}^{T}(c_{\text{P,wood}} - c_{\text{P,tar}})dT\Big) \\ +\dot{\omega}_{k3}\Big(\int_{T_0}^{T}(c_{\text{P,wood}} - c_{\text{P,char}})dT\Big) \\ +\dot{\omega}_{\text{evap}}\Big(\int_{T_0}^{T}(c_{\text{P,water}} - c_{\text{P,vapor}})dT\Big) \\ +(\dot{\omega}_{\text{steam,gasif}} + \dot{\omega}_{\text{oxid}} + \dot{\omega}_{\text{CO}_2\text{,gasif}})\Big(\int_{T_0}^{T}(c_{\text{P,char}} - c_{\text{P,non-cond. gases}})dT\Big) \\ +\dot{\omega}_{k4}\Big(\int_{T_0}^{T}(c_{\text{P,tar}} - c_{\text{P,non-cond. gases}})dT\Big) + \dot{\omega}_{k5}\Big(\int_{T_0}^{T}(c_{\text{P,tar}} - c_{\text{P,char}})dT\Big).\end{aligned} \tag{9}$$

Compared to earlier works by Haberle et al.[19,21] minor corrections were made in the advective terms of the continuity equation, the species equations and the energy equation. The initially used equations suggested by Lu et al.[4] were based on the phase averaged gas density entering the convective term, while based on physical consistency the intrinsic gas density would be required. Compared to earlier works (see Haberle et al.[19,21]) this has been corrected. The corresponding typo in the advection term with respect to intrinsic gas density and phase averaged gas density is also found in the review paper by Haberle et al.[1]

Furthermore, the diffusive terms in the species equations were corrected compared to earlier works, since Kim et al.[22] suggested that the phase averaged diffusive mass flux, $J_{\text{diff,k}}$, should be calculated as

$$J_{\text{diff,k}} = -D_{\text{eff}}\rho_{\text{g}}^{\text{g}}\nabla Y_k \tag{10}$$

if the effective diffusivity is calculated as

$$D_{\text{eff}} = \frac{\Big(\frac{1}{\frac{1}{D_{\text{AB}}}+\frac{1}{D_{\text{Knudsen}}}}\Big)\epsilon}{\tau}, \tag{11}$$

as it is done in this work, where $\tau = \frac{1}{\epsilon}$. Of course it needs to mentioned that depending on the definition of the effective diffusivity, either the intrinsic gas density enters the diffusive term or the phase average gas density.

The density, temperature and pressure of the gas phase are linked together by the equation of state. The gas phase flow is modeled by Darcy's law.[4]

Table 4: List of species source terms and gas phase source term. The fractions of gas species k produced from primary devolatilization reactions are marked by f_k and the fraction of species k formed from secondary reactions is marked by g_k.

Source term		**Equation number**
Species k phase average density	$\rho_k = \rho_{\mathrm{g}}^{\mathrm{g}} \epsilon_{\mathrm{g}} Y_k$	(12)
Steam gasification	$\dot{\omega}_{\mathrm{steam,gasif}} = k_{H_2O} \rho_{H_2O,g} \tilde{s}_{\mathrm{a,char}}$ [1)]	(13)
Char oxidation	$\dot{\omega}_{\mathrm{oxid}} = k_{\mathrm{O_2}} \rho_{\mathrm{O_2}} \tilde{s}_{\mathrm{a,char}}$ [1)]	(14)
CO_2 gasification	$\dot{\omega}_{\mathrm{CO_2,gasif}} = k_{CO_2} \rho_{CO_2} \tilde{s}_{\mathrm{a,char}}$ [1)]	(15)
CO oxidation	$\dot{\omega}_{\mathrm{CO}} = k_{CO} \left(\frac{\epsilon_{\mathrm{g}} \rho_{\mathrm{g}}^{\mathrm{g}} Y_{CO}}{MW_{CO}} \right) \left(\frac{\epsilon_{\mathrm{g}} \rho_{\mathrm{g}}^{\mathrm{g}} Y_{O_2}}{MW_{O_2}} \right)^{0.25} \left(\frac{\epsilon_{\mathrm{g}} \rho_{\mathrm{g}}^{\mathrm{g}} Y_{H_2O,g}}{MW_{H_2O}} \right)^{0.5}$	(16)
Gas phase source term	$\dot{\omega}_{\mathrm{g}} = \dot{\omega}_{\mathrm{oxid}} \frac{2MW_C}{MW_{O_2}} + \dot{\omega}_{\mathrm{steam,gasif}} \frac{MW_C}{MW_{H_2O}} + \dot{\omega}_{\mathrm{CO_2,gasif}} \frac{MW_C}{MW_{CO_2}} + (k_1 + k_2)\rho_{\mathrm{wood}} - k_5 \rho_{\mathrm{tar}} + k_{\mathrm{evap}} \rho_{\mathrm{b}}$	(17)
CO_2 source term	$\dot{\omega}_{\mathrm{CO_2}} = f_{\mathrm{CO_2}} k_1 \rho_{\mathrm{wood}} + g_{\mathrm{CO_2}} k_4 \rho_{\mathrm{tar}} - \dot{\omega}_{\mathrm{CO_2,gasif}} + \dot{\omega}_{\mathrm{CO}} \frac{MW_{\mathrm{CO_2}}}{MW_{\mathrm{CO}}}$	
H_2O (g) source term	$\dot{\omega}_{\mathrm{H_2O,g}} = k_{\mathrm{evap,b}} \rho_{\mathrm{b}} - \dot{\omega}_{\mathrm{steam,gasif}} + f_{\mathrm{H_2O}} k_1 \rho_{\mathrm{wood}} + g_{\mathrm{H_2O}} k_4 \rho_{\mathrm{tar}}$	(18)
CO source term	$\dot{\omega}_{\mathrm{CO,total}} = 2\dot{\omega}_{\mathrm{oxid}} \frac{MW_{\mathrm{CO}}}{MW_{\mathrm{O_2}}} + f_{\mathrm{CO}} k_1 \rho_{\mathrm{wood}} + g_{\mathrm{CO}} k_4 \rho_{\mathrm{tar}} + \dot{\omega}_{\mathrm{steam,gasif}} \frac{MW_{\mathrm{CO}}}{MW_{\mathrm{H_2O}}} + 2\dot{\omega}_{\mathrm{CO_2,gasif}} \frac{MW_{\mathrm{CO}}}{MW_{\mathrm{CO_2}}} - \dot{\omega}_{\mathrm{CO}}$	(19)
H_2 source term	$\dot{\omega}_{\mathrm{H_2}} = f_{\mathrm{H_2}} k_1 \rho_{\mathrm{wood}} + g_{\mathrm{H_2}} k_4 \rho_{\mathrm{tar}} + \dot{\omega}_{\mathrm{steam,gasif}} \frac{MW_{\mathrm{H_2}}}{MW_{\mathrm{H_2O}}}$	(20)
Tar source term	$\dot{\omega}_{\mathrm{tar}} = k_2 \rho_{\mathrm{wood}} - k_4 \rho_{\mathrm{tar}} - k_5 \rho_{\mathrm{tar}}$	
O_2 source term	$\dot{\omega}_{\mathrm{O_2}} = -\dot{\omega}_{\mathrm{oxid}} - \dot{\omega}_{\mathrm{CO}} \frac{1MW_{\mathrm{O_2}}}{2MW_{\mathrm{CO}}}$	(21)
Devolatilization reactions	$k_i = A_i \exp\left(\frac{-Ea_i}{RT}\right),\ i = 1,2,3,4,5$	(22)
Homogeneous reactions	$k_{CO} = A_{CO} \exp\left(\frac{-Ea_{CO}}{RT}\right)$	(23)
Heterogeneous reactions	$k_k = A_k T \exp\left(\frac{-Ea_k}{RT}\right),\ k = CO_2, O_2, steam$	(24)

[1)] marks that the specific surface area used in this reaction term is corrected as follows: $\tilde{s}_{\mathrm{a,char}} = s_{\mathrm{a,char}} \frac{\rho_{\mathrm{char}}}{\rho_{\mathrm{char}} + \rho_{\mathrm{ash}} + \rho_{\mathrm{wood}}}$.

2.1 Boundary conditions

The overall model-set-up is the same for the two different ash handling concepts studied here, with the main difference being that in *Model A* the boundaries are fixed to the same grid point during the entire conversion, while the boundaries are moving inward with the char conversion front in *Model B*. The concept of inward moving boundaries is based on the idea, that as soon as char at a grid point has been consumed, the evolution equations at this grid point are assumed to not change in time anymore. The boundary conditions are then moved to the grid point further inward. Therefore, *Model B* requires the tracking of the char conversion front. Hereby the number of grid points is constantly reduced. When using *Model A* instead, evolution equations are continuously solved for the entire number of grid points that has been assigned to the model at the beginning of the simulations. Therefore boundary conditions are fixed. In *Model A* shrinkage is then modeled such that the cell volume related to a grid point, shrinks due to drying and devolatilization. The new total volume of the wood particle is then calculated by summing up the different cell volumes, and the new grid spacing is calculated, based on the assumption of a structured equidistant grid, as well as a new wood particle radius.

The applied temperature boundary condition (for *Model A* and *Model B*) is[3]

$$\lambda_{\mathrm{eff}} \frac{\partial T}{\partial r} = \sigma \omega_{\mathrm{eff}} \left(T_{\mathrm{wall}}^4 - T_{\mathrm{surface}}^4 \right) + h_{\mathrm{c}} \left(T_{\mathrm{g}} - T_{\mathrm{surface}} \right) \tag{25}$$

with λ_{eff} being the effective thermal conductivity of the solid phase, T_{wall} the furnace wall temperature, ω_{eff} the effective particle emissivity, T_{surface} the particle surface temperature, T_{g} the surrounding gas phase temperature and h_{c} the heat transfer coefficient (reduced by the blowing factor). The current model does not consider the radiative feedback of the flame surrounding the particle.

The boundary condition for the mass fractions of gas species k is defined as[3]

$$D_{\text{eff}} \frac{\partial Y_k}{\partial r} = h_{\text{m}} \Big(Y_{\text{k},\infty} - Y_{\text{k,surface}} \Big) \tag{26}$$

with D_{eff} being the effective diffusivity, h_{m} the mass transfer coefficient corrected by the blowing factor and $Y_{\text{k},\infty}$ and $Y_{\text{k,surface}}$ the mass fractions of gas species k in the bulk and at the surface, respectively.

The reduction of heat and mass transfer coefficients by the blowing of the exiting gases (the Stefan flow) is considered by the following correlations[23]

$$h_{\text{c}} = \frac{\dot{M}_{\text{total}} \bar{c}_{\text{P,g}}}{h_{\text{c},0} \Big(\exp \Big(\frac{\dot{M}_{\text{total}} \bar{c}_{\text{P,g}}}{h_{\text{c},0}} \Big) - 1 \Big)}. \tag{27}$$

for the heat transfer with $h_{\text{c},0}$ being the uncorrected heat transfer coefficient and $\bar{c}_{\text{P,g}}$ being the mass averaged specific heat capacity of the gas mixture and

$$h_{\text{m}} = \frac{\dot{M}_{\text{total}}}{h_{\text{m},0} \Big(\exp \Big(\frac{\dot{M}_{\text{total}}}{h_{\text{m},0}} \Big) - 1 \Big)} \tag{28}$$

for the mass transfer coefficient, with $h_{\text{m},0}$ being the uncorrected mass transfer coefficient, and $\dot{M}_{\text{total}}$ the total gas phase mass flux leaving the particle. Nusselt and Sherwood numbers were calculated with the Ranz-Marshall correlation[2]

$$Nu = 2 + 0.6 Re^{0.5} Pr^{1/3} \tag{29}$$

and

$$Sh = 2 + 0.6 Re^{0.5} Sc^{1/3}. \tag{30}$$

The Ranz-Marshall correlation was used, since the wood particle modeled was near-

spherical.

In *Model B*, the exterior of the char core is tracked and the governing equations are solved for the interior grid points, while the exterior grid points are assumed to not change in time. The definition of exterior and interior grid points in the explanation above is done such that the exterior grid points are the ones of the original mesh whose position is now outside of the boundary between the solid particle and the surrounding gas. Exterior grid points are therefore grid points of the the original mesh that are now located in the surrounding gas phase, since the solid species previously available have been fully consumed and now only the residual solid species ash could remain to be considered. The internal grid points, meanwhile cover the points of the initial mesh, that still span over solid species, i.e. the residual wood and char particle that has not yet been consumed.

The pressure at the particle surface is set to ambient pressure. The surrounding gas phase is assumed to be air. This is a simplification as it neglects that different gas species can be the products of gas phase reactions in the combustion chamber of, for example, a wood stove. The surrounding gas phase temperature was set to 1050 K while the furnace wall temperature was set to 1276 K.

Furthermore, the model development is based on the following assumptions:

1. All present phases are in local thermal equilibrium.
2. An ideal gas is assumed.
3. The superficial gas velocity can be calculated by Darcy's velocity.
4. Shrinkage is calculated from empirical shrinkage factors.
5. The particle is surrounded by air.
6. The effect of a surrounding flame is neglected.
7. Wood properties change linearly from wood to char, as a function of the degree of conversion.

2.2 Numerical set-up

Poplar was modeled, and the chosen properties entering the model are presented in Table 5.

Table 5: Properties used as input values for the drying, devolatilization and char conversion model.

Property	Unit	Value	Ref.
Thermal conductivity (wood cell wall), $\lambda_{\mathrm{wood},\perp}$	[W/(mK)]	0.52	7
Thermal conductivity (water), $\lambda_{\mathrm{l},\perp}$	[W/(mK)]	$0.278 + 1.11 \times 10^{-3}$ T	7
Thermal conductivity (ash), $\lambda_{\mathrm{ash},\perp}$	[W/(mK)]	1.2	4
Thermal conductivity (char), $\lambda_{\mathrm{char},\perp}$	[W/(mK)]	0.071	10
Thermal conductivity (gases), λ_{g}	[W/(mK)]	25.77×10^{-3}	24
Specific heat capacity (wood) (298 - 413 K), $c_{\mathrm{P,\ wood}}$	[J/(kgK)]	-91.2 + 4.4T	10
Specific heat capacity (wood) (350 - 500 K), $c_{\mathrm{P,\ wood}}$	[J/(kgK)]	1500 + T	10
Specific heat capacity (ash), $c_{\mathrm{P,\ ash}}$	[J/(kgK)]	754 + 0.586 (T - 273)	25
Specific heat capacity (gases), $c_{\mathrm{P,\ g}}$	[J/(kgK)]	$770 + 0.629$ T - 1.91×10^{-4} T^2	10
Specific heat capacity (char), $c_{\mathrm{P,\ char}}$	[J/(kgK)]	$420 + 2.09$ T - 6.85×10^{-4} T^2	10
Specific heat capacity (tar), $c_{\mathrm{P,\ tar}}$	[J/(kgK)]	$-100 + 4.4$ T - 1.57×10^{-3} T^2	10
Specific heat capacity (vapor), $c_{\mathrm{P,\ H_2O,g}}$	[J/(kgK)]	1670 + 0.64 T	10
Apparent/true wood density	[kg/m^3]	570 & 1500 ($\rightarrow \epsilon_{\mathrm{pore},0} = 0.62$)	1) & 26
Radiative thermal conductivityλ_{rad}	[W/(mK)]	$\frac{4\omega_{\mathrm{eff}}\epsilon_{\mathrm{pore}}d_{\mathrm{pore}}T^3}{1-\epsilon_{\mathrm{pore}}}$	10
Binary diffusivity, $\mathrm{D_{AB}}$	[m^2/s]	$3 \times 10^{-5} \left(\frac{T}{T_{\mathrm{ref}}}\right)^{1.75}$	4 & 25
Effective diffusivity, $\mathrm{D_{eff}}$	[m^2/s]	$D_{\mathrm{eff}} = \left(1/\left(\frac{1}{D_{\mathrm{AB}}} + \frac{1}{D_{\mathrm{Knudsen}}}\right)\right)\epsilon_{\mathrm{pore}}^2$	4
Particle diameter, $\mathrm{d_P}$	[m]	9.5×10^{-3}	4
Aspect ratio, AR	[-]	1	4
Moisture content, $\mathrm{M_{liquid}}$	[% wet basis]	40	4
Permeability, $\kappa_{\mathrm{wood}\ \perp}$&$\kappa_{\mathrm{char}\ \perp}$	m^2	10^{-16}& 10^{-13}	27
Char emissivity, ω_{char}	[-]	0.95	4
Wood emissivity, ω_{wood}	[-]	0.85	4
Ash emissivity, ω_{ash}	[-]	0.85	2)
Ash porosity, $\epsilon_{\mathrm{pore,ash}}$	[-]	0.8	14
Char porosity, $\epsilon_{\mathrm{pore,char}}$	[-]	0.8	14
Shrinkage factor (drying), θ_{m}	[-]	0.9	20
Shrinkage factor (devolatilization), θ_{devol}	[-]	0.9	20

1) marks that this value was calculated based on knowing the apparent density and the true density.
2) marks that the same emissivity was assumed for char and ash.

The pore diameter, which is required for the calculation of the radiative contribution to the effective thermal conductivity, was based on pore diameters of 4×10^{-5} m for wood and 2×10^{-4} m for char.[10]

One advancement to older works was that instead of using a constant diffusivity for all species, a temperature dependent one is chosen, since it was assumed that the temperature significantly influences the diffusion coefficient. Furthermore, a general D_{AB} was chosen. With respect to all the gaseous species formed from devolatilization only H_2 has a significantly higher diffusivity compared to the residual species. Hydrogen formation from primary and secondary devolatilization is comparably small, compared to carbon monoxide and carbon dioxide as well as tar. Therefore, we assumed that a general D_{AB} was a valid simplifying assumption.

The wood conductivities listed in Table 5 are for wood fiber and are therefore higher than what is commonly observed for effective wood thermal conductivities.

The applied pre-exponential factors, activation energies and heat of reactions used for drying, devolatilization and char conversion are listed in Table 6.

Table 6: Kinetic data used for modeling drying, devolatilization and char gasification and oxidation. *"Gases"* in the following table refer to non-condensable gases.

Reaction	Reaction rate constant	Unit	Ref.	Heat of reaction	Ref.
Wood → Gases	$k_1 = 1.11 \times 10^{11} \exp\left(\frac{-177000}{RT}\right)$	[1/s]	28	-418 [kJ/kg]	29
Wood → Tar	$k_2 = 9.28 \times 10^{9} \exp\left(\frac{-149000}{RT}\right)$	[1/s]	28	-418 [kJ/kg]	29
Wood → Char	$k_3 = 3.05 \times 10^{7} \exp\left(\frac{-125000}{RT}\right)$	[1/s]	28	-418 [kJ/kg]	29
Tar → Gases	$k_4 = 4.28 \times 10^{6} \exp\left(\frac{-107500}{RT}\right)$	[1/s]	30	42 [kJ/kg]	31
Tar → Char	$k_5 = 1 \times 10^{5} \exp\left(\frac{-107500}{RT}\right)$	[1/s]	32	42 [kJ/kg]	31
$\rho_b \rightarrow \epsilon_g \rho_g^g Y_{vap}$	$k_{evap} = 5.13 \times 10^{10} \exp\left(\frac{-880000}{RT}\right)$	[1/s]	33	-2440 [kJ/kg]	4
C + x O_2 → a CO + b CO_2	$k_{oxid} = 1.715T \exp\left(\frac{-74800}{RT}\right)$	[m/s]	7	110 kJ/mol (fraction a) 393.5 kJ/mol (fraction b)	1)
C + H_2O → CO + H_2	$k_{H_2O,gasif} = 3.42T \exp\left(\frac{-130000}{RT}\right)$	[m/s]	4	-10940 [kJ/kg]	1)
C + CO_2 → 2 CO	$k_{CO_2,gasif} = 3.42T \exp\left(\frac{-130000}{RT}\right)$	[m/s]	4	-14370 [kJ/kg]	1)
CO + 0.5O_2 → CO_2	$k_{CO,oxid} = 10^{12.35} \exp\left(\frac{-167000}{RT}\right)$	[1/s]	20	10110 [kJ/kg]	4

1) marks that the heat of reactions have been calculated by assuming char reacting as pure C.

Char oxidation is modeled by the following coefficients,[34] were a refers to the moles of carbon monoxide and b refers to the moles of carbon dioxide

$$a + b = 1 \tag{31}$$

and where x refers to the moles of oxygen,

$$x = \frac{a}{2} + b. \tag{32}$$

The ratio between CO/CO_2 was modeled to be temperature-dependent according to[34]

$$\frac{a}{b} = A \exp\Big(- E_\eta / T \Big). \tag{33}$$

The coefficients A and E_η were taken to be 12 and 3300 K, respectively.[35]

Hydrogen oxidation reaction is not considered due to limited hydrogen production during thermochemical conversion.

2.3 Numerical solver and discretization schemes

The IDA solver, included in the SUNDIALS software package, is used to solve the set of differential and algebraic equations.[36] The convective term is discretized by first order upwinding, while the diffusive terms are discretized by second order central difference. The accuracy in space is therefore 1st order, while the accuracy in time depends on the order of the backward differentiation formula, which can range from 1 to 5. The maximum time step was 10^{-4} s. The simulations were run with 55 grid points spanning over the particle radius, as this number of grid points has been found to yield grid-independent solutions.

3 Results and Discussion

In this section the results of the parametric study, as well as the results of the comparison between the modeling results obtained from the two different ash modeling concepts, are presented. The two different ash modeling concepts, based on fixed boundaries and inward-moving boundary conditions, are referred to as *Model A* and *Model B*, respectively, in this work.

3.1 Comparison of Model A and Model B

All simulations presented in this section were performed with a specific surface area of $10^6 \frac{m^2}{m^3}$. The temperature and the normalized residual solid mass predictions of the two modeling approaches are compared. Only these data are compared in this study since they are thought to be the most representative ones. Therefore based on these data the applicability and

suitability of a modeling approach can be well enough discussed.

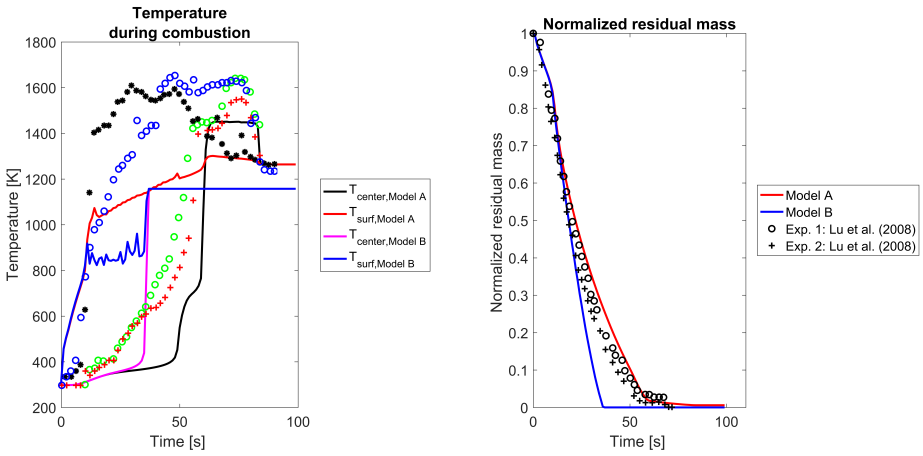

(a) Center and surface temperature predicted by *Model A* and *Model B*.

(b) Normalized residual mass predicted by *Model A* and *Model B*.

Figure 1: Temperature and normalized residual mass predicted by *Model A* and *Model B* with the surrounding gas phase velocity being $u_g = 0.5$ m/s. The surface temperature is presented by T_{surf}; the center temperature by T_{center}. The symbols are experimental data obtained by Lu et al.:[4] The measured T_{surf} are plotted by: $\circ$, $*$. The measured T_{center} are plotted as $\circ$, $+$. The measured data for the normalized residual mass has been plotted by $\circ$, $+$.

From an experimental point of view, Figure 1 clearly shows that there is a significant difference between the different experimental test runs, especially when it comes to the measured surface temperatures. However, this derivation from measured surface temperatures is assumed to arise from the difficulty to exactly measure the surface temperature of a particle that is subject to significant size reduction due to char consumption. It can therefore be assumed that a surface thermocouple might be detached at some point during the measurements which led to the differences in measured data, causing the deviation visible with respect to the two experimental series. Further details on the experiments can be found in the original paper by Lu et al.[4] who conducted the experiments.

Figure 1 shows that the two modeling concepts yield different total thermal conversion times as well as center and surface temperatures. We also found that for *Model A* and

Model B a lower surrounding gas phase velocity (test case was $u_{\mathrm{gas}} = 0.25$ m/s) resulted in negligible influence on the total conversion time.

When the ash layer is removed immediately after char consumption has been accomplished (*Model B*), the thermal conversion is faster than in *Model A*. This is because *Model B* does not consider any limitation to mass transfer of oxygen to the active sites through the ash surrounding the char core. Oxygen transferred from the bulk to the char surface can directly react at the char surface. The additional consideration of diffusion through the porous ash layer, as it is done by *Model A*, reduces the amount of available oxygen at the surface of the residual char core and hereby also the burnout rate, while increasing the burnout time. The differences in initial normalized residual mass predictions obtained by *Model A* and *Model B* are initially minor, but become more prominent after 14 s. The reason for this is that the char at the outermost grid point has then been consumed, and due to the different handling of the boundaries, the models start to predict very different conversion trends from this time on.

Also, the temperature predictions are very different. *Model B* predicts a temperature plateau for $\mathrm{T_{surf}}$ at about 850 K to 950 K. At this temperature char conversion reactions occur. Since *Model B* assumes that the boundary moves one grid point inward, after the char at a certain grid point has dropped below a threshold value, also the plotted surface temperature moves one grid point inward. This explains why the plotted surface temperature fluctuates within a range of enhanced char conversion temperatures around 850 K.

Most interesting is also to see that the final surface and center temperatures predicted by *Model B* remain at a lower level than the temperatures predicted by *Model A*. The reason is, that *Model B* is based on the assumption of inward moving boundary conditions. As soon as the char mass at a grid point has been consumed, the boundary is shifted further inward, and hereby moves closer to the wood particle center. The grid point that had previously been consumed is then, however, neglected in further evolution considerations, as it is assumed to not change in time anymore. This implies that the grid point is not allowed to further heat

up after a complete char conversion. Therefore, the temperature at a grid point will remain at temperatures lower than the furnace wall temperature, if the grid point has not reached the furnace wall temperature before or during complete char conversion.

Assumingly the temperature starts to increase above the previous temperature plateau between 850 to 950K when the char at the last two inner most grid points is consumed. The two grid points degrade simultaneously and the heat release is higher on a particle level. Therefore, the temperature increases again before reaching the temperature plateau at 37 s.

However, it shall be outlined that the flat temperature line in Figure 1 with respect to *Model B* does not have an actual physical meaning, since according to the modeling assumption, there is no solid species left, whose temperature could be measured by thermocouples attached to the particle surface. In fact, the physical meaning of the blue and pink lines in Figure 1a stops at 37 s, which is at the instant when the temperature plateau becomes prominent.

The char consumption of the final char core occurs faster in *Model B* than in *Model A*, since oxygen transfer to the char core is more enhanced due to the missing ash layer. The effective residual particle size is even more reduced compared to what is predicted by *Model A*. A reduced residual particle diameter results in an enhanced mass transfer rate to the residual char core. Consequently, *Model A* and *Model B* are also predicting different mass and heat transfer coefficients since different effective particle diameters are used for their calculations.

One can see the different char conversion behaviors, when plotting the change in char particle radius over time (Figure 2). The initial, rather slow, decrease in particle size is due to volumetric shrinkage during drying and devolatilization, which is then superimposed by the more prominent size reduction of the outer particle areas where char conversion occurs.

Overall it was found that temperature and normalized residual mass predictions obtained with *Model A* are in better agreement with experimental data. Even though we found that the two modeling concepts yield different results, the conclusion is drawn that, based on these results, we cannot generically state which model is more appropriate. In fact it is

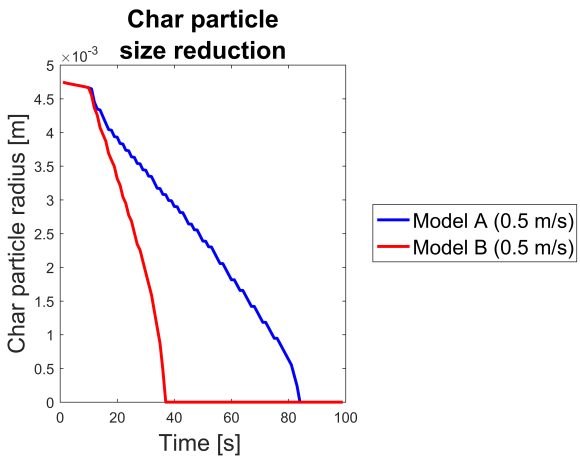

Figure 2: Comparison of char particle size (neglecting ash layer) reduction obtained by *Model A* and *Model B*.

not yet known if the better agreement with experiments observed for *Model A* is due to the applied fuel (and its ash content as well as the chemistry of the ash) or due to the idealized experimental conditions in the single particle reactor. This conclusion is based on the understanding that the validation experiments are performed under idealized conditions in a single particle reactor, i.e.; no influence of other particles. Under such conditions the up-build of an ash layer is not affected by external phenomena. In a wood stove, however, wood logs are stacked. Therefore, fragmentation of upper wood logs might affect the physical appearance of lower wood logs by off-falling parts and the subsequent knock-off of the brittle and fragile ash of the lower wood logs. This implies that under conditions found in wood stoves, it is more likely that the ash layer will not built up undisturbedly, but will rather fall off.

This phenomenon is of course a local structural change of the particle. Therefore, *Model B* and *Model A* are two extreme cases that simplify a structural change by assuming that the entire surface of the particle can be handled equally, e.g. homogeneous boundary conditions. However, to consider a localized knock-off of char, or a localized change in the ash appearance due to fusion which could affect heat and mass transfer, multi-dimensional models are needed.

Therefore, in order to validate which modeling concept is more appropriate for solid phase conversion modeling in wood stove applications, the concept cannot only be linked to the ash content and composition of the fuel, but also has to be chosen in dependence of the operating (experimental) conditions. Further studies and model developments are therefore recommended to eventually be able to obtain an accurate replication of this structural change in numerical models.

3.2 Parametric study

To assess the sensitivity of the model to specific surface areas, thermal conductivities of char and wood as well as gas permeabilities, a parametric study over these parameters was performed. For all these input parameters, there is a wide range of values available in literature. This scattering of available data can affect modeling results and it is therefore needed to study to which extent the results are influenced. The parametric study was done with *Model A* (fixed boundaries) and a surrounding gas phase velocity of 0.5 m/s.

3.2.1 Specific surface area

When studying the sensitivity of the model to the specific surface area of char, a range of values were tested. The maximum value tested was $s_{\mathrm{a,char,max}} = 10^7\ \frac{m^2}{m^3}$ ($=$*Test 6*) and the second largest value was $s_{\mathrm{a,char}} = 10^6\ \frac{m^2}{m^3}$ ($=$*Test 5*), which was the standard value we used in all the other simulations presented in this paper. The minimum value that was tested was $s_{\mathrm{a,char,min}} = 10^2\ \frac{m^2}{m^3}$ ($=$*Test 1*). Furthermore the intermediate values of $s_{\mathrm{a,char}} = 10^3\ \frac{m^2}{m^3}$ (*Test 2*), $s_{\mathrm{a,char}} = 10^4\ \frac{m^2}{m^3}$ (*Test 3*) and $s_{\mathrm{a,char}} = 10^5\ \frac{m^2}{m^3}$ (*Test 4*) were tested. The values were chosen such that they covered a broad range of values, replicating the significant scattering of data found in literature (see Table 2).

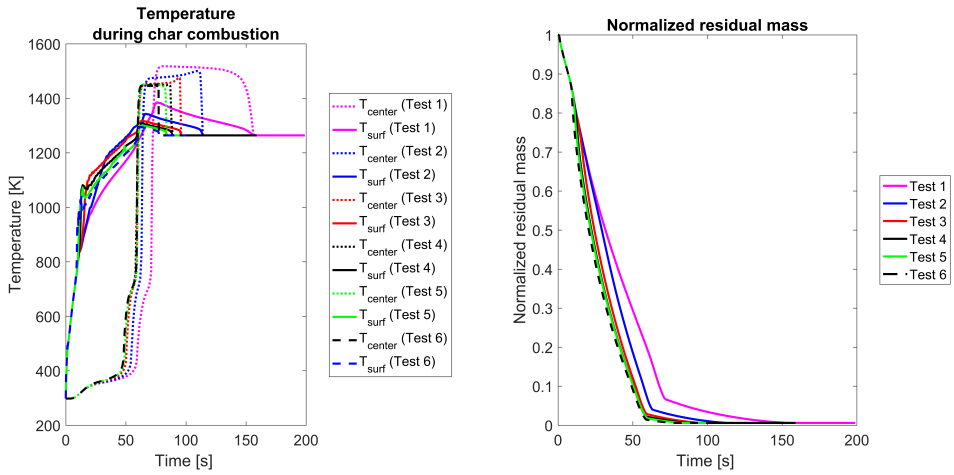

(a) Comparison of modeling results for center and surface temperature.

(b) Comparison of normalized residual mass.

Figure 3: Temperature and normalized residual mass predictions obtained from *Tests 1-6* ($s_{\mathrm{a,char}} = 10^2 \frac{m^2}{m^3} - 10^7 \frac{m^2}{m^3}$). The surface temperature is referred to as T_{surf} and the center temperature is referred to as T_{center}.

It was found (see Figure 3) that the reactivity of the char, has an influence on modeling results, especially on the final char conversion stage. A very low reactivity (implemented in model considerations by a low specific surface area, i.e. *Test 1*) yielded a significantly slower char conversion. The overall conversion times were 156 s for *Test 1*, 113 s for *Test 2*, 96 s for *Test 3*, 88 s for *Test 4*, 84 s for *Test 5* and 77.5 s for *Test 6*. The differences between *Test 5* and *Test 6* are small. One can, however, identify, that *Test 1* led to significantly slower char conversion. In fact, when it comes to the pure char conversion time the results are as theoretically expected; predicting that a significantly low specific surface area results in longer char conversion, due to reduced char oxidation and gasification rates. Still it is interesting to see that even though *Test 1* (and also *Test 2* to a certain extent) differs significantly from the other test runs, the four residual test runs predict a more similar behavior. In fact, the predicted results of the higher specific surface area test runs converge, which implies that the specific surface area does not have a significant influence on the model

results anymore if mass transfer starts to control oxidation. This means that, if the specific surface area is above a certain critical threshold, the char conversion rate is independent of the choice of specific surface area. The reason is that as long as the reactivity is set to be significantly large (large enough surface area), the oxygen diffusion to the active sites is the limiting factor and not the chemistry of char conversion.

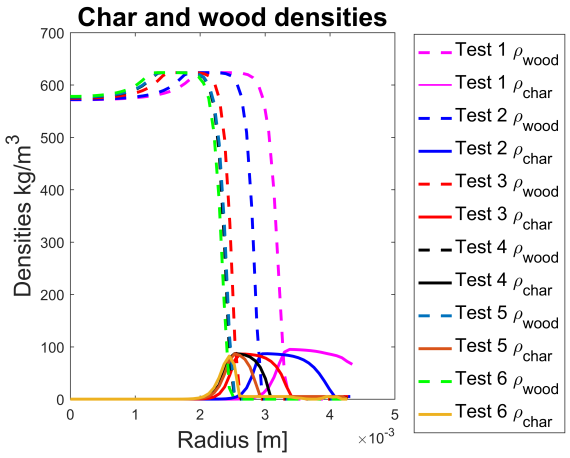

Figure 4: Comparison of predicted wood and char densities predicted with *Tests 1-6* at 25 s.

In Figure 4 one can identify the char conversion layer (thickness and position) as well as the devolatilization zone, plotted at 25 s. The apparent dry wood density increases even above the initial value, which is due to ongoing volumetric shrinkage, which is considered to occur during drying and devolatilization in this model. At this early stage of conversion, one can still identify the ordering of the char conversion front according to the specific surface area. This means that for the highest specific surface area, the char conversion front has moved furthest inside. The reason for this ordering is due to the start of char conversion at the outer most grid point. The rate of this grid point's conversion is not limited by the availability of oxygen, but is controlled by specific surface area. This implies that a higher specific surface area allows this grid point to react faster. Overall, char conversion therefore starts at a slightly earlier time.

As the char conversion front moves inward, the char conversion is diffusion controlled, such that the advancement of the test case with the highest specific surface area is constantly reduced, since for all high specific surface area test cases (*Test 4* to *Test 6*) oxygen diffusion is controlling. Since 25 s, however, is still an early time in the total conversion, we still see the advancement of the highest specific surface area test case rather prominently.

Since the heat release due to char conversion then also occurs to a close to same extent, independent of the choice of specific surface area, and the thermal properties of the char-ash-layer surrounding the dry wood are similar (which is due to the similar degree of conversion), also the heat-transfer controlled phenomena occurring further inside the particle, such as devolatilization, tend to converge for the high surface area test cases (*Test 4-6*) (see Figure 4).

From the right hand panel of Figure 3 one can see, that the kink in normalized residual mass predictions, indicating where devolatilization has been accomplished in the entire particle, and where only char conversion is occurring on a particle scale, varies, depending on the specific surface area. It is highest for the lowest specific surface area, which implies that more char is still available, contributing more to the normalized residual mass, while for higher specific surface areas, the kink occurs at lower residual mass. This suggest that more char has already been consumed in the outer particle area, while devolatilization is still going on in the inner particle areas. These observations outline that in thermally thick particles, all three conversion stages are strictly coupled and cannot be looked at separately in modeling works.

The differences between *Test 6* and *Test 5* are small. In fact, when looking at the final enhanced char conversion time, which is defined as the time, when only a char particle is left, the variation in the contribution of this final conversion stage to the total conversion stage, varies from 29% to about 24%, respectively for *Test 5* and *Test 6*. This final conversion time, can be identified in Figure 3b as the time following after the kink in the normalized residual mass prediction. Compared to *Test 1*, where this final char conversion time is 54 % of the total conversion time, the difference between *Test 5* and *Test 6* can be considered

negligible.

From this study on the influence of specific surface areas it is concluded that as soon as a critical value of specific surface area is exceeded, while at the same time modeling oxygen diffusion to the char core through the ash layer, the char conversion is not affected by the char specific surface area. Accordingly, one might assume, that unless a comparably low char surface area is chosen the influence of char reactivity on modeling results is minor.

However, it needs to be outlined that this critical specific surface area is no generic value, but in fact is case-dependent, as it will be influenced by experimental conditions, i.e. external temperature and heating rate, particle size and fuel properties.

3.2.2 Thermal conductivity

Since both drying and devolatilization are heat-transfer controlled phenomena, it was aimed to investigate how the thermal conductivities affect the modeling results. Only the influence of the thermal conductivities of wood and char were studied, since both will have a significant influence on the heat conduction. The results will be less sensitive to the thermal conductivity of the gas since the fraction of the heat that is conducted by the gas is significantly smaller than it is for the solid species.

Furthermore, the model's sensitivity to the thermal conductivity of ash was not studied. The variation in applied thermal conductivities of ash found in other works was considered minor. In fact, the thermal conductivities of ash applied in simulations, commonly only ranged from 1.03 W/(mK)[25] to 1.2 W/(mK),[4] which led to the conclusion that this model input parameter was not subject to significant scattering in current literature.

Table 7: Tested thermal conductivities for wood and char. Each combination of thermal conductivity of char and wood is labeled as listed in the first column, e.g. *Test A*, which is subsequently used for discussion in the text section.

Test case	$\lambda_{\text{wood},\perp}$ W/(mK)	**Ref.**	$\lambda_{\text{char},\perp}$ W/(mK)	**Ref.**
Test A	0.52	7	$0.071^{1)}$	10
Test B	0.43	37	$0.071^{1)}$	10
Test C	$0.291 + 0.000276T$	38	$0.071^{1)}$	10
Test D	$0.13 + 0.0003$ (T-273)$^{1)}$	39	$0.071^{1)}$	10
Test E	0.52	7	$0.091 + 8.2 \times 10^{-5}$ T$^{1)}$	40
Test F	0.52	7	$1.47 + 1.11 \times 10^{-3}T$	3

$^{1)}$ marks that these thermal conductivities already include the influence of porosity.

All simulations presented in this section were performed with a specific surface area of $10^6\ \frac{m^2}{m^3}$ and a surrounding gas phase velocity of 0.5 m/s. The different conductivities that were tested are listed in Table 7.

The validity of the temperature-dependence of thermal conductivity of wood calculated as suggested in *Test C* is limited to a maximum temperature of 500 °C.[41] For wood devolatilization modeling the thermal conductivity as defined in *Test C* can be used, since most of the wood will have been consumed at temperatures higher than 500 °C.

In the original papers, where the thermal conductivities were taken from, the thermal conductivity of char used in *Test F* is the thermal conductivity of the char without pores, requiring the multiplication by char porosity according to

$$\lambda_{\text{char,eff}} = (1 - \epsilon_{\text{char}})\lambda_{\text{char,fiber}}, \tag{34}$$

in order to model the effective thermal conductivity of char.

It was found that the thermal conductivity of *Test F* led to significantly higher thermal conductivities than the temperature-dependencies of *Test E*.

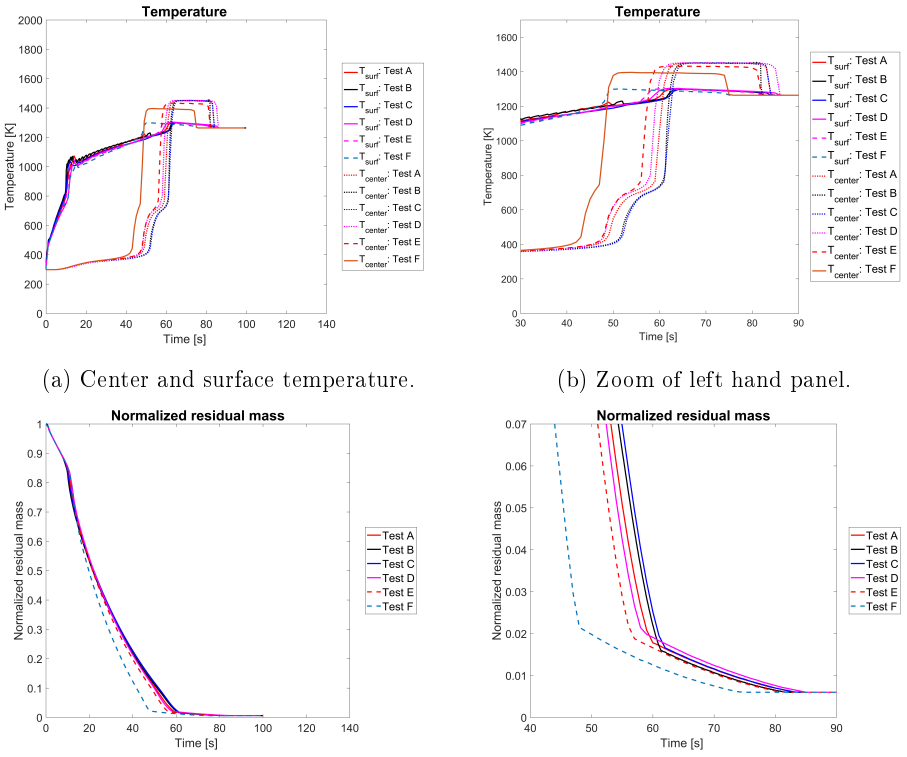

(a) Center and surface temperature.

(b) Zoom of left hand panel.

(c) Normalized residual mass.

(d) Zoom of left hand panel.

Figure 5: Temperature and normalized residual mass predictions obtained from *Tests A-G*. All tests are done with $s_{\mathrm{a,char}} = 10^6 \frac{m^2}{m^3}$ and $u_{\mathrm{gas}} = 0.5\ m/s$. The surface temperature is referred as T_{surf} and the center temperature is referred as T_{center}.

The thermal conductivities of wood and char affect the internal temperature history (as shown in Figure 5). Drying and devolatilization stages are accomplished earliest for *Test F* and are terminated the latest by *Test B* and *Test C*. The difference of *Test B* to *Test C* is minor, since even though the effective wood thermal conductivity of *Test C* is lower at room temperature, it increases as temperature increases while *Test B* considers a constant value. Since the two modeling test runs are so similar, it is somewhat expected that the

difference in thermal conductivities at room temperature is balanced during the conversion as the temperature-dependence becomes more important. Interesting is also, that at room temperature actually *Test D* has the lowest thermal wood conductivity of all test runs, but due to a constant change in porosity, affecting *Test A - C*, leading to a drop in the effective thermal wood conductivity, the thermal wood conductivity of *Test D* becomes larger than the thermal conductivity of wood used in the other three test runs. In fact *Test F* leads to a comparably fast internal heating of the particle, since it has the least insulating char layer of all test cases. Therefore, the heat transferred to the external particle surface can easily be conducted further inside, even though a char layer builds up.

It can be observed that the drying stage is influenced by the choice of thermal conductivity of wood. This can be seen by *Test B* and *Test C*, which have a lower thermal conductivity of wood (at room temperature) compared to *Test A* and therefore predict a slower drying. When both drying and devolatilization are studied, the influence of thermal conductivity of char becomes relevant. The more insulating the char layer is, the more the progress of the devolatilization zone slows down.

When looking at Figure 5, one can observe that for *Test B* and *Test C* the drying and the devolatilization stage are accomplished the latest, compared to other test cases. Drying is considered to have been accomplished in the entire particle when the center temperature starts to exceed 400 K. Devolatilization is assumed to have been accomplished in the entire particle, when the final kink in the normalized residual mass prediction can be seen.

By the choice of thermal conductivity the internal heat transfer is changed, which can result in accelerated or retarded drying and devolatilization of the inner areas of a thermally thick wood particle. The thermal conductivity of wood does not only significantly affect drying but also the *pre-devolatilization-temperature* heating of the particle. This has an effect on the char conversion stage, whose start is accelerated or retarded accordingly.

If internal heat transfer is retarded, the heating of the particle to temperatures where char consumption reactions occur is slower, which then again is reflected by a longer total

conversion time of the particle.

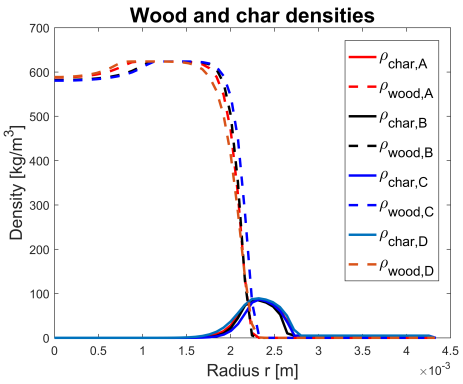

Figure 6: Comparison of devolatilization zoness predicted with *Tests A-D* at 45 s.

In Figure 6 the char and wood densities at 45 s are plotted to outline how the thermal conductivity of wood affects the devolatilization zone. It is seen that the position of the devolatilization zone is affected by the assigned thermal conductivity of wood, even though the predicted shift in the devolatilization zone is minor with respect to the tested range of thermal wood conductivities. The devolatilization zone has moved furthest inside for *Test D*, which has the highest thermal conductivity of wood at high temperatures. A higher thermal conductivity of wood leads to a faster heating of the inner particle areas in pre-devolatilization temperature ranges and therefore fast termination of drying.

After studying the effect of thermal conductivity of wood, the influence of the thermal conductivity of char on the temperature history and residual mass was studied. Modeling of temperature evolution and mass loss trends were performed with char thermal conductivities as used in *Test A*, *Test E* and *Test F*.

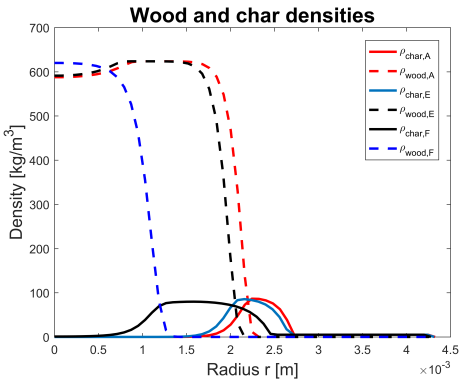

Figure 7: Comparison of devolatilization zones predicted with *Test A*, *Test E* and *Test F* at 45 s.

From Figure 7 it can be seen that the devolatilization zone moves faster when using a higher thermal conductivity of char. This observation agrees with the theoretical understanding that the lower the insulating barrier is, the faster the heat-transfer-controlled phenomena are. Again, the sensitivity of the modeling results to thermal conductivities seems significant, which can be seen by the significant shift in devolatilization zones predicted by *Test A* and *Test F*.

3.3 Gas permeability

When studying the influence of gas permeability on modeling results, three cases were tested. In *Test 2*, the gas permeability for wood was fixed to 10^{-16} m^2 and the one for char was set to 10^{-13} m^2. In the second test (*Test 1*) the wood permeability was set to 10^{-17} m^2 and the char permeability was set to 10^{-14} m^2 and in *Test 3* κ_{wood} was fixed to 10^{-15} m^2 and κ_{char} was fixed to 10^{-12} m^2. The difference between wood and char permeabilities in all test cases was a factor of 1000. The specific surface area for the test runs was set to 10^6 $\frac{m^2}{m^3}$ and the surrounding gas phase velocity was set to 0.5 m/s. The modeling concept presented in *Model A* was used for the study.

A parametric study on the gas permeability was performed in order to study its effect on

the particle temperature history as well as the normalized residual mass predictions. When testing a range of different permeabilities it was observed that higher permeabilities have an effect on the stability of the numerical solution procedure.

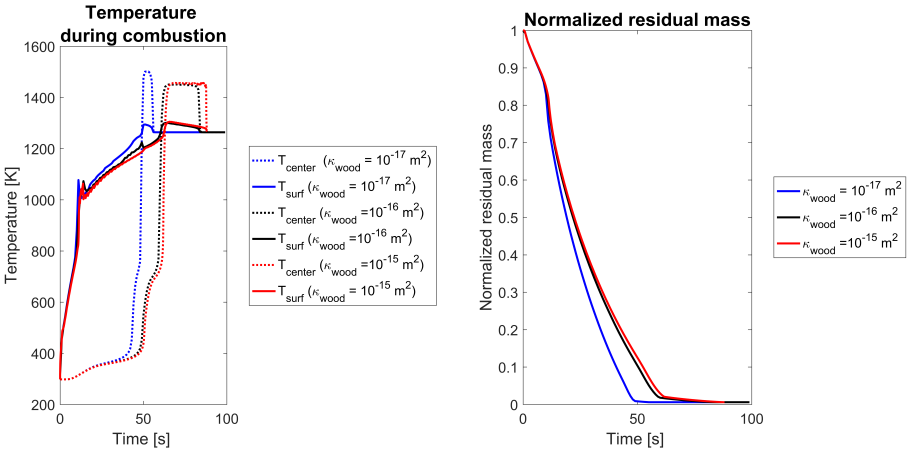

(a) Surface and center temperature predictions obtained from *Test 1*, *Test 2* and *Test 3*.

(b) Normalized residual mass predictions obtained from *Test 1*, *Test 2* and *Test 3*.

Figure 8: Sensitivity of modeling results to assigned wood and char permeabilities. *Test 1* was run with $\kappa_{\text{wood}} = 10^{-17}\ m^2$ and $\kappa_{\text{char}} = 10^{-14}\ m^2$; *Test 2* was run with $\kappa_{\text{wood}} = 10^{-16}\ m^2$ and $\kappa_{\text{char}} = 10^{-13}\ m^2$; *Test 3* was run with $\kappa_{\text{wood}} = 10^{-15}\ m^2$ and $\kappa_{\text{char}} = 10^{-12}\ m^2$.

It can be seen from Figure 8 that the permeabilities influence both the temperature and the normalized residual solid mass predictions. When higher permeabilities are used, the termination of drying and devolatilization is shifted to slightly later times, which therefore also shifts the start of the final char conversion to later times.

The difference between *Test 2* and *Test 3* is only minor, compared to the difference between predictions obtained by *Test 2* and *Test 3* and predictions obtained by *Test 1*. This effect of permeability on devolatilization is due to its influence on the diffusive mass transfer within the particle. The relevant point here is that lower permeabilities yield lower superficial velocity. A lower outward superficial velocity allows for more diffusive mass transfer into the particle. The consequence of this is that the ratio of diffusive transport of oxygen into the particle relative to the outwardly convective transport of oxygen due to the gaseous

flow within the particle becomes larger due to the lower convective velocity. Therefore char conversion is faster, which results in additional heating of the particle, due to exothermic char oxidation, which additionally accelerates the drying and devolatilization.

The total conversion time only increased from 84 s to 87.5 s for *Test 2* and *Test 3*, respectively, while it was only 55 s in *Test 1*. The final char conversion time ranged from 28.6 to 29.3% of the total conversion time for *Test 2* and *Test 3*, respectively, while it covered only 11% of the total conversion time in *Test 1*. Based on these results, one can conclude that for a permeability above a certain value, the total conversion time as well as predicted center and surface temperatures become independent of permeability. However, wood internal pressure distributions will still be affected by the permeabilities, but the variations are of minor influence to general solid phase degradation behavior, e.g. solid mass loss trends. In the opposite case, when the permeability is below the critical value, the influence of gas permeability on the result is significant.

4 Conclusions

In this work, two different modeling approaches for ash-handling in wood combustion modeling were tested. In one approach, an ash-layer builds up around the unreacted char core and therefore has to be considered in heat and mass transfer. In the second modeling approach, the ash remaining after total char conversion at a given point falls off immediately, such that no ash-layer builds up around the char core. Hereby the model operates at the absence of an ash layer, and therefore the lack of influence of the ash layer on heat and mass transfer. It was found, that the two modeling approaches give very different results, with the modeling approach of no-ash-layer-build-up yielding faster thermochemical conversion. However, the modeling approach with the distinct consideration of an up-building ash layer gave temperature and normalized residual mass predictions that were in better agreement with experimental observations. Nonetheless, it was concluded that the better agreement

can also be due to the idealized experimental conditions tested in the single particle reactor, and therefore the unhindered up-building of an ash-layer.

It is therefore expected that for real wood stove conditions, the approach where the ash layer falls off may still be more realistic, since the occurrence of knocking off of ash is more realistic under those conditions. However, it needs to be added, that in the current numerical set up, even the consideration of such a knock-off is simplified, since it is assumed to occur continusously as degradation proceeds and homogeneously at the lateral surface of the wood log. The knock-off as in wood stoves, however, would be a local phenomenon. Therefore *Model A* and *Model B* as presented in this work are two extreme cases. The actual case given in a wood stove, will be a mixture of the two extreme cases. To capture such a mixed case however, which requires the localization of the knock-off phenomenon, is expected to require multi-dimensional models, where the external surface of the wood log is well enough considered. Therefore, future work is recommended to focus on multi-dimensional wood log models.

Furthermore, we also present a parametric study of thermal conductivities of wood and char, the specific surface area and the gas permeabilities. It was found that the model is very sensitive to the thermal conductivity of wood and char. The reason is that drying and devolatilization are both heat-transfer controlled phenomena.

The model is also sensitive to the specific surface area if it is less than a critical value. If the char surface area is large, such that diffusion controls char conversion, the assumed specific surface area is a less critical input data.

When testing the model's sensitivity to gas permeability it was found that total wood combustion depended significantly on assigned permeabilities up until a critical value was reached.

5 Acknowledgments

This work has been carried out within the WoodCFD (243752/E20) project, which is funded by: Dovre AS, Norsk Kleber AS, Jøtulgruppen and Morsø AS together with the Research Council of Norway through the ENERGIX program.

References

(1) Haberle, I.; Skreiberg, Ø.; Łazar, J.; Haugen, N. E. L. *Prog. Energy Combust. Sci.* **2017**, *63*, 204 – 252.

(2) Mehrabian, R.; Zahirovic, S.; Scharler, R.; Obernberger, I.; Kleditzsch, S.; Wirtz, S.; Scherer, V.; Lu, H.; Baxter, L. L. *Fuel Process. Technol.* **2012**, *95*, 96 – 108.

(3) Fatehi, H.; Bai, X. S. *Combust. Sci. Technol.* **2014**, *186*, 574–593.

(4) Lu, H.; Robert, W.; Peirce, G.; Ripa, B.; Baxter, L. L. *Energy Fuels* **2008**, *22*, 2826–2839.

(5) Porteiro, J.; Granada, E.; Collazo, J.; Patiño, D.; Morán, J. C. *Energy Fuels* **2007**, *21*, 3151–3159.

(6) Porteiro, J.; Míguez, J. L.; Granada, E.; Moran, J. C. *Fuel Process. Technol.* **2006**, *87*, 169–175.

(7) Thunman, H.; Leckner, B.; Niklasson, F.; Johnsson, F. *Combust. Flame* **2002**, *129*, 30–46.

(8) Galgano, A.; Di Blasi, C.; De Vita, R. *Energy Fuels* **2018**, *0*, null.

(9) Sadhukhan, A. K.; Gupta, P.; Saha, R. K. *Bioresour. Technol.* **2009**, *100*, 3134 – 3139.

(10) Grønli, M. G. A theoretical and experimental study of the thermal degradation of biomass. PhD thesis, Norwegian University of Science and Technology, Trondheim, 1996.

(11) Strandberg, A.; Thyrel, M.; Skoglund, N.; Lestander, T. A.; Broström, M.; Backman, R. *Fuel Process. Technol.* **2018**, *176*, 211 – 220.

(12) Basu, P. In *Biomass Gasification, Pyrolysis and Torrefaction : Practical Design and Theory*, 2nd ed.; Basu, P., Ed.; Elsevier/AP: Boston, 2013; Chapter 3- Biomass Characteristics, pp 47–86.

(13) Pettersen, R. C. *The Chemistry of Solid Wood*; 1984; Chapter 2 - The Chemical Composition of Wood, pp 57–126.

(14) Fatehi, H. Numerical Simulation of Combustion and Gasification of Biomass Particles. PhD thesis, LTH (Lund University), Lund, Sweden, 2014.

(15) Anca-Couce, A.; Dieguez-Alonso, A.; Zobel, N.; Berger, A.; Kienzl, N.; Behrendt, F. *Energy Fuels* **2017**, *31*, 2335–2344.

(16) Burhenne, L.; Damiani, M.; Aicher, T. *Fuel* **2013**, *107*, 836 – 847.

(17) Link, S.; Arvelakis, S.; Hupa, M.; Yrjas, P.; Külaots, I.; Paist, A. *Energy Fuels* **2010**, *24*, 6533–6539.

(18) Weber, K.; Quicker, P. *Fuel* **2018**, *217*, 240 – 261.

(19) Haberle, I.; Haugen, N. E. L.; Skreiberg, Ø. *Energy Fuels* **2017**, *31*, 13743–13760.

(20) Lu, H. Experimental and modelling investigation of biomass particle combustion. PhD thesis, Brigham Young University, Provo, Utah, 2006.

(21) Haberle, I.; Haugen, N. E. L.; Skreiberg, Ø. *Energy & Fuels* **2018**, *32*, 6847–6862.

(22) Kim, J.-H.; Ochoa-Tapia, J.; Whitaker, S. *Transport in Porous Media* **1987**, *2*, 327–356.

(23) Bird, R. B.; Stewart, W. E.; Lightfoot, E. N. *Transport Phenomena*, 2nd ed.; John Wiley & Sons, Inc.: New York, 2002.

(24) Di Blasi, C. *Chem. Eng. Sci.* **1996**, *51*, 1121 – 1132.

(25) Hermansson, S.; Thunman, H. *Combust. Flame* **2011**, *158*, 988 – 999.

(26) Forest Products Laboratory, *Wood Handbook - Wood as an Engineering Material. General Technical Report FPL-GTR-190.*; 2010.

(27) Larfeldt, J.; Leckner, B.; Melaaen, M. C. *Fuel* **2000**, *79*, 1637–1643.

(28) Wagenaar, B.; Prins, W.; van Swaaij, W. *Fuel Process. Technol.* **1993**, *36*, 291 – 298.

(29) Chan, W.-C. R.; Kelbon, M.; Krieger, B. B. *Fuel* **1985**, *64*, 1505–1513.

(30) Liden, A.; Berruti, F.; Scott, D. *Chem. Eng. Commun.* **1988**, *65*, 207–221.

(31) Koufopanos, C.; Papayannakos, N.; Maschio, G.; Lucchesi, A. *Can. J. Chem. Eng.* **1991**, *69*, 907–915.

(32) Di Blasi, C. *Combust. Sci. Technol.* **1993**, *90*, 315–340.

(33) Bryden, K. M.; Hagge, M. J. *Fuel* **2003**, *82*, 1633 – 1644.

(34) Evans, D.; Emmons, H. *Fire Saf. J.* **1977**, *1*, 57 – 66.

(35) Anca-Couce, A.; Sommersacher, P.; Shiehnejadhesar, A.; Mehrabian, R.; Hochenauer, C.; Scharler, R. *Energy Procedia* **2017**, *120*, 238 – 245.

(36) National Laboratory Lawrence Livermore, SUNDIALS: SUite of Nonlinear and DIfferential/ALgebraic Equation Solvers - IDA. 2016; http://computation.llnl.gov/projects/sundials/ida [accessed 2017-04-07].

(37) Biswas, A. K.; Umeki, K. *Chem. Eng. J.* **2015**, *274*, 181 – 191.

(38) Harada, T.; Hata, T.; Ishihara, S. *J. Wood Sci.* **1998**, *44*, 425–431.

(39) Babu, B.; Chaurasia, A. *Chem. Eng. Sci.* **2004**, *59*, 1999 – 2012.

(40) Alves, S.; Figueiredo, J. *Chem. Eng. Sci.* **1989**, *44*, 2861 – 2869.

(41) Pozzobon, V.; Salvador, S.; Bézian, J. J.; El-Hafi, M.; Maoult, Y. L.; Flamant, G. *Fuel Process. Technol.* **2014**, *128*, 319 – 330.

Errata for Paper IV

This document lists errors found in Paper IV. Only errors that matter from a mathematical viewpoint are listed.

Location	Original text	Correction
pp. 19, Eq.(27)	$h_{\mathrm{c}} = \frac{\dot{M}_{\mathrm{total}} \bar{c}_{\mathrm{P,g}}}{h_{\mathrm{c},0} \left(\exp\left(\frac{\dot{M}_{\mathrm{total}} \bar{c}_{\mathrm{P,g}}}{h_{\mathrm{c},0}} \right) - 1 \right)}$	$h_{\mathrm{c}} = \frac{\dot{M}_{\mathrm{total}} \bar{c}_{\mathrm{P,g}}}{\left(\exp\left(\frac{\dot{M}_{\mathrm{total}} \bar{c}_{\mathrm{P,g}}}{h_{\mathrm{c},0}} \right) - 1 \right)}$
pp. 19, Eq.(28)	$h_{\mathrm{m}} = \frac{\dot{M}_{\mathrm{total}}}{h_{\mathrm{m},0} \left(\exp\left(\frac{\dot{M}_{\mathrm{total}}}{h_{\mathrm{m},0}} \right) - 1 \right)}$	$h_{\mathrm{m}} = \frac{\dot{M}_{\mathrm{total}} / \rho_{\mathrm{g}}^{\mathrm{g}}}{\left(\exp\left(\frac{\dot{M}_{\mathrm{total}}}{\rho_{\mathrm{g}}^{\mathrm{g}} h_{\mathrm{m},0}} \right) - 1 \right)}$

Paper V

Reproduced with permission from Energy & Fuels, submitted for publication

Inge Haberle, Nils Erland L. Haugen and Øyvind Skreiberg, A two-dimensional study on the effect of anisotropy on the devolatilization of a large wood log, Energy & Fuels (submitted), 2018.

A two-dimensional study on the effect of anisotropy on the devolatilization of a large wood log

Inge Haberle,[*,†] Nils Erland L. Haugen,[*,†,‡] and Øyvind Skreiberg[‡]

[1]

†*Department of Energy and Process Engineering, Norwegian University of Science and Technology, Kolbjørn Hejes vei 1 B, 7491 Trondheim, Norway*

‡*Department of Thermal Energy, SINTEF Energy Research, Kolbjørn Hejes vei 1 A, 7491 Trondheim, Norway*

E-mail: inge.haberle@ntnu.no; nils.e.haugen@sintef.no

Abstract

In this work, an existing one-dimensional (1D) model for wood particle drying, devolatilization and char conversion was extended to a two-dimensional (2D) model. The 2D model validated in this work, describes devolatilization of a large, dry, cylindrical birch wood log. Furthermore, the wood log internal distributions of temperature, solid species densities, gas density and gas species mass fractions were studied. In addition, the internal pressure was analyzed and, in combination with this, the gas flow velocities in radial and longitudinal directions were studied. It was found that the internal pressure peak significantly depended on the permeability of char, even though the solid phase devolatilization behavior (e.g. solid mass loss) was hardly affected by the permeability. The highest gas velocities were observed in the axial direction of the hanging wood log and it was observed that the velocity profiles changed as the pressure wave travelled radially inward in the same manner as the devolatilization zone.

In addition to the study on wood anisotropy, which can be accounted for in detail by the presented 2D model, the authors compared the 2D results to results obtained from a 1D model, where only radial heat and mass transfer properties were used. It was found that even though the predictions of the 2D model were in better agreement with experimental observations than the 1D modeling results, 1D models can still be used to sufficiently well predict solid phase degradation behavior and wood internal temperature fields, under the prerequisite that the modeled wood log can be assumed to be infinitely long.

Nomenclature

A	pre-exponential factor $[\frac{1}{\mathrm{s}}]$ / $[\frac{\mathrm{m}}{\mathrm{sK}}]$
AR	aspect ratio
c_{P}	specific heat capacity $[\frac{\mathrm{J}}{\mathrm{kgK}}]$
D_{AB}	diffusivity $[\frac{\mathrm{m}^2}{\mathrm{s}}]$
D_{b}	bound water diffusivity $[\frac{\mathrm{m}^2}{\mathrm{s}}]$
D_{eff}	effective diffusivity $[\frac{\mathrm{m}^2}{\mathrm{s}}]$
D_{Knudsen}	Knudsen diffusion $[\frac{\mathrm{m}^2}{\mathrm{s}}]$
d_{P}	particle diameter [m]
d_{pore}	pore diameter [m]
E_a	activation energy $[\frac{\mathrm{J}}{\mathrm{mol}}]$
f	gas species fraction from primary devolatilization [-]
g	gas species fraction from secondary devolatilization [-]
$\triangle \mathrm{h}$	heat of reaction $[\frac{\mathrm{J}}{\mathrm{kg}}]$
$h_{\mathrm{c,0}}$	heat transfer coefficient $[\frac{\mathrm{W}}{\mathrm{m}^2\mathrm{K}}]$ (without Stefan flow)
h_{c}	heat transfer coefficient $[\frac{\mathrm{W}}{\mathrm{m}^2\mathrm{K}}]$ (with Stefan flow)
$h_{\mathrm{m,0}}$	mass transfer coefficient $[\frac{\mathrm{m}}{\mathrm{s}}]$ (without Stefan flow)
h_{m}	mass transfer coefficient $[\frac{\mathrm{m}}{\mathrm{s}}]$ (with Stefan flow)
k	reaction rate constant $[\frac{1}{\mathrm{s}}]$ or $[\frac{\mathrm{m}}{\mathrm{s}}]$
k_1	reaction: wood to non-condensable gases
k_2	reaction: wood to tar
k_3	reaction: wood to char
k_4	reaction: tar to non-condensable gases
k_5	reaction: tar to char
$\dot{m}_g$	phase averaged convective mass flux $[\frac{\mathrm{kg}}{\mathrm{m}^2\mathrm{s}}]$
M_{liquid}	liquid moisture content [-]
$\dot{M}_{\mathrm{total}}$	total mass flux of exiting gases $[\frac{kg}{sm^2}]$
MW	molecular weight $[\frac{\mathrm{kg}}{\mathrm{mol}}]$

R	ideal gas constant $[\frac{\mathrm{J}}{\mathrm{molK}}]$	$\mathbf{U}_\mathrm{b}$	bound watere velocity in radial direction $[\frac{\mathrm{m}}{\mathrm{s}}]$
r	radius [m]	u_l	liquid free water velocity in radial direction $[\frac{\mathrm{m}}{\mathrm{s}}]$
T	temperature [K]	u_r	gas phase velocity in radial direction $[\frac{\mathrm{m}}{\mathrm{s}}]$
T_gas	surrounding gas phase temperature [K]	V_j	cell volume [m^3]
T_ref	reference temperature [K] (298 K)	Y	mass fraction [-]
T_wall	furnace wall temperature [K]	z	length of the wood log [m]

Greek letters

ϵ	porosity [-]	λ	thermal conductivity $[\frac{\mathrm{W}}{\mathrm{mK}}]$
ω	effective emissivity [-]	ρ	density $[\frac{\mathrm{kg}}{\mathrm{m}^3}]$
Φ_heat	heat source term $[\mathrm{J}/(\mathrm{sm}^3)]$	σ	Stefan-Boltzmann constant $[\frac{\mathrm{W}}{\mathrm{m}^2\mathrm{K}^4}]$
κ	permeability [m^2]	$\dot{\omega}$	reaction rate $[\frac{\mathrm{kg}}{\mathrm{m}^3\mathrm{s}}]$

Subscript

a	ash	$devol, 2$	secondary devolatilization
b	bound water	eff	effective
c	char	H_2O, g	water vapor
$CO_{2,\mathrm{gasif}}$	CO_2 gasification	i	reaction
$devol, 1$	primary devolatilization	$evap$	evaporation

g	gas phase		$steam, gasif$	H_2O gasification	
k	gas species		tar	tar	
$long$	longitudinal		$wall$	furnace wall	
l	liquid free water		w	dry wood	
$mix, total$	mixed gas phase		$\parallel$	parallel to fiber direction	
oxid	char oxidation		$\perp$	perpendicular to fiber direction	
rad	radiative		∞	bulk	
$radial$	radial		$vapor$	water vapor	
ref	reference		$water$	water	

Superscript

g	gas phase	l	liquid phase

1 Introduction

Since 1980 the world primary energy consumption has dramatically increased. This increase was mainly due to an intense rise in the use of oil, coal and natural gas.[1] Biomass can be used to generate heat via combustion, while at the same time biomass combustion is accompanied by limited greenhouse gas effects.[2] In order to confront the problems induced by greenhouse gases, i.e. global warming and climate change, research is focusing on the potential role of biomass in the future energy mix. Thermochemical degradation of biomass, from which energy carriers can be generated, and combustion, used for heat generation, are currently both intensively studied.[3]

During the last years, there has been an increased focus on modeling of thermochemical

wood degradation as well as on conversion of the resulting char. One-dimensional (1D) models were, and are still, the main tool. This is beacuse they allow for fundamental studies on conversion related chemical and physical processes, while at the same time remaining computationally efficient.[4] However, significant simplifications of the chemical and physical processes are required with respect to 1D model development. Multi-dimensional models have, on the other hand, been developed only to a very limited extent.[2,5–7]

For both wood logs and wood chips, the original wood structure is maintained during processing. This means that both of these fuel types have a highly anisotropic structure. In 1D models, fuel properties are simplified by using radial or averaged values, i.e. by neglecting or very much simplifying the anisotropic structure. This simplification implies that e.g. effective thermal conductivity is calculated by weighing the influence of heat transfer parallel and perpendicular to the grain direction by a bridge factor.[8] Accordingly, multi-dimensional models are required in order to account in detail for the influence of the direction-dependent wood properties.

Furthermore, it has been found that even though research is focusing on the modeling of thermochemical wood conversion and char consumption, only very rarely the developed models are focusing on large wood logs, comparable in size to wood logs used in wood log heating appliances, e.g. stoves and boilers.[4]

A one-dimensional pyrolysis model for large wood logs (with a radius of 25mm and a length of 300mm) was developed by Larfeldt et al.[9] They presented experimental data for the devolatilization of a large and dry birch wood cylinder, (detailed explanation on the experiments is available in an earlier work by Larfeldt,[10] where also wet wood logs were tested) and found a discrepancy between the modeling and experimental results, concluding that this difference was partly due to the anisotropy of the wood, which could not be replicated well enough by their 1D model. Furthermore, they also mention that differences in results might arise from the lack of empirical data with respect to heat transfer properties, heat of reactions for devolatilization reactions, as well as shrinkage parameters. One of their findings

was that the pyrolysis time depended significantly on the wood log shrinkage.

A two-dimensional (2D) drying and pyrolysis model was developed by Sand et al.[6] They solved the momentum equations and were studying a leaving gas plume that was observed during thermochemical wood log conversion.

Yang et al.[5] developed a 2D combustion model. However, they only studied wood particles within a size range of 10μm to 20mm. This size range still differs significantly from the wood log used in domestic wood log heating appliances.

Di Blasi[7] studied the anisotropy of wood by a 2D model applied to a wood slab. They found that the dynamics of particle degradation depended on the grain structure of the solid. According to their findings an accurate prediction of the influence of anisotropy is required in order to obtain correct results for conversion time and product yields.

Pozzobon et al.[2] experimentally studied the drying and thermochemical degradation of a thermally thick wood particle, exposed to a high radiative heat flux. In addition to their experiments they developed a 2D unsteady numerical code that described drying and devolatilization in order to understand the observed phenomena.

Even though some research has been conducted with the field of 2D modeling, 3D model development is even more limitedly done. This is primarily due to the fact that fundamental studies of wood particle degradation and combustion can also be done by means of 1D models, which are easier to implement and computationally faster.

Also, experimental research rarely focus on thermochemical degradation and char conversion of large wood logs. This limitation in available experimental data with respect to large wood log conversion is the reason why only devolatilization of a large, dry and hanging wood log cylinder was modeled in this work.

We aim to develop a wood log conversion model that can be coupled to a gas phase model, such that a simulation tool for wood stove design and optimization is established. Since we want to model a large and highly anisotropic wood log in a wood stove, the use of a 2D model yields the ideal trade-off between accuracy and computational costs. This is because

it allows for a detailed study of direction-dependent wood properties, while at the same time remaining computationally faster than three-dimensional (3D) models. It is not only the anisotropy of the wood structure, but also the highly non-homogeneous boundary conditions at the wood log surface in a wood stove, that call for multi-dimensional models. De facto, the boundaries of the wood log can be affected very differently, e.g. due to different exposure to the flame, the furnace wall, blocking by other wood logs in the stack etc. Therefore, multi-dimenional models need to be developed, since only then a local variation in boundary conditions can be accounted for. The development of this 2D standalone code is the first step in developing a wood stove design and optimization tool.

2 Wood log model

In this section it is explained how the existing 1D model is extended to 2D. First, the relevant governing equations are listed in Table 1. It should be mentioned, that the presented equations are only limited to the devolatilization stage, since in the current test run drying and char conversion are not modeled. Further details on the model development can be found in earlier works by Haberle et al. [11,12]

Table 1: List of evolution equations required for the devolatilization model. The last column gives the references the equations have been taken from.

Equation		**Equation number**	**Ref.**
Wood density[1)]	$\frac{\partial \rho_\mathrm{w}}{\partial t} = -(k_1 + k_2 + k_3)\rho_\mathrm{w} - \frac{\rho_\mathrm{w}}{V_j}\frac{\partial V_j}{\partial t}$	(1)	13
Ash density	$\frac{\partial \rho_\mathrm{a}}{\partial t} = -\frac{\rho_\mathrm{a}}{V_j}\frac{\partial V_j}{\partial t}$	(2)	13
Continuity equation[3)]	$\frac{\partial \epsilon \rho_\mathrm{g}^\mathrm{g}}{\partial t} + \frac{1}{r}\frac{\partial}{\partial r}\left(r\rho_\mathrm{g}^\mathrm{g} u_\mathrm{r}\right) + \frac{\partial}{\partial z}\left(\rho_\mathrm{g}^\mathrm{g} u_\mathrm{z}\right) = \dot{\omega}_\mathrm{g}$	(3)	7
Species mass fraction[4)]	$\frac{\partial(\epsilon\rho_\mathrm{g}^\mathrm{g} Y_k)}{\partial t} + \frac{1}{r}\frac{\partial(r\rho_\mathrm{g}^\mathrm{g} Y_\mathrm{k} u_\mathrm{r})}{\partial r} + \frac{\partial(\rho_\mathrm{g}^\mathrm{g} Y_\mathrm{k} u_\mathrm{z})}{\partial z} = \frac{1}{r}\frac{\partial}{\partial r}\left(r\rho_\mathrm{g}^\mathrm{g} D_\mathrm{eff}\frac{\partial Y_\mathrm{k}}{\partial r}\right) + \frac{\partial}{\partial z}\left(\rho_\mathrm{g}^\mathrm{g} D_\mathrm{eff}\frac{\partial Y_\mathrm{k}}{\partial z}\right) + \dot{\omega}_k$	(4)	3
Char density[2)]	$\frac{\partial \rho_\mathrm{c}}{\partial t} = k_3\rho_\mathrm{w} + \epsilon k_5 \rho_\mathrm{tar}^\mathrm{g} - \frac{\rho_\mathrm{c}}{V_j}\frac{\partial V_j}{\partial t}$	(5)	13
Temperature[4)]	$\left(\rho_\mathrm{w} c_{P,\mathrm{w}} + \rho_\mathrm{a} c_{P,\mathrm{a}} + \rho_\mathrm{c} c_{P,\mathrm{c}} + \epsilon\rho_\mathrm{g}^\mathrm{g} c_{P,\mathrm{g}}\right)\frac{\partial T}{\partial t} + \rho_\mathrm{g}^\mathrm{g} c_{\mathrm{P,g}} u_\mathrm{r}\frac{\partial T}{\partial r} + \rho_\mathrm{g}^\mathrm{g} c_{\mathrm{P,g}} u_\mathrm{z}\frac{\partial T}{\partial z} = \frac{1}{r}\frac{\partial}{\partial r}\left(r\lambda_{\mathrm{eff},\perp}\frac{\partial T}{\partial r}\right) + \frac{\partial}{\partial z}\left(\lambda_{\mathrm{eff},\parallel}\frac{\partial T}{\partial z}\right) + \Phi_\mathrm{Heat}$	(6)	14
Radial gas velocity, u_r	$u_\mathrm{r} = u = -\frac{\kappa_\mathrm{radial}}{\mu}\frac{\partial P}{\partial r}$	(7)	13
Longitudinal gas velocity, u_z	$u_\mathrm{z} = v = -\frac{\kappa_\mathrm{long}}{\mu}\left(\frac{\partial P}{\partial z} + g\rho_\mathrm{g}^\mathrm{g}\right)$	(8)	7
Equation of state	$\mathrm{pV} = \mathrm{nRT}$	(9)	7
Effective diffusivity	$D_\mathrm{eff} = \frac{\epsilon}{\tau}\frac{1}{\frac{1}{D_\mathrm{AB}} + \frac{1}{D_\mathrm{Knudsen}}}$	(10)	11

[1)] The reaction rates of wood to non-condensable gases, tar and char are given by k_1, k_2 and k_3, respectively.
[2)] k_5 marks the reactions of tar to char.
[3)] marks that the continuity equation has been transferred to cylindrical coordinates from cartesian coordinates.
[4)] marks that the original equation given in the reference has been extended to 2D by the authors.

In Eq. (10) one can identify that the effective diffusivity is dependent on tortuosity, which is direction dependent. In this model, however, a simplification is made by assuming that pores are homogeneously distributed within the wood, and that tortuosity can be expressed as[15]

$$\tau = \frac{1}{\epsilon}. \tag{11}$$

Based on this assumption the effective diffusivity is not assumed to be different in radial and longitudinal direction.

The heat source term,Φ_{heat}, in Table 1 is defined as

$$\begin{aligned}\Phi_{\mathrm{heat}} = \dot{\omega}_{k1,k2,k3}\triangle h_{\mathrm{devol},1} + \dot{\omega}_{k4,k5}\triangle h_{\mathrm{devol},2} \\ +\dot{\omega}_{k1}\Big(\int_{T_0}^{T}(c_{\mathrm{P,wood}} - c_{\mathrm{P,non-cond.\ gases}})dT\Big) + \dot{\omega}_{k2}\Big(\int_{T_0}^{T}(c_{\mathrm{P,wood}} - c_{\mathrm{P,tar}})dT\Big) \\ +\dot{\omega}_{k3}\Big(\int_{T_0}^{T}(c_{\mathrm{P,wood}} - c_{\mathrm{P,char}})dT\Big) \\ +\dot{\omega}_{k4}\Big(\int_{T_0}^{T}(c_{\mathrm{P,tar}} - c_{\mathrm{P,non-cond.\ gases}})dT\Big) + \dot{\omega}_{k5}\Big(\int_{T_0}^{T}(c_{\mathrm{P,tar}} - c_{\mathrm{P,char}})dT\Big),\end{aligned} \tag{12}$$

since it includes the influence of the heat of reaction of different chemical reactions as well as the changes in sensible enthalpy.

For reactions 1,2,3, which describe the primary devolatilization of wood to non-condensable gases, tar and char respectively, the reaction rate is calculated as

$$\dot{\omega}_i = k_i \rho_{\mathrm{w}}, \tag{13}$$

where ρ_{w} is the apparent wood density. The devolatilization reaction rate constants, k_i, are calculated from[13]

$$k_i = A_i \exp\frac{-E_{\mathrm{a,i}}}{RT} \qquad \text{for i} = 1,2,3,4,5 \tag{14}$$

with A_i being the pre-exponential factor, R the ideal gas constant, T the temperature and $E_{\mathrm{a,i}}$ the activation energy.

The secondary devolatilization ($i = 4$ and 5) reaction rates are calculated as

$$\dot{\omega}_i = k_i \epsilon \rho^{\mathrm{g}}_{\mathrm{tar}} \tag{15}$$

with $\rho^{\mathrm{g}}_{\mathrm{tar}}$ being the intrinsic tar density and ϵ the porosity. However, it needs to be added that tar re-polymerization to secondary char is actually a heterogeneous reaction, which is simplified to a homogeneous reaction by the kinetics implemented here. Accordingly, the consideration of secondary char formation is very much simplified, which of course can affect modeling results, but it is a first attempt to capture a chemical phenomenon that is not yet very well understood.

The source terms of the different gas species equations are

$$\dot{\omega}_{\mathrm{CO}} = f_{\mathrm{CO}}\dot{\omega}_{\mathrm{k}_1} + g_{\mathrm{CO}}\dot{\omega}_{\mathrm{k}_4} \tag{16}$$

$$\dot{\omega}_{\mathrm{H_2}} = f_{\mathrm{H_2}}\dot{\omega}_{\mathrm{k}_1} + g_{\mathrm{H_2}}\dot{\omega}_{\mathrm{k}_4} \tag{17}$$

$$\dot{\omega}_{\mathrm{H_2O,g}} = f_{\mathrm{H_2O}}\dot{\omega}_{\mathrm{k}_1} + g_{\mathrm{H_2O}}\dot{\omega}_{\mathrm{k}_4} \tag{18}$$

$$\dot{\omega}_{\mathrm{CO_2}} = f_{\mathrm{CO_2}}\dot{\omega}_{\mathrm{k}_1} + g_{\mathrm{CO_2}}\dot{\omega}_{\mathrm{k}_4} \tag{19}$$

$$\dot{\omega}_{\mathrm{tar}} = \dot{\omega}_{k_2} - \dot{\omega}_{k_4} - \dot{\omega}_{k_5} \tag{20}$$

where $\dot{\omega}_{k_4}$ represents the reaction rate due to the tar cracking to non-condensable gases and $\dot{\omega}_{k_5}$ represents reaction rate due to the tar re-polymerization to char. The fractions $f_{\mathrm{CO_2}}$, f_{CO}, $f_{\mathrm{H_2}}$ and $f_{\mathrm{H_2O}}$ define how much carbon dioxide, carbon monoxide, hydrogen and water vapor are produced from primary devolatilization reactions, and the fractions $g_{\mathrm{CO_2}}$, g_{CO}, $g_{\mathrm{H_2}}$ and $g_{\mathrm{H_2O}}$ define how much of the corresponding species are formed from tar reactions. Those fractions are user-defined model input data.

In addition to the evolution equations, auxiliary equations are needed to describe wood properties. The effective permeabilities, $\kappa_{\parallel}$ and $\kappa_{\perp}$, are modeled by mass-weighting the influence of primarily wood and char based on the local solid composition

$$\kappa_{\parallel} = \frac{\rho_{\mathrm{w}}}{\rho_{\mathrm{w}} + \rho_{\mathrm{c}} + \rho_{\mathrm{a}}}\kappa_{w,\parallel} + \frac{\rho_{\mathrm{a}} + \rho_{\mathrm{c}}}{\rho_{\mathrm{w}} + \rho_{\mathrm{c}} + \rho_{\mathrm{a}}}\kappa_{c,\parallel} \tag{21}$$

and

$$\kappa_{\perp} = \frac{\rho_{\mathrm{w}}}{\rho_{\mathrm{w}} + \rho_{\mathrm{c}} + \rho_{\mathrm{a}}}\kappa_{w,\perp} + \frac{\rho_{\mathrm{a}} + \rho_{\mathrm{c}}}{\rho_{\mathrm{w}} + \rho_{\mathrm{c}} + \rho_{\mathrm{a}}}\kappa_{c,\perp}. \tag{22}$$

The same permeabilities are assumed for char and ash. The effective particle emissivity, ω, is calculated by mass-weighting every solid component [13]

$$\omega = \frac{\rho_{\mathrm{w}}}{\rho_{\mathrm{w}} + \rho_{\mathrm{c}} + \rho_{\mathrm{a}}}\omega_{\mathrm{w}} + \frac{\rho_{\mathrm{c}}}{\rho_{\mathrm{w}} + \rho_{\mathrm{c}} + \rho_{\mathrm{a}}}\omega_{\mathrm{c}} + \frac{\rho_{\mathrm{a}}}{\rho_{\mathrm{w}} + \rho_{\mathrm{c}} + \rho_{\mathrm{a}}}\omega_{\mathrm{a}}. \tag{23}$$

As Lu et al. [13] already mentioned, a volume-weighted calculation of the emissivity is more appropriate. However, this is not possible in this case due to the applied governing equa-

tions, since all solid components are assumed to occupy the same total volume. Similar challenges arise for the permeability calculation, such that mass-weighting was also used for the calculation of the effective local permeability.

The effective thermal conductivities in radial ($\lambda_{\mathrm{eff,radial}}$) and longitudinal ($\lambda_{\mathrm{eff,long}}$) direction are calculated as

$$\lambda_{\mathrm{eff,long}} = \lambda_{\mathrm{cond,long}} + \epsilon\lambda_{\mathrm{rad}} \tag{24}$$

and

$$\lambda_{\mathrm{eff,radial}} = \lambda_{\mathrm{cond,radial}} + \epsilon\lambda_{\mathrm{rad}} \tag{25}$$

with the conduction part, ($\lambda_{\mathrm{cond,j}}$), being

$$\lambda_{\mathrm{cond,j}} = \epsilon\lambda_{\mathrm{g}} + (1-\epsilon)\Big(\frac{\rho_{\mathrm{w}}}{\rho_{\mathrm{w}}+\rho_{\mathrm{c}}+\rho_{\mathrm{a}}}\lambda_{\mathrm{w,j}} + \frac{\rho_{\mathrm{c}}}{\rho_{\mathrm{w}}+\rho_{\mathrm{c}}+\rho_{\mathrm{a}}}\lambda_{\mathrm{c,j}} + \frac{\rho_{\mathrm{a}}}{\rho_{\mathrm{w}}+\rho_{\mathrm{c}}+\rho_{\mathrm{a}}}\lambda_{\mathrm{a,j}}\Big), \tag{26}$$

where j refers to either longitudinal (*long*) or radial (*radial*) direction within the wood log. The calculation principle of the effective thermal conductivity was taken from Fatehi and Bai,[16] but was corrected to neglect the influence of water, since the wood log modeled here was perfectly dry.

2.1 Boundary conditions

The boundary conditions at the external surfaces are modeled as described in Figure 1. The external particle surfaces (in Figure 1, the right and upper boundary) are influenced by the reactor conditions.

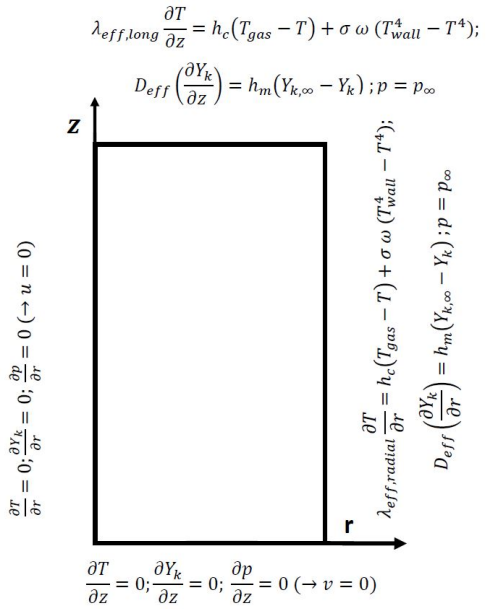

Figure 1: Computational domain and applied boundary conditions. The z-axis marks the wood log length and the r-axis marks the wood log radius.

Due to symmetry conditions, only a part of the total wood log volume is simulated. Symmetry boundary conditions are applied (left and lower boundary), as shown in Figure 1. Heat and mass transfer coefficients, defining convective heat and mass transfer from the bulk to the particle surface, are reduced due to the Stefan flow. The Stefan flow is an outward flow of gas that results from volatile production within the wood. The reduced heat transfer coefficient is modeled as[17]

$$h_{\mathrm{c}} = \frac{\dot{M}_{\mathrm{total}}\bar{c}_{\mathrm{P,g}}}{\left(\exp\left(\frac{\dot{M}_{\mathrm{total}}\bar{c}_{\mathrm{P,g}}}{h_{\mathrm{c},0}}\right) - 1\right)}, \tag{27}$$

with $h_{\mathrm{c},0}$ being the uncorrected heat transfer coefficient, $\dot{M}_{\mathrm{total}}$ the total gas phase mass flux leaving the particle and $\bar{c}_{\mathrm{P,g}}$ the mass averaged specific heat capacity of the gas mixture. The mass transfer coefficient is calculated similarly, as

$$h_{\mathrm{m}} = \frac{\frac{\dot{M}_{\mathrm{total}}}{\rho_{\mathrm{g}}^{\mathrm{g}}}}{\left(\exp\left(\frac{\dot{M}_{\mathrm{total}}}{\rho_{\mathrm{g}}^{\mathrm{g}} h_{\mathrm{m},0}}\right) - 1\right)}, \tag{28}$$

with $h_{\mathrm{m},0}$ being the uncorrected mass transfer coefficient. The Nusselt and Sherwood numbers, which are required for the calculation of the uncorrected heat and mass transfer coefficients,

$$h_{\mathrm{m},0} = \frac{ShD_{\mathrm{AB}}}{l_{\mathrm{c}}} \tag{29}$$

and

$$h_{\mathrm{c},0} = \frac{Nu\lambda_{\mathrm{gas}}}{l_{\mathrm{c}}} \tag{30}$$

with l_{c} being the characteristic length, were calculated from

$$Nu = 0.664 Re^{0.5} Pr^{1/3} \tag{31}$$

and

$$Sh = 0.664 Re^{0.5} Sc^{1/3}. \tag{32}$$

The pressure at the particle surface is set to ambient pressure. The surrounding gas phase is assumed to be nitrogen, i.e. $\mathrm{Y_{N_2}}$=1, all residual $\mathrm{Y}_k = 0$. The surrounding gas phase temperature is set to 973 K, which is equal to the furnace wall temperature.

The applied set of differential and algebraic equations is influenced by the choice of modeling assumptions. The 2D model development in this work is based on the following assumptions:

1. The gas is ideal.
2. Wood and char are anisotropic homogeneous porous media.
3. Darcy's law is used to derive the gas phase velocity, which is valid due to a low pore Reynolds number.
4. Primary devolatilization is described by three independent competitive reactions, and secondary tar reactions are considered.
5. The following solid and gaseous species are modeled: wood, char, ash, CO_2, CO, N_2, tar. No liquid specie is considered, since the wood log is considered to be perfectly dry.

6. The solid and the gas phase are in thermal equilibrium. Therefore, it is enough to solve only one temperature equation. Further explanations on this can be found in other works.[1]

7. The ash content is 1wt% (db).

2.2 Numerical solver

The set of equations is solved by the IDA solver included in the SUNDIALS[18] software package. The equations listed in Table 1 are solved. The advection term in the transport equations is discretized by first-order up-winding, which is sufficient for the smooth flows encounterd within large wood logs. The diffusive terms in the transport equations are discretized by second order differencing. As a consequence, the overall spatial accuracy is first order. The IDA solver implicitly solves the set of equations by a backward differentiation formula, with the order of 1 to 5. The appropriate order is found by the solver based on the local error. The IDA solver was chosen because it follows the same concept as the DASSL solver (written in Fortran), which has already been used for thermochemical degradation modeling of wood by Grønli.[3] Since Grønli did not report any problems arising from their choice of numerical solver, it was assumed that the IDA solver can equally well lead to a suitable simulation tool for thermochemical degradation of wood and char conversion.

2.3 Numerical set-up

Dry birch wood was used in the experiments by Larfeldt et al.[9,10] The wood properties used in the simulations are presented in Table 2.

306

Table 2: Properties used as input values for the devolatilization model.

Property	**Unit**	**Value**	**Ref.**
Thermal conductivity (wood), $\lambda_{w,long}/\lambda_{w,radial}$	[W/(mK)]	0.419 / 0.158	[3]
Thermal conductivity (ash - fiber), $\lambda_{a,long,radial}$	[W/(mK)]	1.2	[13]
Thermal conductivity (char), $\lambda_{c,long}/\lambda_{c,radial}$	[W/(mK)]	0.1046 / 0.071	[7]
Thermal conductivity (gases), λ_g	[W/(mK)]	25.77×10^{-3}	[19]
Specific heat capacity (wood) (298 - 413 K), $c_{P,\ wood}$	[J/(kgK)]	-91.2 + 4.4T	[3]
Specific heat capacity (wood) (350 - 500 K), $c_{P,\ wood}$	[J/(kgK)]	1500 + T	[3]
Specific heat capacity (ash), $c_{P,\ a}$	[J/(kgK)]	754 + 0.586 (T - 273)	[20]
Specific heat capacity (gases), $c_{P,\ g}$	[J/(kgK)]	770 + 0.629 T - 1.91×10^{-4} T^2	[3]
Specific heat capacity (char), $c_{P,\ c}$	[J/(kgK)]	420 + 2.09 T - 6.85×10^{-4} T^2	[3]
Specific heat capacity (tar), $c_{P,\ tar}$	[J/(kgK)]	-100 + 4.4 T - 1.57×10^{-3} T^2	[3]
Apparent wood density, ρ_w (porosity, ϵ_{pore})	[kg/m^3]	410 ($\epsilon_{pore} = 0.4$)	[9]
Radiative thermal conductivity, λ_{rad}	[W/(mK)]	$\frac{4\omega\epsilon d_{pore} T^3}{1-\epsilon}$	[3]
Binary diffusivity, D_{AB}	[m^2/s]	$3 \times 10^{-5} \left(\frac{T}{T_{ref}}\right)^{1.75}$	[13]&[20]
Particle diameter, d_P	[m]	50×10^{-3}	[9]
Aspect ratio, AR	[-]	6	[9]
Moisture content, M_{liquid}	[% wet basis]	0	[9]
Permeability, $\kappa_{w,\ long}$	m^2	2.96×10^{-15}	[3]
Permeability, $\kappa_{w,\ rad}$	m^2	1.29×10^{-18}	[3]
Permeability, $\kappa_{c,\ long}$	m^2	10^{-12}	1)
Permeability, $\kappa_{c,\ rad}$	m^2	10^{-13}	[9]
Char emissivity, ω_c	[-]	0.95	[13]
Wood emissivity, ω_w	[-]	0.85	[13]
Ash emissivity, ω_a	[-]	0.85	2)
Ash porosity, $\epsilon_{pore,a}$	[-]	0.8	[14]
Char porosity, $\epsilon_{pore,c}$	[-]	0.8	[14]
Shrinkage factor (devolatilization)	[-]	0.9	[21]

1) It was assumed that the radial char permeability was smaller than the longitudinal permeability and the difference was assumed to be a factor of 10.
2) The same emissivity was assumed for wood and ash, since they were present in a solid mixture before devolatilization.

307

308 The pore diameter, which is required for the calculation of the radiative contribution to

the effective thermal conductivity, was set to 4×10^{-5} m for wood and 2×10^{-4} m for char.[3] The pore diameter changed linearly from its value in wood to its value in char, depending on the local degree of conversion, which was calculated on a mass-weighted fraction of wood or char in the total available solid phase.

It shall be pointed out that the difference between radial and longitudinal char permeabilities is smaller than what could theoretically be expected. This small difference arises from numerical instabilities that were observed when larger char permeabilities were applied. The authors assume that pre-conditioning can be implemented in the solver to confront those instabilities. However, this is the task of future research, as it goes beyond the scope of this work.

Since volumetric shrinkage factors are given, it has to be defined how the wood log shrinks along and across the wood fibers. Since shrinkage in the longitudinal direction is typically negligible,[3] the length of the wood log is considered unchanged in this work. The wood log radius, however, decreases due to shrinkage. Based on this relative contribution of longitudinal and radial shrinkage to the volumetric shrinkage, the volumetric shrinkage calculated with the given shrinkage factor could be coupled to a definition of the radial shrinkage.

The applied pre-exponential factors, activation energies and heat of reactions used for phase change and chemical reactions included in the model are listed in Table 3.

Table 3: Kinetic data used for modeling drying, devolatilization and char gasification and oxidation. *"Gases"* in the following table refer to non-condensable gases.

Reaction	Reaction rate constant	Unit	Ref.	Heat of reaction [kJ/kg]	Ref.
Wood → Gases	$k_1 = 1.11 \times 10^{11} \exp\left(\frac{-177000}{RT}\right)$	[1/s]	[22]	0	[1)]
Wood → Tar	$k_2 = 9.28 \times 10^{9} \exp\left(\frac{-149000}{RT}\right)$	[1/s]	[22]	0	[1)]
Wood → Char	$k_3 = 3.05 \times 10^{7} \exp\left(\frac{-125000}{RT}\right)$	[1/s]	[22]	0	[1)]
Tar → Gases	$k_4 = 4.28 \times 10^{6} \exp\left(\frac{-107500}{RT}\right)$	[1/s]	[23]	42	[24]
Tar → Char	$k_5 = 1 \times 10^{5} \exp\left(\frac{-107500}{RT}\right)$	[1/s]	[25]	42	[24]

[1)] The heat of reaction was obtained by fitting the modeling results to the experimental data.

In this work, the primary devolatilization reactions were initially assumed to be endothermic as suggested by Chan et al.[26] Experimentally, however, no significant temperature plateau was observed for the center temperature. Commonly, such temperature plateaus can be observed and their extent depends on how endothermic primary devolatilization reactions are assumed. Due to the lack of such a temperature plateau in the experiments, it was assumed that primary devolatilization reactions are only slightly endothermic and can rather be assumed to be heat neutral. Due to this, the heat of reaction of the primary devolatilization reactions was set to zero. This assumption, with respect to heat of reaction is justified, since Ström and Thunman[27] already reported that the identification of heat of pyrolysis is challenging. Primary devolatilization is commonly assumed to be endothermic, while secondary devolatilization is exothermic. For some wood species, the heat of reaction of primary devolatilization has nevertheless been reported to range from endothermic to exothermic values.[28]

3 Results and Discussion

The 2D numerical simulation tool is used to predict the devolatilization of a large hanging wood log, as described by Larfeldt et al.[9,10] and as was also already modeled by Sand et al.[6] In the experiments, which were conducted by Larfeldt et al.,[10] the thermocouples were fixed at different radial positions of a wood log with a radius of 25mm and a length of 300mm via axially drilled holes.

3.1 Grid-independence study

Before studying the distribution of different variables within the wood log, a grid-independence study was performed. Three differently fine grids were tested and the modeling results were compared, to identify how dense the mesh had to be to guarantee grid-independent results. The coarsest mesh was composed of 15×31 grid points (GPs) in the radial and longitudinal

directions, respectively. A medium coarse mesh was composed of 37×61 GPs and the finest mesh was composed of 67×161 GPs.

The differences between the predicted center and surface temperatures as well as the predicted normalized residual mass of the finest and the medium coarse mesh were small (see Figure 2), such that it was concluded that the medium coarse mesh already yielded grid-independent results. By comparing also the results of surface and center temperature as well as normalized residual mass, predicted by the coarsest mesh, to the two finer meshes, it was found that the deviation in modeling results was small, but more prominent to what was observed when comparing the medium coarse and the fine mesh. However, when plotting the temperature field in the wood log interior, see Figure 3, it was found that the predicted temperatures deviated from what was obtained by the medium coarse and the finest mesh, with the contour lines of the latter two actually overlapping. Hence, for the current test case of a large wood log with a radius of 25mm and length of 300mm, the medium coarse mesh (37×61 GPs) is sufficient to obtain grid-independent results.

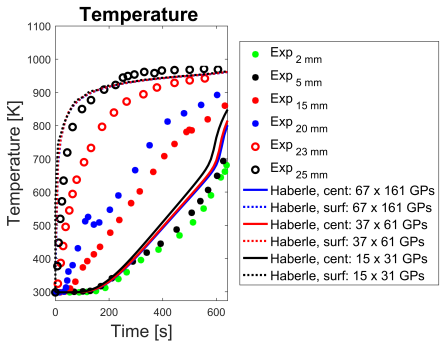

(a) Predicted center and surface temperatures validated against the first experimental series conducted by Larfeldt.[10]

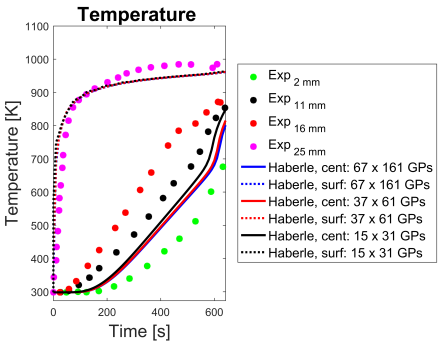

(b) Predicted center and surface temperatures validated against the second experimental series conducted by Larfeldt.[10]

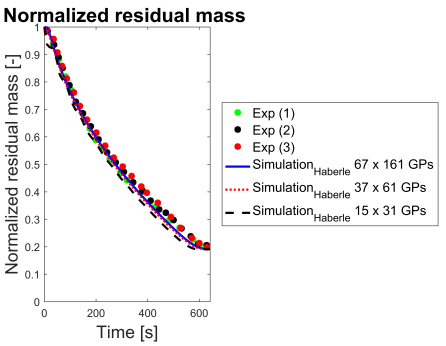

(c) Predicted normalized residual solid mass.

Figure 2: Results of the grid-independence study. The results of a fine mesh (67 × 161 GPs) are compared with the results of a medium coarse mesh (37 × 61 GPs) and the results of a very coarse mesh (15 × 31 GPs). The plotted experimental data was taken from Larfeldt.[10]

The steeper the gradients within the wood log, the finer the mesh has to be. The steepest gradient to be expected for the current devolatilization test case is the temperature gradient, since the surface of the wood log is quickly heated by radiation while the internal heat transfer is slow (large Biot number). Since char conversion is not subject of the current test case, the steepness of the oxygen gradient is not influencing the requirements for mesh fineness.

It must be highlighted that the grid-independence study is case-dependent. For the given case of devolatilization of a large, dry cylindrical wood log with the given external heating conditions, the medium coarse mesh is suitable. However, if the model is extended to also

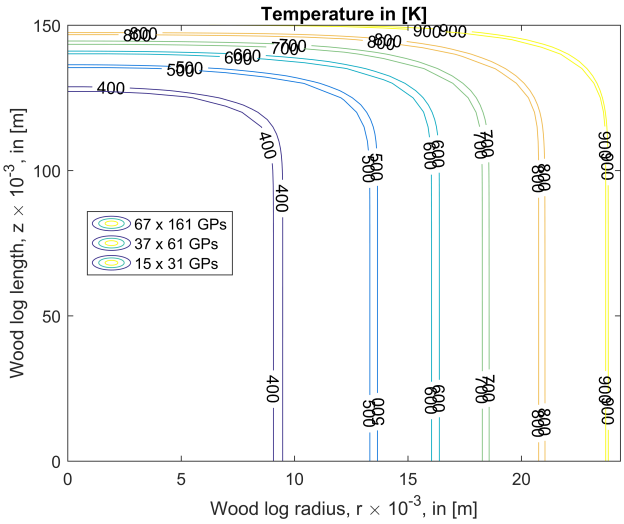

Figure 3: Comparison of the wood internal temperature distribution obtained from a fine mesh (67 × 161 GPs), a medium coarse mesh (37 × 61 GPs) and the coarsest mesh (15 × 31 GPs) at 200s. The contour lines that have moved closer to the wood log center are the ones predicted by the coarsest mesh.

consider char conversion, a finer mesh will be required since the steep oxygen gradients will affect mesh-requirements. Drying can as well affect the mesh-requirements, since ongoing drying in the wood log center and extensive radiative heating at its surface, can increase the steepness of the wood-internal temperature gradient, potentially resulting in the need of a finer grid.

The modeling results discussed in the following sections are based on the medium coarse mesh of 37 × 61 GPs (radius × wood log length).

3.2 Study of anisotropy of wood

In this section the spatial distribution of temperature, densities (solid and gas) and mass fraction of gaseous species within the simulation domain is studied and the results at 200s and at 450s are shown in Figure 4 to Figure 8. The two different times of 200s and 450s were chosen since by that one can observe the propagation of the devolatilization inward.

The temperature distribution shown in Figure 4 is smooth. Steep temperature gradients, which would be due to either strongly endothermic or exothermic reactions, cannot be observed. This is the result of lacking drying, which would be highly endothermic, heat neutral primary devolatilization and lacking char conversion (highly exothermic). Secondary devolatilization reactions are only mildly exothermic. Furthermore, one can identify that the devolatilization zone is rather narrow, since the wood density quickly drops from its initial value to zero in both the longitudinal and the radial directions (see Figure 5).

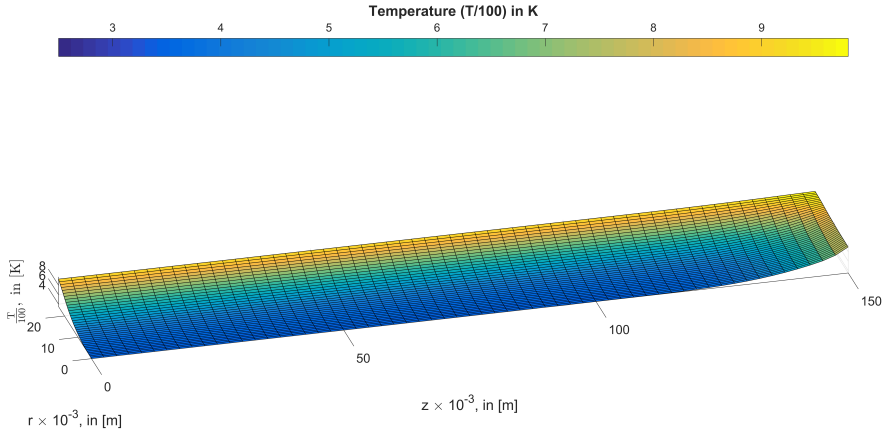

(a) Predicted temperature in [K] at 200s.

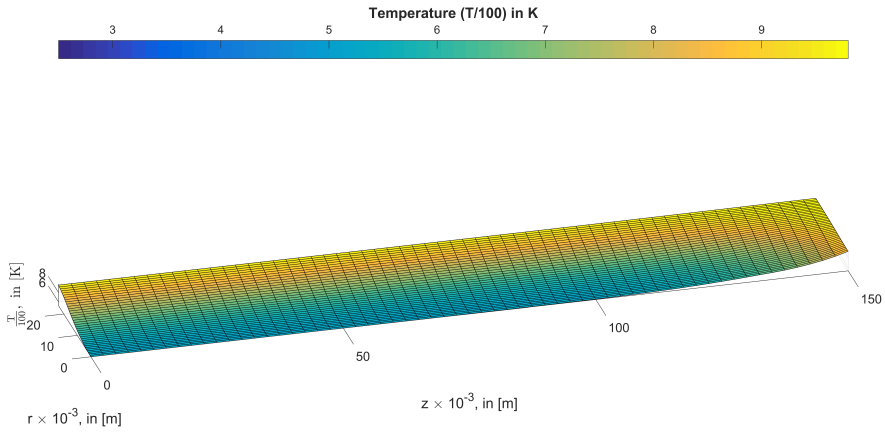

(b) Predicted temperature in [K] at 450s.

Figure 4: Wood internal temperatures in [K] at 200s and 450s during devolatilization. The top of the wood log is at z = 150mm, and the lateral shell surface of the wood log is at r=25mm.

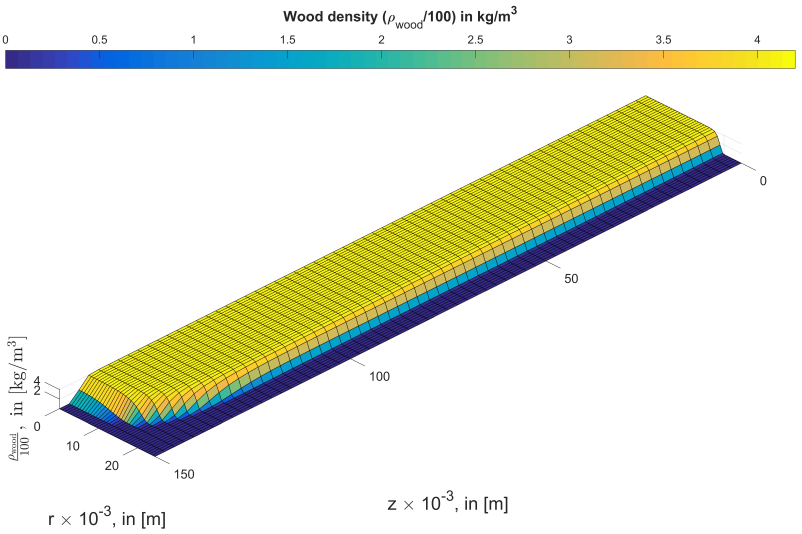

(a) Predicted wood density in [kg/m^3] at 200s.

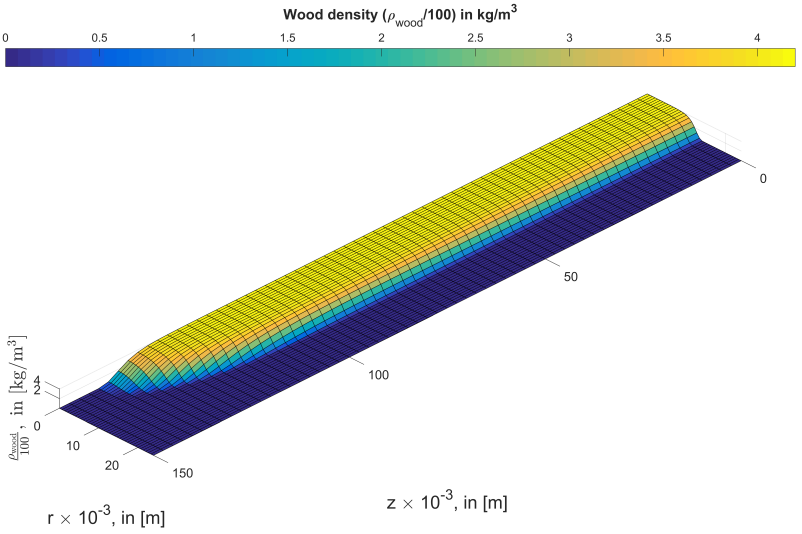

(b) Predicted wood density in [kg/m^3] at 450s.

Figure 5: Wood densities in [kg/m^3] at 200s and 450s during devolatilization. The top of the wood log is at z = 150mm, and the lateral shell surface of the wood log is at r=25mm.

394 Even though the thermal conductivity is higher in the longitudinal than in the radial
395 direction, the wood is primarily converted by the devolatilization zone moving in the radial

direction. This is a result of the ratio between the radial and the longitudinal dimensions of the wood log. The wood log is six times longer (L) than its diameter (D), which means that the (initial) ratio between the total surface of the devolatilization front moving in the radial (S_R) and longitudinal (S_L) directions is given by $S_R/S_L = L/D = 12$. (Here, the devolatilization front is defined as the surface within the devolatilization zone with the highest primary devolatilization rate.) The result of this S_R/S_L ratio is that even though the devolatilization front moves faster in the longitudinal than in the radial direction, the fact that the majority of the surface area of the combined devolatilization front is moving in the radial direction means that most of the wood devolatilzation is due to the radially moving front.

When comparing the progress of the devolatilization, one can clearly see how far the devolatilization has moved inside from 200s (Figure 5a) to 450s (Figure 5b). At 200s the devolatilzation zone is only at slightly less than 150mm in the longitudinal direction and 20mm in the radial direction, while the devolatilization zone has not even reached 125mm in the longitudinal direction and less than 10mm in the radial direction at 450s.

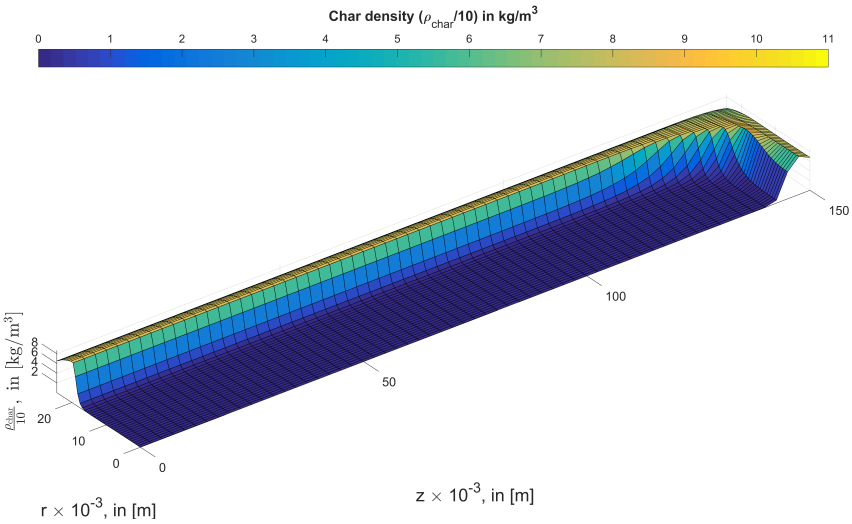

(a) Predicted char density in [kg/m^3] at 200s.

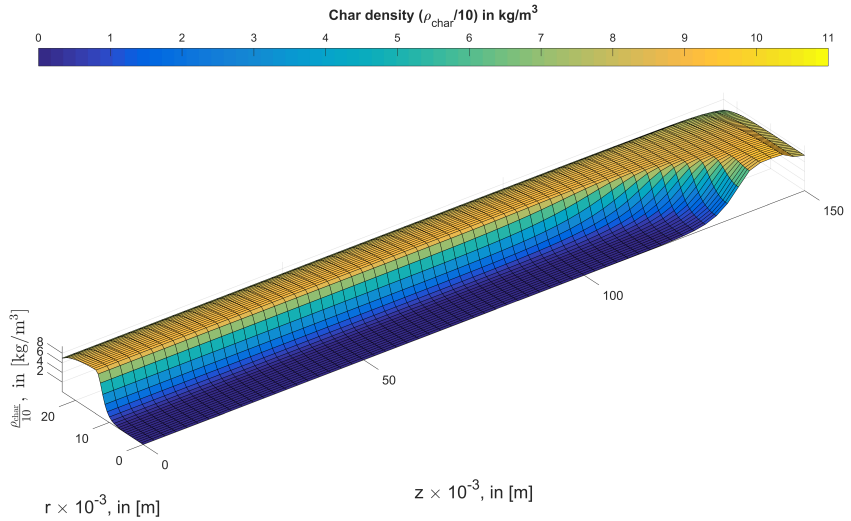

(b) Predicted char density in [kg/m^3] at 450s.

Figure 6: Char densities in [kg/m^3] at 200s and 450s during devolatilization. The top of the wood log is marked at z = 150mm, and the lateral shell surface of the wood log is at r=25mm.

Corresponding to the drop in wood density one can clearly observe the notable char density increase in Figure 6. It can also be observed that the char density is slightly lower

close to the external surface. Thermally thick particles have a faster heat transfer to the wood log surface compared to the heat transfer from the external surface to the wood log center. The outer zones of the wood log are therefore quickly heated. In those zones, more tar is formed, which comes at the expense of char production. As a consequence, the char density is lower closer to the external wood log surface. As the char formation zone moves further inside, one can see that the char density forms a plateau at about 90 kg/m^3. The final char yield is predicted to be about 20 % of the initial dry wood log mass, see Figure 2c, which also agrees well with experimental observations.

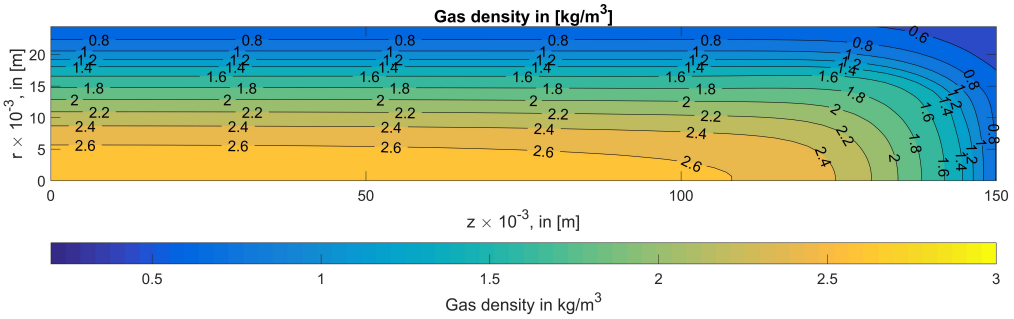

(a) Predicted gas density in [kg/m^3] at 200s.

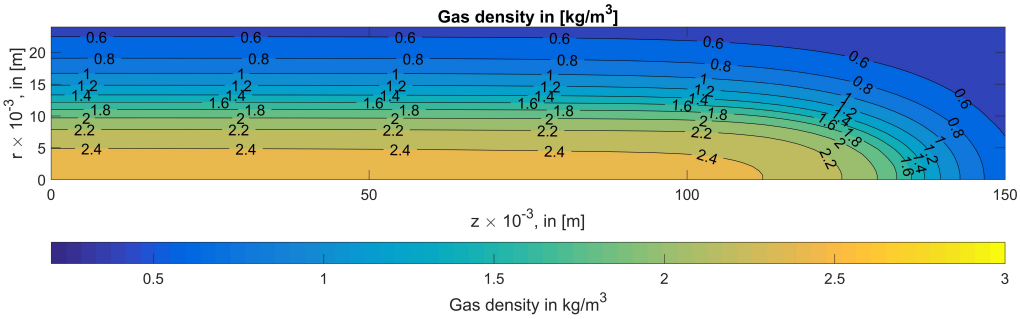

(b) Predicted gas density in [kg/m^3] at 450s.

Figure 7: Gas densities in [kg/m^3] at 200s and 450s during devolatilization. The top of the wood log is at z = 150mm, and the lateral shell surface of the wood log is at r=25mm.

The maximum gas density inside the wood log shown in Figure 7 is about 2.6kg/m^3 at 200s and about 2.4 kg/m^3 at 450s. This is a result of the permeabilities and therefore a function of mass transfer limitations but also volatile release rate, which is influenced by

wood internal heat transfer and therefore thermal conductivities. As will also be discussed in Section 3.4, a higher longitudinal and radial char permeability leads to a drop in the peak value of the gas density and also the internal pressure. Vice versa the internal pressure increases when permeabilities are assumed to be small. However, besides mass transfer properties, a slower heat transfer and therefore a slower devolatilization rate as well lead to lower internal pressure and gas densities, since gases are less quickly produced and have time to leave the wood matrix before newly formed gases add to the already existing volatiles, filling the pores.

The pressure increases steeply within the zones of low permeabilities (high mass transfer limitations) and flattens out within the zones of high permeabilities (low mass transfer limitations), which is where char has already been formed.

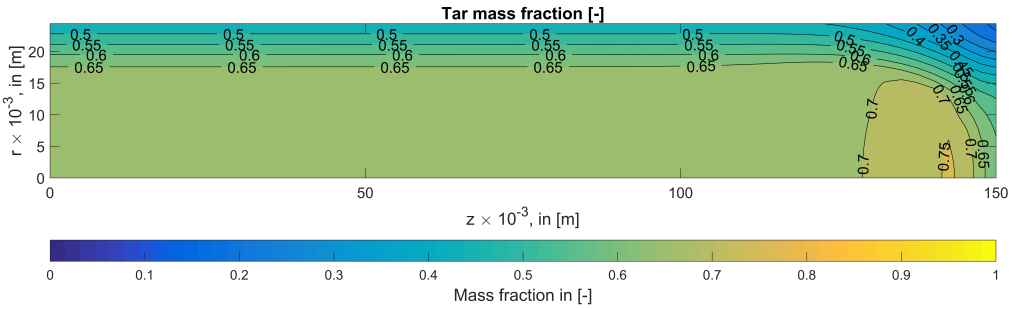

(a) Predicted tar mass fraction, Y_{tar}, at 200s.

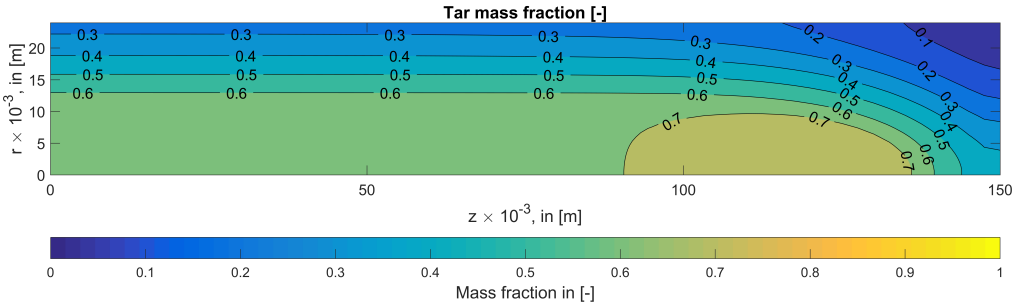

(b) Predicted tar mass fraction, Y_{tar}, at 450s.

Figure 8: Tar mass fractions [-] at different times during devolatilization. The top of the wood log is at z = 150mm, and the lateral surface of the wood log is at r=25mm.

As can be seen in Figure 8a, the tar mass fraction rises to a value as high as 75 % inside the wood log at 200s. Most interesting though is to see that the highest tar mass fraction is observed close to the top of the wood log. This zone of high tar fractions close to the top of the wood log, is a result of primary tar formation, faster outward convection of tar in longitudinal direction and therefore reduced secondary tar cracking. Tar can either be transported outward or be consumed by secondary tar reactions, which yield either secondary char or additional non-condensable gases. One can observe that the tar mass fraction decreases toward the external surface. This is partly due to inward diffusing nitrogen, since the assumption is that the reactor is filled with nitrogen. The nitrogen to some extent dilutes the tar in the wood log pore structure. In addition, however, secondary tar reactions also contribute to tar reduction.

When plotting the char densities (Figure 6) one cannot identify a significant char density increase toward the surface of the wood log, which would imply significant tar repolymerization to char as tar leaves the wood log. One rather sees a plateau in the char density, and a rather even distribution at about 90 kg/m^3 throughout the wood log. This implies that char formation from tar in this case plays only a minor role compared to primary char formation. In fact, tar cracking to non-condensable gases is faster than secondary char formation. When comparing the secondary tar kinetics, one can see that even though the activation energies of the two secondary tar reaction paths are the same, the pre-exponential factor of the tar to char reaction is about 40 times lower than the one for tar to non-condensable gases. Therefore, the drop in tar mass fraction is a combination of outward-diffusion of tar, and mostly tar reacting to non-condensable gases. Since the gases are mostly transported out of the wood log in longitudinal direction, and u_z is higher than u_r, the tars have shorter residence times in longitudinal direction than in radial direction. Therefore, tar fractions are lower in radial direction, since tar has more time to convert to non-condensable gases, while via the top of the wood log, higher tar mass fractions are released to the wood log surroundings.

The internal pressure fields at different times of thermochemical conversion are not discussed in detail in this section, since they are discussed in a following section (Section 3.4) in connection with the discussion of the effect of permeabilities on wood internal pressure and velocities.

3.3 Study of primary devolatilization kinetics

In the 1D model presented by Larfeldt et al.,[9] they used kinetics to predict devolatilization of a large wood that differed from what is used in the base case of this work (see Table 3). In order to identify how the choice of kinetics alters modeling results, two different sets of primary devolatilization kinetics were used below.

By analyzing the reaction rate constants plotted in Figure 9 it can be observed that the two different sets of kinetics yield rather different conversion rates, and therefore also different product yields.

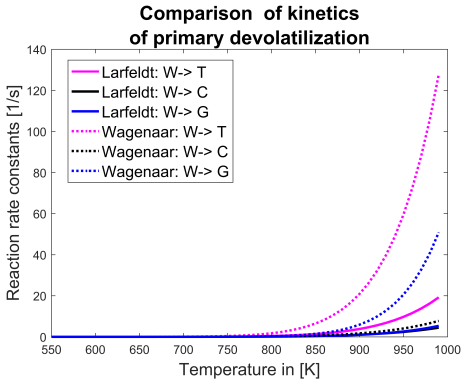

Figure 9: Comparison of kinetics used for primary devolatilization. The solid lines correspond to kinetics used to describe wood degrading to tar (W $\rightarrow$ T), wood to char (W $\rightarrow$ C) and wood to non-condensable gases (W $\rightarrow$ G) as used by Larfeldt et al.[9] The dotted lines correspond to kinetics used to describe the same three degradation reaction paths, but with kinetics taken from Wagenaar.[22]

The kinetics suggested by Wagenaar et al.[22] yield significant tar formation. We therefore expect large amounts of tar being produced from primary devolatilization, which we found

to be confirmed when analyzing Figure 8. Unless this tar is fully converted to char or non-condensable gases subsequently, it will be emitted to the freeboard above the wood log. The final char yield predicted by means of the kinetics suggested by Wagenaar et al.[22] agreed very well with experimental observations.

In order to clearly illustrate the effect the kinetics have on the degradation dynamics, the normalized residual solid mass curves are plotted (see Figure 10c).

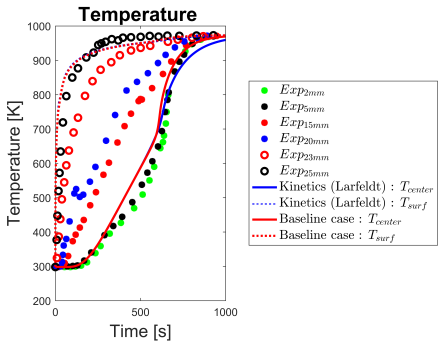

(a) Predicted center and surface temperatures validated against the first experimental series by Larfeldt et al.[9]

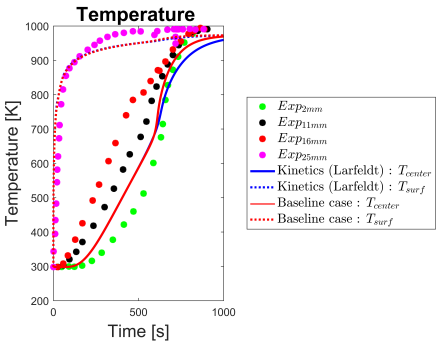

(b) Predicted center and surface temperatures validated against the second experimental series by Larfeldt et al.[9]

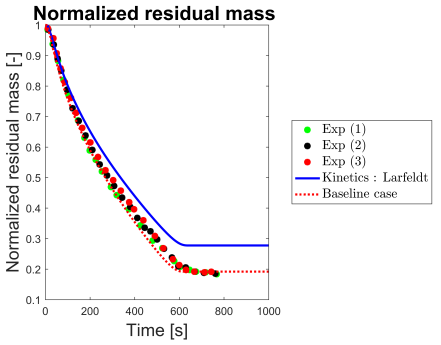

(c) Predicted normalized residual solid mass.

Figure 10: Comparison of the degradation dynamics predicted by two different sets of kinetics describing primary devolatilization. One kinetic set was the same as the one used in the 1D model by Larfeldt et al.[9] and the second one was taken from Wagenaar et al.[22]

Better agreement was found for the set of kinetics as suggested by Wagenaar et al.,[22] especially since the final char yield agreed better with what had been observed experimentally

(see Figure 10). The kinetics used by Larfeldt et al.[9] led to significantly higher char densities (see Figure 11), and therefore a higher final char yield.

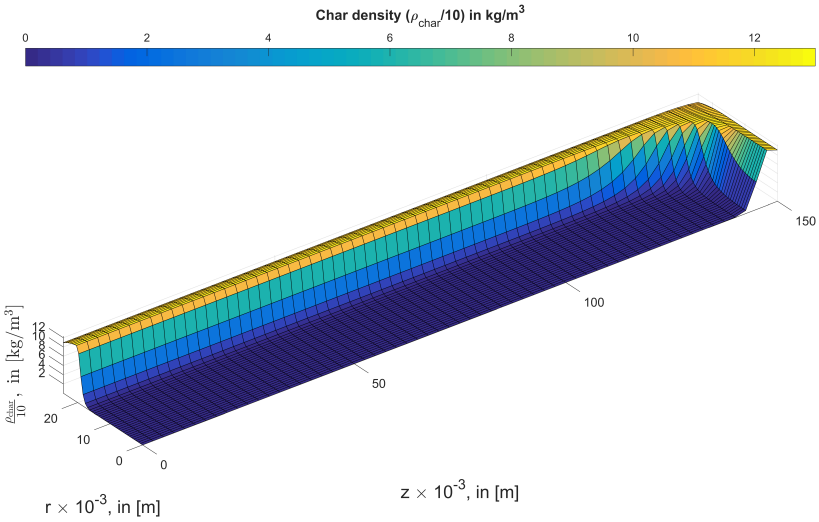

(a) Predicted char density in [kg/m^3] at 200s.

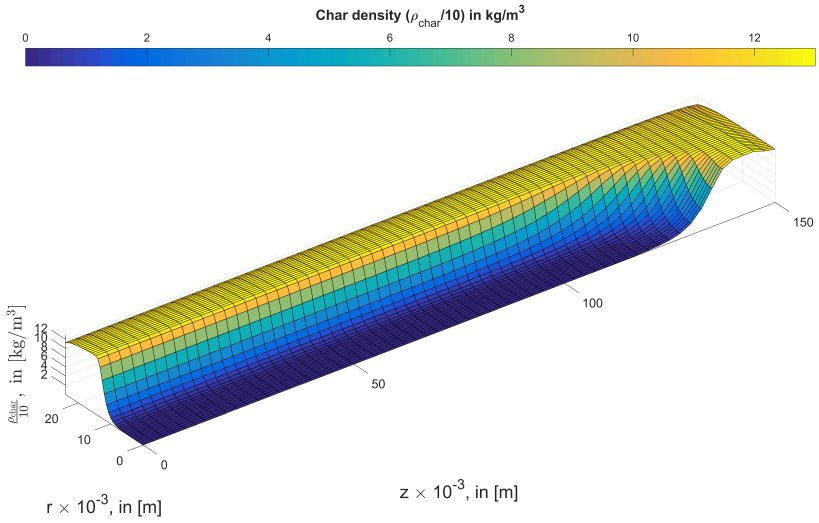

(b) Predicted char density in [kg/m^3] at 450s.

Figure 11: Char densities in [kg/m^3] at 200s and 450s during devolatilization, predicted with the kinetics used in Larfeldt et al.[9]

The char density obtained from the kinetics used by Larfeldt et al.[9] even exceeded

120kg/m^3, while the base case predicted a char density of 90kg/m^3. The base case is the one performed with the wood properties and kinetics listed in Table 2 and Table 3. For early times, the progress of the devolatilization does not differ significantly, but it starts to deviate as devolatilization proceeds (see Figure 10c). This is due to the thicker char layer that is predicted to build up when applying the kinetics used by Larfeldt et al.[9] A thicker char layer implies a more prominent insulation barrier to heat transfer inward and therefore slower devolatilization.

When plotting the tar fractions predicted by the kinetics of Larfeldt et al.,[9] lower tar fractions as in the base case were modeled (see Figure 12).

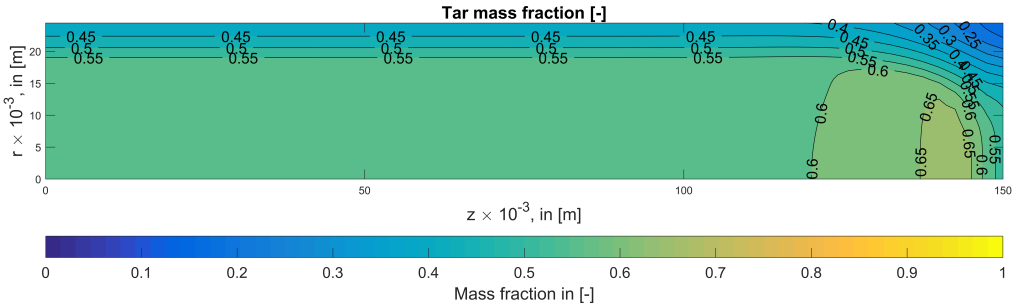

(a) Predicted tar mass fraction, Y_{tar}, at 200s.

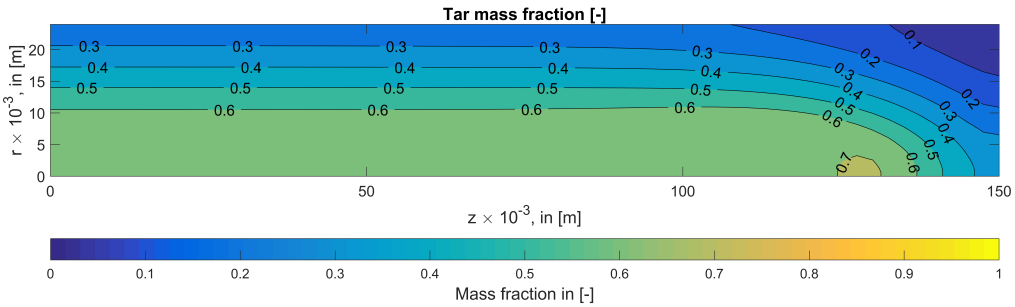

(b) Predicted tar mass fraction, Y_{tar}, at 450s.

Figure 12: Tar mass fractions [-] at 200s and 450s during devolatilization, predicted with the kinetics used in Larfeldt et al.[9] The top of the wood log is at z = 150mm, and the lateral shell surface of the wood log is at r=25mm.

In Figure 12b, which shows the mass fraction of tar obtained with the kinetics used

by Larfeldt et al.,[9] the main difference to the base case is that there is slightly less tar in Figure 12. Overall, the difference in tar fraction distribution in the wood log interior is not significantly altered by the choice of kinetics at 450s. At 450s only the area of the highest tar mass fraction (70%) is larger when using primary devolatilization kinetics suggested by Wagenaar et al.[22] At 200s (Figure 12a) the tar mass fraction predicted close to the wood log top, is slightly smaller (peak at 65% in Figure 12a) than the predictions from the base case (peak at 75% in Figure 8a). However, overall the difference is minor. The kinetics used in the base case were still considered more suitable, due to the better agreement in final char yield.

This section outlines that the chosen kinetics used for degradation modeling are a significant uncertainty entering a thermochemical degradation model. Different gas species production yields are predicted, as well as different yields of char. Different char yields then again affect the heating of the residual wood log, since the thermal mass is altered accordingly. Such an effect on internal heat transfer can reflect back on the prediction of normalized residual solid mass.

3.4 Effect of wood and char permeabilities on pressure and gas phase flow in radial and longitudinal direction

The necessity of multi-dimensional models is often discussed, and they are clearly needed if one wants to study the effect of wood anisotropy. Only multi-dimensional models can account for the fact that mass transfer properties, e.g. permeabilties, strictly depend on the fiber direction. In addition, heat transfer along and across the fiber direction can differ significantly. The choice of dimensionality of a model also depends on its purpose. One cannot draw a general conclusion on how well 2D and 1D models balance accuracy and CPU time, since most likely the two modeling set-ups are used for entirely different purposes. While 1D models are commonly used when simplified and fast models are needed, with

the main purpose of predicting total conversion time and center and surface temperatures, multi-dimensional models are developed when more comprehensive studies on wood internal distributions of a range of variables shall be performed. Furthermore, a detailed prediction of product yields can only be obtained from multi-dimensional models, since mass transfer limitations are very different in axial and radial direction and therefore also residence times of tars and consequently the extent of secondary tar reactions. One can clearly see that the degree of detail for the two modeling concepts varies significantly. Valuable information on the suitability and applicability of the model can therefore not be obtained by purely comparing the CPU time and the accuracy of the model.

In this work, the influence of anisotropy on modeling results is studied, which require multi-dimensional models. The base case was run with the wood and char permeabilities given in Table 2. The difference between radial and longitudinal permeabilities of wood was of the order of 10^3, while the difference was reduced to roughly 10 for char.

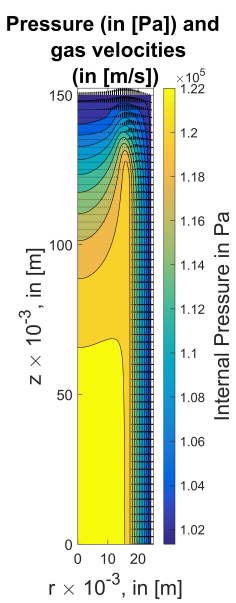

(a) Predicted internal pressure, P_{gas}, in [Pa] and radial and longitudinal velocities in [m/s] at 200s.

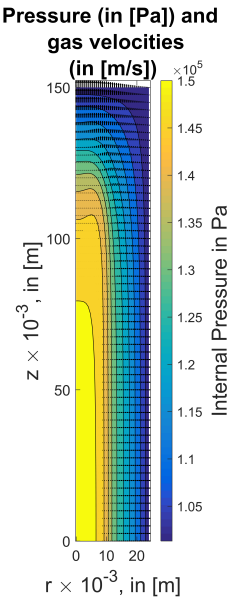

(b) Predicted internal pressure, P_{gas}, in [Pa] and radial and longitudinal velocities in [m/s] at 450s.

Figure 13: Wood internal pressure [Pa] and gas velocities (radial and longitudinal) in [m/s] at 200s and 450s during devolatilization - base case.

In Figure 13 it is shown that the maximum velocities in the z-direction (u_{z}), which is the direction following the fiber orientation, are higher than the maximum velocities in the radial direction (u_{r}). This is the result of the permeabilities, since the mass flow resistance is ten times higher in the radial direction than it is in the longitudinal direction. Furthermore, it is shown that the velocity profile at the wood log top is coupled to the position of the pressure peak. The highest u_{z} at the top of the wood log at 200s is positioned where we have the highest wood internal pressure (see Figure 13). The highest velocity crossing the wood log top surface is predicted where the pressure wave, travelling into the particle radially, is closest to the external top surface of the hanging wood log. As the pressure peak travels inward from the wood log surface to its center, also the u_{z} profile changes accordingly (compare Figure 13a and Figure 13b). Similar connections between pressure

peaks (also sometimes referred to as pressure wave) to the velocity profile at the wood log surface have been presented by Di Blasi[29] when discussing the importance of physical transport phenomena in wood devolatilization modeling. Based on the results shown in Figure 13, it seems that the volume flow of volatiles exits the wood primarily via the top of the log.

In Figure 13 one can also study the significance of the char permeabilities in radial and longitudinal direction to the up-building wood internal pressure. For the permeabilities used in the base case, the maximum wood internal pressure was found to be 1.22×10^5 Pa at 200s and 1.5×10^5 Pa at 450s. When decreasing the assigned char permeabilities by a factor of 10, i.e. $\kappa_{c,\parallel} = 10^{-13}$ m^2 and $\kappa_{c,\perp} = 10^{-14}$m^2, the wood internal pressure increased significantly. The maximum pressures at 200s and 450s were then about 2.4×10^5 Pa and 4×10^5 Pa, respectively (see Figure 14).

The reason for these high wood internal pressures is that the permeability, together with the heat transfer controlled volatiles formation rate, are the only parameter controlling wood internal pressure decrease. This means that pressure increase is a combined result of both heat and mass transfer processes. However, the current model does not include the effect of cracking and the connected sudden gas release rate in case of crack formation and the resulting pressure drop. Instead, it is assumed that the structural integrity of both the initial wood log as well as the resulting char log is always high enough to avoid any crack formation. This might be an acceptable assumption for virgin wood, which has a high structural integrity, but in case of char, this assumption is less accurate, since char is more brittle and fragile than wood. A high internal pressure will lead to crack formation if the pressure exceeds the strength of the remaining char matrix. In order to set a limit to the wood internal pressure up-build, it is therefore recommended to include crack formation in the model and hereby increase the accuracy of the model.

The velocity profiles for the low permeability case, as shown in Figure 14, are similar to the profiles predicted by the base case, while the velocity profiles of the base case and

the case with the same premeabilities along the fiber direction but 10 times smaller radial permeabilities differed at 450s (compare Figure 13b and Figure 15b). In Figure 15b it is shown that the radially moving pressure wave has not yet reached the wood log center.

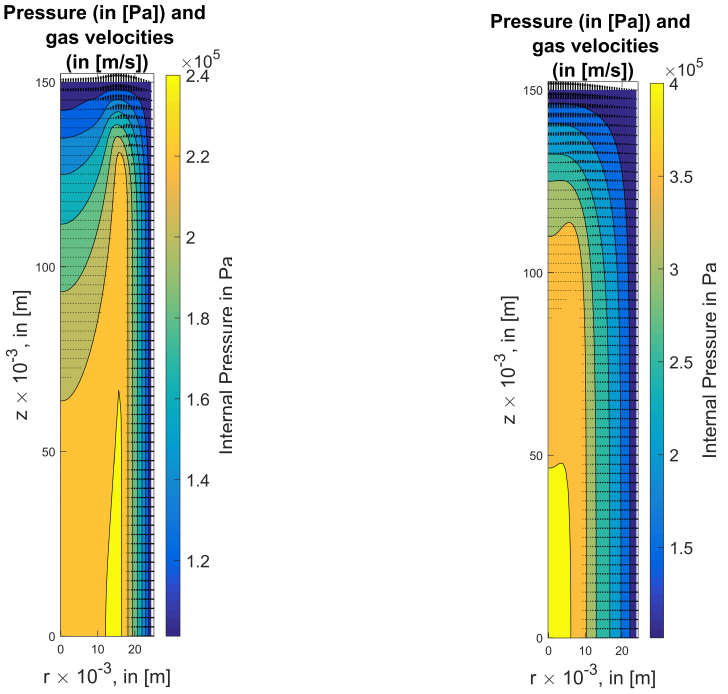

(a) Predicted internal pressure, P_{gas}, in [Pa] and radial and longitudinal velocities in [m/s] at 200s.

(b) Predicted internal pressure, P_{gas}, in [Pa] and radial and longitudinal velocities in [m/s] at 450s.

Figure 14: Wood internal pressure [Pa] and gas velocities (radial and longitudinal) in [m/s] at different times during devolatilization - higher permeability test case. The char permeabilities were decreased to 10^{-14} m^2 in radial direction and 10^{-13} m^2 in longitudinal direction.

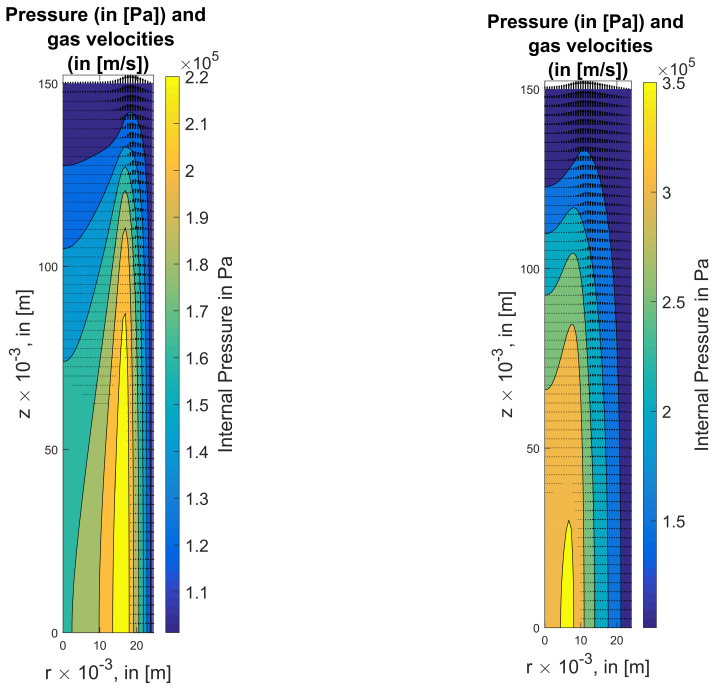

(a) Predicted internal pressure, P_{gas}, in [Pa] and radial and longitudinal velocities in [m/s] at 200s.

(b) Predicted internal pressure, P_{gas}, in [Pa] and radial and longitudinal velocities in [m/s] at 450s.

Figure 15: Wood internal pressure [Pa] and gas velocities (radial and longitudinal) in [m/s] at different times during devolatilization. The char permeabilities were decreased to 10^{-14} m^2 in radial direction and kept unchanged at 10^{-12} m^2 in longitudinal direction.

The different radial and axial velocity profiles predicted by the three cases have primarily two effects. Firstly, the tar residence time is altered by the mass transfer limitations, i.e. by the char permeabilities. As a consequence, the extent of secondary tar reactions differs in the radial and longitudinal direction, which means that also the tar release rate at the top and across the radial surface differs. The residence time of tar in the radial direction is higher, implying that more tar can be converted and less tar is released to the wood log surroundings. This highlights the importance of multi-dimensional models when the purpose of the solid phase model is to be coupled to a gas phase model. The different release rates might potentially have an effect on the combustion in the freeboard above the wood

log. Secondly, the difference in velocity profiles, i.e. Stefan flow profiles, between the top and the radial surfaces means that the heat and mass transfer coefficient over the surfaces will differ. For common combustion processes, such as in a wood stove, the effect of the convective heat transfer coefficient on the overall degradation dynamics is minor, since the wood log is primarily heated by the radiative feedback of the flame. However, differences in the convective mass transfer coefficients might potentially have a significant effect on the char oxidation since oxygen will less easily diffuse into the porous char structure via the top of the char log. The opposing effect of the convective outward flow will be less in radial direction, which facilitates the oxygen diffusion into the porous wood log in the radial direction. This effect on mass transfer coefficients are expected to be of any significant importance only as long as devolatilization still occurs in the wood log core, i.e. as long as char conversion and wood devolatilization overlap on the wood log scale. This is because only then convection is sufficiantly high. It is, however, recommended that the effect of mass transfer coefficients on char conversion is studied in more detail in future works.

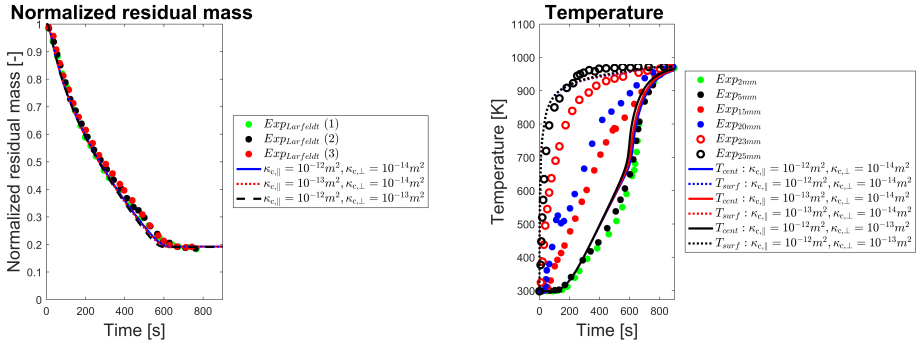

(a) Normalized residual mass. (b) Center and surface temperatures.

Figure 16: Normalized residual mass and center and surface temperatures predicted by the base case, and two additional test runs. The char permeabilities were reduced to 10^{-14} m^2 in radial direction and 10^{-13} m^2 in longitudinal direction in the second test run, and 10^{-14} m^2 in radial direction and 10^{-12} m^2 in longitudinal direction in the third test run. Experimental data also plotted was taken from Larfeldt et al.[9]

From the above it can be concluded that in order to predict the correct velocity profiles

within the wood log, a higher dimensional code is required. At the same time, it is also clear that the velocity profile does not have a significant influence on the mass loss rate of the wood log (see 16a). The mass loss rate is controlled by the heat transfer, which is also directional dependent through the thermal conductivities. This means that even though the directional dependence of the permeability does not require a higher dimensional code in order to predict the correct mass loss rate, the directional dependence of the thermal conductivity does.

3.4.1 Comparison of 1D to 2D modeling results

The 2D model allows a detailed consideration of wood anisotropy by allowing for different heat and mass transfer properties in the radial and longitudinal direction of the wood log. However, this increase in detail comes at the cost of increased computational time. The question arises, if such a detailed model operating at this increased computational cost, is always needed to accurately predict conversion. Therefore this section is dedicated to studying how 1D and 2D models compare in their prediction of solid degradation dynamics.

The 2D model, used for comparison in this section, was the base case presented earlier in this paper. The 1D model was run purely with the radial heat and mass transfer properties of the 2D model. The results of this comparison are shown in Figure 17.

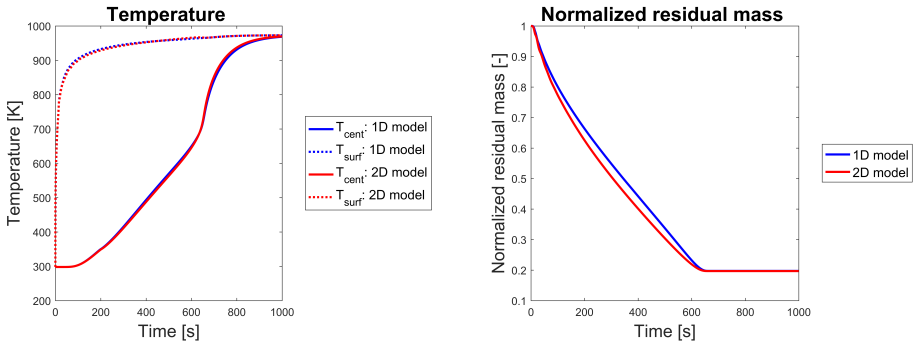

(a) Predicted center and surface temperatures.

(b) Predicted normalized residual solid mass.

Figure 17: Comparison of degradation dynamics predicted by the 1D model and by a detailed 2D model.

For the particular conditions that are studied in this paper, the difference in the prediction of the solid degradation dynamics between the 1D and the 2D simulations is not significant, as shown in Figure 17. Therefore, it is concluded that for studying the conversion fundamentals, such as total devolatilization time as well as center and surface temperature, a simplified 1D model is sufficient. However, if the aspect ratio between the longitudinal and the radial extent of the cylindrical wood log is decreased from the current value of 6, 2D models might become more relevant since the heat transfer in the longitudinal direction becomes more influential on the overall degradation dynamics. This is not the given case in the base study, where the mass loss of the wood log is mostly occurring due to the inward propagation of the devolatilization zone in radial direction.

However, a 2D model will always be needed if one aims to get detailed information on wood internal distributions. Those cannot be accurately predicted by 1D models. Furthermore, inhomogeneous boundary conditions demand multi-dimensional models. Also, if one aims to get correct volatile release rates at different positions of the wood log surface, multi-dimensional models are needed.

One can conclude that degradation trends obtained under simple boundary conditions, i.e. constant heat fluxes to the particle all over its surface, can be well enough predicted by

1D models. At least if the aspect ratio of the cylinder is large enough to assume an infintely long wood log. But, if one aims to couple the solid and the gas phase model to obtain an overall combustion simulation tool, multi-dimensional models are strictly required. This is primarily because wood logs in e.g. wood stoves are not subject to idealized simple and homogeneous boundary conditions, and also because volatile release rate (its composition and flow rate) from the wood log is not uniform all over the wood log external surface. Since this volatile release enters the gas phase model, it needs to be predicted accurately in order to predict the combustion in the wood stove correctly.

4 Conclusions and recommendations

In this work, a 2D model for wood log devolatilization was presented. The modeling results were validated against experimental data obtained for the devolatilization of a dry, large, birch wood cylinder. Good agreement was found between modeling results and experimental data.

A grid independence study was performed, and it was found that for the given modeling case a grid with 37×61 (radius $\times$ length) grid points was sufficient. This is, however, not a generic mesh-requirement, since the required mesh resolution will vary with e.g. heating rate and which wood conversion stages that are considered.

In addition, it was studied how the anisotropic wood structure affects pressure magnitude and distribution and therefore also radial and longitudinal gas velocities. It was found that the pressure peak is very sensitive to the assigned permeabilities. The relative contribution of radial and longitudinal gas flow depends on the permeabilities in radial and longitudinal directions. Wood degradation dynamics, however, did not show a significant dependence on permeabilities, and hence also not on pressure and gas phase velocities. This of course only applies to the solid mass loss. Product yields will be affected by the differences in mass transfer limitations.

Lastly, it was studied how 1D and 2D models compare. For the given case of a large wood log, solid phase degradation dynamics were acceptably well predicted by the 1D model. Nevertheless, the 2D model yielded better agreement with experiments. Since 1D models are much faster and more computationally efficient than higher dimensional models, it is important to understand how high dimensionality that is required for a given study. As a general rule, we found that higher dimensional simulations (>1) are required when

- the wood logs have non-uniform boundary conditions (like in e.g. wood stoves),
- the detailed distribution of any variable within the log is studied,
- the ratio between the longitudinal and the radial extent of the log is low,
- the log cannot be approximated as neither cylindrical nor spherical.

5 Acknowledgments

This work has been carried out within the WoodCFD (243752/E20) project, which is funded by: Dovre AS, Norsk Kleber AS, Jøtulgruppen and Morsø AS together with the Research Council of Norway through the ENERGIX program.

References

(1) Pozzobon, V.; Salvador, S.; Bézian, J. J. *Fuel* **2018**, *214*, 300 – 313.

(2) Pozzobon, V.; Salvador, S.; Bézian, J. J.; El-Hafi, M.; Maoult, Y. L.; Flamant, G. *Fuel Process. Technol.* **2014**, *128*, 319 – 330.

(3) Grønli, M. G. A theoretical and experimental study of the thermal degradation of biomass. PhD thesis, Norwegian University of Science and Technology, Trondheim, 1996.

(4) Haberle, I.; Skreiberg, Ø.; Łazar, J.; Haugen, N. E. L. *Prog. Energy Combust. Sci.* **2017**, *63*, 204 – 252.

(5) Yang, Y. B.; Sharifi, V. N.; Swithenbank, J.; Ma, L.; Darvell, L. I.; Jones, J. M.; Pourkashanian, M.; Williams, A. *Energy Fuels* **2008**, *22*, 306–316.

(6) Sand, U.; Sandberg, J.; Larfeldt, J.; Fdhila, R. B. *Applied Energy* **2008**, *85*, 1208 – 1224.

(7) Di Blasi, C. *Int. J. Heat Mass Transfer* **1998**, *41*, 4139 – 4150.

(8) Biswas, A. K.; Umeki, K. *Chem. Eng. J.* **2015**, *274*, 181 – 191.

(9) Larfeldt, J.; Leckner, B.; Melaaen, M. *Fuel* **2000**, *79*, 1637 – 1643.

(10) Larfeldt, J. Drying and pyrolysis of logs of wood. PhD thesis, Chalmers University of Technology, Göteborg, Sweden, 2000.

(11) Haberle, I.; Haugen, N. E. L.; Skreiberg, Ø. *Energy Fuels* **2018**, *32*, 6847–6862.

(12) Haberle, I.; Haugen, N. E. L.; Skreiberg, Ø. *Energy Fuels* **2017**, *31*, 13743–13760.

(13) Lu, H.; Robert, W.; Peirce, G.; Ripa, B.; Baxter, L. L. *Energy Fuels* **2008**, *22*, 2826–2839.

(14) Fatehi, H. Numerical Simulation of Combustion and Gasification of Biomass Particles. PhD thesis, LTH (Lund University), Lund, Sweden, 2014.

(15) Mehrabian, R.; Zahirovic, S.; Scharler, R.; Obernberger, I.; Kleditzsch, S.; Wirtz, S.; Scherer, V.; Lu, H.; Baxter, L. L. *Fuel Process. Technol.* **2012**, *95*, 96 – 108.

(16) Fatehi, H.; Bai, X. S. *Combust. Sci. Technol.* **2014**, *186*, 574–593.

(17) Bird, R. B.; Stewart, W. E.; Lightfoot, E. N. *Transport Phenomena*, 2nd ed.; John Wiley & Sons, Inc.: New York, 2002.